Nonclassical states of light and atomic ensembles: Generation and New Applications

A thesis presented

by

Axel André

to

The Department of Physics

in partial fulfillment of the requirements

for the degree of

Doctor of Philosophy

in the subject of

Physics

Harvard University

Cambridge, Massachusetts

May 2005

Thesis advisor

Mikhail D. Lukin

Author

Axel André

Nonclassical states of light and atomic ensembles:

Generation and New Applications

Abstract

This thesis considers several novel methods for generating nonclassical states of light and atomic ensembles, and describes applications of these methods to precision measurements, generation of Fock states with controllable waveform and few-photons nonlinear optics.

We study the generation of spin-squeezed states of an ensemble of N atoms, and the conditions necessary to achieve high degree of squeezing taking into account imperfections such as decay and finite number of atoms. A specific implementation of this model based on atom-atom interactions via quantized photon exchange is presented in detail.

We analyze the effect of realistic noise sources for an atomic clock consisting of a local oscillator that is actively locked to a spin-squeezed (entangled) ensemble of N atoms. We show that the use of entangled states with a moderate degree of entanglement yields the maximal clock stability.

We study the dynamics of Raman scattering in optically thick atomic media, and the ensuing correlations between the atomic spin coherence and the Stokes photons created via Raman generation. The theoretical model and experimental highlights

are presented, demonstrating generation of pulses of light with controllable photon numbers, propagation direction, timing, and pulse shapes.

We describe two methods to dynamically control the propagation of light in atomic media using EIT. We show that propagating light pulses can be coherently converted into stationary excitations with nonvanishing photonic components, and present highlights of an experiment demonstrating this effect. We then show that these ideas can be further extended to localize optical pulses in all three spatial dimensions, and to dramatically enhance nonlinear interactions between weak optical pulses. Finally, we report on experimental progress towards nonlinear optical interactions in atomic media confined inside hollow-core photonic crystal fibers. We describe the experimental setup used to load Rubidium atoms along with a buffer gas inside the optical fiber, and report our preliminary results towards achieving this goal.

Contents

Citations to Previously Published Work

Some of the introductory material appears in

> "Quantum Control of Light Using Electromagnetically Induced Transparency", A. André, M. D. Eisaman, R. L. Walsworth, A. S. Zibrov, and M. D. Lukin, Journal of Physics B **38**, S589 *Special Issue: Einstein Year*, 2005.

The material of Chapter 2 has been published as

> "Atom Correlations and Spin Squeezing near the Heisenberg Limit: Finite-size Effect and Decoherence", A. André and M. D. Lukin, Phys. Rev. A **65**, 053819 (2002), `quant-ph/0112126`;

and appears also partly in

> "Coherent Atom Interactions Mediated by Dark-state Polaritons", A. André, L.-M. Duan, and M. D. Lukin, Phys. Rev. Lett. **88**, 243602 (2002), `quant-ph/0107075`;

Chapter 3 is based on

> "Stability of Atomic Clocks Based on Entangled Atoms", A. André, A. S. Sørensen, and M. D. Lukin, Phys. Rev, Lett. **92**, 230801 (2004), `quant-ph/0401130`

as well as

> "Long-term Stability of Atomic Clocks Based on Entangled Atoms", A. André, A. S. Sørensen, and M. D. Lukin, *in preparation*

Experimental results from Chapter 4 appear partly in

> "Atomic Memory for Correlated Photon States", C. H. Van der Wal, M. D. Eisaman, A. André, R. L. Walsworth, D. F. Phillips, A. S. Zibrov, and M. D. Lukin, Science **301**, 196 (2003).

and in

> "Shaping Quantum Pulses of Light Via Coherent Atomic Memory", M. D. Eisaman, L. Childress, A. André, F. Massou, A. S. Zibrov, and M. D. Lukin, Phys. Rev, Lett. **93**, 233602 (2004), `quant-ph/0406093`

The material of Chapter 5 is based partly on

> "Manipulating Light Pulses via Dynamically Controlled Photonic Band Gap", A. André and M. D. Lukin, Phys. Rev, Lett. **89**, 143602 (2002), `quant-ph/0205072`

and the experimental data presented in Chapter 5 appeared in

> "Stationary Pulses of Light in an Atomic Medium", M. Bajcsy, A. S. Zibrov, and M. D. Lukin, Nature **426**, 638 (2003), `quant-ph/0311092`

Chapter 6 appears partly as

> "Nonlinear Optics with Stationary Pulses of Light", A. André, M. Bajcsy, A. S. Zibrov, and M. D. Lukin, Phys. Rev, Lett. **94**, 063902 (2005), `quant-ph/0410157`

Electronic preprints (shown in `typewriter font`) are available on the Internet at the following URL:

> `http://xxx.lanl.gov`

Acknowledgments

First, I would like to thank my advisor Mikhail Lukin for his support and encouragement during the completion of the work presented in this thesis. His enthusiasm in conducting research and his relentless curiosity, have been an inspiration and have kept me challenged during those years that I had the privilege to be his student. Thank you Misha for giving me the opportunity to learn from you.

I would also like to thank Eric Heller for his support while I was in his group. His willingness to let me explore various topics in quantum physics finally led me to quantum optics, and was very fruitful to my development as a researcher. I would also like to thank the other members of my thesis committee, John Doyle and Ronald Walsworth, for the useful discussions we had during this work. The discussions I had with Ron on how to observe spin-squeezing experimentally were particularly stimulating.

During the completion of this work, I had the privilege of working with many inspiring colleagues, in particular with Lu-Ming Duan and Anders Sørensen; their contributions to this work is gratefully acknowledged. For the experimental parts of this thesis, I had the opportunity to collaborate with the very talented experimentalists of the Lukin and Walsworth group: Matthew Eisaman, Michal Bajcsy, Lilian Childress, Caspar van der Wal, Florent Massou, Sasha Zibrov, Gene-Wei Li, Irina Novikova, and David Phillips. Sasha Zibrov was particularly patient with me during my Lab work, and he was very generous with sharing his wisdom about experimental physics.

I would also like to thank all members of the Lukin group for many useful and intellectually stimulating discussions: Jacob Taylor, Michael Hohensee, Darrick Chang,

Mohammed Hafezi, Arjyesh Mukherjee, Gurudev Dutt, Alexey Gorshkov, Jiang Qian, John Calsamiglia and Ludwig Mathey.

The support of the Harvard-Smithsonian Institute for Theoretical Atomic, Molecular and Optical Physics (ITAMP) is gratefully acknowledged, and many thanks to Kate Kirby for the various discussions we had. Both ITAMP and the Harvard-MIT Center for Ultracold Atoms (CUA) were key in making my years at Harvard intellectually stimulating, through their seminars and the various social events they organized.

During this work, at Harvard and while travelling at conferences, I have greatly benefited from discussions with Roy Glauber, David Wineland, Peter Zoller, Ignacio Cirac, Michael Fleischhauer, Steve Harris, Eugene Polzik, Suzanne Yelin, Alexei Trifonov, and Klaus Mølmer.

The Physics Department staff at Harvard has been a great source of support and help. I would like to thank in particular Sheila Ferguson, Marilyn O'Connor, and Carol Davis for all their help.

Finally, I thank my friends and family for all their support during these years at Harvard, I could not have achieved this without them. In particular, thank you Victoria for putting up with me during the difficult times and keeping your trust in me.

A mon père

Chapter 1

Introduction

1.1 Motivation

We consider in this thesis several novel methods for generating nonclassical states of light and atomic ensembles. Nonclassical states of light or atoms have properties that challenge the usual notions of classical physics. These states illustrate some of the fundamental differences between quantum and classical physics, and thus enable to experimentally test the validity of quantum mechanics. Many of the original thought experiments conceived by the founders of quantum mechanics to illustrate its "strangeness" have now been experimentally realized and have confirmed its validity (see [41] for a recent snapshot of experiments). Besides these fundamental considerations, nonclassical states of light and atoms play an essential role in quantum networks where the goal is to enable quantum communication between distant parties, as well as processing of quantum information [28]. From a more directly applied standpoint, certain types of nonclassical states have reduced fluctuations compared to classical

states, which may lead to improvements in the field of precision measurements, as compared to what can be achieved with classical states.

The superposition principle is at the heart of many of the non-intuitive and most interesting aspects of quantum physics. A quantum system may exist in a linear superposition of states, in a way "suspended" between different classical outcomes: a particle may be at two positions at the same time, a spin may point in two directions at the same time...etc. Applying the concept of superposition to composite systems, immediately leads to the idea of entanglement. When the components of a composite system interact with one another, they quickly evolve into an entangled state: the state of one subsystem becomes correlated with the state of the other. But there is more to entanglement than just correlations, in fact as the EPR state of two spin $\frac{1}{2}$ systems shows

$$\left|\psi^{-}\right\rangle \;=\; \frac{1}{\sqrt{2}}\left(|\uparrow\downarrow\rangle - |\downarrow\uparrow\rangle\right), \tag{1.1}$$

the two spins are always anti-parallel to each other, yet at the same time neither of them is pointing in any definite direction. Thus, it is not until one spin has been measured that the direction of the other spin becomes determined. These correlations cannot be understood in classical terms. Moreover, the statistical predictions of quantum theory contradict any "local" theory, as expressed in the famous Bell inequalities [18, 12, 169, 11]. EPR correlations between two quantum bits (or qubits) can be used to perform cryptographic key distribution, quantum state teleportation, entanglement swapping and many other fundamental tasks of quantum communication (see [28] for reviews and references).

Squeezed states of light are such that the fluctuations in one of the two quadra-

ture phase amplitudes of the electromagnetic field drop below the level of fluctuations associated with the vacuum state of the field. Squeezed states are therefore in some sense quieter than the vacuum state and hence can be employed to improve measurement precision beyond the standard quantum limits [89]. Similarly, entangled states of an ensemble of N spin $\frac{1}{2}$ systems can have reduced fluctuations in one component of the total angular momentum operator compared to the benchmark classical state when all spins are 100% polarized and pointing in the same direction. These so-called spin-squeezed states [91] can be used to improve the precision with which phase can be measured, with direct implications for the long-term stability of atomic clocks [165].

Many of the ideas and developments of quantum information come from quantum optics. The reason is the spectacular experimental advances in this field over the last few years [41, 28]. The internal quantum states of atoms can be manipulated very efficiently using lasers and their state of motion can be controlled with laser cooling techniques. These methods when combined appropriately allow in principle to perform quantum computations and to implement quantum communications. The paradigm system consists of single atoms located inside high-Q optical cavities, with optical fibers connecting spatially separated "nodes" of the network [28]. Recently, it has been recognized that similar tasks can be realized with atomic ensembles, instead of single atoms or single ions [104]. Using a collective degree of freedom of the atomic ensemble, the atoms do not need to be manipulated one by one, and do not need to be cooled.

For teleportation and quantum communication, a goal is to create an EPR pair of

high fidelity between two distant locations. However, this distance is limited because of errors occuring in the communication channels used to distribute the entangled pair. For example, in optical fibers the error (absorption and/or depolarization) scales exponentially with the length of the channel. To overcome this problem, a quantum repeater can be used [34, 50, 48]. The idea is to divide the channel into shorter segments, which are purified separately before they are connected. Once connected, an entanglement swapping procedure is used to swap the entanglement to pairs separated by twice the segment length. Further rounds of purification and swapping, using a nested purification protocol, enables the distribution of entanglement over long distances, while keeping the necessary resources (initial fidelity over the length of one segment and time required for the whole procedure) from growing exponentially with channel length. The quantum repeater therefore combines the methods of entanglement purification and teleportation. A quantum repeater based on Raman scattering and quantum memories in atomic ensembles was proposed in [48]. The theory and experiments presented in chapter 4 constitute one of the basic building blocks of such a quantum repeater and may enable quantum communications over long distances.

Quantum networks consist of spatially distant nodes where information is stored and locally processed, and quantum communication channels connecting the nodes. Atoms, ions, and more generally matter is well-suited for storing qubits and for performing quantum gates because their quantum states can be efficiently manipulated using electromagnetic fields. On the other hand, photons are ideally suited for communication because of the long distance over which they can be carried using optical

fibers. Consequently, techniques for coherently and reversibly mapping the quantum state of light onto atoms and vice versa are essential to realize such a quantum network. Such an interface between atoms and photons can be implemented using Electromagnetically Induced Transparency in optically thick atomic ensembles [56]. Moreover, combining this ability to interface between light and atoms with techniques that allow for local quantum processing of quantum information (i.e. quantum gates), opens the possibility for distributed quantum computing [28].

In this work, we show that the well-known weak nonlinearity provided by Raman scattering [24] leads to the generation of atom-photon entangled states. In combination with techniques to coherently map the quantum states of atoms to photons and vice versa [56], we show that this method can be used to engineer atom-atom entanglement in atomic ensembles, generate controllable photon number states, and achieve optical nonlinearity at the single photon level.

1.2 Overview

In the following section of this introduction, we briefly review background material relevant to the rest of this thesis. We review EIT and its use to control the group velocity of light pulses, in particular to map the quantum state of light pulses onto atoms.

In Chapter 2, we describe a new technique [3, 5] to induce effective coherent interactions between atoms in metastable states. The technique is based on a resonantly enhanced nonlinear process involving Raman scattering into a "slow" optical mode [31], which creates a pair of spin-flipped atom and slowly propagating coupled exci-

tation of light and matter (dark-state polariton [56]). When the group velocity of the polariton is reduced to zero [103, 128], this results in pairs of spin flipped atoms. This can be used for fast generation of entangled atomic ensembles, spin squeezing [91] and applications in quantum information processing [28]. The conditions for achieving strong spin squeezing with this mechanism are analyzed, taking into account imperfections such as decay and finite number of atoms.

In Chapter 3, we analyze the effect of realistic noise sources on an atomic clock consisting of a local oscillator that is actively locked to a spin-squeezed (entangled) ensemble of N atoms [7]. Such noise sources include the frequency noise of the local oscillator that is used to interrogate the atoms and that is actively locked to the atomic resonance. Also, uncontrollable environmental noise sources are considered, and their effect on the precision of the atomic clock is analyzed. A detailed model of the frequency control loop is presented, and the long-term stability of the stabilized clock is obtained from this model. We have also performed numerical simulations of the active stabilization process, including atomic noise, local oscillator noise and the frequency control feedback loop. We show that the use of entangled states with a moderate degree of entanglement yields the maximal clock stability.

In Chapter 4, we study the dynamics of Raman scattering in optically thick atomic media. We develop a three-dimensional quantum theoretical model of Raman generation of Stokes scattered light and of the associated atomic excitation. The ensuing correlations between the atomic spin coherence and the Stokes photons are analyzed and shown to be nonclassical. We show that this method can be use to generate pulses of light with controllable photon numbers, propagation direction, timing, and

pulse shapes. We present highlights of two experiments [159, 52] we performed in this area, demonstrating excellent agreement with our theory. Finally, we describe how a counter-propagating geometry [4] can improve conditional single-photon generation using this technique.

In Chapter 5, we describe two methods to dynamically control the propagation of light in atomic media using EIT. Spatial modulation of the index of refraction leads to the well-known formation of photonic bandgaps [83]. We show that these can be created using EIT, and furthermore that they can be dynamically controlled, i.e. switched on and off. We show that propagating light pulses can be coherently converted into stationary excitations, trapped inside the atomic medium. In addition to such a dispersive modulation, we show that modulation of the absorption can also be used to control the propagation properties of light pulses. We present highlights of an experiment demonstrating this effect.

We then show in Chapter 6 that these ideas can be further extended to localize optical pulses in all three spatial dimensions. In contrast to the challenge of achieving three-dimensional confinement through purely dispersive modulations [83] (e.g. the high index contrast and complicated structures required to achieve three-dimensional photonic bandgaps), combination of an absorptive modulation with a smooth transverse variation of the index of refraction immediately leads to a transverse waveguiding effect, and three-dimensional confinement of light pulses. The combination of waveguiding and long atom-photon interaction times allows to dramatically enhance nonlinear interactions between weak optical pulses. The usual limits of nonlinear optics to high intensities and tightly focused beams do not apply anymore in the sit-

uation we describe, so that a new regime of nonlinear optics is thus accessible, where coherent nonlinear interactions at the single-photon level appear accessible.

Finally, we report on experimental progress towards nonlinear optical interactions in atomic media confined inside hollow-core photonic crystal fibers. In hollow-core photonics fibers [142] light is guided by a periodic array of microscopic air holes inside a hollow core channel, with extremely low loss. We describe the experimental setup used to load Rubidium atoms along with a buffer gas inside the optical fiber, and report our preliminary results towards achieving this goal.

1.3 Quantum Control of Light

In general, the strength of the interaction between light and atoms is a function of the frequency of light. When the light frequency matches the frequency of a particular atomic transition, a resonance condition occurs. In this case, the optical response of the medium is greatly enhanced. Light propagation is then accompanied by strong absorption and dispersion [147], as the atoms are actively promoted into fluorescing excited states. This is one of the consequences of the relation between stimulated and spontaneous emission rates. Research over the past few decades has shown, however, that this is not always the case. Specifically, under conditions of Electromagnetically Induced Transparency (EIT), a resonant, opaque medium can be made transparent by means of interference [69].

To illustrate this effect, consider the situation shown in Fig. 1.1a in which the atoms have a pair of long-lived lower energy states $|g\rangle$ and $|s\rangle$. Such is the case for sublevels of different angular momentum (spin) states within the electronic ground

state of alkali atoms. In order to modify the propagation through this atomic medium of a light field that couples the ground state $|g\rangle$ to an electronically excited state $|e\rangle$ (the signal field), one can apply a second control field that is at resonance with the transition $|s\rangle \rightarrow |e\rangle$. The combined effect of these two fields is to stimulate the atoms into a so-called dark superposition of the states $|g\rangle$ and $|s\rangle$. In such a case, the two possible pathways in which light can be absorbed by atoms ($|g\rangle \rightarrow |e\rangle$ and $|s\rangle \rightarrow |e\rangle$) can interfere and cancel each other. The atoms are then said to be in dark states. With such destructive interference, none of the atoms are promoted to the excited state, leading to vanishing light absorption [69].

Many of the important properties of EIT result from the fragile nature of interference in a material that is initially opaque. Ideal transparency is attained only if the frequency difference between the two laser fields precisely matches the frequency separation between the atomic states. When the frequency difference is non-zero, the interference is not ideal and the medium becomes optically active. As a consequence, transparency is accompanied by steep dispersion of the refractive index, resulting in substantial reduction of the group velocity of light pules in EIT medium [54, 74, 35, 87, 31, 104, 113]. Additionally, vanishing absorption is accompanied by an enhanced nonlinear response [105]. A variety of interesting manifestations and potential applications of EIT, ranging from single-cycle pulse generation [148] to nonlinear optics at ultra-low light level [70, 71, 170, 33], have been demonstrated over the last decade. Thus, EIT has by now been firmly established as a powerful technique for coherent control of resonant propagation of classical light pulses.

At the same time, it is interesting to consider if similar ideas can be extended

to control pulses where quantum mechanical properties of light become apparent. In particular, the ability to control quantum states as well as propagation properties of weak quantum signals, such as single photon pulses, is central to the emerging field of quantum information science. It has been shown recently that EIT-based techniques can be used to create, store and manipulate single-photon pulses [104]. One of the particularly important potential applications of these techniques are in the area of long-distance quantum communication.

1.3.1 Strong coupling of light and matter

Photons are robust and efficient carriers of quantum information, while atoms are well-suited to precise quantum state manipulation. Moreover, long-lived atomic states provide ideal storage of quantum information. Quantum networks [38] require a technique for coherent transfer of quantum states from photons to atoms and vice versa. It is thus necessary to have a quantum memory that is capable of storing, releasing and manipulating quantum states at the level of individual quanta. Such coherent transfer techniques are essential, e.g., for quantum communication over long distances [34, 28, 48, 36].

A conceptually simple approach to quantum memory is to store quantum states of single photons in individual atoms. This approach involves, in essence, coherent absorption and emission of single photons by single atoms. However, implementing this idea in practice is difficult: strong coupling of a single atom to a single cavity mode is required. Trapped atoms placed inside high-Q optical cavities offer an elegant approach to coherent light-atom interactions [90]. The spectacular experi-

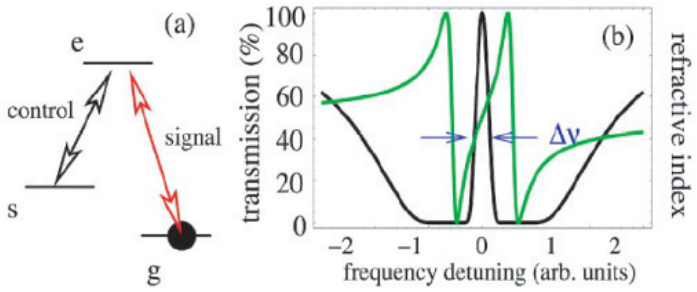

Figure 1.1: Electromagnetically induced transparency: (a) Prototype atomic system for EIT. (b) Spectrum of transmission and refractive index for signal field corresponding to EIT. Rapid variation of the refractive index (gray curve) causes a reduction of group velocity.

mental progress in this field, most notably by the groups of J. Kimble and G. Rempe [96, 117, 118], makes it a viable avenue for studying the fundamental physics of atom-photon interaction as well as for quantum networking with possibilities ranging from deterministic single-photon sources to quantum logic operations.

Recently a number of protocols have been developed [95, 100, 67, 55] that utilize a dispersive light-matter interaction and the ideas of quantum teleportation to achieve continuous-variable quantum state mapping into atomic samples. These ideas have been recently probed in pioneering experiments involving weak coherent state pulses [84].

1.3.2 Electromagnetically Induced Transparency (EIT)

EIT can be used to make a resonant, opaque medium transparent by means of quantum interference. In the case when the resonant control field is strong and its intensity is constant in time but the signal field is weak, the response of the atomic

ensemble can be described in terms of the linear susceptibility spectrum $\chi(\omega)$:

$$\chi(\omega) \;=\; g^2 N \frac{\gamma_{gs} + i\omega}{(\gamma_{ge} + i\omega)(\gamma_{gs} + i\omega) + |\Omega|^2} \tag{1.2}$$

where γ_{ij} corresponds to the relaxation rate of the $|i\rangle\langle j|$ coherence, Ω is the Rabi frequency of the control field (proportional to the electric field amplitude [147]), N is the total number of atoms in the sample, g is the atom-signal field coupling constant $g = \wp\sqrt{\frac{\omega_0}{2\hbar\epsilon_0 V}}$ ($\wp$ is the $g-e$ dipole matrix element, ω_0 the $g-e$ transition frequency, and V the quantization volume), and ω is the difference between the signal field frequency and the frequency of the atomic transition $|g\rangle \rightarrow |e\rangle$ (with $\omega \rightarrow 0$ corresponding to the exact atom-field resonance). The imaginary part of the susceptibility describes absorptive properties of the medium (thereby modifying the intensity transmission coefficient T), whereas the real part determines the refractive index n:

$$T(\omega) \;=\; \exp\left[-\mathrm{Im}\chi(\omega)kL\right], \quad n(\omega) = 1 + \mathrm{Re}\chi(\omega)/2 \tag{1.3}$$

where L is the length of the medium. Ideal transparency is obtained in the limit when the relaxation of the low-frequency (spin) coherence vanishes ($\gamma_{gs} = 0$), in which case there is no absorption at atomic resonance (see Fig. 1.1b). Ideal transparency is attained only at exact resonance, i.e., when the frequency detuning $\omega = 0$. Away from this resonance condition, the interference is not ideal and the medium becomes absorbing. The transparency spike that appears in the absorption spectrum is typically very narrow [Fig. 1.1b], however the tolerance to frequency detuning (transparency window $\Delta\nu$) can be increased by using stronger coupling fields, since in this case interference becomes more robust.

Since atoms are decoupled from the light fields in an ideal EIT medium, at resonance the susceptibility vanishes, and the refractive index is equal to unity. This

means that the propagation velocity of a phase front (i.e., the phase velocity) is equal to that in vacuum. However, the narrow transparency resonance is accompanied by a very steep variation of the refractive index with frequency. As a result, the envelope of a wave packet propagating in the medium moves with a group velocity v_g [56], where

$$v_g = \frac{c}{1 + g^2 N/|\Omega|^2} \tag{1.4}$$

which can be much smaller than the speed of light in vacuum c [54, 31, 104]. Note that v_g depends on the control field intensity and the atomic density: decreasing the control power or increasing the atom density makes v_g slower, as demonstrated by Hau et al. [74] and then by others [35, 87].

1.3.3 Dark-state polaritons

Consider the situation where the signal pulse is initially outside the medium. The front edge of the pulse then enters the medium and is rapidly decelerated. Being outside of the medium the back edge still propagates with vacuum speed c. As a result, upon entrance into the cell, the spatial extent of the pulse is compressed by the ratio c/v_g , while its peak amplitude remains unchanged. Clearly the energy of the light pulse is much smaller when it is inside the medium. Photons are being expended to establish the coherence between the states $|g\rangle$ and $|s\rangle$, or, in other words, to change the atomic state, with the excess energy carried away by the control field. As the signal pulse exits the medium its spatial extent increases again and the atoms return to their original ground state; the pulse, however, is delayed as a whole by the group delay $\tau = \frac{L}{v_g} - \frac{L}{c}$.

Inside the medium, the wave of flipped spins propagates together with the signal pulse. The photons in the pulse are therefore strongly coupled to the atoms, with an associated quasiparticle called a dark-state polariton [56] that is a combined excitation of photons and spins. For the case when the decay rate of coherence between states $|g\rangle$ and $|s\rangle$ is negligible, we can describe the propagating signal by the electric field operator $\hat{\mathcal{E}}(z,t) = \sum_k \hat{a}_k(t)e^{ikz}$, where the sum is over the free-space photonic modes with wave vectors k and corresponding bosonic operators $\hat{a}_k$. To describe the properties of the medium, we use collective atomic operators $\hat{\sigma}_{\mu\nu}(z,t) = \frac{1}{N_z}\sum_{j=1}^{N_z} |\mu_j\rangle\langle\nu_j|e^{-i\omega_{\mu\nu}t}$ averaged over small but macroscopic volumes containing $N_z \gg 1$ particles at position z.

In particular, the operator $\hat{\mathcal{P}}(z,t) = \sqrt{N}\hat{\sigma}_{ge}(z,t)$ describes the atomic polarization oscillating at an optical frequency, whereas the operator $\hat{\mathcal{S}}(z,t) = \sqrt{N}\hat{\sigma}_{gs}(z,t)$ corresponds to a low-frequency spin wave. The control field is assumed to be strong and is treated classically. The atomic evolution is governed by a set of Heisenberg equations: $i\hbar\partial_t\hat{A} = \left[\hat{A}, \hat{H}\right]$, where $\hat{H}$ is the atom-field interaction Hamiltonian and $\hat{A} = \{\hat{\mathcal{P}}, \hat{\mathcal{S}}\}$. These equations can be simplified assuming that the signal field is weak and that Ω and $\hat{\mathcal{E}}$ change in time sufficiently slowly, i.e., adiabatically [57]. To leading order in the signal field $\hat{\mathcal{E}}$ we find

$$\hat{\mathcal{P}}(z,t) \;=\; -\frac{i}{\Omega}\partial_t\hat{\mathcal{S}}, \qquad \hat{\mathcal{S}}(z,t) = -\frac{g\sqrt{N}\hat{\mathcal{E}}}{\Omega}. \tag{1.5}$$

The evolution of the signal field is described by the Heisenberg equation

$$\left(\frac{\partial}{\partial t} + c\frac{\partial}{\partial z}\right)\hat{\mathcal{E}}(z,t) \;=\; ig\sqrt{N}\hat{\mathcal{P}}(z,t). \tag{1.6}$$

The solution of Eqs. (1.5,1.6) can be obtained by introducing a new quantum field

$\hat{\Psi}(z,t)$ that is a superposition of photonic and spin-wave components:

$$\hat{\Psi}(z,t) = \cos\theta\hat{\mathcal{E}}(z,t) - \sin\theta\hat{\mathcal{S}}(z,t) \tag{1.7}$$

$$\cos\theta = \frac{\Omega}{\sqrt{\Omega^2+g^2N}}, \quad \sin\theta = \frac{g\sqrt{N}}{\sqrt{\Omega^2+g^2N}}. \tag{1.8}$$

The field $\hat{\Psi}(z,t)$ obeys the equation of motion:

$$\left[\frac{\partial}{\partial t} + c\cos^2\theta\frac{\partial}{\partial z}\right]\hat{\Psi}(z,t) = 0, \tag{1.9}$$

which describes a shape-preserving propagation with velocity $v_g = c\cos^2\theta$ that is proportional to the magnitude of its photonic component.

1.3.4 Quantum memory using dynamic EIT

The idea for quantum memory is closely related to the dark-state polariton concept. When a polariton propagates in an EIT medium, it preserves its amplitude and shape,

$$\hat{\Psi}(z,t) = \hat{\Psi}\left[z - c\int_0^t d\tau\cos^2\theta(\tau), t=0\right] \tag{1.10}$$

but its properties can be modified by simply changing the intensity of the control beam. As the control intensity is decreased, $\cos^2\theta \sim |\Omega|^2$ becomes very small, and the group velocity is slowed. At the same time the contribution of photons to the polariton state is reduced. In particular, if the control beam is turned off [$\Omega(t) \to 0$], v_g is reduced to zero as $\theta(t) \to \pi/2$ and the polariton becomes purely atomic: $\hat{\Psi}(z,t) \to -\hat{\mathcal{S}}(z,t)$.

At this point, the photonic quantum state is mapped onto long-lived spin states of atoms (a "spin wave"). As long as the storage process is sufficiently smooth [57], the

entire procedure has no loss and is completely coherent. The stored photonic state can be easily retrieved by simply reaccelerating the stopped polariton by turning the control field back on. In recent years, it was shown experimentally that weak classical light pulses can be stored and retrieved in optically thick atomic media using dynamic EIT [103, 128], and that the storage process preserves phase coherence [111]. Also, a novel form of dynamic optical bistability was recently demonstrated experimentally [123]. Very recently, an experiment demonstrating quantum state transmission of an incident squeezed vacuum field through EIT medium was carried out [1].

1.4 Entanglement Generation in Atomic Ensembles

In the following, we study several applications of the quantum state mapping technique described in the previous section, when used in conjunction with methods for generating entangled states of light and atoms. In particular, Raman scattering is used to create entangled states of light in a frequency-shifted Stokes mode, with a collective excitation of the atomic spin. These atom-photon entangled states can be mapped onto atom-atom entangled states upon mapping of the photonic (Stokes) part of the state onto atoms. As we demonstrate, the atomic entanglement thus generated is of the spin-squeezing type. This process is very efficient at generating large amounts of squeezing in atomic ensembles [3]. Conversely, these same atom-photon entangled states can be mapped to correlated photon states. Upon mapping the atomic part of the state to photons, correlated Stokes/anti-Stokes photon pairs are

generated where the number of photons in the two channels are quantum-mechanically correlated. We describe this process theoretically and review our experiments on the generation of correlated photon pairs, and conditional photon Fock state generation [159, 52]. Another aspect of the strong atom-photon coupling associated with EIT is that the propagation properties of light pulses can be very efficiently manipulated and controlled. Further developments of these ideas [6] led to the idea of "stationary light pulses" [15], in which a spatial modulation of the properties of the atomic medium is used to give rise to a vanishing group velocity for light pulses, while at the same time preserving the electromagnetic character of the excitation. This greatly enhances the interaction time of photons with atoms, enabling us to engineer effective photon-photon interactions (quantum nonlinear optics).

Chapter 2

Spin squeezing and Heisenberg-limited spectroscopy

2.1 Motivation

Interacting quantum systems that start in uncorrelated states generally evolve towards entangled states due to quantum correlations building up in time. These correlations and the form they take depend crucially on the interaction that gives rise to them. For example in parametric down conversion or in the optical parametric oscillator (OPO) pairs of photons can be created in distinct modes of the electromagnetic field. The fact that *pairs* of photons are generated leads to quantum correlations between the two modes. Since each mode is described by a harmonic oscillator, one can think of the state of the field as the quantum state of two fictitious particles in harmonic oscillator potentials. The quantum correlations correspond to e.g. the positions of the particles being strongly correlated, in the ideal case $\Delta(X_1 - X_2)^2 \to 0$ and

their momenta being anticorrelated $\Delta(P_1 + P_2)^2 \to 0$. For the electromagnetic field modes, the position and momenta correspond to quadratures of the field modes and it is between these that correlations are produced [89, 162]. These correlations are essential to quantum communication e.g. quantum teleportation of information from one location to another [115, 125]. Entanglement is also crucial for many schemes in quantum cryptography and for long-distance quantum communication through lossy channels [48].

Since the mechanism for producing correlations in electromagnetic field modes is conceptually simple (photons created in pairs) it is natural to wonder if such a mechanism may lead to entanglement of atoms when they are interacting in a similar manner. In complete analogy to the OPA mechanism, a process that transfers *pairs* of atoms from their ground state to two well defined final states also gives rise to quantum correlations between atoms. When a collection of N two level atoms is thought of as an ensemble of effective spin $\frac{1}{2}$ particles with total pseudo-angular momentum $J = N/2$, it turns out [91] that the quantum correlations produced by an interaction that transfers atoms in pairs from the lower state to the upper state show up as reduced fluctuations in a component of the angular momentum e.g. $\Delta J_x^2 \to 0$.

The possibility of coherently controlling interacting quantum systems has lead to many new developments in the field of quantum information science [28]. These are expected to have an impact in a broad area ranging from quantum computation and quantum communication [122] to precision measurements [165, 164, 25, 80, 119] and controlled modeling of complex quantum phenomena [143]. Entangled systems realized in the laboratory range in size from few qbits [144], to macroscopic ensemble

of particles [85]. Controllable coherent interactions between atoms [156, 120] may also open the way for modelling of complex quantum phenomena such as quantum phase transitions [143] in which quantum correlations play a crucial role.

Entanglement of a single atomic ensemble, i.e. quantum correlations between atoms in the same ensemble, has been shown to be potentially very useful in the field of precision measurements [165, 164, 25]. Certain types of interactions between atoms lead to entanglement and spin squeezing, characterized by reduced variance in an observable and increased fluctuations in the canonically conjugate observable. This reduction of fluctuations directly translates into an improved accuracy for measurements sensitive to that observable. A typical figure of merit for spin squeezed states is the phase accuracy $\delta\phi$ on estimating accumulated dynamical phase in the Ramsey interferometric experiment. With all experimental uncertainties controlled below this noise level, the dominant source of noise in such experiments is the "quantum projection noise" [81] associated with e.g. the noise in measurements of the x-component of the spin of an ensemble of two-level atoms (effective spin $\frac{1}{2}$) all prepared in the lower level (the $|\downarrow\rangle$ state). This noise leads to a lower limit on phase accuracy $\delta\phi = 1/\sqrt{N}$ called the standard quantum limit (SQL), where N is the number of atoms in the ensemble. The Heisenberg uncertainty principle however allows for phase accuracies consistent with the basic principles of quantum mechanics that are as low as $\delta\phi = 1/N$, called the Heisenberg limit.

2.2 Overview

In this chapter, we will discuss entanglement of atoms with one another in an atomic ensemble for which an effective interaction leads to the transfer of atoms in pairs to well defined final states and we will use the concept of spin squeezing to quantify the amount of quantum correlations produced in such a case. As for squeezed states of light, decoherence mechanisms and dissipation are acting in such a way as to destroy or limit the amount of squeezing achievable in practice. We also analyze the influence of such dissipation mechanisms and find relations between the spin squeezing interaction rate, the dissipation rate and the amount of squeezing achievable in the presence of damping mechanisms. The coherent control of the dynamical evolution of complex systems such as atomic ensembles may lead to the production of entangled non-classical states such as spin squeezed states [91] (analogous to squeezed states of light [162]) and correlated collective atomic modes (similar to twin photons generated by a non-degenerate OPO).

The main result of this chapter is that for a collection of N atoms with average single atom nonlinearity χ (two atom interaction rate) and with single atom loss rate Γ, the condition for achieving some spin squeezing is that $N\chi \gtrsim \Gamma$. In order to achieve reduction of uncertainty in say J_x (see Appendix A.1 for a definition of the operators $J_{x,y,z}$ for N two-level atoms) compared to the uncertainty in the Bloch state $|J = N/2, J_z = N/2\rangle$ for which $(\Delta J_x)^2 = N/4$ by an amount s (i.e. $(\Delta J_x)^2 = N/(4s)$) with $1 \leq s \leq N$, one requires that $N\chi \gtrsim s\Gamma$ and the interaction time needed scales as $t \sim (\log s)/(N\chi)$ while the maximum number of atoms than can be lost without destroying the squeezing scales as $\Delta N \sim (N/s)\log s$. To achieve Heisenberg limited

precision (i.e. maximum spin squeezing $s \sim N$), one needs a large single atom nonlinearity $\chi \gtrsim \Gamma$. This means that the interaction time needed to achieve this strongly correlated state is $t \sim (\log N)/(N\chi)$ and the maximum number of atoms that can be lost without compromising this optimal squeezing is $\Delta N \sim \log N$ i.e. a very small number of atoms lost may prevent reaching the Heisenberg limit. This analysis remains valid and agrees with a specific implementation based on an effective atom-atom interaction via quantized photon exchange in a cavity, for which the decoherence mechanism corresponds to spontaneous emission and leakage of photons from the cavity.

We also discuss in more detail a technique [3] based on a resonantly enhanced nonlinear process involving Raman scattering into a "slow" optical mode [74, 87, 35], which creates a pair of spin-flipped atom and slowly propagating coupled excitation of light and matter (dark-state polariton). When the group velocity of the polariton is reduced to zero [103, 128, 109, 56], this results in pairs of spin flipped atoms. The dark-state polariton can be easily converted into corresponding states of photon wavepackets "on demand" [109, 56], which makes the present approach most suitable for implementing protocols in quantum information processing that require a combination of deterministic sources of entangled states and long-lived quantum memory [48, 38, 160].

This chapter is divided into five sections. In Section 2.3, we discuss Ramsey spectroscopy and the use of spin-squeezed states in precision measurements. In particular we analyze the situation where N two level atoms with levels $|g\rangle$ and $|e\rangle$ are prepared in a correlated state and subsequently probed by separated fields of frequency ω in

the Ramsey interferometric configuration, which we review in Appendix A.1. We also discuss spin-squeezed states and develop pictorial representation of those states which we compare to squeezed states of light and in appendix A.2 we introduce the Wigner representation for a particular class of spin squezed states.

In Section 2.4, we analyze a model for spin squeezing based on the analogy with the optical parametric oscillator. We also seek to understand the influence of loss processes on the coherent spin-squeezing interaction and the way in which it limits the correlations achievable for a given interaction rate. The model consists of two bosonic modes (a "spin up" state and a "spin down" state) with loss rates and a coherent interaction that transfers pairs of atoms from one mode to the other. For our simple model, analytical results can be obtained in the perturbative regime of small number of excitations (most atoms in the lower state) and low loss rate. We estimate the conditions for which Heisenberg-limited spin squeezed states can be produced.

In Section 2.5, we present a scheme for inducing effective coherent interactions between atoms in an atomic ensemble. These coherent interactions lead to massive entanglement of the ensemble and to characterize the degree of entanglement thus obtained, we calculate the squeezing or reduction in fluctuations of one particular observable. The coherent interaction is based on Raman scattering into a cavity mode for which the atomic medium is made transparent by Electromagnetically Induced Transparency (EIT). The slowly propagating mode is then best described by a polariton: a collective excitation that is partly photonic and partly "spin" excitation of the atomic ensemble (the up and down states of the spin being two metastable

states). The overall process leads to the creation of pairs of excitations, one being a "spin flip" created by Raman scattering, the other being a polariton which can be "steered" into a photon or spin flip excitation "on demand". We find that substantial spin squeezing can be obtained for atomic ensembles in low finesse cavities, without the strong coupling requirement of cavity QED. In the limit of unity finesse this corresponds to free-space configuration and substantial correlations can still be produced in this case. In the opposite limit of high finesse, very strong correlations are obtained and in particular we estimate the regime for which Heisenberg limited spin-squeezed states are produced.

2.3 Ramsey Spectroscopy with Correlated Atoms

In appendix A.1, Ramsey spectroscopy is reviewed and in particular we show how the phase accuracy in phase estimation based on the Ramsey fringe signal is, at the maximum sensitivity point, given by

$$\delta\phi = \frac{\Delta J_x}{|\langle \hat{J}_z \rangle|} \tag{2.1}$$

where ΔJ_x is the variance in the x-component of the pseudo angular momentum (of length $J = N/2$) representing the state of N two-level atoms and $\langle \hat{J}_z \rangle$ is the expectation value of the z-component of the pseudo angular momentum (both the variance and the expectation value are calculated in the initial state).

For an uncorrelated state of atoms e.g. with all atoms in their lower state so that the state of the ensemble is described by $|J_z = -N/2\rangle$, it is found that $\Delta J_x = \sqrt{J/2}$ and $\langle \hat{J}_z \rangle = -J$ so that $\delta\phi = \sqrt{1/N}$. In order to improve the phase accuracy, one must

use a state for which the variance in $\hat{J}_x$ is reduced while $\langle \hat{J}_z \rangle$ is little changed. Consider therefore a state such as an eigenstate of $\hat{J}_x$, for example $|J_x = 0\rangle$. Calculating the expectation values and variances we find $\langle \hat{J}_x \rangle = \langle \hat{J}_y \rangle = \langle \hat{J}_z \rangle = 0$, $\Delta J_x = 0$ and $\Delta J_y = \Delta J_z = \sqrt{J(J+1)/2}$. However the Ramsey signal has amplitude proportional to $\langle J_z \rangle$ and therefore vanishes for all phase angles ϕ, which means that even though the noise or fluctuation properties of the signal may be improved, its average is zero. Note that this is because we have chosen $\hat{J}_z(\phi)$ as our observable, other observables such as $\hat{J}_z^2(\phi)$ for example may lead to non-zero average signal together with reduced variance [29, 88]. However, it turns out their signal to noise ratio is very much reduced compared to that of the Ramsey scheme [88]. It is thus necessary to consider states that lead to a reduced variance ΔJ_x while maintaining a large signal amplitude, i.e. a large $\langle \hat{J}_z \rangle$. We therefore consider states such as

$$|\psi(a)\rangle = \frac{1}{\sqrt{1+a^2}}(i|J_x = 0\rangle + a\frac{|J_x = +1\rangle - |J_x = -1\rangle}{\sqrt{2}}) \tag{2.2}$$

where a is a real number parametrizing the state $|\psi(a)\rangle$. It is straightforward to calculate the expectation values

$$\begin{aligned} \langle \hat{J}_x \rangle &= 0 \\ \langle \hat{J}_y \rangle &= 0 \\ \langle \hat{J}_z \rangle &= \frac{2a}{1+a^2}\sqrt{\frac{J(J+1)}{2}} \end{aligned} \tag{2.3}$$

and

$$\langle \hat{J}_x^2 \rangle = \frac{a^2}{1+a^2} \tag{2.4}$$

$$\langle \hat{J}_y^2 \rangle = \frac{1}{1+a^2}\frac{J(J+1)}{2} \tag{2.5}$$

$$\langle \hat{J}_z^2 \rangle = \frac{1/2}{1+a^2}\left\{J(J+1) + a^2\left[J(J+1) + \frac{(J-1)(J+2)}{2}\right]\right\} \tag{2.6}$$

and the variances

$$\begin{aligned} \Delta J_x &= \frac{a}{\sqrt{1+a^2}} \\ \Delta J_y &= \frac{1}{\sqrt{1+a^2}}\sqrt{\frac{J(J+1)}{2}} \\ \Delta J_z &= \sqrt{\frac{J(J+1)}{2}}\left[1 - \frac{4a^2}{(1+a^2)^2}\right]^{1/2}. \end{aligned} \tag{2.7}$$

The signal amplitude which depends on $\langle \hat{J}_z \rangle$ can thus be rather large ($O[N]$) while the noise amplitude characterized by ΔJ_x is minimized ($O[1]$). The Ramsey signal and phase accuracy for such a state is shown in Fig. 2.1, compared to the case of uncorrelated atoms (Fig. 2.1).

These states are minimum uncertainty states i.e. $(\Delta J_x)(\Delta J_y) = \frac{1}{2}|\langle \hat{J}_z \rangle|$ for all values of the parameter a. Also, their phase accuracy is given by

$$\delta\phi(\pm\pi/2) = \sqrt{\frac{1+a^2}{2}}\frac{1}{\sqrt{J(J+1)}} \tag{2.8}$$

which is of order $1/N$. The best phase accuracy is obtained for $a \to 0$ in which case the optimal phase accuracy is $\delta\phi(\pm\pi/2) = \sqrt{2}/N$. Note that in this case the signal amplitude ($\propto \langle \hat{J}_z \rangle$) becomes vanishingly small ($\langle \hat{J}_z(\phi) \rangle \to 0$ for all ϕ) and also the range of values of ϕ for which improved phase accuracy is achieved becomes vanishingly small around $\phi = \pm\pi/2$. For these reasons, the optimally spin squeezed

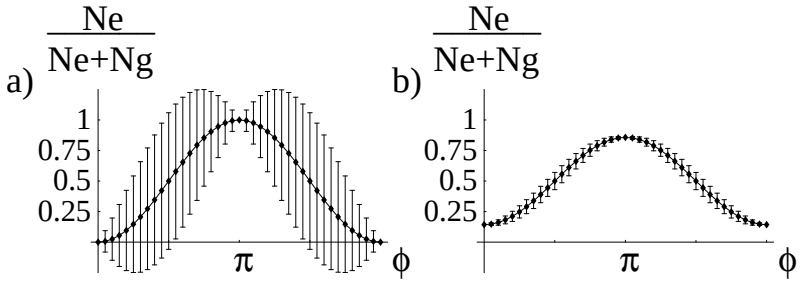

Figure 2.1: Number of atoms detected in the upper state (N_e) relative to total number of atoms (the total number is $N = N_e + N_g$ and thus $N_e/(N_e + N_g) = (N/2 + \langle J_z(\phi)\rangle)/N$) vs. accumulated phase $\phi = (\omega - \omega_0)T$ for a) uncorrelated atoms and b) correlated atoms in a spin-squeezed state $|\psi(a)\rangle$, for $N = 100$ and $a = -1$ (error bars have been magnified by a factor of 10 for clarity). Note how squeezing of the variance improves the phase accuracy.

state $|\psi(a = 0)\rangle$ may prove impractical. Note however that for finite a i.e. for $|a| = 1$, the signal amplitude is large ($\sim N/\sqrt{8}$) and the phase accuracy is independent of ϕ

$$\delta\phi(\phi) = \frac{1}{\sqrt{J(J+1)}} \simeq \frac{2}{N} \tag{2.9}$$

i.e. twice the Heisenberg limit.

In Fig. 2.2 we show the signal and variance for various spin squeezed states along with the phase accuracy $\delta\phi(\phi)$.

We can gain a better understanding of the squeezing in the states (2.2) $|\psi(a)\rangle$ by looking at various representations of them. The simplest representation is to project the state onto eigenstates of the three components of the angular momentum

$$P_i(m) = |\langle J_i = m|\psi(a)\rangle|^2 \tag{2.10}$$

where $|J_i = m\rangle$ is the eigenstate of the i-component of angular momentum with eigenvalue m.

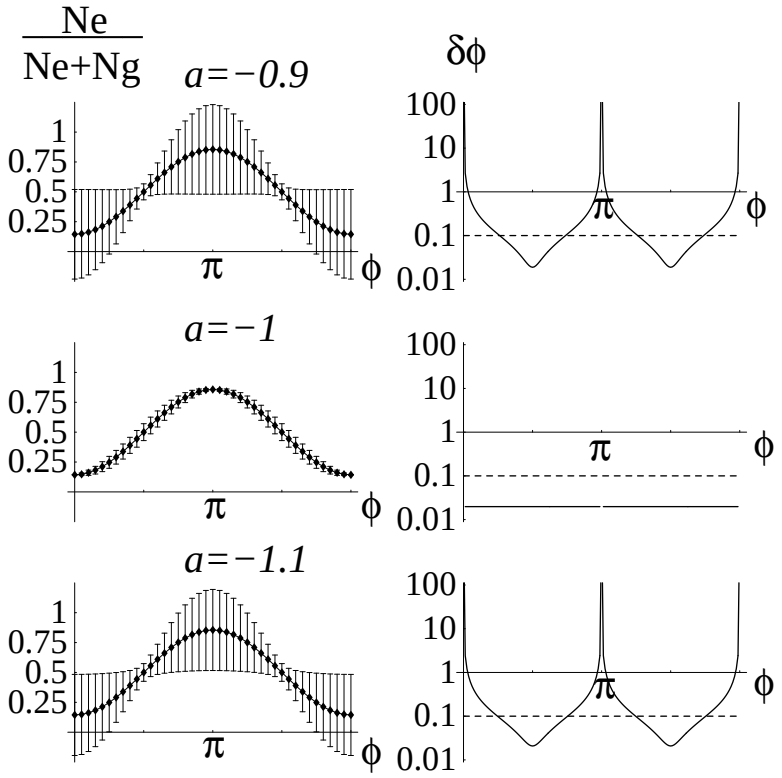

Figure 2.2: Number of atoms detected in the upper state vs. accumulated phase $\phi = (\omega - \omega_0)T$ for correlated atoms in various spin-squeezed states $|\psi(a)\rangle$, for $N = 100$ and $a = -0.9$, $a = -1$ and $a = -1.1$ (error bars have been magnified by a factor of 10 for clarity). Also shown is the phase accuracy $\delta\phi(\phi)$ vs. accumulated phase (the dashed line represents the standard quantum limit $\delta\phi = 1/\sqrt{N}$). Note how $\delta\phi(\phi)$ gets to a minimum value of order $2/N = 0.02$.

From Fig. 2.3 it is clear that the expectation value of $\hat{J}_x$ and $\hat{J}_y$ are zero in such a state, whereas (for $a = -1$) the expectation value of $\hat{J}_z$ is large and negative, the variances are clearly given by (2.7). It is interesting to note the similarity of these angular momentum squeezed states and those of a harmonic oscillator (i.e. squeezed states of light). In both cases, the probability distributions vanish for odd number of quanta (note that for simplicity we consider only N even here). For even number of quanta, the behaviour is nearly exponential $P_z(m) \propto e^{-c(m+j)}$ for some constant c. A

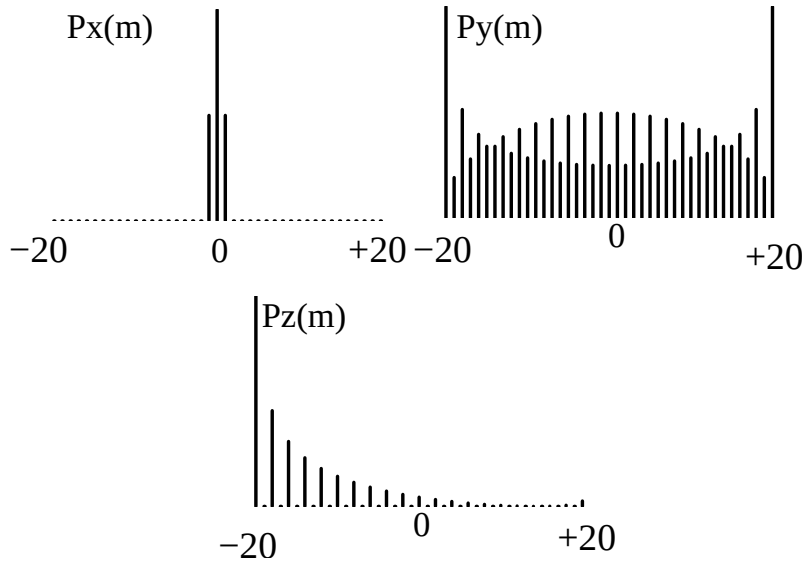

Figure 2.3: Projection of the state $|\psi(a)\rangle$ onto eigenstates of the angular momentum operators $\hat{J}_x$, $\hat{J}_y$ and $\hat{J}_z$ for $J = N/2 = 20$ and $a = -1$. The $P_x(m)$ distribution is sharply peaked since the state $|\psi(a)\rangle$ is a superposition of the $m_x = -1, 0, +1$ components only; the $P_y(m)$ distribution is broad and symmetric; the $P_z(m)$ distribution vanishes for m odd and the even components decrease roughly exponentially with m.

mechanism for generating such states starting from the uncorrelated state $|J_z = -J\rangle$ must therefore be one in which atoms are excited in pairs, i.e. two atoms in the ground state are transferred to the excited state $|g\rangle|g\rangle \rightarrow |e\rangle|e\rangle$. Consider the similarities with squeezed states of light: in particular the photon number distribution vanishes for odd photon number in the case of squeezed vacuum due to the form of the squeezing Hamiltonian $\hat{H} = -i\chi[\hat{a}^{\dagger 2} - \hat{a}^2]$, which creates and destroys photons in pairs. Since we find a similar cancellation of the probability of there being odd number of excitations for the states $|\psi(a)\rangle$, the interaction giving rise to such states starting from all atoms in their lower states must likewise create and destroy excitations in pairs and thus be of the form $\hat{H} = -i\hbar\chi[\hat{L}_+^2 - \hat{L}_-^2]$. This process can also be viewed as a coherent collision mechanism. Moreover, for the whole atomic ensemble to become entangled

(not just particular atom pairs), this process must occur completely symmetrically for all atoms. It should not be two particular atoms that get transferred to the excited state, rather it should be two collective excitations that get created

$$|g_1 \cdots g_N\rangle \;\; \rightarrow \;\; \sqrt{\frac{2}{N(N-1)}} \sum_{i>j} [|g \cdots e_i \cdots e_j \cdots g\rangle] \tag{2.11}$$

which is the state obtained by letting $\hat{J}_+^2$ operate on $|J_z = -J\rangle$. The simplest Hamiltonian giving rise to this type of interaction is analyzed in section 2.4 to quantify the squeezing generated by this mechanism. This form of interaction was considered by Kitegawa and Ueda [91] in their classic study of spin squeezing and was dubbed the "two axis countertwisting" interaction.

2.4 Two Axis Counter-twisting Model

We now turn to the analysis of the two axis countertwisting Hamiltonian [91]

$$\begin{aligned} \hat{H} &= -i\frac{\hbar\chi}{2}\left(\hat{L}_+^2 - \hat{L}_-^2\right) \\ &= \hbar\chi\left(\hat{L}_x\hat{L}_y + \hat{L}_y\hat{L}_x\right). \end{aligned} \tag{2.12}$$

As argued in last section it is this type of Hamiltonian that most closely parallels squeezed state generation for light.

We now present a general theory that allows to quantify atom correlations and takes into account decoherence and finite system size. Specifically, we consider two bosonic modes (such as for a two component Bose-Einstein condensate or for an

atomic ensemble with two relevant atomic levels) with annihilation operators $\hat{a}_1$ and $\hat{a}_2$. The system is also subject to damping i.e. loss of atoms at rates which may depend on the internal state. The equations of motion for the two modes are then (with $\hat{L}_+ = \hat{a}_2^\dagger \hat{a}_1$ and $\hat{L}_- = \hat{a}_1^\dagger \hat{a}_2$)

$$\begin{aligned} \dot{\hat{a}}_1 &= -\gamma_1 \hat{a}_1 + \chi \hat{a}_1^\dagger \hat{a}_2^2 + \hat{F}_1(t) \\ \dot{\hat{a}}_2 &= -\gamma_2 \hat{a}_2 - \chi \hat{a}_2^\dagger \hat{a}_1^2 + \hat{F}_2(t) \end{aligned} \tag{2.13}$$

where $\hat{F}_j(t)$ are delta-correlated Langevin noise forces with appropriate diffusion coefficients $D_{ij} = \langle \hat{F}_i(t) \hat{F}_j(t) \rangle$.

In order to discuss spin squeezing, it is easier to rewrite the equations of motion in terms of the Stokes parameters

$$\begin{aligned} \hat{L}_0 &= \hat{N} = \hat{a}_1^\dagger \hat{a}_1 + \hat{a}_2^\dagger \hat{a}_2 \\ \hat{L}_x &= (\hat{a}_2^\dagger \hat{a}_1 + \hat{a}_1^\dagger \hat{a}_2)/2 \\ \hat{L}_y &= (\hat{a}_2^\dagger \hat{a}_1 - \hat{a}_1^\dagger \hat{a}_2)/2i \\ \hat{L}_z &= (\hat{a}_2^\dagger \hat{a}_2 - \hat{a}_1^\dagger \hat{a}_1)/2 \end{aligned} \tag{2.14}$$

for which the equations are

$$\begin{aligned} \dot{\hat{L}}_0 &= -2\Gamma \hat{L}_0 + 4\gamma \hat{L}_z + \hat{F}_0(t) \\ \dot{\hat{L}}_x &= -2\Gamma \hat{L}_x + \chi(\hat{L}_x \hat{L}_z + \hat{L}_z \hat{L}_x) + \hat{F}_x(t) \\ \dot{\hat{L}}_y &= -2\Gamma \hat{L}_y - \chi(\hat{L}_y \hat{L}_z + \hat{L}_z \hat{L}_y) + \hat{F}_y(t) \\ \dot{\hat{L}}_z &= -2\Gamma \hat{L}_z + \gamma \hat{L}_0 - 2\chi(\hat{L}_x^2 - \hat{L}_y^2) + \hat{F}_z(t) \end{aligned} \tag{2.15}$$

where $\Gamma = (\gamma_1 + \gamma_2)/2$, $\gamma = (\gamma_1 - \gamma_2)/2$ and $\hat{F}_j(t)$ are new delta-correlated noise forces associated with the damping.

Since (2.15) are non-linear operator equations, in the equations of motion for the first order moments $\langle \hat{L}_i \rangle$ there are terms that depend on those first order moments but also terms depending on the second order moments $\langle \hat{L}_i \hat{L}_j \rangle$. Similarly the equations of motion for the second order moments depend on themselves and also on the third order moments, and so on, leading to the BBGKY hierarchy of equations of motion for the expectation values of operator products. In order to solve this set of equations, the hierarchy must be truncated at some order [8]. Keeping the first and second order moments, we truncate the BBGKY hierarchy by the approximation

$$\begin{aligned} \langle \hat{L}_i \hat{L}_j \hat{L}_k \rangle &\approx \langle \hat{L}_i \hat{L}_j \rangle \langle \hat{L}_k \rangle + \langle \hat{L}_j \hat{L}_k \rangle \langle \hat{L}_i \rangle + \langle \hat{L}_k \hat{L}_i \rangle \langle \hat{L}_j \rangle \\ &- 2 \langle \hat{L}_i \rangle \langle \hat{L}_j \rangle \langle \hat{L}_k \rangle. \end{aligned} \tag{2.16}$$

The equations of motion for the expectation values $l_i \equiv \langle \hat{L}_i \rangle$ and the second order moments $\Delta_{ij} \equiv \langle \hat{L}_i \hat{L}_j + \hat{L}_j \hat{L}_i \rangle - 2 \langle \hat{L}_i \rangle \langle \hat{L}_j \rangle$ are then obtained from (2.15). We are interested in the case when all atoms start in mode 1, i.e. $l_0(0) = N, l_x(0) = l_y(0) = 0, l_z(0) = -N/2$ and $\Delta_{xx}(0) = \Delta_{yy}(0) = N/2$ (all other second moments vanish) and for simplicity we take $\gamma_1 = \gamma_2 = \Gamma$, $\gamma = 0$. Writing only the relevant equations and omitting vanishing terms (such as those proportional to Δ_{xz} and Δ_{yz} which are zero for all times), we have (after some algebra)

$$\begin{aligned}
\dot{l}_0 &= -2\Gamma l_0 \\
\dot{l}_z &= -2\Gamma l_z - \chi(\Delta_{xx} - \Delta_{yy}) \\
\dot{\Delta}_{xx} &= -4\Gamma\Delta_{xx} + \Gamma l_0 + 4\chi l_z \Delta_{xx} \\
\dot{\Delta}_{yy} &= -4\Gamma\Delta_{yy} + \Gamma l_0 - 4\chi l_z \Delta_{yy}
\end{aligned} \tag{2.17}$$

and $l_x(t) = l_y(t) = 0$. These equations are non-linear and cannot be solved analytically nor perturbatively in Γ/χ. For short enough times, the number of excitations into mode 2 is small and $l_z \simeq -N/2$, so that plugging this in (2.17) we have

$$\begin{aligned}
\Delta_{xx}(t) &\simeq \frac{N}{2} e^{-2N\chi t} + O[\Gamma/\chi] \\
\Delta_{yy}(t) &\simeq \frac{N}{2} e^{2N\chi t} + O[\Gamma/\chi]
\end{aligned} \tag{2.18}$$

i.e. the variance of the x-component of the pseudo-angular momentum is squeezed while that of the y-component is anti-squeezed. Plugging these back in the equation of motion of l_z, we obtain $l_z(t) \simeq -N/2 + (\cosh 2N\chi t - 1)/2 + O[\Gamma/\chi]$. This equation predicts growth of l_z without bound, however we know that because l_z is the z-component of an angular momentum vector, we must have $|l_z| \leq N/2$. The phase space of this angular momentum vector is the Bloch sphere and in essence we have neglected the small curvature of the Bloch sphere (of radius $R = N/2$) and have approximated the phase space by the flat planar phase space of a harmonic oscillator. We call this approximation the bosonic approximation, since it predicts infinite squeezing in the long time limit and in the absence of dissipation, similar to the case of squeezed light. Formally this is equivalent to assuming

$$\begin{aligned}[\hat{a}_2^\dagger \hat{a}_1, \hat{a}_1^\dagger \hat{a}_2] &= \hat{a}_2^\dagger \hat{a}_2 - \hat{a}_1^\dagger \hat{a}_1 \\ &\simeq -N \end{aligned} \tag{2.19}$$

i.e. the operator $\hat{S}_+ = \hat{a}_2^\dagger \hat{a}_1/\sqrt{N}$ obeys bosonic commutation relations. Under this approximation the Hamiltonian (2.12) becomes $\hat{H} = -i(\hbar\chi N/2)(\hat{S}_+^2 - \hat{S}_-^2)$ which is identical to the Hamiltonian describing squeezing of light [162].

In order to take into account the curvature of phase space and the non-bosonic nature of the angular momentum operators, we use the following transformation

$$\begin{aligned}\hat{N} &= N\hat{h}_0 \\ \hat{L}_x &= \sqrt{N}\hat{h}_x \\ \hat{L}_y &= \sqrt{N}\hat{h}_y \\ \hat{L}_z &= \hat{h}_z - \frac{N}{2}\hat{h}_0 \end{aligned} \tag{2.20}$$

in terms of which the commutation relations become

$$\begin{aligned}\left[\hat{h}_{x,y,z}, \hat{h}_0\right] &= 0 \\ \left[\hat{h}_z, \hat{h}_\pm\right] &= \pm\hat{h}_\pm \\ \left[\hat{h}_+, \hat{h}_-\right] &= 2\frac{\hat{h}_z}{N} - \hat{h}_0 \end{aligned} \tag{2.21}$$

where $\hat{h}_\pm = \hat{h}_x \pm i\hat{h}_y$. In the limit $N \to \infty$ these commutation relations become those of bosonic operators i.e. $\lim_{N\to\infty}[\hat{h}_0, \hat{h}_z, \hat{h}_+, \hat{h}_-] = [\hat{1}, \hat{a}^\dagger\hat{a}, \hat{a}^\dagger, \hat{a}]$, a process for-

mally known as a group contraction [9]. The linear transformation of operators (2.20) does not introduce any extra approximation.

The Hamiltonian (2.12) can be re-expressed as

$$\begin{aligned} \hat{H} &= \hbar\chi N\left(\hat{h}_x\hat{h}_y + \hat{h}_y\hat{h}_x\right) \\ &= -i\frac{\hbar\xi}{2}\left(\hat{h}_+^2 - \hat{h}_-^2\right) \end{aligned} \tag{2.22}$$

where we have defined $\xi = \chi N$. We can now obtain equations of motion for the expectation values $h_j = \langle\hat{h}_j\rangle$ and the second order moments $\delta_{ij} = \langle\hat{h}_i\hat{h}_j\rangle - 2\langle\hat{h}_i\rangle\langle\hat{h}_j\rangle$ from (2.17). Letting $\tau = N\chi t = \xi t$ be a rescaled time, $\kappa = \Gamma/(N\chi) = \Gamma/\xi$ be the rescaled dissipation rate and writing $\epsilon = 1/N$ and $\dot{x} = \mathrm{d}x/\mathrm{d}\tau$, we have

$$\begin{aligned} \dot{h}_0 &= -2\kappa h_0 \\ \dot{h}_z &= -2\kappa h_z - (\delta_{xx} - \delta_{yy}) \\ \dot{\delta}_{xx} &= -4\kappa\delta_{xx} + \kappa h_0 - 2h_0\delta_{xx} + 4\epsilon h_z\delta_{xx} \\ \dot{\delta}_{yy} &= -4\kappa\delta_{yy} + \kappa h_0 + 2h_0\delta_{yy} - 4\epsilon h_z\delta_{yy}. \end{aligned} \tag{2.23}$$

Note that these equations are formally equivalent to (2.17), no approximation has been made from (2.17) to (2.23). Letting $\epsilon \to 0$ reproduces the results of the bosonic approximation obtained above in the limit of $l_z \simeq -N/2$. Terms of order ϵ and higher represent corrections to the bosonic approximation and, as shown below, they give rise to a limit to the amount of squeezing achievable.

Solving (2.23) to first order in ϵ and κ we obtain, writing only the relevant terms,

$$\delta_{xx}(\tau) \;=\; \frac{1}{2}\left[e^{-2\tau} + (\kappa + \epsilon/2) + \cdots\right] \tag{2.24}$$

which shows that the variance $\Delta J_x = \sqrt{(N/2)\delta_{xx}}$ is squeezed. Second order terms in κ and ϵ come multiplied by an exponentially growing term $e^{2\tau}$ so that as a function of time, the variance reaches a minimum value $\delta_{xx} \sim \max[\kappa, \epsilon]$ at a time $e^{-\tau_*} \sim \max[\kappa, \epsilon]$, after which it grows exponentially and the squeezing is lost. Note that this behaviour ($\delta_{xx}(t)$ reaches a minimum value and then increases again) also occurs when $\kappa \to 0$, indicating that it is a generic feature of the finite system size. This model predicts that a variance $\delta_{xx} \sim \epsilon = 1/N \to \Delta J_x^2 \sim 1$ is achievable as long as losses are small enough, i.e. $\kappa \lesssim \epsilon$, which in terms of χ and Γ means

$$\chi \gtrsim \Gamma \quad \text{or} \quad \xi \gtrsim N\Gamma \tag{2.25}$$

where χ corresponds to the single-atom nonlinear interaction rate and Γ represents the single-atom loss rate.

In order to achieve any squeezing ($\delta_{xx} \leq 1/2$) it is necessary to have $\kappa \lesssim 1$ i.e. $N\chi \gtrsim \Gamma$. In the regime $N\chi \gg \Gamma$ very strong correlations can be obtained. Note that the single-atom nonlinearity can still be relatively weak compared to the single particle loss rate ($\chi \ll \Gamma$). For example when the dissipation rate is such that $\kappa \sim \sqrt{\epsilon}$ i.e. $\sqrt{N}\chi \sim \Gamma$, the amount of squeezing obtained (2.24) is $\delta_{xx} \sim 1/\sqrt{N}$. It takes a time $e^{-2\tau} \sim \sqrt{\epsilon}$ to reach this state and the number of particles lost during that time is $\Delta N \sim N \times 2\kappa\tau \sim \sqrt{N}\log N$. This number can therefore also be thought of as the maximum number of particles that can be lost from the ensemble without destroying squeezing beyond $\delta_{xx} \sim 1/\sqrt{N}$.

In order to reach the Heisenberg limit it is required that the single atom nonlinearity χ be larger than the decay rate Γ. Note that in this case, the number of atoms lost by the time optimal squeezing is achieved is $\Delta N \sim \log N$ which indicates that a very small number of atoms is lost. This number also corresponds to the maximum number of particles that can be lost from the ensemble and not destroy squeezing at the Heisenberg limit level. Clearly the more squeezed the state of the atoms is, the more sensitive it becomes to atom loss and in general to any form of dissipation.

2.5 Coherent Atom Interactions via Slow Light

We now describe a technique to induce effective coherent interactions between atoms in metastable states [3]. The technique is based on a resonantly enhanced nonlinear process involving Raman scattering into a "slow" optical mode [74, 87, 35], which creates a pair of spin-flipped atoms and a slowly propagating coupled excitation of light and matter (dark-state polariton). When the group velocity of the polariton is reduced to zero [103, 128, 109, 56], this results in pairs of spin flipped atoms. The fact that pairs of atomic excitations are created in this process can also be viewed as a coherent interaction between atoms, i.e. a controlled "collision" leading to entanglement of the state of each atom with that of every other atom in the ensemble.

A number of proposals have been made for generating entangled states of atomic ensembles and resulting in so-called spin squeezed states. Some are based on interatomic interactions at ultra-cold temperatures [49, 141], whereas others involve mapping the states of non-classical light fields into atoms [98, 66], QND measure-

ments of spins [99] with light or dipole blockade for Rydberg atoms [26]. Also note the recent experiments on number-phase squeezed states and the Mott insulator phase in BEC [124, 64]. In contrast to some of these mechanisms the present approach does not require coherence of the atomic motion or sources of non-classical light and is completely deterministic thereby significantly simplifying possible experimental realizations. We further show that the present technique can be made robust with respect to realistic decoherence processes such as spontaneous emission and leakage of slow photons from the medium.

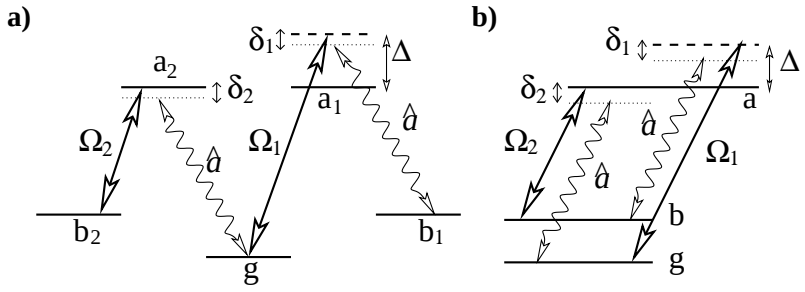

Figure 2.4: Energy levels scheme for the effective coherent interaction leading to creation of pairs of atoms a) in different final states ("non-degenerate" scheme) and b) in identical final states("degenerate" version).

We consider a system of N atoms (Fig. 2.4a) interacting with two classical driving fields $\Omega_{1,2}$ and one quantized mode $\hat{a}$ of a running wave cavity that is initially in a vacuum state. Note that we consider a cavity configuration for ease of theorerical treatment, the results of this analysis however remain valid in the limit of unity finesse, i.e. in free space configuration. Relevant atomic sublevels include two manifolds of metastable states (e.g hyperfine sublevels of electronic ground state) and excited states that may be accessed by optical transitions. The atoms are initially prepared in their ground states $|g\rangle$. One of the classical fields, of Rabi frequency Ω_1, is detuned

from the atomic resonance by an amount roughly equal to the frequency splitting between ground state manifolds. The other field of Rabi frequency Ω_2 is resonant with an atomic transition $|b_2\rangle \rightarrow |a_2\rangle$. The quantized field can be involved in two Raman transitions corresponding to Stokes and anti-Stokes processes. Whereas the former corresponds to the usual Stokes scattering in the forward direction, the latter establishes an Electromagnetically Induced Transparency (EIT) and its group velocity is therefore substantially reduced.

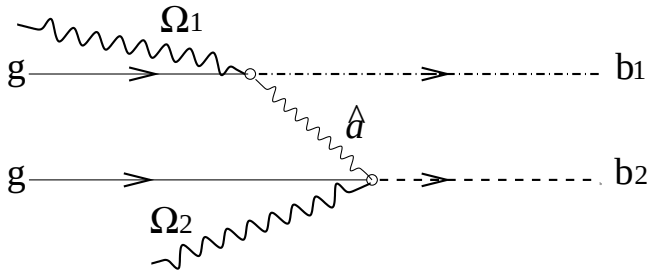

Figure 2.5: Diagram illustrating coherent atom-atom interaction mediated by dark-state polariton, leading to the creation of a pair of spin-flipped atoms.

The pair excitation can be viewed as resulting from quantized photon exchange between atoms (Fig. 2.5) in a two-step process. The first flipped spin is created due to Stokes Raman scattering, which also results in photon emission in a corresponding Stokes mode. In the presence of EIT, this photon is directly converted into a dark-state polariton which becomes purely atomic when the group velocity is reduced to zero. This implies that atomic spins are always flipped in pairs. In Fig. 2.4a the two final states involved in Raman transitions are different and atomic pairs in different states are created. In Fig. 2.4b the final states of the two Raman processes are identical, in which case atomic pairs in the same state result. The analysis of this "degenerate" version of the scheme is similar to the "non-degenerate" case and we

will consider only the latter case here.

For conceptual simplicity we assume that the quantized field corresponds to a single mode of a running-wave cavity with a creation operator $\hat{a}^\dagger$ and atom-field coupling constants g_1 and g_2. The interaction Hamiltonian for the system of N atoms and light can be split into two parts $H = H_{Ram} + H_{res}$ corresponding to the Stokes Raman process and the anti-Stokes process respectively:

$$\begin{aligned} H_{Ram} &= -\hbar\Delta\Sigma_{a1a1} - \hbar\delta_1\Sigma_{b_1b_1} \\ &+ [\hbar\Omega_1\Sigma_{a_1g} + \hbar g_1 a\Sigma_{a_1b_1} + \text{h.c.}], \qquad (2.26) \\ H_{res} &= \hbar\delta_2\Sigma_{b_2b_2} + \hbar\delta_2\Sigma_{a_2a_2} \\ &+ [\hbar g_2 a\Sigma_{a_2g} + \hbar\Omega_2\Sigma_{a_2b_2} + \text{h.c.}], \qquad (2.27) \end{aligned}$$

where $\Sigma_{\mu\nu} = \sum_i |\mu\rangle_{ii}\langle\nu|$ are collective atomic operators corresponding to transitions between atomic states $|\mu\rangle, |\nu\rangle$, Δ is the detuning of the classical field Ω_1 from the single-photon transition $|g\rangle \rightarrow |a_1\rangle$, δ_1 and δ_2 are the two-photon detunings from the $|g\rangle \rightarrow |b_1\rangle$ and $|g\rangle \rightarrow |b_2\rangle$ transitions respectively as shown in Fig. 2.4.

In the limit of large detuning Δ and ignoring two-photon detunings for the moment, the Hamiltonian H_{Ram} describes off-resonant Raman scattering. We take into account realistic decoherence mechanisms such as spontaneous emission from the excited states in all directions and decay of the cavity mode with a rate κ. The evolution of atomic operators is then described by Heisenberg-Langevin equations:

$$\dot{\Sigma}_{\mu\nu} = -\gamma_{\mu\nu}\Sigma_{\mu\nu} + \frac{i}{\hbar}[H, \Sigma_{\mu\nu}] + F_{\mu\nu}, \qquad (2.28)$$

where $\gamma_{\mu\nu}$ is a decay rate of coherence $\mu \rightarrow \nu$ and $F_{\mu\nu}$ are associated noise forces.

The latter have zero average and are δ-correlated with associated diffusion coefficients that can be found using the Einstein relations.

After a canonical transformation corresponding to adiabatic elimination of the excited state (see Appendix A.3 for details), H_{Ram} becomes equivalent to the effective Hamiltonian

$$\tilde{H}_{Ram} = \hbar\chi\hat{a}^\dagger\hat{S}_1^\dagger + \text{h.c.} \tag{2.29}$$

where $\hat{S}_1 = \Sigma_{gb_1}/\sqrt{N}$ and $\chi = g_1\sqrt{N}\Omega_1^*/\Delta$. This effective hamiltonian thus describes the process in which a Stokes photon is emitted necessarily accompanied by a spin flip. The quantum state of the Stokes mode is thus perfectly correlated with the state of the atomic spin flip mode.

The resonant part of the Hamiltonian H_{res} is best analyzed in terms of dark and bright-state polaritons [57]

$$\begin{aligned} P_D &= \frac{\Omega_2 a - g_2\sqrt{N}S_2}{\sqrt{g_2^2N + \Omega_2^2}}, \\ P_B &= \frac{g_2\sqrt{N}a + \Omega_2 S_2}{\sqrt{g_2^2N + \Omega_2^2}}, \end{aligned} \tag{2.30}$$

which are superpositions of photonic and atomic excitations $\hat{a}$ and $S_2 = \Sigma_{gb_2}/\sqrt{N}$.. In particular, H_{res} has an important family of dark-states:

$$|D^n\rangle \sim (P_D^\dagger)^n|g\rangle|\text{vac}\rangle \tag{2.31}$$

with zero eigenenergies. This means that once in the dark state, the system stays in the dark state. Note that all other eigenstates of H_{res} have, in general, non-vanishing interaction energy. Under conditions of Raman resonance and sufficiently slow excitation ("adiabatic condition", see Appendix A.4 for details) the Stokes photons emitted

by Raman scattering, Eq.(2.29), will therefore couple solely to the dark-states (2.31). In this case the coherent part of the evolution of the entire system is described by an effective Hamiltonian:

$$H_{eff} = -i\hbar\xi(P_D^\dagger S_1^\dagger - S_1 P_D), \tag{2.32}$$

with $\xi = \Omega_1\Omega_2/\Delta \times g_1\sqrt{N}/\sqrt{g_2^2 N + \Omega_2^2}$ (without loss of generality, ξ was chosen imaginary here for simplified calculations). The Hamiltonian (2.32) describes the coherent process of generation of pairs of excitations involving polaritons and spin-flipped atoms. Note that for small number of excitations the spin waves and polaritons obey bosonic commutation relations and this Hamiltonian is formally equivalent to that describing optical parametric amplification (OPA) of two modes [162]. In the non-bosonic limit, this Hamiltonian is also analogous to the "counter-twisting" model of (2.12). In appendix A.4 we show that the coupled equations for the polariton P_D and the spin flip S_1 are given by

$$\dot{S}_1^\dagger = (\frac{|g_1|^2}{|g_2|^2}\gamma_L - \gamma_L - \gamma_0 - i\delta_1)S_1^\dagger + \xi P_D + \tilde{F}_{S_1}^\dagger(t) \tag{2.33}$$

$$\dot{P}_D = -(\kappa/\eta + \gamma_L + \gamma_0 + i\delta_2)P_D + \xi S_1^\dagger + \tilde{F}_D(t) \tag{2.34}$$

where the polariton decay rate includes an atomic part $\gamma_L + \gamma_0$ and a photonic part κ/η due to leakage of photons out of the medium (at a rate reduced by the factor $\eta = |g_2|^2 N/|\Omega_2|^2$ equal to the ratio of vacuum light velocity to the group velocity of slowly propagating Stokes photons). The spin flip operator equation (2.33) is seen to contain both a decay term and a gain term due to spontaneous emission into the bright polariton mode. Note that this apparent decrease in dissipation is however

accompanied by increased fluctuations denoted by the new noise force operator $\tilde{F}_{S_1}(t)$. The effective detuning between the polariton and spin flip mode is seen to correspond to the difference in two-photon detunings $\delta_1 - \delta_2$.

We now consider the scenario in which the system is evolving for a time τ under the Hamiltonian H_{eff}, after which both fields are turned off. If the procedure is adiabatic upon turn-off of the coupling fields $\Omega_{1,2}$ the polaritons are converted into pure spin excitations $P_D \rightarrow S_2$. Hence the entire procedure will correspond to the following state of the system:

$$\begin{aligned} |\Psi\rangle = \quad & \frac{1}{\cosh \xi\tau} \sum_n (\tanh \xi\tau)^n \frac{1}{n!} (P_D^\dagger)^n (S_1^\dagger)^n |g\rangle |\text{vac}\rangle \\ & \rightarrow \frac{1}{\cosh \xi\tau} \sum_n (\tanh \xi\tau)^n |n_{b_1}, n_{b_2}\rangle |\text{vac}\rangle. \end{aligned} \tag{2.35}$$

Here $|n_{b_1}, n_{b_2}\rangle = 1/n!(S_2^+)^n (S_1^+)^n |g\rangle$ are Dicke-like symmetric states of atomic ensemble and we assumed $n_{b_{1,b_2}} \ll N$. For non-zero $\xi\tau$ this state describes an entangled state, for which relative fluctuations between the two modes decreases exponentially to values well below the standard quantum limit (SQL) corresponding to uncorrelated atoms.

The present technique can also be viewed as a new mechanism for coherent "collisions" [120] between atoms mediated by light. In particular, the case when atomic pairs are excited into two different levels (as e.g. in Fig. 2.4a) closely resembles coherent spin-changing interactions that occur in degenerate atomic samples [152], whereas the case when atomic pairs are stimulated into the identical state (Fig. 2.4b) is reminiscent of dissociation of a molecular condensate [75]. To put this analogy in perspective we note that the rate of the present optically induced process can exceed that of weak interatomic interactions by orders of magnitude. Therefore the present

work may open up interesting new possibilities for studying many-body phenomena of strongly interacting atoms.

To quantify the resulting correlations established between the polariton mode P_D and the pure spin flip mode S_1, we introduce the quadratures of both modes (which are bosonic for small number of excitations) in direct analogy to the optical parametric case. We define the quadratures $X_1 = (S_1 + S_1^+)/\sqrt{2}$, $Y_1 = i(S_1 - S_1^+)/\sqrt{2}$ and similarly for the polarition mode; these can be measured e.g. by converting spin excitations to light. Correlations between the modes appear due to dynamical evolution and squeezing is found in certain quadratures of the sum and difference modes $X_- = (X_1 - X_D)/\sqrt{2}$ and $Y_+ = (Y_1 + Y_D)\sqrt{2}$. In the language of harmonic oscillators, the positions in mode 1 and $2 = D$ are correlated ($X_1 \simeq X_D$), while the momenta are anti-correlated ($Y_1 \simeq -Y_D$). For small number of excitations the sum and difference modes obey standard commutation relations $[X_\alpha, Y_\beta] = -i\delta_{\alpha,\beta}$ where $\alpha, \beta = +, -$ or $1, D$. A quadrature $Y_\pm$ is squeezed when $\Delta Y_\pm(t)^2 < 1/2$ and the Heisenberg limit corresponds to $\Delta Y_\pm(t)^2 \sim 1/N$.

We find that squeezing is optimal under conditions of four-photon resonance ($\delta_1 = \delta_2$) and in the limit of $\eta \gg 1$ (Fig. 2.6). Evolution leads to squeezing of Y_+ and X_-, anti-squeezing of Y_- and X_+. The squeezing in Y_+ reaches a minimum value at $t = t^*$ after which the growing fluctuations in X_+ give rise to increased noise in Y_+. Note that the total number of excitations (both modes) in the system, equal to $\langle X_+^2 + X_-^2 + Y_+^2 + Y_-^2 \rangle$, grows exponentially with time (Fig. 2.6c). Specifically, in the case $g_1 = g_2 = g$ and thus $\gamma_1 = \gamma_2 = \gamma$, for $\xi t > 1$, we have:

$$(\Delta Y_+(t))^2 = 1/2\left\{e^{-2\xi t} + \frac{2\kappa/\eta + 5\gamma_L + 4\gamma_0}{4\xi} + \left(\frac{\kappa/\eta + \gamma_L}{4\xi}\right)^2 e^{2\xi t}\right\} \tag{2.36}$$

where we have neglected terms of higher order in $(\gamma_L + \gamma_0)/\xi$ and $\kappa/(\eta\xi)$. The maximum amount of squeezing is obtained after an interaction time t^* such that $e^{-2\xi t^*} = (\kappa/\eta + \gamma_L)/4\xi$ and is given by

$$(\Delta Y_+)^2 = \frac{4\kappa/\eta + 7\gamma_L + 4\gamma_0}{8\xi} \tag{2.37}$$

i.e. of the order of the damping rate divided by the coherent interaction rate.

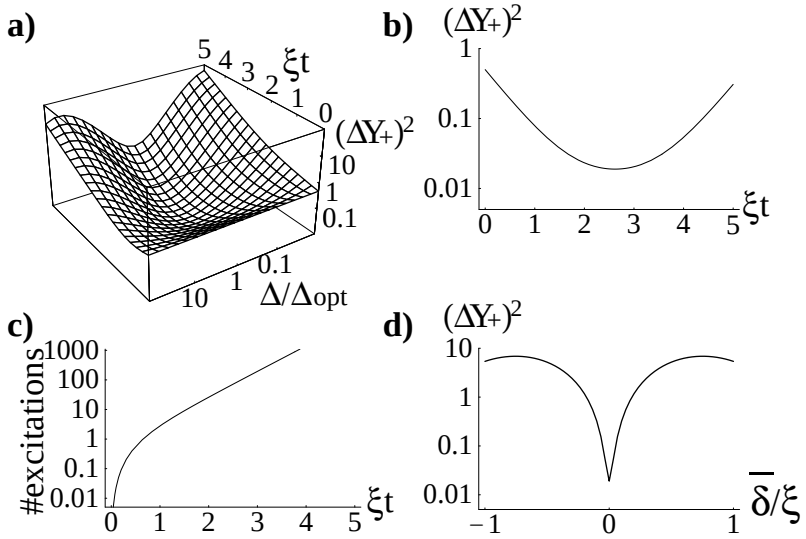

Figure 2.6: (a) Quadrature variance ΔY_+^2 vs. single-photon detuning Δ and interaction time ξt, (b) same for $\Delta = \Delta_{opt}$ and $\delta_1 = \delta_2$ showing maximum squeezing $\Delta Y_+^2 \simeq 0.01$ (for $\sqrt{g^2 N/\gamma\kappa} = 100$), (c) Number of excitations pumped in the system vs. time (same conditions as in b) and (d) $\Delta Y_+(t^*)^2$ vs. two-photon detuning $\bar{\delta} \equiv (\delta_1 - \delta_2)/2$ for $\Delta = \Delta_{opt}$ and where t^* gives maximum squeezing.

Since both the interaction parameter ξ and the relaxation rate of the polariton

$\gamma_D = \gamma_L + \gamma_0 + \kappa/\eta$ depend on the single photon detuning Δ (Fig. 2.6a), we find that squeezing is optimized for

$$\Delta_{opt} = \gamma \sqrt{\frac{7|\Omega_1|^2}{4|\Omega_2|^2} \frac{|g|^2 N}{\gamma\kappa}} \Big/ \sqrt{1 + \frac{\gamma_0 \eta}{\kappa}} \tag{2.38}$$

and with this optimal value of the detuning, the squeezing reaches a minimum value of

$$(\Delta Y_{+opt})^2 = \sqrt{\frac{\gamma\kappa}{|g|^2 N}} \times \sqrt{\frac{7}{4}(1 + \frac{\gamma_0 \eta}{\kappa})} \tag{2.39}$$

Note that the factor $g^2 N/\kappa\gamma$ is equal to the atomic density-length product multiplied by the empty cavity finesse and can easily exceed 10^4 even for modest values of the density-length product and cavity finesse. The factor $\gamma_0\eta/\kappa$ is small as long as the effective group delay η/κ is smaller that the ground state relaxation time $1/\gamma_0$, which is easily achievable. Furthermore, although a cavity configuration was used for simplicity, the results of the present analysis remain qualitatively valid in the limit of unity finesse, i.e. free space.

We consider a possible implementation of our degenerate scheme (Fig. 2.4b): levels $|g\rangle$ and $|b\rangle$ correspond to the $5^2S_{1/2}, F = 1, m_F = 1$ and $5^2S_{1/2}, F = 2, m_F = 1$ levels in ^{87}Rb (i.e. D_1 line) and level $|a\rangle$ to the $5^2P_{1/2}, F = 2, m_F = 2$ level. With all fields σ^+ polarized and atoms prepared in state $5^2S_{1/2}, F = 1, m_F = 1$ by optical pumping or magnetic state selection in atom traps, this implements the scheme of Fig. 2.4b. For these conditions the typical generation rate resulting in optimal squeezing $\Omega_1\Omega_2/\Delta_{opt}$ can easily be on the order of fraction of MHz. In such a case other decoherence mechanisms are negligible. Doppler shifts can also be disregarded as long as all fields are co-propagating.

For the "degenerate" version of the interaction (i.e. with identical final states for the spin flips, see Fig. 2.4b), the effective hamiltonian can be written as

$$H_{eff} = i\hbar\xi(\hat{S}^{\dagger 2} - \hat{S}^2) \tag{2.40}$$

where the limit $\eta \gg 1$ has been used to write $P_D \simeq -S$, with $S = 1/\sqrt{N}\Sigma_{gb}$ the spin flip operator. In this case the correlations lead to squeezing of $X = (S + S^\dagger)/\sqrt{2}$ and anti-squeezing of $Y = i(S - S^\dagger)/\sqrt{2}$. The analysis for this configuration is very similar to the non-degenerate version, in particular the maximum amount of squeezing achievable is also given by an expression of the form (2.39).

We can now obtain a condition for achieving Heisenberg-limited spin squeezed states, i.e. $(\Delta Y_{+opt})^2 \simeq 1/N$. We see from (2.37) that this requires

$$\xi \gtrsim N\Gamma \tag{2.41}$$

where $\Gamma = (4\kappa/\eta + 7\gamma_L + 4\gamma_0)/4$ is the effective damping rate of the system. This is in complete agreement with the estimate based on our simple bosonic model of section 2.4 (2.25). In terms of the single photon Rabi frequency g, the cavity decay rate κ, the spontaneous emission rate γ and the number of atoms N, the condition for achieving some squeezing i.e. $(\Delta Y_+)^2 \lesssim 1/2$ is

$$|g|^2 N \gtrsim \kappa\gamma \tag{2.42}$$

which can be easily achieved in the laboratory since it simply corresponds to the condition that the density length product multiplied by the cavity finesse be larger than one. In the cavity QED regime of strong coupling $|g|^2 \sim \kappa\gamma$, very strong

quantum correlations i.e. $(\Delta Y_+)^2 \sim 1/\sqrt{N}$ between atoms can be produced. In order to obtain Heisenberg limited spin squeezed states i.e. $(\Delta Y_+)^2 \sim 1/N$, one requires a more stringent condition

$$|g|^2 \gtrsim N\kappa\gamma \tag{2.43}$$

which can be fulfilled only in the strong coupling regime of cavity QED for a limited number of atoms. Note that this regime has been achieved experimentally by several groups [129, 79] and would allow for Heisenberg limited spin squeezing for as many as $\sim 10^3$ atoms. We have analyzed in this chapter the situation of a running-wave cavity, so that all atoms couple equally apart from a possible phase to the cavity mode irrespective of their position. In order to fulfill the cavity QED regime, small cavity volume is needed i.e. standing wave cavities. For atoms in such a cavity the coupling to the cavity mode is position dependent and it becomes necessary to localize atoms accurately at the antinodes of a trapping mode. Note that significant experimental progress has been made towards this direction by several groups [168, 130]. Once the atoms are well localized in the cavity, the interaction can proceed via a neighbouring mode b (e.g. different from the trapping mode a) so that for atoms localized within a small region in the cavity the two modes have essentially the same wavelength and atoms would therefore couple equally to the b mode as well, irrespective of their position.

2.6 Discussion and Conclusion

We have reviewed Ramsey spectroscopy and the use of spin squeezed states in precision measurements of this type. With the experimental motivation of minimizing the phase accuracy in phase estimation with Ramsey fringes, we introduced a particular class of squeezed states. These states lead to Heisenberg limited phase accuracy and we developed various pictorial representations for them. The strong similarities of these representations of spin squeezed states to those of squeezed states of light suggests an analogy extending to the type of interaction that gives rise to squeezing. We are thus lead to consider the so-called "counter twisting" Hamiltonian, which has been shown to lead to maximal spin squeezing. We have studied this model for spin squeezing in the presence of a dissipation mechanism and analyzed the effect of damping and finite system size on the amount of squeezing achievable with such an interaction. The analysis was based on a decorrelation approximation to the BBGKY hierarchy of equations of motion, followed by the use of a linear transformation which in the limit of large number of atoms $1/N \to 0$ "contracts" the angular momentum operators onto bosonic operators. This allows for the systematic inclusion of finite system size effects. It appears that Heisenberg limited spin squeezed states may be produced when the single atom nonlinearity exceeds the single atom loss rate. In this case the maximum number of atoms that can be lost before quantum correlations are destroyed to the point of compromising the spin squeezing is of the order $\Delta N \sim \log N$. For spin squeezing at a more modest level than the Heisenberg limit, larger number of atoms may be lost without compromising the squeezing, indicating the stronger sensitivity of spin squeezed states to dissipation for larger amounts of

squeezing.

We have also presented in detail a scheme based on the interaction of coherent classical light with an optically dense ensemble of atoms that leads to an effective coherent spin-changing interaction involving pairs of atoms. Atoms may be transferred to the same final state leading to spin squeezing (analogous to squeezing of light by degenerate OPO) or to different final states in this case leading to quantum correlations between different atomic modes (analogous to quantum correlations between electromagnetic modes by non-degenerate OPO). We have shown that this process is robust with respect to realistic decoherence mechanisms and can result in rapid generation of correlated (spin squeezed) atomic ensembles. The amount of correlations created by this effective interaction can be simply expressed in terms of the single photon Rabi frequency g, the atomic spontaneous emission rate γ and the cavity decay rate κ. We find that the generation of spin squeezed states requires $g^2 N \sim \kappa\gamma$, which can easily be achieved in low finesse cavities with e.g. room temperature atomic vapours. Very strongly correlated states can be produced when the strong coupling regime $g^2 \sim \kappa\gamma$ of cavity QED is achieved and the generation of Heisenberg limited spin squeezed states requires $g^2 \sim N\kappa\gamma$. The effective interaction rate $\xi = \Omega_1\Omega_2/\Delta$ which depends on the Rabi-frequency of two applied classical fields $\Omega_{1,2}$ and a detuning from an atomic transition Δ can be fast and is controllable. Furthermore, the resulting spin excitations can be easily converted into photons on demand, which facilitates applications in quantum information processing. Possible applications involving high-precision measurements in atomic clocks can be also foreseen.

Chapter 3

Stability of Realistic Atomic Clocks Based on Entangled Atoms

3.1 Introduction

Quantum entanglement is the basis for many of the proposed applications of quantum information science [28]. The experimental implementation of these ideas is challenging since entangled states are easily destroyed by decoherence. To evaluate the potential usefulness of entanglement it is therefore essential to include a realistic description of noise in experiments of interest. Although decoherence is commonly analyzed in the context of simple models [59], practical sources of noise often possess a non-trivial frequency spectrum, and enter through a variety of different physical processes. In this chapter, we analyze the effect of realistic decoherence processes and noise sources in an atomic clock that is actively locked to a spin-squeezed (entangled) ensemble of atoms.

The performance of an atomic clock can be characterized by its frequency accuracy and stability. Accuracy refers to the mean frequency offset from the ideal value, whereas stability describes the fluctuations around, and drift away from the average frequency. To have a precise clock, one must use a good atomic transition, for which there is little or no decay from the excited state, and that is relatively insensitive to external perturbations. In the presence of uncontrollable noisy perturbations, the atomic transition frequency becomes a randomly varying, noisy reference. To improve the long-term clock stability, it has been suggested to use entangled atomic states [81, 164, 25], and in this chapter we analyze such proposals in the presence of realistic decoherence and noise.

In practice, an atomic clock operates by locking the frequency of a local oscillator (L.O.) to the transition frequency between two levels of an atom. This locking is achieved by a spectroscopic measurement (such as Ramsey spectroscopy, as described in appendix A.1) determining the L.O. frequency offset $\delta\omega$ from the atomic resonance, followed by a feedback mechanism which steers the L.O. frequency so as to null the mean frequency offset. The spectroscopic precision and its dependence on the quantum state of the atoms, on the interrogation time, and on the presence of uncontrollable noise sources, is discussed further in this chapter.

A true atomic clock is achieved by incorporating the spectroscopic measurement in a frequency control loop that steers the local oscillator frequency in order to correct random drifts of the frequency. The problem of filtering the detection process [102] in order to obtain the optimal estimate of the frequency offset is a complex one, which we do not attempt to solve exactly. Rather we present two approaches, one based on

a linear approximation and the other taking into account the nonlinear dependence of the detection signal on the frequency offset. The problem of frequency control thus combines elements of quantum parameter estimation theory and control of stochastic systems via feedback [60, 155].

3.2 Quantum Projection Noise

The spectroscopic measurement of the atomic transition frequency is typically achieved through Ramsey spectroscopy [134], in which the atoms are illuminated by two short, near-resonant pulses from the local oscillator, separated by a long period of free evolution, referred to as the Ramsey time T. During the free evolution the atomic state and the L.O. acquire a relative phase difference $\delta\phi = \delta\omega T$, which is subsequently determined by a projection measurement. If a long time T is used, then Ramsey spectroscopy provides a very sensitive measurement of the L.O. frequency offset $\delta\omega$. Here, we investigate the situation relevant to trapped particles, such as atoms in an optical lattice [154] or trapped ions [132]. In this situation, the optimal value of T is determined by atomic decoherence (caused by imperfections in the experimental setup) which therefore determines the ultimate performance of the clock.

We consider an ensemble of N two-level particles with lower (upper) state $|\downarrow\rangle$ ($|\uparrow\rangle$). Adopting the nomenclature of spin-1/2 particles, we introduce the total angular momentum (i.e., Bloch vector) $\vec{J} = \sum_{j=1}^{N} \vec{S}_j$, where e.g. $S_z^j = (|\uparrow\rangle_j\langle\uparrow| - |\downarrow\rangle_j\langle\downarrow|)/2$. Initially the state of the atoms has mean $\langle\vec{J}\rangle$ along the z direction and $\langle J_x\rangle = \langle J_y\rangle = 0$. Unavoidable fluctuations in the x and y components $\langle J_x^2\rangle = \langle J_y^2\rangle \neq 0$, result in the so-called atomic projection noise. These fluctuations give rise to an uncertainty in

the Ramsey phase $\delta\phi_R \simeq \Delta J_y/|\langle \hat{J}_z \rangle|$ (see appendix A.1) as indicated geometrically in Fig. 3.2 [145, 81]. For uncorrelated spins aligned along the z axis, the uncertainty from independent spins are added in quadrature, resulting in the projection noise $\Delta J_y = \sqrt{N}/2$. To reduce the measurement error it has been proposed [164, 91, 141] and demonstrated [119] to use entangled atomic states (so called spin squeezed states), which have reduced noise in one of the transverse spin components (e.g., J_y) and non-zero noise ΔJ_z in the mean spin direction. Ideally this gives an improvement by a factor $\xi = \sqrt{N}\Delta J_y/\langle J_z \rangle$, which can be as low as $\xi = 1/\sqrt{N}$ for maximally entangled states [25].

An example of a mildly spin squeezed state is shown in Fig.3.1 with $\Delta J_y = N^{1/3}$. Note that noise reduction in the $\hat{J}_y$ component also introduces noise $\Delta J_z = (\langle \hat{J}_z^2 \rangle - \langle \hat{J}_z \rangle^2)^{1/2}$ in the mean spin direction. This unavoidable noise plays an important role in the long-term stability of atomic clocks using entangled atoms.

Using a simple noise model it was shown in Ref. [80] that entanglement provides little gain in spectroscopic sensitivity in the presence of atomic decoherence. In essence, random fluctuations in the phase of the atomic coherence cause a rapid smearing of the error contour in Fig. 3.2a. For example, dephasing of individual particles results in an additional contribution $(N/4)\langle \delta\phi^2 \rangle$ to the noise, where $\langle \delta\phi^2 \rangle$ denotes the variance of the phase fluctuations (increasing with T as $\langle \delta\phi^2 \rangle = \gamma T$ for white noise, where γ is the dephasing rate). In practice, the stability of atomic clocks is often limited primarily by fluctuations of the L.O. As we show below, the L.O. fluctuations result in the added noise $\Delta J_z^2 \langle \delta\phi^2 \rangle$, where ΔJ_z^2 is the initial variance in J_z. This added noise is due to the error in the feedback loop, caused by the

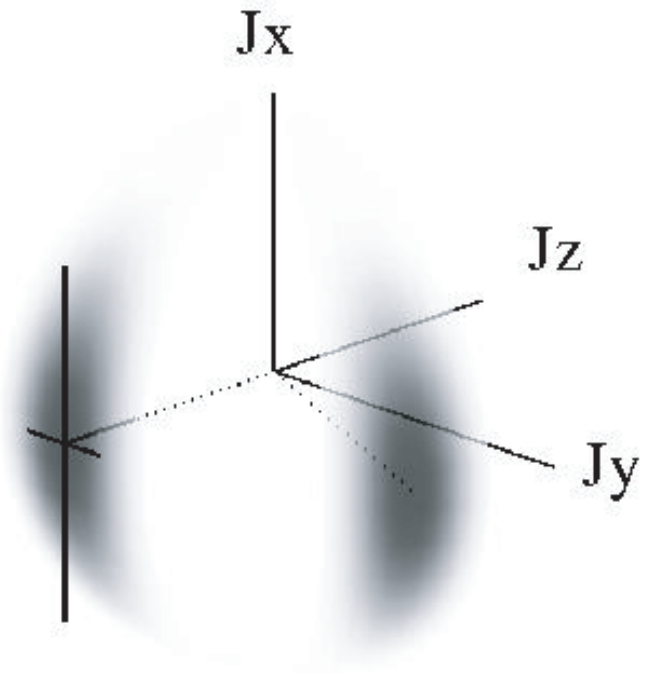

Figure 3.1: Probability distribution on the Bloch sphere for a spin-squeezed state polarized along the $\hat{J}_z$ direction (i.e. with $\langle \hat{J}_z \rangle \simeq -N/2$). Also shown is the probability distribution for atoms initially in that state, but shown at the end of the Ramsey cycle, immediately before $\hat{J}_z$ is measured. $N = 20$ atoms, $\langle \hat{J}_z \rangle \simeq -N/2$, and $\Delta J_y = N^{1/3}$. Thick lines indicate quantum uncertainties $\Delta J_{x,y,z}$.

longitudinal noise ΔJ_z. For weakly entangled states, the added noise is considerably smaller than in the case of atomic dephasing and the use of entangled states can lead to a significant improvement in clock stability.

3.3 Local Oscillator and Environmental Noise

In what follows we present a model that incorporates the effects of atomic noise and spin squeezing as well as that of the feedback loop. Before proceeding, we note that qualitative considerations along these lines were noted in Ref. [166]. At the operating point, the error signal in Ramsey spectroscopy [164] measured at time t_k is determined by the operator

$$\hat{E}(t_k) \simeq \sum_{j=1}^{N} \hat{S}_z^j \sin[\delta\phi_j(t_k)] + \hat{S}_y^j \cos[\delta\phi_j(t_k)], \tag{3.1}$$

where $\delta\phi_j(t_k)$ is the phase acquired by the jth atom during the interrogation time T and all operators refer to the initial atomic state. We separate the phase into two parts $\delta\phi_j = \delta\phi_O + \delta\phi_E^j$, where $\delta\phi_O(t_k) = \int_0^T \delta\omega(t_k - t)dt$ is the phase due to the frequency fluctuations $\delta\omega(t)$ of the L.O., and $\delta\phi_E^j$ is a phase induced by the interaction of the jth atom with the environment.

In the model, the interrogating oscillator has frequency $\omega_{LO}(t) = \bar{\omega} + \delta\omega(t)$, where $\bar{\omega}$ is the mean frequency of the L.O. and $\delta\omega(t)$ is a stochastic process representing the frequency fluctuations. We therefore assume $\langle\delta\omega(t)\rangle = 0$, while the fluctuations are characterized by the noise spectrum of frequency fluctuations. Letting the Fourier transform of $\delta\omega(t)$ be $\delta\Omega(\nu) = \int dt\ e^{i\nu t}\delta\omega(t)$, the noise spectrum is defined by

$$\langle\delta\Omega(\nu)\delta\Omega(\nu')\rangle \;=\; 2\pi\delta(\nu + \nu')S_\Omega(\nu). \tag{3.2}$$

For example for white frequency noise $\langle \delta\omega(t)\delta\omega(t')\rangle = \gamma\delta(t-t')$, the noise spectrum $S_\Omega(\nu) = \gamma$ is independent of frequency ν (white). Assuming the oscillator phase is the same for all atoms, the acquired phase is $\delta\phi_{LO}(t_k, T) = \int_0^T dt\ \delta\omega(t_k - t)$. The environmental noise likewise results in a random phase at atom j of $\delta\phi_{j,E}(t_k, T)$, which we model by a noise source of frequency fluctuations $\delta\omega_{j,E}(t)$ with noise spectrum $S_E(\nu)$.

In order to lock the L.O. to the atomic frequency, the interrogation time should be short enough that $\langle \delta\phi(t_k)^2\rangle \lesssim 1$. Expanding in terms of $\delta\phi(t_k)$, we find the measured error signal

$$\begin{aligned} \mathcal{E}(t_k) &\simeq \langle \hat{J}_z\rangle \left(\delta\phi_O(t_k) - \frac{\delta\phi_O(t_k)^3}{3!}\right) + \sum_{j=1}^{N} \mathcal{S}_z^j \delta\phi_E^j(t_k) \\ &+ [\mathcal{J}_y(t_k) + \delta\mathcal{J}_z(t_k)\delta\phi_O(t_k)] + \cdots . \end{aligned} \tag{3.3}$$

Here $\delta\mathcal{J}_z(t_k) = \mathcal{J}_z(t_k) - \langle \hat{J}_z\rangle$, where $\mathcal{J}_z(t_k)$ and $\mathcal{J}_y(t_k)$ are random numbers with a distribution corresponding to the initial atomic state (we consider here states for which $\langle \hat{J}_y\hat{J}_z\rangle = 0$, so that we may treat $\mathcal{J}_z(t_k)$ and $\mathcal{J}_y(t_k)$ as independent random variables). The term multiplying $\langle \hat{J}_z\rangle$ in (3.3) is used to estimate the frequency offset, while the remaining terms represent measurement noise.

The spectroscopic estimate of the phase $\delta\phi_{LO}$ acquired due to the frequency offset can be obtained from the linear approximation $\delta\tilde{\phi}_{LO,k} = \frac{\mathcal{E}_k}{\langle \hat{J}_z}$ from which the estimate for the average frequency offset $\delta\bar{\omega}_k(T) = \frac{1}{T}\int_0^T \delta\omega(t_k - t)dt$ is simply given by $\delta\tilde{\omega}_k = \frac{\delta\tilde{\phi}_{LO,k}}{T}$. Intuitively, we can see that this will yield an accurate estimate for interrogation times short enough that the oscillator phase has not drifted too much i.e. $\langle \delta\phi_{LO,k}^2\rangle \ll 1$.

The error in our estimate is characterized by $\langle \delta\tilde{\phi}_{LO,k} - \delta\phi_{LO,k}\rangle$ for any systematic

bias in the estimate, and by $\langle\left(\delta\tilde{\phi}_{LO,k}-\delta\phi_{LO,k}\right)^2\rangle$ for the variance, i.e. the typical size of the uncontrollable error in the estimate. Using the statistical properties of the measurement results, we find that there is no systematic bias $\langle\delta\tilde{\phi}_{LO,k}-\delta\phi_{LO,k}\rangle=0$, and that the variance is given by, in the small oscillator noise limit $\langle\delta\phi_{LO}^2\rangle\ll 1$,

$$\langle\left(\delta\tilde{\phi}_{LO,k} - \delta\phi_{LO,k}\right)^2\rangle = \frac{1}{\langle\hat{J}_z\rangle^2}\left[\frac{N}{4}\langle\delta\phi_E^2\rangle + \Delta J_y^2 + \Delta J_z^2\langle\delta\phi_{LO}^2\rangle\right]. \qquad (3.4)$$

For uncorrelated atoms, $\Delta J_z=0$ and $\Delta J_y=N/4$, so that the variance becomes independent of the local oscillator noise.

Our estimate of the phase offset $\delta\phi(\tau)=\int_0^\tau\delta\omega(\tau-t)dt$ after n Ramsey cycles (corresponding to a total measurement time $\tau=nT$) is

$$\delta\tilde{\phi}(\tau) = \sum_{k=1}^{n}\delta\tilde{\phi}_{LO,k}. \qquad (3.5)$$

The average frequency offset during the time $\tau=nT$ is $\delta\bar{\omega}_{LO}(\tau)=\frac{1}{\tau}\int_0^\tau\delta\omega_{LO}(\tau-t)dt$, and it is estimated by $\delta\tilde{\omega}(\tau)=\frac{1}{\tau}\delta\tilde{\phi}(\tau)$. The variance of the error in the phase estimate is

$$\langle\left(\delta\tilde{\phi}(\tau)-\delta\phi(\tau)\right)\right)^2\rangle = \langle\left[\sum_{k=1}^{n}\left(\delta\tilde{\phi}_{LO,k}-\delta\phi_{LO,k}\right)\right]^2\rangle \qquad (3.6)$$

When the environmental dephasing noise is white (i.e. uncorrelated during different interrogation times $\langle\delta\phi_{E,k}\delta\phi_{E,k'}\rangle=0$ for $k\neq k'$), we have

$$\begin{aligned}\langle(\delta\tilde{\omega}(\tau)-\delta\bar{\omega}(\tau))^2\rangle &= \frac{1}{T\tau}\langle\left(\delta\tilde{\phi}(T)-\delta\phi(T)\right)^2\rangle \\ &= \frac{1}{T\tau\langle\hat{J}_z\rangle^2}\left[\frac{N}{4}\langle\delta\phi_E(T)^2\rangle+\Delta J_y^2+\Delta J_z^2\langle\delta\phi_{LO}(T)^2\rangle\right]. \qquad (3.7)\end{aligned}$$

When the environmental noise is the dominant source of noise, so that we may neglect the fluctuations of the local oscillator, and when it has a white spectrum, we

have $\langle \delta\phi_E(T)^2 \rangle = \gamma T$ where γ is the dephasing rate. In this situation, the spectroscopic precision becomes

$$\langle (\delta\tilde{\omega}(\tau) - \delta\bar{\omega}(\tau))^2 \rangle = \frac{1}{T\tau \langle \hat{J}_z \rangle^2} \left[\frac{N}{4}\gamma T + \Delta J_y^2 \right]. \tag{3.8}$$

As shown in [80], no spectroscopic gain is achieved by using spin-squeezed states: the phase precision improvement due to spin squeezing becomes lost when the interrogation time is such that $\gamma T \frac{N}{4} \sim \Delta J_y^2$, thus implying a shorter interrogation time for spin-squeezed states than for uncorrelated states. The net result is that, assuming one is free to choose the interrogation time so as to optimize the spectroscopic precision (i.e. no other sources of noise except environmental noise), spin-squeezed states and uncorrelated states give essentially the same spectroscopic precision [80, 158].

3.4 Simple Model of Frequency Control

A detailed description of the frequency control loop and a discussion of the stabilized oscillator noise spectrum is given in appendix B.1. We here present a simplified model of the frequency control loop. Additionally, linear and nonlinear feedback are discussed in details in appendix B.2 where a stochastic differential equation approach is used to obtain the long-term stability of the clock.

The feedback is started at $t = 0$ and, at the end of each Ramsey cycle, at $t_k = kT$ ($k = 1, 2, ...$), the detection signal is used to steer the frequency of the oscillator to correct for the fluctuations accumulated during the last cycle $\delta\omega(t_k^+) = \delta\omega(t_k^-) + \Delta\omega(t_k)$, where t_k^- and t_k^+ refer to before and after the correction, and $\Delta\omega(t_k)$ is the frequency correction. Assuming that negligible time is spent performing the $\pi/2$

pulses and in preparing and detecting the state of the atoms, the mean frequency offset after running for a period $\tau = nT$ is then

$$\begin{aligned} \delta\bar{\omega}(\tau) &= \frac{1}{\tau}\int_0^\tau \delta\omega(t)dt \\ &= \frac{T}{\tau}\sum_{k=1}^{n}\left[\frac{\delta\phi_O(t_k)}{T} + \Delta\omega(t_k)\right]. \end{aligned} \tag{3.9}$$

We begin by analyzing the simplest case of linear feedback (in $\mathcal{E}(t_k)$) and later extend to the more optimal nonlinear feedback case. With $\Delta\omega(t_k) = \frac{-\mathcal{E}(t_k)}{\langle\hat{J}_z\rangle T}$, using (3.3) and substituting in (3.9), we find, ignoring for now the $\delta\phi_O(t_k)^3$ term,

$$\begin{aligned} \delta\bar{\omega}(\tau) &= \frac{-1}{\tau\langle\hat{J}_z\rangle}\sum_{k=1}^{n}[\mathcal{J}_y(t_k) + \delta\mathcal{J}_z(t_k)\delta\phi_O(t_k) \\ &+ \sum_{j=1}^{N}\mathcal{S}_z^j\delta\phi_E^j(t_k)] \end{aligned} \tag{3.10}$$

Note that the acquired offsets $\delta\phi_O(t_k)/T$ $(k = 1, ..., n)$ due to L.O. frequency fluctuations are corrected by the feedback loop and do not appear in (3.10), while measurement noise is added at the detection times t_k. The first two terms in (3.10) are uncorrelated for different t_k since the atomic noise for different detection events is uncorrelated. If the dephasing noise is uncorrelated for different t_k, then the fractional frequency fluctuation (Allan deviation) [16] $\sigma_y(\tau) = \langle(\delta\bar{\omega}(\tau)/\omega)^2\rangle^{1/2}$, is

$$\sigma_y(\tau) = \frac{\left[\Delta J_y^2 + \Delta J_z^2\langle\delta\phi_O^2\rangle + (\lambda\langle J_z^2\rangle)\langle\delta\phi_E^2\rangle\right]^{1/2}}{\omega\sqrt{\tau T}\langle\hat{J}_z\rangle}. \tag{3.11}$$

Here λ accounts for the possibility of collective decoherence, so that for atoms dephasing collectively (independently) $\lambda \to 1$ ($\lambda \to (N/4)/\langle\hat{J}_z^2\rangle$). The L.O. noise affects the atoms in a similar fashion than collective dephasing. Note, however, the significant difference between collective environmental dephasing, which enters expression

(3.11) as $\langle \hat{J}_z^2 \rangle \langle \delta\phi_E^2 \rangle$, and L.O. noise, for which $\Delta J_z^2 \langle \delta\phi_O^2 \rangle$ is the relevant expression. The feedback loop results in a large cancellation of the effect of the L.O. noise on the stability; the uncanceled part of the noise is now proportional to $\Delta J_z^2 \ll \langle \hat{J}_z^2 \rangle$.

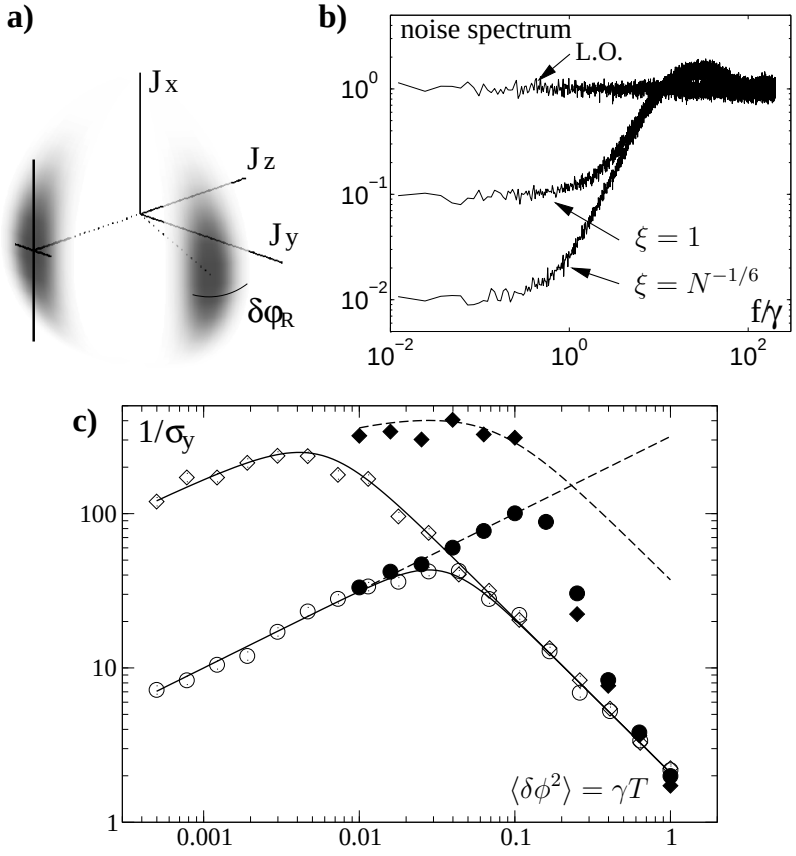

Figure 3.2: a) Representation of the probability distribution on the Bloch sphere for a spin squeezed state $|\psi(\kappa)\rangle$, with $\kappa = N^{1/4}$ corresponding to the squeezing parameter $\xi = N^{-1/4}$ ($N = 10$, both the initial state and the state just before detection are shown for clarity). Thick lines indicate initial uncertainties in $\vec{J}$. b) Noise spectra due to L.O. frequency fluctuations when free running, when stabilized to unsqueezed atoms ($\xi = 1$), and when stabilized to spin squeezed atoms ($\xi = N^{-1/6}$), $N = 10^3$ and $\gamma T = 10^{-2}$. c) Inverse fractional frequency stability $1/\sigma_y$ (arbitrary units) vs. Ramsey time for white L.O. noise, $N = 10^5$, with linear feedback to uncorrelated atoms ($\circ$); linear feedback to correlated atoms ($\diamond$, $\xi = N^{-1/4}$); nonlinear feedback to uncorrelated atoms ($\bullet$); and nonlinear feedback to correlated atoms (filled $\diamond$, $\xi = N^{-1/4}$). Points: numerical simulations, lines: analytical results.

3.5 Long Term Stability of the Atomic Clock

The long-term stability of the clock, the optimal Ramsey time and the optimal scaling with the number of atoms is discussed in details in appendix B.3, both for the case of linear and nonlinear feedback. We here present a simplified discussion, for ease of presentation.

When decoherence is negligible, $\langle \delta\phi_O^2 \rangle = \langle \delta\phi_E^2 \rangle = 0$, the long term frequency stability is given by $\sigma_y(\tau) = \Delta J_y / \omega\sqrt{\tau T}\langle \hat{J}_z \rangle$ as shown in Refs. [81, 164]. For an uncorrelated atomic state, the stability improves with increasing number of atoms as $N^{-1/2}$ [145]. The maximum possible improvement using spin-squeezed states is a factor of $N^{-1/2}$, yielding a stability $\sigma_y(\tau) \propto N^{-1}$ [25].

The best long term stability is obtained with the longest possible interrogation time T. When the interrogation time is limited by environmental decoherence, the latter cannot be ignored. This corresponds to the situation considered in Refs. [80, 158], in which case no substantial improvement is possible using spin-squeezed states. This conclusion however relies on a model of white environmental noise, where the local oscillator fluctuations are ignored (i.e. negligible compared to environmental noise). By choosing the atomic transition properly and by shielding the atom from the environment, these sources of noise can be reduced and eventually completely eliminated. The local oscillator noise however, is never negligible: this is the reason for building an atomic clock in the first place, i.e. to stabilize the (noisy) oscillator to the atoms and generate a stabilized, less noisy oscillator signal that can be used as a frequency reference. In the practically relevant case where the main source of noise is from the L.O. [23, 132, 44] the situation is quite different. In this case it

is undesirable to use a very highly squeezed state with $\Delta J_y \sim 1$ because it has a very large uncertainty in the z-component of the spin $\Delta J_z \sim N$, which according to Eq. (3.11) has a large contribution to the noise. A moderately squeezed state can, however, lead to a considerable improvement in the stability. This observation is the main result of the present chapter.

To find the optimal stability, we first optimize (3.11) with respect to the interrogation time. Considering uncorrelated atoms first, we have $\Delta J_y = \sqrt{N}/2$ and $\Delta J_z = 0$; Eq. (3.11) then predicts that $\sigma_y(\tau)$ decreases indefinitely as $1/\sqrt{T}$. To derive Eq. (3.11), however, we have linearized the expression in Eq. (3.1), and this linearization breaks down when the (neglected) cubic term in (3.3) is comparable to the noise term that we retained, i.e., when $\delta\phi(t_k)^3 \sim \Delta J_y/\langle \hat{J}_z \rangle$. In a more careful analysis based on Eq. (3.3), including perturbatively the nonlinear terms in a stochastic differential equation, we find the optimal time $\gamma T = (2\Delta J_y^2/\langle \hat{J}_z \rangle^2)^{1/3}$. At this point the stability is given by $\sigma_y(\tau) = \zeta N^{-1/3}\gamma/\omega\sqrt{\gamma\tau}$ where

$$\zeta = \frac{3}{2^{4/3}} N^{1/3} \left[\left(\frac{\Delta J_y}{\langle \hat{J}_z \rangle} \right)^{4/3} + \frac{2^{4/3}}{3} \left(\frac{\Delta J_z}{\langle \hat{J}_z \rangle} \right)^2 \right]^{1/2} . \tag{3.12}$$

To evaluate the potential improvement in stability by using squeezed states (i.e., the scaling with increasing number of atoms N, in the limit $N \gg 1$), it is convenient to use a family of states parametrized by a small number of parameters. A one-parameter family of states that includes the uncorrelated state as well as spin squeezed states is given by the Gaussian states (discussed in appendix B.5) $|\psi(\kappa)\rangle = \mathcal{N}(\kappa) \sum_m (-1)^m e^{-(m/\kappa)^2} |m\rangle$, where $|m\rangle$ are eigenstates of the J_y operator with eigenvalue m and the total angular momentum quantum number is $J = N/2$, and $\mathcal{N}(\kappa)$ is a normalization factor. The transverse noise for these states is given by

$\Delta J_y = \kappa/2$. For a large number of atoms $N \gg 1$, the uncorrelated state is well approximated by $|\psi(\kappa = \sqrt{N})\rangle$, while highly-squeezed states are obtained when $\kappa \to 1$. Within this family of states the optimal value is $\zeta \simeq 1.42N^{-1/6}$ for $\kappa \simeq 2^{1/16}N^{1/4}$ ($\xi \sim N^{-1/4}$) giving a stability scaling as $N^{-1/2}$. This represents an improvement by a factor of $N^{1/6}$ compared to uncorrelated states, for which $\zeta = 3/2^{4/3}$ and the stability scales as $N^{-1/3}$. We emphasize that these results are derived assuming a linear feedback loop.

To confirm these predictions, we have made extensive numerical simulations of the frequency control loop, along the lines of Ref. [13, 63]. The noise spectrum of the free-running oscillator is defined by $S(f)\delta(f + f') = \langle \delta\omega(f)\delta\omega(f')\rangle$, where $\delta\omega(f)$ is the Fourier transform of the stochastic process $\delta\omega(t)$. We generate the corresponding time-series and at the detection times $t_k = kT$, the accumulated phase $\delta\phi_O(t_k)$ is calculated and the atomic noise is generated from the probability distributions of $\mathcal{J}_y$ and $\mathcal{J}_z$. The error signal $\mathcal{E}(t_k)$ is found and a frequency correction $\Delta\omega(t_k)$ is generated. The noise spectrum of the slaved oscillator, see Fig. 3.2b, clearly shows that while for short time scales ($\lesssim T$, high frequencies) the noise is given by that of the free-running oscillator, at longer time scales (lower frequencies) the oscillator is locked to the atoms and the remaining (white) noise is determined by the atomic fluctuations. The low-frequency white noise floor determines the long-term stability of the clock and is the quantity we seek to optimize. In Fig. 3.2c we compare our analytical results with the results of the numerical simulations as a function of Ramsey time T, and in Fig. 3.3a we show the scaling with the number of atoms. The analytical and numerical approaches are in excellent agreement.

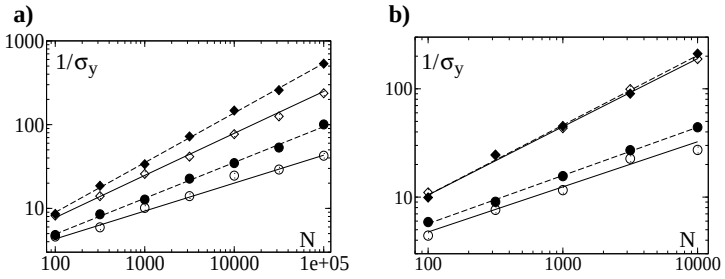

Figure 3.3: Inverse fractional frequency stability $1/\sigma_y$ (arbitrary units) vs. number of atoms N, with Ramsey time optimized for a) white noise and b) $1/f$ noise. Points: numerical simulations, lines: analytical results. Uncorrelated atoms ($\circ$) and optimal spin squeezed atoms ($\diamond$), both for linear feedback (full lines, open symbols) and nonlinear feedback (dashed lines, filled symbols).

So far we have assumed linear feedback and white noise; we now relax these assumptions. The stability limit identified above is mainly determined by the breakdown of the assumption of small (i.e., linear) phase fluctuations. In fact, the stability can be improved considerably by using a feedback $\Delta\omega$ which is a nonlinear function of the error signal $\mathcal{E}$. To investigate this we have included a nonlinear feedback $\Delta\omega(t_k) \propto \arcsin[\mathcal{E}(t_k)/J]$ in our numerical simulations. In Fig. 3.2c it is seen that nonlinear feedback performs better, and that it extends the validity of Eq. (3.11) all the way to $\gamma T \sim 0.1$. For larger γT, the feedback loop fails, resulting in a rapid decrease in stability. If we optimize the Allan deviation in Eq. (3.11) for nonlinear feedback, under the condition $\gamma T \leq 0.1$, we find that the optimally squeezed states have $\Delta J_y \sim N^{1/3}$ ($\xi \sim N^{-1/6}$) resulting in a stability scaling as $N^{-2/3}$. This represents again a relative improvement in scaling of $N^{1/6}$ compared to the uncorrelated state for which the stability scales as $N^{-1/2}$. Detailed derivation of these results are presented in appendices B.2 and B.3.

The assumption of white noise $\langle\delta\phi^2\rangle = \gamma T$, is convenient for theoretical calcula-

tions, but in practice very-low-frequency noise is likely to have nontrivial spectrum such as $1/f$ noise. To find the scaling with the number of atoms in this situation, we replace $\langle \delta\phi^2 \rangle = \gamma T$ with the behaviour expected for $1/f$ noise: $\langle \delta\phi^2 \rangle \sim (\gamma T)^2$. Repeating all the calculations above we again find an improvement by a factor of $N^{1/6}$ by using squeezed states for the nonlinear feedback loop, and a factor of $N^{5/24}$ for linear feedback. In Fig. 3.3b we compare these scaling arguments to the numerical simulations and the two approaches are seen to be in very good agreement.

3.6 Conclusions

To summarize, we have shown that entanglement can provide a significant gain in the frequency stability of an atomic clock when it is limited by the stability of the oscillator used to interrogate the atoms. The optimal stability is achieved by using moderately squeezed states, with a relative improvement that scales approximately as $N^{1/6}$ with the number of atoms. These results are in contrast to previous studies using simplified decoherence models, which found that no practical improvement can be achieved with entangled states. Finally, we note a few interesting questions raised by our work. First, it would be interesting to see if there exists special quantum states of atoms and feedback mechanisms which optimize the performance of the clock. Second, the present results highlight that it is essential to have a realistic model of the noise (and possible stabilization mechanism) present in specific realizations of quantum information protocols. Although the protocol considered in this chapter exploits entanglement to stabilize a classical system (the local oscillator), it would be interesting to study how similar considerations (e.g. $1/f$ noise and collective

decoherence) affect protocols such as quantum error correction codes [28], which use entanglement to stabilize a quantum system and protect it from decoherence.

Chapter 4

Raman Generation of Quantum States of Light and Atoms

4.1 Motivation

As shown by Raymer [135], the weak nonlinearity of Raman scattering, when analyzed from a quantum-mechanical point of view, generates strong atom-photon correlations. The creation of atom-photon entangled states can be understood with the following simple model, see Fig. 4.1. Optical pumping prepares the atoms in the ground state $|g\rangle$, following which a pulse of Raman excitation induces the spontaneous generation of a frequency-shifted Stokes photon. At the same time, one atom changes state from $|g\rangle$ to $|s\rangle$. Note that the states $|g\rangle, |s\rangle$ are analogous to the $|\downarrow\rangle, |\uparrow\rangle$ states of an effective spin $\frac{1}{2}$ particle. However, since it is impossible (even in principle) to distinguish which atom changed state, elementary quantum mechanics implies that the collective atomic superposition state is generated $|\psi\rangle_{atom} = \frac{1}{\sqrt{N}} \sum_{j=1}^{N} |g \cdots s_j \cdots g\rangle$,

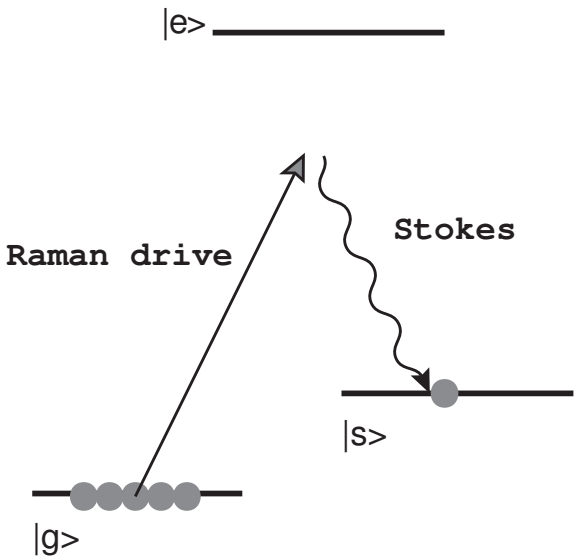

Figure 4.1: Atomic level configuration for Raman scattering and generation of atom-photon entanglement.

where the summation is over all N atoms in the ensemble. The collective atomic mode corresponds to a collective "spin", as described by the spin raising operator $\hat{\mathcal{S}}^{\dagger} = \frac{1}{\sqrt{N}} \sum_{j=1}^{N} |s\rangle_j \langle g|$. Note that with all atoms initially pumped in state $|g\rangle$, the collective spin degree of freedom obeys bosonic commutation rules $[\hat{\mathcal{S}}, \hat{\mathcal{S}}^{\dagger}] = 1$.

Before the Raman transition, the Raman mode at the shifted optical frequency and the atomic spin mode $\hat{\mathcal{S}}$ are in the vacuum state $|0\rangle_{phot} \otimes |0\rangle_{spin}$. The Raman transition is a spontaneous but coherent process in which the classical drive field induces coherent evolution from the vacuum state to a superposition of number states

$$|\Psi\rangle \;=\; \sum_{n=0}^{\infty} c_n \, |n\rangle_{phot} \otimes |n\rangle_{spin} \, . \tag{4.1}$$

The probability amplitudes c_n have a thermal distribution $|c_n|^2 = \frac{\overline{n}^n}{(\overline{n}+1)^{n+1}}$, where $\overline{n}$ is the mean number of photons in the Raman mode. This Raman field and the spin wave form a coherent superposition with entanglement between the number of

photons and collective spin excitations. Subsequent measurement of the intensity (or photon number) of the Raman Stokes field is destructive for the photonic part of (4.1), but projects the spin part on a number state and leaves the atomic ensemble in a Fock state. Obviously, measurement of the number of spin excitations should show very strong correlations with the number of photons measured in the Stokes field (twin-mode intensity squeezing [162]).

The possibility of creating and manipulating entangled states of systems of many particles is of significant interest for quantum information processing [28]. Such capability would have an impact in a broad area ranging from quantum computation and quantum communication [122], to the more traditional field of precision measurements. Controllable, coherent atomic interactions [120] could be used to entangle atoms with one another, and lead to the the generation of collective entangled states in atomic ensembles, such as spin-squeezed states [91]. Such states have the property of having reduced fluctuations in one component of the collective spin of N spin $\frac{1}{2}$ systems, perpendicular to the direction in which the mean collective spin is directed. Thus, these states act as very thin pointers that can be rotated and used to measure phase very accurately. In fact, their interest lies in the fact that they offer higher phase accuracy than any non-entangled (factorizable) state, such as that corresponding to all elementary spins pointing in the same direction. Precision measurements would thus greatly benefit from the availability of such states, in particular atomic clocks could be greatly improved with such atomic states [81].

Techniques to coherently map the quantum states of light pulses to that of atoms in optically thick atomic ensembles [56] have now been developed. They are based on

Electromagnetically Induced Transparency [147, 69] (EIT), and permit for example to map the photonic superposition state $|\psi\rangle_{photon} = \sum_{n=0}^{\infty} c_n |n\rangle$ to the atomic superposition state $|\psi\rangle_{atom} = \sum_{n=0}^{\infty} c_n \left(\hat{\mathcal{S}}^{\dagger}\right)^n |0\rangle_{atom}$, where as described earlier the state $|0\rangle_{atom}$ corresponds to all atoms pumped to the lower atomic "spin" state $|g\rangle$. Ideally, the mapping is perfectly coherent and reversible so that the atomic ensemble can be used as a quantum memory for quantum states of light. Thus, the atom-photon entangled states created by Raman scattering (as described earlier) can be mapped, upon mapping of the photonic part of the state onto atoms, into atom-atom entangled states. In fact, the atomic entanglement thus generated is precisely of the spin-squeezing type and this process is very efficient at generating large amounts of squeezing in atomic ensembles [3].

Conversely, atom-photon entangled states in which a Stokes photon is correlated with an atomic collective spin excitation, can be mapped to a correlated photon state. Upon mapping the atomic part of the state to photons, correlated Stokes/anti-Stokes photon pairs are generated where the number of photons in the two channels are quantum-mechanically correlated [159, 97, 48].

4.2 Introduction

In this section we describe a novel technique for generating pulses of light with controllable, well-defined photon numbers, propagation direction, timing, and pulse shapes by exploiting Raman preparation and retrieval of atomic excitations. This technique is particularly important in the contexts of long-distance quantum communication [28, 48], and EIT-based quantum nonlinear optics [104]. Following the

early experiments by Kuzmich and co-workers [97] and van der Wal and co-workers [159], in which non-classical correlations were demonstrated, there has been exciting experimental progress in this area. This chapter presents detailed theoretical analysis of these processes as well as brief highlights of our experiments in this area.

Our approach, using Raman preparation and EIT-based retrieval of atomic excitations, has resulted in generation of single photon pulses with controllable propagation direction, timing and pulse shapes [52, 53]. Concurrently, the experiments at Caltech [37, 131], have demonstrated non-classical photon pair creation and single photon production via conditional measurement of the light from optically thick atomic ensembles. Also noteworthy are experiments demonstrating coherent quantum state transfer between matter and light using optically thick atomic ensembles [114], and experiments on low-light level four-wave mixing in atomic ensembles using EIT [32].

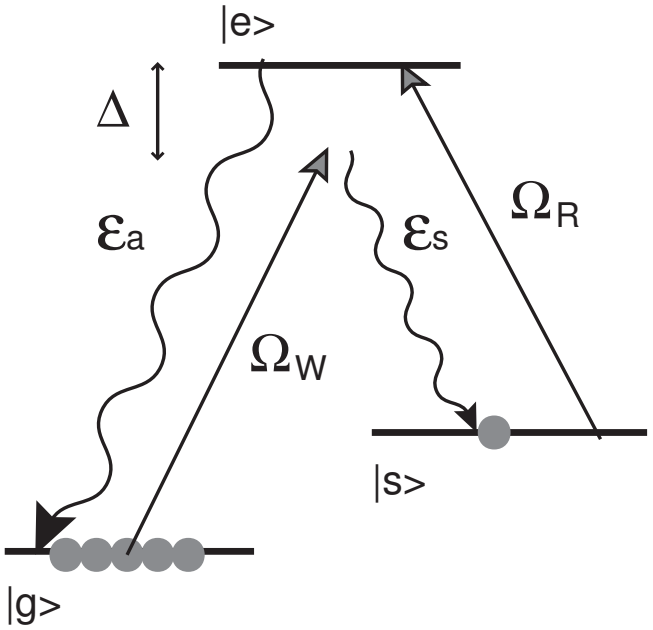

Figure 4.2: Atomic energy level configuration for preparation of nonclassical states of light and atoms via Ramam scattering.

The use of Raman scattering for nonclassical light generation can be understood qualitatively by considering three atomic states coupled by a pair of optical control fields in a "double-Λ" configuration (Fig. 4.2). A large ensemble of atoms is initially prepared in the ground state $|g\rangle$. Atomic spin excitations are produced via spontaneous Raman scattering [135], induced by an off-resonant control beam with Rabi frequency Ω_W and detuning Δ, which we refer to as the write beam. In this process, correlated pairs of frequency-shifted photons (so-called Stokes photons) and flipped atomic spins are created (corresponding to atomic Raman transitions into the state $|s\rangle$). Energy and momentum conservation ensure that for each Stokes photon emitted in a particular direction, there exists exactly one flipped spin quantum in a well-defined spin-wave mode. As a result, the number of spin-wave quanta and the number of photons in the Stokes field are strongly correlated. These atom-photon correlations closely resemble those between two electromagnetic field modes in parametric down-conversion [72, 78]

Thus, measurement of the Stokes photon number n_S ideally projects the spin-wave into a nonclassical collective state with n_S spin quanta [48]. After a controllable delay time τ_d, the stored spin-wave can be coherently converted into a light pulse by applying a second near-resonant laser beam with Rabi fequency Ω_R (retrieve laser), see Fig. 4.2. The physical mechanism for this retrieval process is identical to that employed in earlier stored light experiments [128, 111]. The direction, delay time τ_d, and rate of retrieval are determined by the direction, timing, and intensity of the retrieve laser, allowing control over the spatio-temporal properties of the retrieved pulse (referred to as the anti-Stokes pulse).

In the following, we present a quantum theory of Raman scattering, describing the Stokes field created in the process and the associated atomic excitation. We describe this interaction in three dimensions and show that an effective one-dimensional description can be used, under the conditions relevant for our experiments. Our theory describes spontaneous Raman scattering, which is an intrinsically quantum-mechanical process initiated by the quantum fluctuations of the vacuum field. In addition, our theory describes the retrieval process whereby the atomic excitation is coherently converted into a light pulse. By studying the three-dimensional theory of atomic state preparation and retrieval, we suggest an improved geometry for the experiments, designed to maximize the nonclassical correlations observed between Stokes and anti-Stokes photons. We also study the quantum correlations present under continuous-wave Raman excitation, and the dynamics of correlated photon pair creation and propagation through the atomic sample.

We then briefly highlight some of the experimental results obtained in our lab in this area. First, we present our measurements on continuous-wave Raman preparation and retrieval, in which nonclassical correlations were observed between the generated Stokes and anti-Stokes fields. We then present some of our more recent experimental results on pulsed preparation and retrieval of excitations with controllable, well-defined photon numbers, propagation direction, timing, and pulse shapes. Lastly, we describe ongoing experimental efforts using our new geometry for preparation and retrieval, and present initial results showing improvement of nonclassical correlations. Quantitative agreement with the experiments demonstrate the validity of our approach.

4.3 Quantum Description of Raman Scattering

Hamiltonian and equations of motion

We consider a medium of length L (volume V) consisting of N Λ-atoms interacting with one classical driving field (called the "write" field) of Rabi frequency $\Omega_W(\vec{r},t)e^{i\vec{k}_W\cdot\vec{r}}$ and a quantized field (the Stokes field) $\hat{E}_s(\vec{r},t)$, as shown in Fig. 4.3. When the write field corresponds to a focused beam, the Rabi frequency can be written as $\Omega_W(\vec{r},t) = \Omega_W(t)U(\vec{r})$, where $U(\vec{r})$ is the mode function of the field, such as a Hermite-Gaussian mode [149]. Both fields are propagating in the forward direction ($\vec{k}_W = k_W\hat{z}$), and we treat the propagation of the weak quantized field in the paraxial approximation (see appendix C for details).

Spontaneous Raman scattering [135] is induced by the weak, off-resonant laser beam with Rabi frequency Ω_W and detuning Δ. This two-photon process flips an atomic spin into the metastable state $|s\rangle$ while producing a correlated frequency-shifted photon (a so-called Stokes photon).

The Stokes electric field is thus given by $\hat{E}_s(\vec{r},t) = \sqrt{\frac{\hbar\omega_s}{2\epsilon_0 V}}\left[\hat{\mathcal{E}}_s(\vec{r},t)e^{i(\vec{k}_s\cdot\vec{r}-\omega_s t)} + \text{h.c.}\right]$, where $\hat{\mathcal{E}}_s(\vec{r},t)$ is a slowly varying envelope operator, and where $\omega_s = |\vec{k}_s|c$ ($\vec{k}_S = k_S\hat{z}$). The driving field Ω_W is detuned by Δ from the $|g\rangle \rightarrow |e\rangle$ transition frequency and the quantum field is detuned by $\delta = \omega_W - (\omega_s + \omega_{gs})$ from two-photon resonance.

To describe the quantum properties of the medium, we use the atomic operators [47]

$$\hat{\sigma}_{\mu\nu}(\vec{r},t) = \frac{1}{N_{\vec{r}}}\sum_{j=1}^{N_{\vec{r}}} |\mu_j\rangle\langle\nu_j| e^{-i\omega_{\mu\nu}t}, \tag{4.2}$$

where the sum is performed over a small but macroscopic volume containing $N_{\vec{r}} \gg 1$

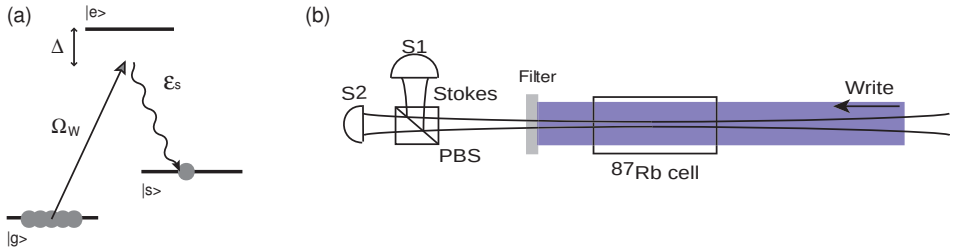

Figure 4.3: (a) Atomic level Λ-configuration for Raman scattering. (b) Co-propagating geometry for Raman Stokes scattering and detection of Stokes light in single transverse mode. The "write" beam is filtered out from the Stokes scattered light, which is then coupled to single mode fibers and photodetectors. Detection of a number n of Stokes photons projects the atomic state onto a state with n atomic excitations. In the limit of plane-wave "write" fields, detection of a Stokes photon projects the atomic excitation in a single transverse mode.

atoms around position $\vec{r}$. In the continuum limit, the collective atomic operators $\hat{\sigma}_{\mu\nu}(\vec{r},t)$ satisfy the commutation relations

$$\left[\hat{\sigma}_{\alpha\beta}(\vec{r},t),\hat{\sigma}_{\mu\nu}(\vec{r'},t)\right] = \frac{V}{N}\delta(\vec{r}-\vec{r'})\left(\delta_{\beta\mu}\hat{\sigma}_{\alpha\nu}(\vec{r},t)-\delta_{\nu\alpha}\hat{\sigma}_{\mu\beta}(\vec{r},t)\right) \tag{4.3}$$

while the slowly varying electric field operator $\hat{\mathcal{E}}_s(\vec{r},t)$ obeys the commutation relations

$$\left[\hat{\mathcal{E}}_s(\vec{r},t),\hat{\mathcal{E}}_s^{\dagger}(\vec{r'},t)\right] = V\delta(\vec{r}_\perp-\vec{r'}_\perp)\delta\left[z-z'-c(t-t')\right], \tag{4.4}$$

where $\vec{r_\perp} = (x,y)$. The atomic operators obey Heisenberg-Langevin equations of motion [59]

$$\partial_t\hat{\sigma}_{\mu\nu} = -\gamma_{\mu\nu}\hat{\sigma}_{\mu\nu}-(i/\hbar)\left[\hat{\sigma}_{\mu\nu},\hat{H}\right]+\hat{F}_{\mu\nu}(\vec{r},t) \tag{4.5}$$

where $\hat{F}_{\mu\nu}(\vec{r},t)$ are Langevin "noise forces" associated with the decay terms $-\gamma_{\mu\nu}\hat{\sigma}_{\mu\nu}$. They have zero average and are delta correlated, with correlation coefficients that can be found from the Einstein relations [59]. This provides a complete and rigorous

treatment of dissipation and the associated fluctuations of the atomic medium, such that all commutation relations of atomic and field operators are preserved during time evolution and spatial propagation [47].

In the undepleted pump approximation (i.e., we assume the scattering process does not substantially deplete the write field, so that its Rabi frequency is unchanged), the interaction hamiltonian is, in a rotating frame,

$$\hat{H} = \frac{N}{V}\int d\vec{r}\left\{\Delta\hat{\sigma}_{ee} - \delta\hat{\sigma}_{ss} - \left[g\hat{\mathcal{E}}_s e^{i\vec{k}_s\cdot\vec{r}}\hat{\sigma}_{es} + \Omega_W e^{i\vec{k}_W\cdot\vec{r}}\hat{\sigma}_{eg} + \text{h.c.}\right]\right\} \quad (4.6)$$

where $g = \wp\sqrt{\frac{\omega_{es}}{2\hbar\epsilon_0 V}}$ is the atom-field coupling constant, $\wp$ being the dipole moment of the $e-s$ transition, N the number of atoms and V the quantization volume. For simplicity, and without loss of generality, we consider g to be purely real.

In the following, we study the growth of the Stokes field due to spontaneous Raman scattering [136], when the initiation is due to the vacuum fluctuations of the Stokes field. We assume the Stokes field amplitude is at all times much smaller than that of the classical driving field and we only keep terms that are linear in $\hat{\mathcal{E}}_s$ in the atomic equations of motion. In addition, we assume that the atomic medium is initially optically pumped to state $|g\rangle$ and the number of atoms scattered to $|s\rangle$ is at all times much smaller than N, so that we may put $\sigma_{gg} \simeq 1 \gg \sigma_{ee,ss}$.

The propagating quantized field obeys the equation of motion (see appendix C for a detailed derivation of this equation)

$$\left(\frac{\partial}{\partial t} + c\frac{\partial}{\partial z} - i\frac{c\nabla_\perp^2}{2k_s}\right)\hat{\mathcal{E}}_s(\vec{r},t) = igN\hat{\sigma}_{se}(\vec{r},t)e^{-i\vec{k}_s\cdot\vec{r}} \quad (4.7)$$

and the atomic variables obey (assuming $\sigma_{gg} \simeq 1$), to first order in the quantized field

$\hat{\mathcal{E}}_s$

$$\partial_t \hat{\sigma}_{se} = -(\gamma + i\Delta - i\delta)\hat{\sigma}_{se} + i\Omega_W e^{i\vec{k}_W\cdot\vec{r}}\hat{\sigma}_{sg} + \hat{F}_{se} \tag{4.8}$$

$$\partial_t \hat{\sigma}_{sg} = -(\gamma_0 + i\delta)\hat{\sigma}_{sg} + i\Omega_W^* e^{-i\vec{k}_W\cdot\vec{r}}\hat{\sigma}_{se} - ig\hat{\mathcal{E}}_s e^{i\vec{k}_s\cdot\vec{r}}\hat{\sigma}_{eg} + \hat{F}_{sg} \tag{4.9}$$

$$\partial_t \hat{\sigma}_{eg} = -(\gamma - i\Delta)\hat{\sigma}_{eg} - i\Omega_W^* e^{-i\vec{k}_W\cdot\vec{r}}\hat{\sigma}_{gg} + \hat{F}_{eg}. \tag{4.10}$$

For simplicity we assume the excited state $|e\rangle$ decays with rate γ towards $|g\rangle$ and with rate γ towards $|s\rangle$, and the coherence σ_{gs} decays with rate γ_0, e.g., due to collisions. The detuning Δ is assumed to be large, in particular $\Delta \gg |\Omega_W|, \gamma, \delta$, so that we can adiabatically eliminate [147] the optical coherences σ_{ge} and σ_{es}, and obtain

$$\hat{\sigma}_{se} \simeq \frac{\Omega_W}{\Delta}\left(1 + i\frac{\gamma}{\Delta}\right)e^{i\vec{k}_w\cdot\vec{r}}\sigma_{sg} \tag{4.11}$$

$$\hat{\sigma}_{eg} \simeq \frac{\Omega_W^*}{\Delta}e^{-i\vec{k}_W\cdot\vec{r}} + \frac{i}{\Delta}\hat{F}_{eg}. \tag{4.12}$$

Substituting these results in the remaining atomic equation of motion for $\hat{\mathcal{S}} \equiv \sqrt{N}\hat{\sigma}_{gs}e^{-i\Delta\vec{K}\cdot\vec{r}}$, and the Stokes field $\hat{\mathcal{E}}_s$, we find

$$\left(\frac{\partial}{\partial t} + c\frac{\partial}{\partial z} - i\frac{c\nabla_\perp^2}{2k_s}\right)\hat{\mathcal{E}}_s(\vec{r},t) = i\chi\hat{\mathcal{S}}^\dagger \tag{4.13a}$$

$$\partial_t\hat{\mathcal{S}}^\dagger = -(\gamma_S + i\delta_S)\hat{\mathcal{S}}^\dagger - i\chi^*\hat{\mathcal{E}}_s + \hat{F}_S^\dagger(\vec{r},t) \tag{4.13b}$$

where $\Delta\vec{K} = \vec{k}_W - \vec{k}_s$, $\delta_S = \delta + \delta_L$ with $\delta_L = |\Omega_W|^2/\Delta$ being the light shift, $\gamma_S = \gamma_L + \gamma_0$ with $\gamma_L = \gamma\frac{|\Omega_W|^2}{\Delta^2}$ the optical pumping rate, and $\hat{F}_S^\dagger$ is the noise force associated with the decay terms $-\gamma_S\hat{\mathcal{S}}^\dagger$. Finally, $\chi(\vec{r},t) = \frac{g\sqrt{N}\Omega_W(\vec{r},t)}{\Delta}$ is the effective coupling rate between the collective "spin" excitation $\hat{\mathcal{S}}$ and the Stokes field $\hat{\mathcal{E}}_s$.

Equations 4.13 describe the coupling of the Stokes field $\hat{\mathcal{E}}_s$ to the atomic spin wave $\hat{\mathcal{S}}^\dagger$, and the propagation of the generated field through the atomic sample. The fact

that a field annihilation operator $\hat{\mathcal{E}}_s$ is coupled to an atomic creation operator $\hat{\mathcal{S}}^\dagger$ indicates that in the Raman scattering process, a pump photon is destroyed while both a Stokes photon and an atomic spin-flip is created (i.e., originating from a term $\propto \hat{\mathcal{E}}_s^\dagger \hat{\mathcal{S}}^\dagger$ is the effective Hamiltonian). This is reminiscent of nonlinear optical processes such as non-degenerate Optical Parametric Amplification (OPA) [162] in which a pump photon of frequency ω_P is absorbed while two photons of frequency ω_s (the "signal" photon) and ω_i (the "idler" photon) are created. Energy conservation implies that $\omega_P = \omega_s + \omega_i$. Energy and momentum conservation ensure that for each Stokes photon emitted in certain direction there exists exactly one flipped spin quantum in a well-defined spin-wave mode. The number of spin wave quanta and the number of photons in the Stokes field thus exhibit strong correlations, analogous to the correlations between photons emitted in parametric down conversion [151].

The noise force $\hat{F}_S(\vec{r},t)$ has correlations

$$\langle \hat{F}_S(\vec{r},t)\hat{F}_S^\dagger(\vec{r'},t')\rangle = 2\gamma_S V\delta(\vec{r}-\vec{r'})\delta(t-t') \tag{4.14}$$

$$\langle \hat{F}_S^\dagger(\vec{r},t)\hat{F}_S(\vec{r'},t')\rangle = 0 \tag{4.15}$$

and the commutation relations for the spin wave are

$$\left[\hat{\mathcal{S}}(\vec{r},t),\hat{\mathcal{S}}^\dagger(\vec{r'},t)\right] = V\delta(\vec{r}-\vec{r'}). \tag{4.16}$$

4.4 Three-dimensional Theory of Raman Scattering

In the experiments [52], Stokes photons are coupled to single mode fibers and detected on photodetectors. Thus, the Stokes field is approximately projected on a set

of Hermite-Gaussian modes whose beam waist is determined by optical collimation before coupling to the fiber. Moreover, the write field mode function $U(\vec{r})$ can be approximated by another Hermite-Gaussian mode (whose waist does not necessarily correspond to the waist of the detected Stokes mode).

Writing out the mode function $U(\vec{r})$ explicitely, and letting $\chi_0(t) = \frac{g\sqrt{N}\Omega_W(t)}{\Delta}$, we have the coupled spin-wave and Stokes field equations

$$\left(c\frac{\partial}{\partial z'} - i\frac{c\nabla_\perp^2}{2k_s}\right)\hat{\mathcal{E}}_s(\vec{r'},t') = i\chi_0(t')U(\vec{r'})\hat{\mathcal{S}}^\dagger \quad , \quad (4.17a)$$

$$\partial_{t'}\hat{\mathcal{S}}^\dagger = -(\gamma_S + i\delta_S)\hat{\mathcal{S}}^\dagger - i\chi_0(t')U^*(\vec{r'})\hat{\mathcal{E}}_s + \hat{F}_S^\dagger(\vec{r'},t') \quad , \quad (4.17b)$$

where we have used the moving coordinates $t' = t - z/c$, $z' = z$, and we assume $\chi_0(t')$ depends only on t'.

Hermite-Gaussian mode expansion

Let the Hermite-Gaussian modes [149] be $U_{nm}(x,y,z) = u_n(x,z)u_m(y,z)$, where

$$\begin{aligned} u_n(x,z) &= (2/\pi)^{1/4}\sqrt{\frac{\exp[-i(2n+1)\psi(z)]}{2^n n! w(z)}}H_n(\sqrt{2}x/w(z)) \\ &\times \exp[-ikx^2/(2R(z)) - x^2/w^2(z)]. \end{aligned} \quad (4.18)$$

The beam waist is $w(z) = w_0\sqrt{1+(z/z_R)^2}$, the radius of curvature $R(z) = z + z_R^2/z$, and the phase shift is $\psi(z) = \arctan(z/z_R)$, where the Rayleigh range is defined as $z_R = \pi w_0^2/\lambda$. The Hermite-Gaussian modes are eigenfunctions of the paraxial equation,

$$[\nabla_\perp^2 + 2ik_0\partial_z]U_{nm}(x,y,z) = 0, \quad (4.19)$$

so that the vacuum field can be written as

$$\hat{\mathcal{E}}(\vec{r},t) = \sum_{nm} \hat{\mathcal{E}}_{nm}(z,t)U_{nm}(z,\vec{r}_\perp), \tag{4.20}$$

with the commutation relations

$$\left[\hat{\mathcal{E}}_{nm}(z,t),\hat{\mathcal{E}}^\dagger_{kl}(z',t')\right] = \delta_{nk}\delta_{ml}V\delta\left[z-z'-c(t-t')\right]. \tag{4.21}$$

Using the completeness relation $\sum_{nm} U^*_{nm}(z,\vec{r}_\perp)U_{nm}(z,\vec{r'}_\perp) = \delta(\vec{r}_\perp - \vec{r'}_\perp)$, we recover the paraxial commutation relations 4.4.

We now expand the Stokes field and the spin wave using Hermite-Gaussian mode functions

$$\hat{\mathcal{E}}_s(\vec{r'},t') = \sum_{nm} \hat{\mathcal{E}}_{s,nm}(z',t')U_{nm}(\vec{r'}), \tag{4.22}$$

$$\hat{\mathcal{S}}^\dagger(\vec{r'},t') = \sum_{nm} \hat{\mathcal{S}}^\dagger_{nm}(z',t')U_{nm}(\vec{r'}), \tag{4.23}$$

so that the equations of motion now become

$$c\partial_{z'}\hat{\mathcal{E}}_{s,nm} = i\chi_0 \sum_{lk} M_{nm,lk}(z')\hat{\mathcal{S}}^\dagger_{lk} \tag{4.24a}$$

$$\partial_{t'}\hat{\mathcal{S}}^\dagger_{lk} = -\Gamma_0\hat{\mathcal{S}}^\dagger_{lk} - \Gamma_L\sum_{nm} A_{lk,nm}\hat{\mathcal{S}}^\dagger_{nm} - i\chi_0\sum_{nm} M^*_{nm,lk}\hat{\mathcal{E}}_{s,nm} + \hat{F}^\dagger_{S,lk} \tag{4.24b}$$

where $\Gamma_0 = \gamma_0 - i\delta$, and $\Gamma_L = \gamma\frac{|\Omega_W|^2}{\Delta^2} - i\frac{|\Omega_W|^2}{\Delta}$, and

$$M_{nm,lk}(z') = \int d\vec{r}_\perp U^*_{nm}UU_{lk} \tag{4.25}$$

$$A_{nm,lk} = \int d\vec{r}_\perp U^*_{nm}|U|^2U_{lk}. \tag{4.26}$$

When the "write" field mode can be considered constant on the scale of the beam waist of the Stokes and spin wave modes, we obtain an effective one-dimensional model since $M_{nm,lk}, A_{nm,lk} \to \delta_{nl}\delta_{mk}$. This situation is realized when the "write"

beam waist is much larger than the Stokes beam waist, and yields the effective theory

$$c\partial_{z'}\hat{\mathcal{E}}_{s,nm} = i\chi_0\hat{\mathcal{S}}^\dagger_{nm} \tag{4.27a}$$

$$\partial_{t'}\hat{\mathcal{S}}^\dagger_{nm} = -\Gamma_S\hat{\mathcal{S}}^\dagger_{nm} - i\chi_0\hat{\mathcal{E}}_{s,nm} + \hat{F}^\dagger_{S,nm}, \tag{4.27b}$$

where $\Gamma_S = \gamma_S + i\delta_S$.

The active volume participating in the Raman scattering process is defined by the Stokes mode. Since by construction the shape of the active atomic volume is matched to the Stokes Hermite-Gaussian mode, its Fresnel number $\mathcal{F} = \frac{\pi w(0)^2}{\lambda L}$ is equal to 1 (where L is the length of the atomic sample, $w(0)$ is the Stokes beam waist at the center of the cell, and λ is the Stokes photon wavelength). This is the regime of "pencil-shaped" atomic samples, for which it is well-known that a one-dimensional theory is justified when $\mathcal{F} \simeq 1$ [136].

The general case of Raman scattering when the gain profile is transversely dependent [126] (i.e., not the plane-wave limit considered here) leads to many interesting effects such as gain-guiding and excess noise [42, 17, 163], which we will not consider here.

4.5 Dynamics: One-dimensional Model

We consider a single Hermite-Gaussian mode coupled $\hat{\mathcal{E}}_{s,nm}$ to the corresponding spin-wave $\hat{\mathcal{S}}^\dagger_{nm}$, for which the equations of motion are (dropping subscripts for ease

of notation)

$$c\partial_{z'}\hat{\mathcal{E}} = i\chi\hat{\mathcal{S}}^\dagger \tag{4.28a}$$

$$\partial_{t'}\hat{\mathcal{S}}^\dagger = -\Gamma_S\hat{\mathcal{S}}^\dagger - i\chi\hat{\mathcal{E}} + \hat{F}_S^\dagger. \tag{4.28b}$$

Solution to equations of motion

To solve the equations of motion we first Laplace transform the Stokes field equation ($\partial_{z'} \to s$)

$$\mathcal{E}(s,t') = \frac{1}{s}\left[\mathcal{E}(z'=0,t') + i\chi/c\mathcal{S}^\dagger\right] \tag{4.29}$$

and plug it in the spin wave equation to get

$$\partial_{t'}\mathcal{S}^\dagger(s,t') = [\frac{\chi(t')^2}{cs} - \Gamma_S(t')]\mathcal{S}^\dagger - i\frac{\chi(t')}{s}\mathcal{E}(0,t') + F_S^\dagger(s,t'). \tag{4.30}$$

The last equation is easily integrated to give

$$\begin{aligned}
\mathcal{S}^\dagger(s,t') &= e^{\frac{g(t')}{cs}-\Gamma(t')}\mathcal{S}^\dagger(s,0) + \int_0^{t'} e^{\frac{g(t')-g(t'')}{cs}-[\Gamma(t')-\Gamma(t'')]}[F_S^\dagger(s,t'') - i\frac{\chi(t'')}{s}\mathcal{E}(0,t'')]dt'' \\
\mathcal{E}(s,t') &= i\frac{\chi(t')}{cs}\left\{e^{\frac{g(t')}{cs}-\Gamma(t')}\mathcal{S}^\dagger(s,0) + \int_0^{t'} e^{\frac{g(t')-g(t'')}{cs}-[\Gamma(t')-\Gamma(t'')]}[F_S^\dagger(s,t'') - i\frac{\chi(t'')}{s}\mathcal{E}(0,t'')]dt''\right\} \\
&+ \frac{\mathcal{E}(0,t')}{s}.
\end{aligned} \tag{4.31}$$

where $g(t') = \int_0^{t'}\chi(t'')^2dt''$ and $\Gamma(t') = \int_0^{t'}\Gamma_S(t'')dt''$.

We can perform the inverse Laplace transforms, using that $\mathcal{L}^{-1}[e^{a/s}] = \delta(z) + \sqrt{\frac{a}{z}}I_1(2\sqrt{az})$, $\mathcal{L}^{-1}[(1/s)e^{a/s}] = I_0(2\sqrt{az})$ and $\mathcal{L}^{-1}[(1/s^2)e^{a/s}] = \sqrt{\frac{z}{a}}I_1(2\sqrt{az})$, where $I_n(x)$ denotes the modified Bessel function of the first kind of order n.

The solution is

$$\begin{aligned}
\mathcal{S}^\dagger(z',t') &= e^{-\Gamma(t')}\mathcal{S}^\dagger(z',0) + \int_0^{t'} e^{-[\Gamma(t')-\Gamma(t'')]}F_S^\dagger(z',t'')dt'' \\
&- i\int_0^{t'} \chi(t'')e^{-[\Gamma(t')-\Gamma(t'')]}H(z',0,t',t'')\mathcal{E}(0,t'')dt'' \\
&+ e^{-\Gamma(t')}\int_0^{z'} G_s(z',z'',t',0)\mathcal{S}^\dagger(z'',0)dz'' \\
&+ \int_0^{t'} e^{-[\Gamma(t')-\Gamma(t'')]}\int_0^{z'} G_s(z',z'',t',t'')F_S^\dagger(z'',t'')dz''dt'' \qquad (4.32) \\
\mathcal{E}(z',t') &= \mathcal{E}(0,t') + i(\chi(t')/c)e^{-\Gamma(t')}\int_0^{z'} H(z',z'',t',0)\mathcal{S}^\dagger(z'',0)dz'' \\
&+ i(\chi(t')/c)\int_0^{t'} e^{-[\Gamma(t')-\Gamma(t'')]}\int_0^{z'} H(z',z'',t',t'')F_S^\dagger(z'',t'')dz''dt'' \\
&+ (\chi(t')/c)\int_0^{t'} \chi(t'')e^{-[\Gamma(t')-\Gamma(t'')]}G_e(z',0,t',t'')\mathcal{E}(0,t'')dt'' \qquad (4.33)
\end{aligned}$$

where

$$\begin{aligned}
H(z',z'',t',t'') &= I_0(2\sqrt{[g(t')-g(t'')][z'-z'']/c}) \\
G_s(z',z'',t',t'') &= \sqrt{\frac{g(t')-g(t'')}{c(z'-z'')}}I_1(2\sqrt{[g(t')-g(t'')][z'-z'']/c}) \\
G_e(z',z'',t',t'') &= \frac{c(z'-z'')}{g(t')-g(t'')}G_s(z',z'',t',t''). \qquad (4.34)
\end{aligned}$$

This is the solution of Raymer *et al.* [136], for pencil-shaped atomic samples. It allows us to calculate all expectation values and correlation functions of the field and atomic operators. In particular, we will study here the mean Stokes intensity and the mean number of spin-flips in the atomic sample as a function of time.

For simplicity, we assume in the following that the pump field is switched on suddenly at $t = 0$, i.e., $\Omega(t) = \Omega\theta(t)$, $\delta = -\delta_L$ so that $\Gamma_S = \gamma_S$ and also assume $\gamma_0 = 0$ so that $\gamma_S = \gamma_L = \gamma\frac{\Omega^2}{\Delta^2}$. The growth rate of atomic and Stokes excitations is $g(t)L/c = \frac{|\chi|^2 tL}{c} = \frac{g^2N}{\gamma c/L}\gamma_S t$, i.e., it is equal to the optical depth $\frac{g^2N}{\gamma c/L} = \frac{3}{4\pi}(N/V)\lambda^2 L \equiv$

$d_0 \gg 1$ times $\gamma_S t$ (optical pumping rate times time). For optically thick atomic samples ($d_0 \gg 1$, which is very easy to achieve at room temperature or for cold atomic samples), we thus find that there is a "collective" enhancement of the rate at which excitations are created in the sample $d_0\gamma_S$, as compared to the single atom scattering rate γ_S.

The photon flux at the end of the atomic cell (number of photons per unit area per unit time) is given by $I_s(t) = \frac{c}{V}\langle \mathcal{E}^\dagger(L,t)\mathcal{E}(L,t)\rangle$, while the total number of spins flipped in the cell is $N_s(t) = \frac{1}{V}\int_0^L \langle \mathcal{S})^\dagger(z,t)\mathcal{S}(z,t)\rangle dz$. Fig. 4.4 shows the photon flux at time t, and the number of photons and spin flips up to time t, when the optical depth is $d_0 = 10$.

At short times $d_0\gamma_S t \ll 1$, we have the spontaneous regime of Raman scattering, where the mean number of emitted Stokes photons is very small $\ll 1$. The probability of Stokes emission is very small and the photon flux is very nearly constant (i.e., a Stokes photon could be emitted at any time). At longer times, when $d_0\gamma_S t \gtrsim 1$, we enter the stimulated regime of Raman scattering. The mean number of emitted Stokes photons is now significant ($\gtrsim 1$). Since emission of a Stokes photon is accompanied by a flipped atomic spin, the subsequent probability of Stokes emission is increased by Bose stimulation due to the presence of flipped spin, resulting in a photon flux that increases very fast as time increases. Note that for times such that $\gamma_S t \lesssim d_0$, the number of emitted Stokes photons precisely equals the number of flipped spins (as shown in Fig. 4.4), as expected for the strongly correlated atom-photon excitations produced in Raman scattering. It is only once $\gamma_S t \gtrsim d_0$ that the atomic spin decay (the $-\gamma_S \hat{\mathcal{S}}^\dagger$ term in 4.28) leads to a steady-state mean number of flipped atomic spins

and a steady-state photon flux. This determines the maximum amplification factor of the atomic ensemble when used as a continuous-wave Raman amplifier.

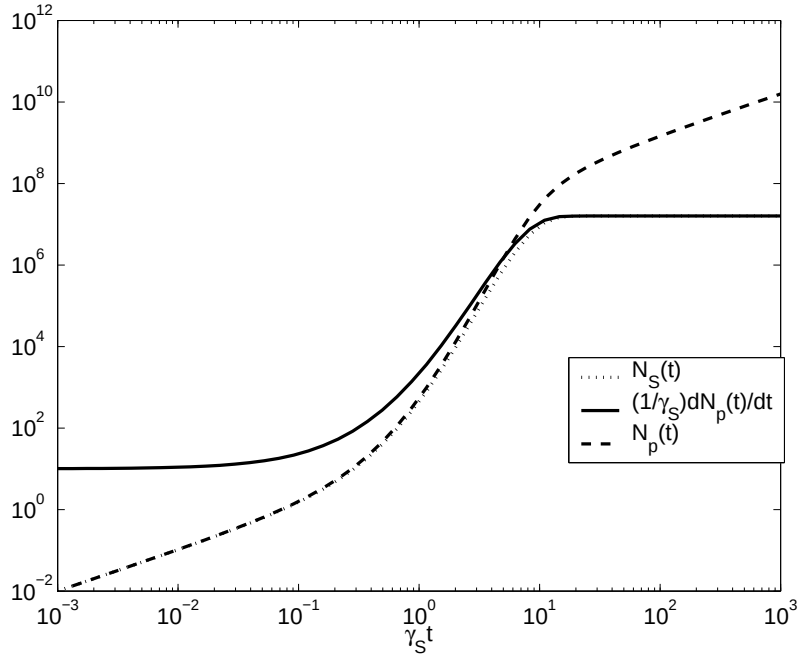

Figure 4.4: Number of flipped spins $N_S(t)$, number of photons $N_p(t)$ emitted in $[0, t]$, and rate of photon emission $(1/\gamma_S)\frac{dN_p(t)}{dt}$ versus $\gamma_S t$, for an optical depth $d_0 = 10$. Note the spontaneous regime for $\gamma_S t \lesssim 1/d_0 = 10^{-1}$, the stimulated transient regime for $1/d_0 \lesssim \gamma_S t \lesssim d_0 = 10$, and the steady-state regime for $\gamma_S t \gtrsim d_0 = 10$.

4.5.1 Transient regime

In this section, we study the transient regime of Raman scattering, i.e., for times such that $\gamma_S t \lesssim d_0$. Note that a large number of Stokes photons can be emitted while still in the transient regime, when the optical depth is large. In the experiments [52], weak pulses of Stokes light are generated corresponding to mean numbers of photons ranging from very small $\ll 1$ to a few. Typical values of the resonant optical depth

in such experiments are $d_0 = 10 - 20$.

In the transient regime, the atomic spin-wave decay and the associated noise source can be ignored, leading to the simplified equations of motion

$$c\partial_{z'}\hat{\mathcal{E}} = i\chi\hat{\mathcal{S}}^\dagger \tag{4.35a}$$

$$\partial_{t'}\hat{\mathcal{S}}^\dagger = -i\chi\hat{\mathcal{E}} \quad , \tag{4.35b}$$

and the simplified solution (only terms contributing to normally-ordered expectation values are written)

$$\mathcal{S}^\dagger(z',t') = -i\int_0^{t'} \chi(t'')H(z',0,t',t'')\mathcal{E}(0,t'')dt'' \tag{4.36}$$

$$\mathcal{E}(z',t') = i(\chi(t')/c)\int_0^{z'} H(z',z'',t',0)\mathcal{S}^\dagger(z'',0)dz''. \tag{4.37}$$

We use these expressions in the formula for the photon flux $I_s(t) = \frac{c}{L}\langle\mathcal{E}^\dagger(L,t)\mathcal{E}(L,t)\rangle$, and the number of flipped spins $N_s(t) = \frac{1}{L}\int_0^L\langle\mathcal{S})^\dagger(z,t)\mathcal{S}(z,t)\rangle dz$. The number of flipped spins at position z is

$$\begin{aligned} n_S(z,t) &= \langle\mathcal{S}^\dagger(z,t)\mathcal{S}(z,t)\rangle = \int_0^{d_0\gamma_S t} dx\; I_0(2\sqrt{x\frac{z}{L}})^2 \\ &= d_0\gamma_S t\left[I_0(2\sqrt{d_0\gamma_S t\frac{z}{L}})^2 - I_1(2\sqrt{d_0\gamma_S t\frac{z}{L}})^2\right] \end{aligned} \tag{4.38}$$

and the total number of flipped spins is

$$\begin{aligned} N_S(t) &= \frac{1}{L}\int_0^L dz\; n_S(z,t) \\ &= d_0\gamma_S t\left[I_0(2\sqrt{d_0\gamma_S t})^2 - 2I_1(2\sqrt{d_0\gamma_S t})^2 + I_0(2\sqrt{d_0\gamma_S t})I_2(2\sqrt{d_0\gamma_S t})\right]. \end{aligned} \tag{4.39}$$

Fig. 4.5 shows the spin flip density as a function of position through the atomic sample, for various corresponding total numbers of spin flips. When the total number

of flipped spins is $\gtrsim 1$, the spin flip density becomes larger towards the latter part of the atomic sample. This indicates that Bose stimulation causes the probability of Stokes emission (and of flipping an atomic spin) to grow as the field propagates through the atomic sample.

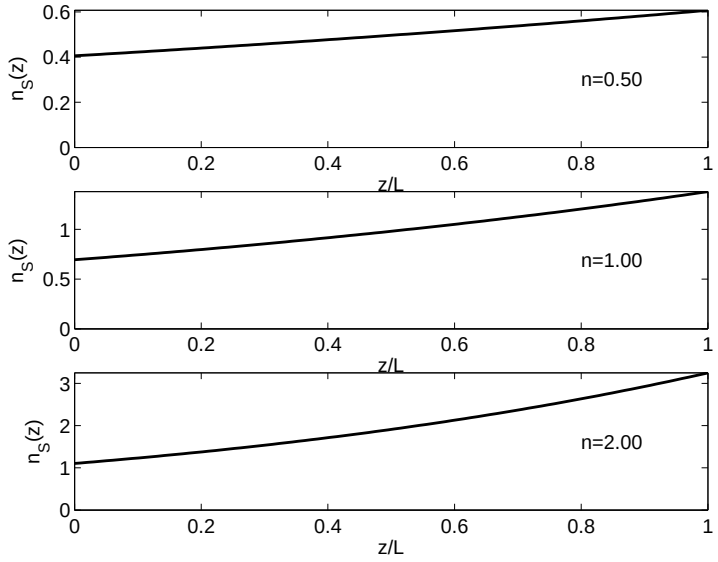

Figure 4.5: Spin flip density $n_S(z)$ in transient high-gain regime, corresponding to a total number of Stokes photons $n = 0.5$, $n = 1$, and $n = 2$.

The Stokes photon flux is

$$\frac{dN_p}{dt}(t) = \frac{c}{L}\langle \mathcal{E}^\dagger(L,t)\mathcal{E}(L,t)\rangle = d_0\gamma_S \left[I_0(2\sqrt{d_0\gamma_S t})^2 - I_1(2\sqrt{d_0\gamma_S t})^2 \right] \quad (4.40)$$

and the total number of photons emitted in $[0,t]$ is

$$\begin{aligned} N_p(t) &= \int_0^t dt' \frac{dN_p}{dt'}(t') \\ &= d_0\gamma_S t \left[I_0(2\sqrt{d_0\gamma_S t})^2 - 2I_1(2\sqrt{d_0\gamma_S t})^2 + I_0(2\sqrt{d_0\gamma_S t}) I_2(2\sqrt{d_0\gamma_S t}) \right] \\ &= N_S(t). \end{aligned} \quad (4.41)$$

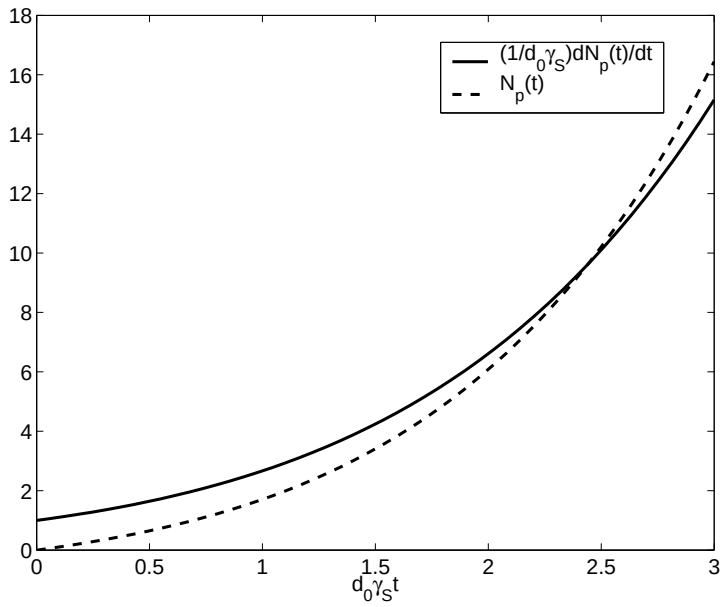

Figure 4.6: Number of photons $N_p(t)$ emitted in $[0, t]$, and rate of photon emission $(1/d_0\gamma_S)\frac{dN_p(t)}{dt}$ versus $d_0\gamma_S t$, in the high-gain transient regime ($\gamma_S t \ll d_0$).

We see that in the transient regime, the number of flipped spins exactly equals the number of Stokes photons emitted.

Given the mean number of photons contained in a pulse, the theoretical pulse shape can be compared to experimental data, as was done in [52] (see also highlights in section 4.8.2). The agreement is excellent, with the fitting parameters determined from experimental data (mean photon number and detection efficiency).

For large values of $d_0\gamma_S t$ (but small enough that the transient regime applies), we find the asymptotic expression for the number of excitations

$$N_S(t) \quad \sim \quad \frac{3}{16\pi} e^{4\sqrt{d_0\gamma_S t}} \tag{4.42}$$

which shows the unusual growth as $\exp[\sqrt{d_0\gamma_S t}]$ in the transient regime [135].

High-gain transient and steady-state regime

Taking into account the atomic spin-flip decay term and the associated fluctuating noise force in 4.27, we find the number of flipped spins at position z is

$$n_S(z,t) = \langle \mathcal{S}^\dagger(z,t)\mathcal{S}(z,t)\rangle = d_0 \int_0^{\gamma_S t} dx\, e^{-2x} I_0(2\sqrt{d_0 x \frac{z}{L}})^2 \tag{4.43}$$

and the total number of flipped spins is

$$\begin{aligned} N_S(t) &= \frac{1}{L}\int_0^L dz n_S(z,t) \\ &= d_0 \int_0^{\gamma_S t} dx\, e^{-2x}\left[I_0(2\sqrt{d_0 x})^2 - I_1(2\sqrt{d_0 x})^2\right]. \end{aligned} \tag{4.44}$$

The number of photons per unit time passing through the cell area is

$$\begin{aligned} \frac{dN_p}{dt}(t) &= \frac{c}{L}\langle \mathcal{E}^\dagger(L,t)\mathcal{E}(L,t)\rangle \\ &= d_0\gamma_S\left\{e^{-2\gamma_S t}\left[I_0(2\sqrt{d_0\gamma_S t})^2 - I_1(2\sqrt{d_0\gamma_S t})^2\right]\right. \\ &\quad \left. +2\int_0^{\gamma_S t} dx\, e^{-2x}\left[I_0(2\sqrt{d_0 x})^2 - I_1(2\sqrt{d_0 x})^2\right]\right\} \end{aligned} \tag{4.45}$$

and the total number of photons emitted in $[0,t]$ is

$$\begin{aligned} N_p(t) &= \int_0^t dt' \frac{dN_p}{dt'}(t') \\ &= d_0\int_0^{\gamma_S t} dx\, \left\{e^{-2x}\left[I_0(2\sqrt{d_0 x})^2 - I_1(2\sqrt{d_0 x})^2\right]\right. \\ &\quad \left. +2\int_0^x dy\, e^{-2y}\left[I_0(2\sqrt{d_0 y})^2 - I_1(2\sqrt{d_0 y})^2\right]\right\} \\ &= N_S(t) + 2d_0\int_0^{\gamma_S t} dx\, \int_0^x dy\, e^{-2y}\left[I_0(2\sqrt{d_0 y})^2 - I_1(2\sqrt{d_0 y})^2\right]. \end{aligned} \tag{4.46}$$

In the steady-state limit, the number of flipped spins at position z is

$$n_S(z, t\to\infty) = \frac{d_0}{2} e^{d_0 z/L} I_0(d_0 z/L) \tag{4.47}$$

and the total number of flipped spins is

$$N_S(t \to \infty) \;=\; \frac{d_0}{2} e^{d_0} \left[I_0(d_0) - I_1(d_0) \right]. \tag{4.48}$$

The number of photons emitted per unit time goes to the steady-state value

$$\frac{dN_p}{dt}(t \to \infty) \;=\; d_0 \gamma_S e^{d_0} \left[I_0(d_0) - I_1(d_0) \right] \tag{4.49}$$

which in the limit $d_0 \gg 1$ becomes [135]

$$\frac{dN_p}{dt}(t \to \infty) \;\sim\; \frac{\gamma_S}{2\sqrt{\pi}} \frac{e^{2d_0}}{\sqrt{2d_0}}. \tag{4.50}$$

4.6 Retrieval of Stored Atomic Excitation

Hamiltonian and equations of motion

We consider the same medium of length L consisting of N Λ-atoms. The atoms are now interacting with a classical driving field Ω_R (the "retrieve" field) tuned close to resonance and a quantized field $\hat{\mathcal{E}}_a$. The driving field Ω_R is tuned on resonance with the $|s\rangle \to |e\rangle$ transition frequency and the quantum field $\hat{\mathcal{E}}_a$ is on two-photon resonance, as shown in Fig. 4.7.

Initially, the medium contains an atomic excitation in the form of a spin wave $\mathcal{S}(z,0) = \sqrt{N}\sigma_{gs}(z,0)$ with N_s flipped spins. This excitation is prepared via Raman scattering and detection of a number N_s of Stokes photons by e.g. a photocounting module.

In an effective one-dimensional description (as before valid for pencil-shaped atomic

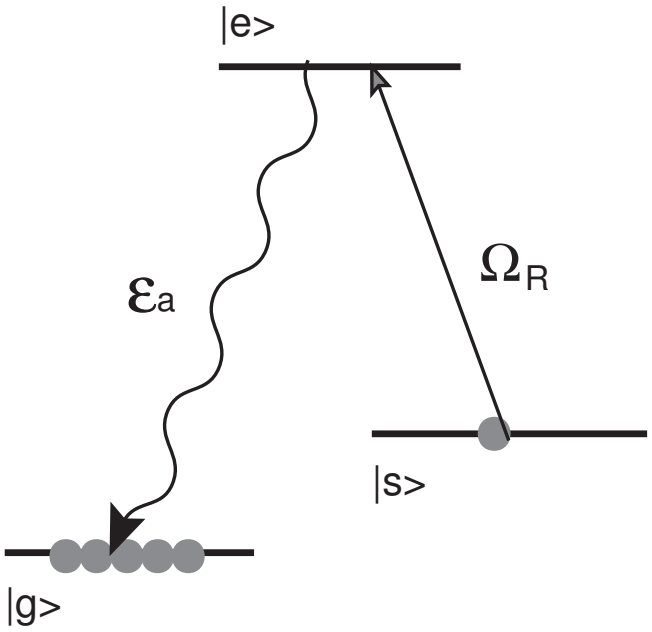

Figure 4.7: Atomic level Λ-configuration for retrieval of stored atomic excitation via Electromagnetically Induced Transparency.

samples), the corresponding equations of motion are

$$(\partial_t + c\partial_z)\hat{\mathcal{E}}_a(z,t) = ig\sqrt{N}\hat{\mathcal{P}} \tag{4.51a}$$

$$\partial_t\hat{\mathcal{P}} = -\gamma\hat{\mathcal{P}} + i\Omega_R\hat{\mathcal{S}} + ig\sqrt{N}\hat{\mathcal{E}}_a + \hat{F}_P \tag{4.51b}$$

$$\partial_t\hat{\mathcal{S}} = -\gamma_S\hat{\mathcal{S}} + i\Omega_R\hat{\mathcal{P}} + \hat{F}_S \tag{4.51c}$$

where $\hat{\mathcal{P}} = \sqrt{N}\hat{\sigma}_{ge}$ and $\hat{\mathcal{S}} = \sqrt{N}\hat{\sigma}_{gs}$.

The "retrieve" field Ω_R beats with the stored spin coherence $\hat{\mathcal{S}}$ to generate an optical polarization $\hat{\mathcal{P}}$ which then decays into the anti-Stokes photon $\hat{\mathcal{E}}_a$. Moreover, the presence of the retrieve field prevents re-absorption of the anti-Stokes photon by the (optically thick) atomic sample through Electromagnetically Induced Transparency (EIT) [147]. The resulting coupled atom-photon excitation ("dark-state" polariton [56]) then propagates at the group velocity $v_g = \frac{|\Omega_R|^2}{g^2N}c$, as we show below.

The only non-vanishing noise correlations are

$$\langle \hat{F}_S(z,t)\hat{F}_S^\dagger(z',t')\rangle = 2\gamma_S V\delta(z-z')\delta(t-t') \quad (4.52)$$

$$\langle \hat{F}_P(z,t)\hat{F}_P^\dagger(z',t')\rangle = 2\gamma V\delta(z-z')\delta(t-t') \quad (4.53)$$

and the commutation relations are

$$\left[\hat{\mathcal{S}}(z,t),\hat{\mathcal{S}}^\dagger(z',t)\right] = V\delta(z-z') \quad (4.54)$$

$$\left[\hat{\mathcal{P}}(z,t),\hat{\mathcal{P}}^\dagger(z',t)\right] = V\delta(z-z') \quad (4.55)$$

$$\left[\hat{\mathcal{E}}_a(z,t),\hat{\mathcal{E}}_a^\dagger(z',t')\right] = V\delta[(z-z')-c(t-t')]. \quad (4.56)$$

4.6.1 Adiabatic solution

Zeroth order adiabatic solution

As before, we want to solve the boundary value problem where the initial polarization wave and the input field correspond to vacuum while an initial non-zero spin wave is present. Again we change variables $t' = t - z/c$, $z' = z$ and Laplace transforming so that $\partial_{z'} \to s$, we have

$$\hat{\mathcal{E}}_a(s,t) = \frac{1}{s}\left[\hat{\mathcal{E}}_a(0,t) + i(g\sqrt{N}/c)\hat{\mathcal{P}}(s,t)\right] \quad (4.57)$$

$$\partial_t\hat{\mathcal{P}}(s,t) = -\left[\gamma + \frac{g^2N}{cs}\right]\hat{\mathcal{P}}(s,t) + i\Omega\hat{\mathcal{S}}(s,t) + i\frac{g\sqrt{N}}{s}\hat{\mathcal{E}}_a(0,t) + \hat{F}_P(s,t). \quad (4.58)$$

For optically thick atomic samples, $\frac{g^2N}{\gamma(c/L)} \gg 1$, so that to zeroth order we can neglect γ compared to $\frac{g^2N}{\gamma cs}$ (which corresponds to a coarsened description for length

scales comparable to or larger than the absorption length L_{abs}). Adiabatically eliminating the polarization, and plugging back the result in the spin wave equation, we get

$$\hat{\mathcal{E}}_a(s,t) \simeq -\frac{\Omega_R}{g\sqrt{N}}\hat{\mathcal{S}}(s,t) + i\frac{1}{g\sqrt{N}}\hat{F}_P(s,t) \tag{4.59}$$

$$\hat{\mathcal{P}}(s,t) \simeq \frac{cs}{g^2N}\left[i\Omega_R\hat{\mathcal{S}}(s,t) + i\frac{g\sqrt{N}}{s}\hat{\mathcal{E}}_a(0,t) + \hat{F}_P(s,t)\right] \tag{4.60}$$

$$\partial_t\hat{\mathcal{S}} = -\left[\gamma_S + \frac{|\Omega_R|^2}{g^2N}cs\right]\hat{\mathcal{S}} - c\frac{\Omega_R}{g\sqrt{N}}\hat{\mathcal{E}}_A(0,t) + \hat{F}_S + i\frac{\Omega_R cs}{g^2N}\hat{F}_P. \tag{4.61}$$

These equations are easily solved, letting $l_d(t) = \int_0^t c\frac{|\Omega_R(t')|^2}{g^2N}dt'$, then

$$\begin{aligned}\hat{\mathcal{S}}(s,t) &= e^{-[\gamma_S t + s l_d(t)]}\hat{\mathcal{S}}(s,0) \\ &- \int_0^t \frac{c\Omega_R(t')}{g\sqrt{N}}e^{-[\gamma_S(t-t') + s(l_d(t)-l_d(t'))]}\left[\hat{\mathcal{E}}_a(0,t') + \hat{F}_S(s,t') - \frac{i}{g\sqrt{N}}\hat{F}_P(s,t')\right]dt',\end{aligned} \tag{4.62}$$

so that, ignoring terms that do not contribute to normally ordered expectation values, we have

$$\hat{\mathcal{E}}_a(z,t) = -\frac{\Omega_R(t)}{g\sqrt{N}}e^{-\gamma_S t}\theta[z - l_d(t)]\hat{\mathcal{S}}[z - l_d(t), 0]. \tag{4.63}$$

Thus, the generated field is given by the retrieved spin wave, which then propagates at the group velocity to the end of the atomic sample. Note that the field is generated instantaneously in this adiabatic approximation, which obviously cannot hold at the beginning of the pulse. Some transient dynamics take place and die down on a time scale given by $1/\gamma$ where γ is the spontaneous emission rate.

First order non-adiabatic correction

Letting $\hat{\alpha}(z,t) = \hat{\mathcal{E}}(z,t)/\Omega_R(t)$, and $\sqrt{\eta(t)} = g\sqrt{N}/\Omega_R(t)$, we can write

$$(\partial_t + c\partial_z)\hat{\alpha}(z,t) \;=\; i\sqrt{\eta(t)}\hat{\mathcal{P}}(z,t). \tag{4.64}$$

We are interested in the "adiabatic" solution corresponding to a small frequency window around zero frequency. Alternatively, we are interested in slow time variations. Solving for the polarization and spin wave adiabatically and ignoring noise terms, we find

$$\begin{aligned} \hat{\mathcal{P}} &= \frac{-i}{\Omega_R}(\partial_t + \gamma_S)\hat{\mathcal{S}} \\ \hat{\mathcal{S}} &= -g\sqrt{N}\hat{\alpha} - \frac{i}{\Omega_R}(\partial_t + \gamma)\hat{\mathcal{P}} \end{aligned} \tag{4.65}$$

iterating a couple of times gives the leading order terms in ∂_t (neglecting ∂_t compared to γ)

$$\begin{aligned} \hat{\mathcal{P}} &= i\sqrt{\eta}(\partial_t + \gamma_S)\hat{\alpha} - \frac{i}{g\sqrt{N}}\sqrt{\eta}(\partial + \gamma_S)\frac{\gamma}{g\sqrt{N}}\eta(\partial_t + \gamma_S)\hat{\alpha} \\ \hat{\mathcal{S}} &= -g\sqrt{N}\hat{\alpha} + \frac{\gamma}{\Omega_R}\sqrt{\eta}(\partial_t + \gamma_S)\hat{\alpha}. \end{aligned} \tag{4.66}$$

Plugging these results in the field equation of motion, we have

$$(\partial_t + c\partial_z)\hat{\alpha} \;=\; -\eta(\partial_t + \gamma_S)\hat{\alpha} + \eta(\partial_t + \gamma_S)\frac{\gamma}{g^2N}\eta(\partial_t + \gamma_S)\hat{\alpha} \tag{4.67}$$

letting $\hat{\alpha} = \tilde{\alpha}e^{-\gamma_S t}$ and assuming $\eta(t) \gg 1$ and letting $\tau(t) = \int_0^t 1/\eta(t')dt'$, we finally find

$$c\partial_z\tilde{\alpha} \;=\; -\partial_\tau[1 - \frac{\gamma}{g^2N}\partial_\tau]\tilde{\alpha}. \tag{4.68}$$

The adiabatic approximation gives $\partial_\tau \alpha = -c\partial_z \alpha$, so that to the same accuracy we can put $\partial_\tau^2 \alpha = (c\partial_z)^2 \alpha$ and get

$$\partial_\tau \alpha = -c\partial_z [1 - \frac{\gamma}{g^2 N} c\partial_z]\alpha. \tag{4.69}$$

The intial conditions are given by

$$\hat{\alpha}(0,z) = -\hat{\mathcal{S}}(0,z)/g\sqrt{N}, \tag{4.70}$$

corresponding to the initial stored atomic excitation.

Fourier transforming the spatial variable and integrating we find,

$$\hat{\alpha}(k,\tau) = \exp\left[-\left(ikc + \frac{\gamma(kc)^2}{g^2 N}\right)\tau\right]\hat{\alpha}(k,0) \tag{4.71}$$

so that

$$\begin{aligned}\hat{\mathcal{E}}_a(L,t) &= \Omega_R(t) e^{-\gamma_S t}\tilde{\alpha}(L,t) \\ &= -\frac{\Omega_R(t)}{g\sqrt{N}} e^{-\gamma_S t}\int_0^L dz\, \frac{1}{\sqrt{2\pi}\Delta z(t)} \exp\left[-\frac{1}{2}\left(\frac{L-z}{\Delta z(t)}\right)^2\right]\hat{\mathcal{S}}(z - c\tau(t), 0)\end{aligned}$$

where $\Delta z(t) = \sqrt{2\frac{Lc\tau(t)}{d_0}}$.

This corresponds to a convolution with a normalized Gaussian function of width $\Delta z(t)$, which increases with time as $\sqrt{t}$. This smoothing process in the spatial domain corresponds precisely to the absorption of non-zero Fourier components in an EIT medium due to the finite width of the transparency window [57]. The resulting loss scales as $1/\sqrt{d_0}$, which can be made negligibly small in an optically thick atomic medium.

Note that in the limit $d_0 \to \infty$ ($\Delta z(t) \to 0$), we recover the zeroth order adiabatic result

$$\hat{\mathcal{E}}(L,t) = -\frac{\Omega_R(t)}{g\sqrt{N}} e^{-\gamma_S t}\hat{\mathcal{S}}(L - c\tau(t), 0).$$

Retrieved pulse shape

Taking the initial spin wave to correspond to the outcome of Raman scattering due to a short "write" pulse of duration T (so we may use expressions valid in the transient regime), we have (writing only terms contributing to normally ordered expectation values)

$$\hat{\mathcal{S}}^{\dagger}(z,0) \;=\; -i\chi \int_0^T dt'\; I_0(2\sqrt{d_0\gamma_S(T-t')z/L})\hat{\mathcal{E}}_s(0,t') \tag{4.72}$$

The number of anti-Stokes photons emitted per unit time is thus

$$\begin{aligned} n_a(t) &= \frac{c}{L}\langle \mathcal{E}_a^{\dagger}(L,t)\mathcal{E}_a(L,t)\rangle \\ &= \frac{v_g}{L}\int_0^1 d\zeta_1 \int_0^1 d\zeta_2\; G(1-\zeta_1,t)G(1-\zeta_2,t) \\ &\quad \int_0^{d_0\gamma_S T} dx\; I_0(2\sqrt{x(\zeta_1 - v_g t/L)})I_0(2\sqrt{x(\zeta_2 - v_g t/L)}) \end{aligned} \tag{4.73}$$

where $G(\zeta,t) = e^{-\gamma_0 t}\frac{L}{\sqrt{2\pi}\Delta z(t)}\exp\left[-\frac{1}{2}\left(\frac{\zeta L}{\Delta z(t)}\right)^2\right]$.

The retrieved pulse shapes obtained from 4.73 can be compared to experimental pulse shapes as in [52] (see also section 4.8.2), and again the agreement is excellent.

4.6.2 Fast read-out

We consider now the possibility that, at $t = 0$, a π pulse transfers population in $|s\rangle$ to $|e\rangle$, with the result that $\hat{\mathcal{S}}(z,0) \to \hat{\mathcal{P}}(z,0)$. Assuming thus an initial polarization wave $\hat{\mathcal{P}}(z,0)$ created at $t = 0$, the atom-field equations of motion are

$$c\partial_{z'}\hat{\mathcal{E}} \;=\; ig\sqrt{N}\hat{\mathcal{P}} \tag{4.74}$$

$$\partial_{t'}\hat{\mathcal{P}} \;=\; -\gamma\hat{\mathcal{P}} + ig\sqrt{N}\hat{\mathcal{E}} + \hat{F}_P \tag{4.75}$$

where $t' = t - z/c$ and $z' = z$.

Let's use dimensionless coordinates to simplify notation, put $\zeta = z/L$, and $\tau = \gamma t$, lastly redefine $\tilde{\mathcal{E}} = \sqrt{c/(L\gamma)}\hat{\mathcal{E}}$ (which we write $\hat{\mathcal{E}}$ from now on). We then have ($d_0 = \frac{g^2 N}{\gamma c/L}$)

$$\partial_\zeta \hat{\mathcal{E}} = i\sqrt{d_0}\hat{\mathcal{P}} \tag{4.76}$$

$$\partial_\tau \hat{\mathcal{P}} = i\sqrt{d_0}\hat{\mathcal{E}} + [\hat{\mathcal{P}}_{in} - \hat{\mathcal{P}}] \tag{4.77}$$

where $\hat{F}_P = \sqrt{2\gamma}\hat{\mathcal{P}}_{in}$. The relevant commutators are

$$\left[\hat{\mathcal{E}}(\zeta,\tau), \hat{\mathcal{E}}(\zeta,\tau')^\dagger\right] = \delta(\tau - \tau') \tag{4.78}$$

$$\left[\hat{\mathcal{P}}(\zeta,\tau), \hat{\mathcal{P}}(\zeta',\tau)^\dagger\right] = \delta(\zeta - \zeta') \tag{4.79}$$

$$\left[\hat{\mathcal{P}}_{in}(\zeta,\tau), \hat{\mathcal{P}}_{in}(\zeta',\tau')^\dagger\right] = 2\delta(\zeta - \zeta')\delta(\tau - \tau'). \tag{4.80}$$

Let's ignore the decay and associated noise of $\hat{\mathcal{P}}$. We solve as usual by Laplace transform of $\zeta \to s$, so that

$$\hat{\mathcal{E}}(s,\tau) = \frac{1}{s}\hat{\mathcal{E}}_{in}(\tau) + i\frac{\sqrt{d_0}}{s}\hat{\mathcal{P}}(s,\tau) \tag{4.81}$$

$$\partial_\tau \hat{\mathcal{P}} = -\frac{d_0}{s}\hat{\mathcal{P}} + i\frac{\sqrt{d_0}}{s}\hat{\mathcal{E}}_{in}(\tau) \tag{4.82}$$

where $\hat{\mathcal{E}}_{in}(\tau) = \hat{\mathcal{E}}(\zeta = 0, \tau)$.

Integrating, we thus have

$$\begin{aligned}\hat{\mathcal{P}}(\zeta,\tau) &= \hat{\mathcal{P}}(\zeta,0) - \int_0^\zeta d\zeta' \hat{\mathcal{P}}(\zeta - \zeta', 0)\sqrt{\frac{d_0\tau}{\zeta'}} J_1(2\sqrt{d_0\tau\zeta'}) \\ &+ i\sqrt{d_0}\int_0^\tau d\tau' \hat{\mathcal{E}}_{in}(\tau') J_0(2\sqrt{d_0(\tau - \tau')\zeta})\end{aligned} \tag{4.83}$$

$$\begin{aligned}\hat{\mathcal{E}}(\zeta,\tau) &= \hat{\mathcal{E}}_{in}(\tau) - d_0\int_0^\tau d\tau' \hat{\mathcal{E}}_{in}(\tau')\sqrt{\frac{\zeta}{d_0(\tau - \tau')}} J_1(2\sqrt{d_0(\tau - \tau')\zeta}) \\ &+ i\sqrt{d_0}\int_0^\zeta d\zeta' \hat{\mathcal{P}}(\zeta', 0) J_0(2\sqrt{d_0\tau(\zeta - \zeta')}).\end{aligned} \tag{4.84}$$

Keeping only terms that contribute to normally ordered expectation values, we have thus the output field

$$\hat{\mathcal{E}}(\zeta,\tau) \;=\; i\sqrt{d_0}\int_0^{\zeta} d\zeta' \hat{\mathcal{P}}(\zeta',0) J_0(2\sqrt{d_0\tau(\zeta-\zeta')}), \tag{4.85}$$

which indicates that the polarization wave results in an oscillatory pulse, reminiscent of the ringing regime of superadiance [65, 86]. Further work on this fast retrieve technique is under way.

4.6.3 Optimal geometry for retrieval of stored excitation

We now discuss in more detail the effective one-dimensional treatment of the retrieval process.

Forward propagating retrieve

Applying a retrieve drive propagating in the forward direction, we have the equations of motion

$$\begin{aligned}\left[\partial_t + c\partial_z - i\frac{c\nabla_\perp^2}{2k_0}\right]\hat{\mathcal{E}}(\vec{r},t) &= ig\sqrt{N}\hat{\mathcal{P}} \\ \partial_t\hat{\mathcal{P}} &= -\gamma\hat{\mathcal{P}} + i\Omega_R\hat{\mathcal{S}} + ig\sqrt{N}\hat{\mathcal{E}} + \hat{\mathcal{F}}_P \\ \partial_t\hat{\mathcal{S}} &= i\Omega_R^*\hat{\mathcal{P}}\end{aligned} \tag{4.86}$$

where for simplicity we neglect the spin coherence decay.

Expanding over Hermite-Gaussian modes as before, and letting $\Omega_R = \Omega_0 U(\vec{r})$, we

now have

$$\begin{aligned}
[\partial_t + c\partial_z]\hat{\mathcal{E}}_{nm} &= ig\sqrt{N}\hat{\mathcal{P}}_{nm} \\
\partial_t\hat{\mathcal{P}}_{nm} &= -\gamma\hat{\mathcal{P}}_{nm} + i\Omega_0\sum_{lk} A_{nm,lk}(z)\hat{\mathcal{S}}_{lk} + ig\sqrt{N}\hat{\mathcal{E}}_{nm} + \hat{\mathcal{F}}_{p,nm} \\
\partial_t\hat{\mathcal{S}}_{nm} &= i\Omega_0^*\sum_{lk} A^{\dagger}_{nm,lk}(z)\hat{\mathcal{P}}_{lk}
\end{aligned} \tag{4.87}$$

where

$$A_{nm,lk}(z) = \int dxdy\; U^*_{nm}(x,y,z)U(x,y,z)U^*_{lk}(x,y,z). \tag{4.88}$$

The "write" and "retrieve" steps described here as separated in time may also take place simultaneously, in which case the strong correlations established between Stokes and anti-Stokes photons would be described in terms of four-wave mixing [30, 24]. Phase matching considerations then suggest that strongest coupling between Stokes and anti-Stokes is achieved when they are phase-conjugate of each other. These simple considerations then suggest that an optimal geometry that maximizes correlations between Stokes and anti-Stokes photons is one where the "write" and "retieve" beams are counter-propagating plane-waves. In such a case one can ensure that one and only one transverse momentum component of the anti-Stokes beam is correlated with a given momentum component of the Stokes beam.

This can also be seen from the above expressions: even when the beam waist chosen in the mode expansion becomes much smaller than the waist of the "retrieve" beam $U(\vec{r})$, there is substantial coupling among the various transverse modes of the anti-Stokes light since $A_{nm,lk} \neq \delta_{nl}\delta_{mk}$ in the limit of constant $U(x,y,z)$ (because the two conjugate modes U^*_{nm} and U^*_{lk} appear in 4.88, instead of one conjugate mode and one non-conjugate mode). Thus, in a forward propagating "retrieve" beam geometry,

preparation of an atomic excitation in a single Hermite-Gaussian mode does not lead to the generation of anti-Stokes light in a single transverse mode. It is desirable to generate anti-Stokes light in single transverse modes as these are easily selected with standard optical lenses and apertures, and can be further efficiently coupled into single-mode optical fibers for distribution in a quantum network.

Backward propagating retrieve beam

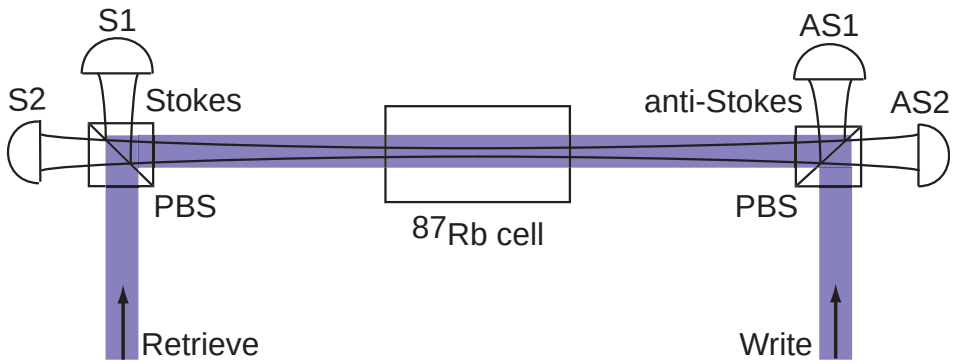

Figure 4.8: Counter-propagating geometry for improved Stokes/anti-Stokes correlations. Detection of a Stokes photon projects the atomic state onto a state with definite number of excitations. In the limit of plane-wave "write" and "retrieve" drives, the Stokes photon detected in a single transverse mode (Hermite-Gaussian mode) is uniquely correlated with an atomic excitation in a single transverse mode. Retrieval of this excitation by a counterpropagating plane-wave beam results in the creation of an anti-Stokes photon in a single transverse mode, uniquely correlated with the detected Stokes photon.

We now analyze the phase-conjugate geometry discussed in the previous paragraph, also shown in Fig. 4.8.

In the case of a backward propagating "retrieve" drive, we expand the field $\hat{\mathcal{E}}$ and polarization $\hat{\mathcal{P}}$ over backward propagating Hermtie-Gaussian modes. These modes correspond to the complex conjugate of forward propagating modes i.e., $U_{nm}(x, y, -z) =$

$U^*_{nm}(x,y,z)$. The spin wave however is expanded over forward propagating modes since these correspond to the write step in which a forward propagating Stokes photon is detected in a single transverse mode in order to prepare the atomic state,

$$\begin{aligned}\hat{\mathcal{E}}(\vec{r},t) &= \sum_{nm}\hat{\mathcal{E}}_{nm}(z,t)U^*_{nm}(\vec{r}) \\ \hat{\mathcal{P}}(\vec{r},t) &= \sum_{nm}\hat{\mathcal{P}}_{nm}(z,t)U^*_{nm}(\vec{r}) \\ \hat{\mathcal{S}}(\vec{r},t) &= \sum_{nm}\hat{\mathcal{S}}_{nm}(z,t)U^*_{nm}(\vec{r}).\end{aligned} \tag{4.89}$$

The equations of motion then take the form

$$\begin{aligned}[\partial_t - c\partial_z]\hat{\mathcal{E}}_{nm} &= ig\sqrt{N}\hat{\mathcal{P}}_{nm} \\ \partial_t\hat{\mathcal{P}}_{nm} &= -\gamma\hat{\mathcal{P}}_{nm} + i\Omega_0\sum_{lk}A_{nm,lk}(z)\hat{\mathcal{S}}_{lk} + ig\sqrt{N}\hat{\mathcal{E}}_{nm} + \hat{\mathcal{F}}_{P,nm} \\ \partial_t\hat{\mathcal{S}}_{nm} &= i\Omega_0^*\sum_{lk}A^\dagger_{nm,lk}(z)\hat{\mathcal{P}}_{lk}\end{aligned} \tag{4.90}$$

where now we have $A_{nm,lk}(z) = \int dxdy\; U_{nm}(x,y,z)U(x,y,z)U^*_{lk}(x,y,z)$.

In such a geometry, when the beam waist chosen for the mode expansion is much smaller than the beam waist of the retrieve beam $U(\vec{r})$, we find $A_{nm,lk} = \delta_{nl}\delta_{mk}$, so that an atomic excitation prepared in a single transverse mode leads to the generation of an anti-Stokes photon in a single transverse mode. We may thus describe the retrieval process in this limit with an effective one-dimensional theory, as was done previously to obtain the retrieved pulse shapes. Here, in the ideal limit of plane-wave write and retrieve lasers, the Stokes and anti-Stokes photons are emitted in counter-propagating single modes owing to the phase conjugation property of the underlying four-wave mixing interaction (see also section 4.8.2 for initial results demonstrating improvements of nonclassical state preparation in the counter-propagating geometry described here).

4.7 Four-wave Mixing: Continuous Wave Picture

When both "write" and "retrieve" fields are simultaneously interacting with the atoms as in Fig. 4.2, both Stokes and anti-Stokes photons are generated, in a correlated manner. In this continuous wave configuration, atomic state preparation and retrieval happen simultaneously and continuously. We thus expect the Stokes intensity $I_s(t)$ is strongly correlated (quantum-mechanically) with the anti-Stokes intensity $I_a(t+\tau)$, where τ allows for a possible delay between the Stokes and anti-Stokes photons, e.g., due to different speeds of propagation.

In a one-dimensional model, the equations of motion are, after adiabatic elimination of the excited state (we consider here, as in the experiments, co-propagating Stokes and anti-Stokes fields),

$$(\partial_t + c\partial_z)\hat{\mathcal{E}}_s = i\chi\hat{\mathcal{S}}^\dagger \tag{4.91}$$

$$(\partial_t + c\partial_z)\hat{\mathcal{E}}_a^\dagger = -ig\sqrt{N}\hat{\mathcal{P}}^\dagger \tag{4.92}$$

$$\partial_t\hat{\mathcal{P}}^\dagger = -\gamma\hat{\mathcal{P}}^\dagger - ig\sqrt{N}\hat{\mathcal{E}}_a^\dagger - i\Omega_R^*\hat{\mathcal{S}}^\dagger + \hat{\mathcal{F}}_P \tag{4.93}$$

$$\partial_t\hat{\mathcal{S}}^\dagger = -\gamma_S\hat{\mathcal{S}}^\dagger - i\chi^*\hat{\mathcal{E}}_s - i\Omega_R\hat{\mathcal{P}}^\dagger + \hat{\mathcal{F}}_S, \tag{4.94}$$

where $\chi = \frac{g\sqrt{N}\Omega_W}{\Delta}$, and $\gamma_S = \gamma_0 + \gamma\frac{|\Omega_W|^2}{\Delta^2}$.

The noise forces have non-vanishing diffusion coefficients

$$\langle\hat{\mathcal{F}}_S(z,t)\hat{\mathcal{F}}_S^\dagger(z't,')\rangle = 2\gamma_s L\delta(z-z')\delta(t-t') \tag{4.95}$$

$$\langle\hat{\mathcal{F}}_P(z,T)\hat{\mathcal{F}}_P^\dagger(z',t')\rangle = 2\gamma L\delta(z-z')\delta(t-t'), \tag{4.96}$$

and the field commutation relations are

$$[\hat{\mathcal{E}}_i(z,t),\hat{\mathcal{E}}_j^\dagger(z',t')] = \delta_{ij}L\delta\left[z-z'-c(t-t')\right], \tag{4.97}$$

where $i, j = a, s$.

The initial atomic state corresponds to all atoms in state $|g\rangle$, i.e., vacuum spin and polarization waves, with commutation relations

$$[\hat{\mathcal{P}}(z,t), \hat{\mathcal{P}}^\dagger(z',t)] = L\delta(z-z'), \tag{4.98}$$

and similarly for $\hat{\mathcal{S}}(z,t)$.

CW configuration

When both driving fields are on at all times and we are in the regime of strong cross-coupling, we can solve adiabatically for the atomic variables $\hat{\mathcal{S}}, \hat{\mathcal{P}}$,

$$\hat{\mathcal{P}}^\dagger = \frac{i}{\Omega_R}[(\partial_t + \gamma_s)\hat{\mathcal{S}}^\dagger + i\chi^*\hat{\mathcal{E}}_s - \hat{\mathcal{F}}_S^\dagger] \tag{4.99}$$

$$\hat{\mathcal{S}}^\dagger = \frac{i}{\Omega_R^*}[(\partial_t + \gamma)\hat{\mathcal{P}}^\dagger + ig\sqrt{N}\hat{\mathcal{E}}_a^\dagger - \hat{\mathcal{F}}_P^\dagger] \tag{4.100}$$

so that iterating a couple of times gives

$$\hat{\mathcal{P}}^\dagger = -\frac{\chi^*}{\Omega_R}\hat{\mathcal{E}}_s - \frac{g\sqrt{N}}{|\Omega_R|^2}(\partial_t + \gamma_S)\hat{\mathcal{E}}_a^\dagger - \frac{i}{\Omega_R}\hat{\mathcal{F}}_S^\dagger \tag{4.101}$$

$$\hat{\mathcal{S}}^\dagger = -\frac{g\sqrt{N}}{\Omega_R^*}\hat{\mathcal{E}}_a^\dagger - i\frac{\gamma\chi^*}{|\Omega_R|^2}\hat{\mathcal{E}}_s - \frac{i}{\Omega_R^*}\hat{\mathcal{F}}_P^\dagger + \frac{\gamma}{|\Omega_R|^2}F_S^\dagger. \tag{4.102}$$

The equations of motion for the fields then become

$$(\partial_t + c\partial_z)\hat{\mathcal{E}}_s = -i\alpha\hat{\mathcal{E}}_a^\dagger + \eta\gamma_L\hat{\mathcal{E}}_s + \hat{\mathcal{F}}_s(z,t) \tag{4.103a}$$

$$(\partial_t + c\partial_z)\hat{\mathcal{E}}_a^\dagger = -\eta\,(\partial_t + \gamma_S)\,\hat{\mathcal{E}}_a^\dagger + i\alpha\hat{\mathcal{E}}_s + \hat{\mathcal{F}}_a^\dagger(z,t) \tag{4.103b}$$

where $\eta = g^2N/|\Omega_R|^2 = c/v_g$ is the ratio of speed of light in vacuum to the group velocity, $\alpha = \eta\Omega_R\Omega_W/\Delta$ is the cross-coupling nonlinearity, $\gamma_L = \gamma|\Omega_W|^2/\Delta^2$ is the optical pumping rate, and where we assumed for simplicity that α is real.

The noise forces are $\hat{\mathcal{F}}_s = (\chi/\Omega_R^*)\hat{\mathcal{F}}_P^\dagger$ and $\hat{\mathcal{F}}_a = -(g\sqrt{N}/\Omega_R^*)\hat{\mathcal{F}}_S$. Note that equations 4.103 describe Raman gain for the Stokes field $\eta\gamma_L$ that scales like $1/\Delta^2$, along with a small absorption of the anti-Stokes field $\eta\gamma_S$, as well as the cross-coupling nonlinearity α that scales like $1/\Delta$. In the following we neglect the Raman gain (negligible compared to cross-coupling nonlinearity when $\Delta \gg \gamma$ and in large gain limit i.e., $\alpha L/c \gg 1$) and the loss $\eta\gamma_S$, i.e., this corresponds to the noiseless regime of EIT enhanced four-wave mixing.

Solution of four-wave mixing equations

To solve, we Fourier transform the time variable $f(t) = \int d\omega\, e^{-i\omega t}\tilde{f}(\omega)$ (so that $\partial_t \to -i\omega$) and Laplace transform the spatial variable (so that $c\partial_z \to s$) and obtain

$$(\tilde{s} + i\sigma(\omega))\hat{\mathcal{E}}_s(s,\omega) - i\alpha\hat{\mathcal{E}}_a^\dagger(s,\omega) = \hat{\mathcal{E}}_s(0,\omega) \quad (4.104)$$

$$i\alpha^*\hat{\mathcal{E}}_s(s,\omega) + (\tilde{s} - i\sigma(\omega))\hat{\mathcal{E}}_2^\dagger(s,\omega) = \hat{\mathcal{E}}_2^\dagger(0,\omega) \quad (4.105)$$

where $\sigma(\omega) = \eta\omega/2$, $\tilde{s} = s - i\sigma(\omega)$.

These algebraic equations can be easily solved and the inverse Laplace transform taken, to give

$$\hat{\mathcal{E}}_s^\dagger(z,\omega) = A_-(z,\omega)\hat{\mathcal{E}}_s^\dagger(0,\omega) + iB(z,\omega)\hat{\mathcal{E}}_a(0,\omega) \quad (4.106)$$

$$\hat{\mathcal{E}}_s(z,\omega) = A_-(z,\omega)\hat{\mathcal{E}}_s(0,\omega) - iB(z,\omega)\hat{\mathcal{E}}_a^\dagger(0,\omega) \quad (4.107)$$

$$\hat{\mathcal{E}}_a^\dagger(z,\omega) = iB(z,\omega)\hat{\mathcal{E}}_s(0,\omega) + A_+(z,\omega)\hat{\mathcal{E}}_a^\dagger(0,\omega) \quad (4.108)$$

$$\hat{\mathcal{E}}_a(z,\omega) = -iB(z,\omega)\hat{\mathcal{E}}_s^\dagger(0,\omega) + A_+(z,\omega)\hat{\mathcal{E}}_a(0,\omega) \quad (4.109)$$

where

$$A_{\pm}(z,\omega) = e^{i\sigma(\omega)z/c}\left[\cosh(\xi(\omega)z/c) \pm i\frac{\sigma(\omega)}{\xi(\omega)}\sinh(\xi(\omega)z/c)\right] \quad (4.110)$$

$$B(z,\omega) = e^{i\sigma(\omega)z/c}\frac{\alpha}{\xi(\omega)}\sinh(\xi(\omega)z/c) \quad (4.111)$$

and with $\xi(\omega) = \sqrt{\alpha^2 - \sigma(\omega)^2}$.

Correlation functions

The instantaneous intensity operator for field j ($j = a, s$) is

$$\begin{aligned}\hat{I}_j(z,t) &= \hat{\mathcal{E}}_j(z,t)^{\dagger}\hat{\mathcal{E}}_j(z,t) \\ &= \int d\omega d\omega'\, e^{i(\omega+\omega')t}\hat{\mathcal{E}}_j^{\dagger}(z,\omega)\hat{\mathcal{E}}_j(z,\omega'),\end{aligned} \quad (4.112)$$

while variances in intensity involve expressions of the form

$$\begin{aligned}\hat{I}_i(z,t)\hat{I}_j(z,t+\tau) &= \int d\omega_1 d\omega_2 d\omega_3 d\omega_4\, e^{i[(\omega_1+\omega_2)t+(\omega_3+\omega_4)(t+\tau)]} \\ &\times\ \hat{\mathcal{E}}_i^{\dagger}(z,\omega_1)\hat{\mathcal{E}}_i(z,\omega_2)\hat{\mathcal{E}}_j^{\dagger}(z,\omega_3)\hat{\mathcal{E}}_j(z,\omega_4).\end{aligned} \quad (4.113)$$

We are in particular interested in the fluctuations of the difference in intensity between Stokes and anti-Stokes fields. Due to quantum correlations, this difference is a fluctuating quantity with variance below that of the corresponding expression for uncorrelated fields (which defines the shot noise level). In the frequency domain, we look at the spectrum of intensity difference noise [162] $S_d(\omega) = S_{ss}(\omega) + S_{aa}(\omega) - S_{sa}(\omega) - S_{as}(\omega)$, where

$$\begin{aligned}S_{ij}(\omega) &= \frac{1}{2\pi}\int_{-\infty}^{\infty} e^{-i\omega\tau}\langle I_i(z,t), I_j(z,t+\tau)\rangle d\tau \\ &= \int d\omega_1 d\omega_2 d\omega_3 d\omega_4 \delta[\omega - (\omega_3+\omega_4)]\langle\hat{\mathcal{E}}_i^{\dagger}(z,\omega_1)\hat{\mathcal{E}}_i(z,\omega_2), \hat{\mathcal{E}}_j^{\dagger}(z,\omega_3)\hat{\mathcal{E}}_j(z,\omega_4)\rangle.\end{aligned}$$

(4.114)

Nonclassical correlations exist if $S_d(\omega) < \langle \hat{I}_s \rangle + \langle \hat{I}_a \rangle$, i.e., when the fluctuations of the intensity difference is below the shot noise level.

Growth dynamics and delay compensation

In the experiments [159] (see also highlights in section 4.8.1) it was essential to correlate Stokes and anti-Stokes signals detected at different times. Indeed, due to slow light effects, the anti-Stokes photons travel at a reduced group velocity and they are delayed compared to the Stokes photons. Initially (at the beginning of the atomic cell), Stokes photons are generated and travel approximately at the speed of light in vacuum. As more Stokes photons are generated and correlated with flipped atomic spins, the "retrieve" field can beat with these coherences and generate the anti-Stokes photons, at the same time establishing an Electromagnetically Induced Transparency which ensures that the anti-Stokes photons are not subsequently re-absorbed. Strong correlations of Stokes and anti-Stokes result from the cross-coupling nonlinearity, so that after a short propagating distance Stokes and anti-Stokes envelopes lock to each other, stimulate growth of one another, and propagate together at the same speed (as shown in section 4.8.1). Thus after initially lagging behind the Stokes pulse and acquiring a delay, the anti-Stokes light is subsequently locked to the Stokes component and the delay does not accumulate further, as shown in the experiments and accompanying theory [159]. The delay depends only on the cross-coupling nonlinearity and is given by $\tau_d = \frac{1}{2}(\Omega_W \Omega_R / \Delta)^{-1}$.

Mathematically, delaying the signals with respect to one another by τ_0, results in

$S_{sa}(\omega) \rightarrow e^{i\omega\tau_0} S_{sa}(\omega)$ and $S_{as}(\omega) \rightarrow e^{-i\omega\tau_0} S_{as}(\omega)$. The mean intensities are

$$\begin{aligned} \langle \hat{I}_s(L) \rangle &= \langle \hat{I}_a(L) \rangle \\ &= \frac{L}{2\pi c} \int |B(L,\omega)|^2 d\omega \end{aligned} \tag{4.115}$$

For the intensity noise spectra we need the expressions

$$\langle \hat{\mathcal{E}}_s^\dagger(L,\omega_1)\hat{\mathcal{E}}_s(L,\omega_2), \hat{\mathcal{E}}_s^\dagger(L,\omega_3)\hat{\mathcal{E}}_s(L,\omega_4)\rangle = \left(\frac{L}{2\pi c}\right)^2 |A_-(L,\omega_2)|^2 \delta(\omega_2+\omega_3)$$

$$\times |B(L,\omega_1)|^2 \delta(\omega_1+\omega_4) \tag{4.116}$$

$$\langle \hat{\mathcal{E}}_a^\dagger(L,\omega_1)\hat{\mathcal{E}}_a(L,\omega_2), \hat{\mathcal{E}}_a^\dagger(L,\omega_3)\hat{\mathcal{E}}_a(L,\omega_4)\rangle = \left(\frac{L}{2\pi c}\right)^2 |B(L,\omega_1)|^2 \delta(\omega_1+\omega_4)$$

$$\times |A_+(L,\omega_2)|^2 \delta(\omega_2+\omega_3) \tag{4.117}$$

$$\langle \hat{\mathcal{E}}_s^\dagger(L,\omega_1)\hat{\mathcal{E}}_s(L,\omega_2), \hat{\mathcal{E}}_a^\dagger(L,\omega_3)\hat{\mathcal{E}}_a(L,\omega_4)\rangle = \left(\frac{L}{2\pi c}\right)^2 A_-(L,\omega_2) B(L,-\omega_2)\delta(\omega_2+\omega_4)$$

$$\times \quad B(L,\omega_1) A_+(L-z',-\omega_1)\delta(\omega_1+\omega_3) \tag{4.118}$$

$$\langle \hat{\mathcal{E}}_a^\dagger(L,\omega_1)\hat{\mathcal{E}}_a(L,\omega_2), \hat{\mathcal{E}}_s^\dagger(L,\omega_3)\hat{\mathcal{E}}_s(L,\omega_4)\rangle = \left(\frac{L}{2\pi c}\right)^2 B(L,\omega_1) A_-(L,-\omega_1)\delta(\omega_1+\omega_2)$$

$$\times \quad A+(L,\omega_2) B(L',-\omega_2)\delta(\omega_4+\omega_4) \tag{4.119}$$

The noise spectra are thus (including electronic delay τ_0)

$$\begin{aligned} S_{ss}(\omega) &= \left(\frac{L}{2\pi c}\right)^2 \int |A_-(L,\omega')|^2 |B(L,\omega-\omega')|^2 d\omega' \\ &= S_{aa}(\omega) \end{aligned} \tag{4.120}$$

$$\begin{aligned} S_{sa}(\omega) &= \left(\frac{L}{2\pi c}\right)^2 \int B(L,\omega') A_+(L,-\omega') A_-(L,\omega-\omega') B(L,\omega'-\omega) d\omega' e^{i\omega\tau_0} \\ &= S_{as}(\omega)^* \end{aligned} \tag{4.121}$$

The cross-correlations and the amount of noise subtraction in the difference intensity spectrum are determined by the real part of $S_{sa}(\omega)$. As can be seen from inspection of the relevant expressions, the phase of the complex function $A_-(\omega)B(-\omega)$ varies

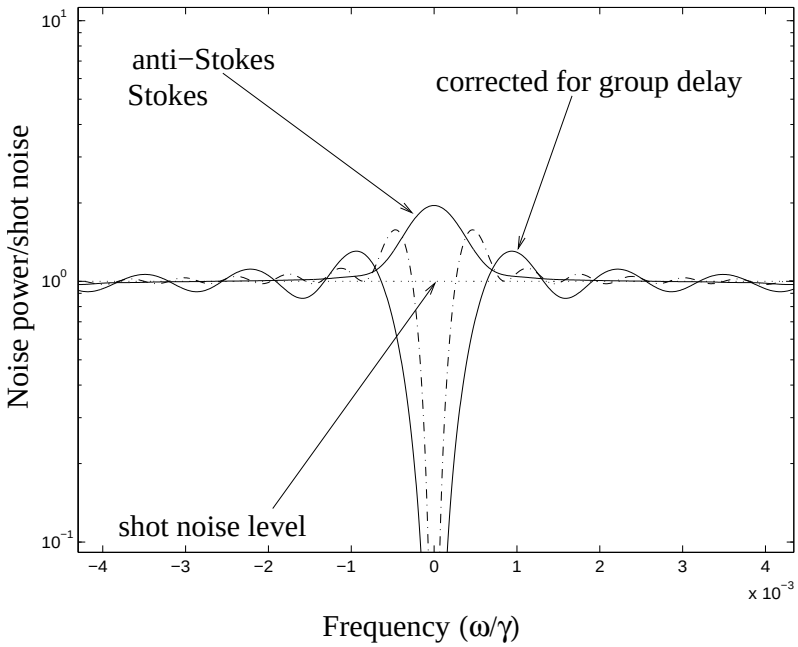

Figure 4.9: Intensity noise spectrum in low gain regime (GAIN $= \alpha L/c = 1$): Intensity noise (full line labeled by "anti-Stokes/Stokes") and intensity difference noise spectra (the dash-dotted line is not corrected for any delay while the full line is corrected for delay). Parameters are: on-resonance optical depth $d_0 = 100$, $\Omega_W/\gamma = 0.02$, $\Omega_R/\gamma = 0.1$ and $\Delta/\gamma = 20$.

linearly with frequency around $\omega = 0$, as it also does for frequencies well outside the Raman bandwidth $\Omega_R\Omega_W/\Delta$. For maximal noise subtraction, the real part of $S_{sa}(\omega)$ should be largest and that is achieved when the phase of A_B is near zero. We can correct for linear variation of the phase with frequency by delaying the traces $I_{s,a}(t)$ with respect to one another by some chosen delay τ_0. The delay maximizing noise subtraction may be different depending on the frequency at which cross-correlations are maximized. In the high gain regime near $\omega = 0$ the delay optimizing correlations is $\tau = (1/2)\Delta/(\Omega_R\Omega_W)$, while for higher frequencies ($\omega \gtrsim \Omega_R\Omega_W/\Delta$) the optimal delay is given by the group delay $\tau = (1/2)L/v_g$.

Low gain regime

In the low gain regime, we can approximate $A_\pm \simeq e^{i[\sigma(\omega)\pm\sigma(\omega)]z/c}$ and $B \simeq \alpha e^{i\sigma(\omega)z/c}$. In this case the delay is given by the group delay $\tau = \eta L/c$.

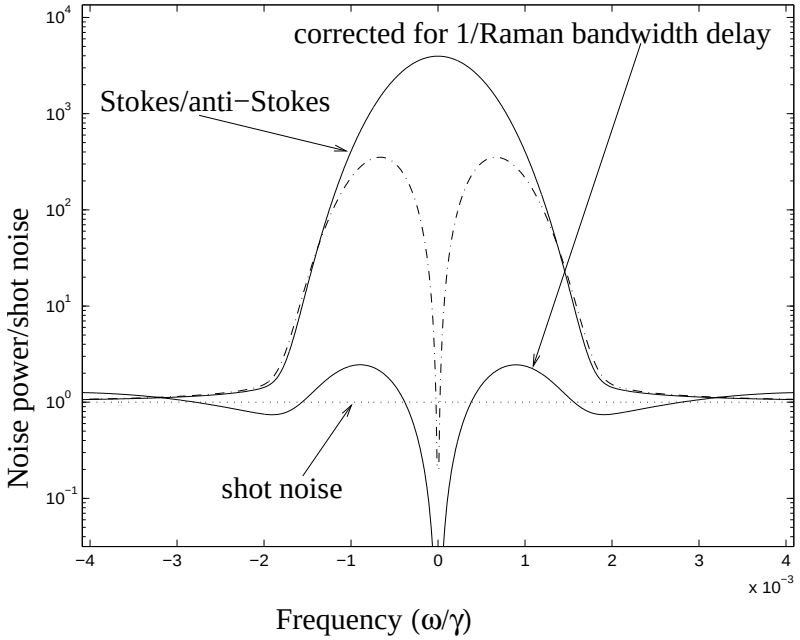

Figure 4.10: Intensity noise spectrum in high gain regime (GAIN $= \alpha L/c = 5$): Intensity noise (full line labeled by "Stokes/anti-Stokes") and intensity difference noise spectra (the dash-dotted line is not corrected for delay, while the full line is corrected for delay). Parameters are: on-resonance optical depth $d_0 = 100$, $\Omega_W/\gamma = 0.02$, $\Omega_R/\gamma = 0.1$ and $\Delta/\gamma = 4$.

High gain regime

In this case we can write $A_\pm \simeq e^{\xi(\omega)z/c}[1 \pm i\sigma(\omega)/\xi(\omega)]$, so that for $|\omega| \ll \Delta_L$, we have $A_\pm \simeq e^{\alpha z/c}e^{\pm i\omega/(2\Delta_L)}$. The delay here is given by the inverse Raman bandwidth $\Delta_L = |\Omega_R\Omega_W|/\Delta$. In this regime, the rate $\Omega_W\Omega_R/\Delta$ is the rate at which atoms are pumped from $|g\rangle$ to $|s\rangle$ back to $|g\rangle$ and this is the delay between the generated fields.

4.8 Experimental Highlights

4.8.1 Quantum correlations and delay in multi-photon experiments

We now describe an experiment [159] in which we study correlations between the photon fields associated with the preparation and the retrieval of the atomic spin state. The onset of quantum-mechanical correlations between the photon numbers of the Stokes and delayed anti-Stokes light (analogous to twin-mode photon-number squeezing [14, 151]) provides evidence for the storage and retrieval of non-classical states. A schematic of the experimental apparatus is shown in Fig. 4.11B. A warm ^{87}Rb vapor cell (length of 4 cm) is maintained at a temperature of typically $\approx$ 85 ^{o}C, corresponding to an atom number density of $\approx$ 10^{12} cm^{-3}. Long-lived hyperfine sublevels of the electronic ground state are used as the storage states $|g\rangle$ and $|s\rangle$.

Fig. 4.12 presents an example of synchronously detected signals at the Stokes and anti-Stokes frequencies. The observed Stokes light (Fig. 4.12A) is a sequence of spontaneous pulses, each containing a macroscopic number of photons, but with significantly fluctuating intensities and durations.

The observed fluctuations are due to the spontaneous nature of the Raman scattering process, which corresponds to thermal, i.e., super-Poissonian, photon-number statistics for the emitted photons, and is described by a Bose-Einstein distribution. The observation of such photon statistics indicates that the transverse mode structure of the Raman fields is approximated reasonably well by a single spatial mode [135]. In essence, each pulse corresponds to a spontaneously emitted Stokes photon that subse-

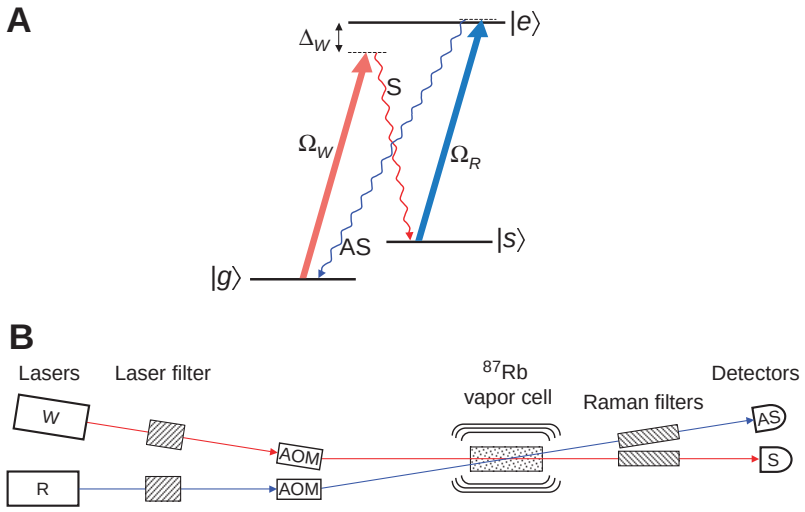

Figure 4.11: (**A**) Optical pumping prepares the atoms in the $|g\rangle$ state. The write Raman process creates a Stokes signal field (S), and a small population in the $|s\rangle$ state with a corresponding $|g\rangle\langle s|$ coherence. In the retrieve step (blue) this coherence is mapped back into an anti-Stokes field (AS). with a near-resonant retrievecontrol beam with Rabi frequency Ω_R. (**B**) Schematic of the experimental setup. The Stokes (anti-Stokes) signal field co-propagates with the write (retrieve) control beam, and a small angle (10mrad) between the control beams allows for spatially separated detection of the Stokes and anti-Stokes signals. Filters before the detectors block the transmitted control beams such that only the Stokes and anti-Stokes fields are detected.

quently stimulates the emission of a number of other photons. As each Stokes photon emission results in an atomic transition from the state $|g\rangle$ into the spin-flipped state $|s\rangle$, the Stokes light fluctuations are mirrored in the anti-Stokes light, as shown in Fig. 4.12B. Striking intensity correlations between the two beams are evident. These observations can be viewed as resulting from a resonant four-wave frequency mixing process in a highly dispersive medium [108, 76], as described in section 4.7.

The delay in Fig. 4.12 corresponds to the finite time required for the retrieve beam to convert the atomic excitation into anti-Stokes light, it originates from the time interval after the atomic spin flip (from $|g\rangle$ to $|s\rangle$) in which the anti-Stokes pulse

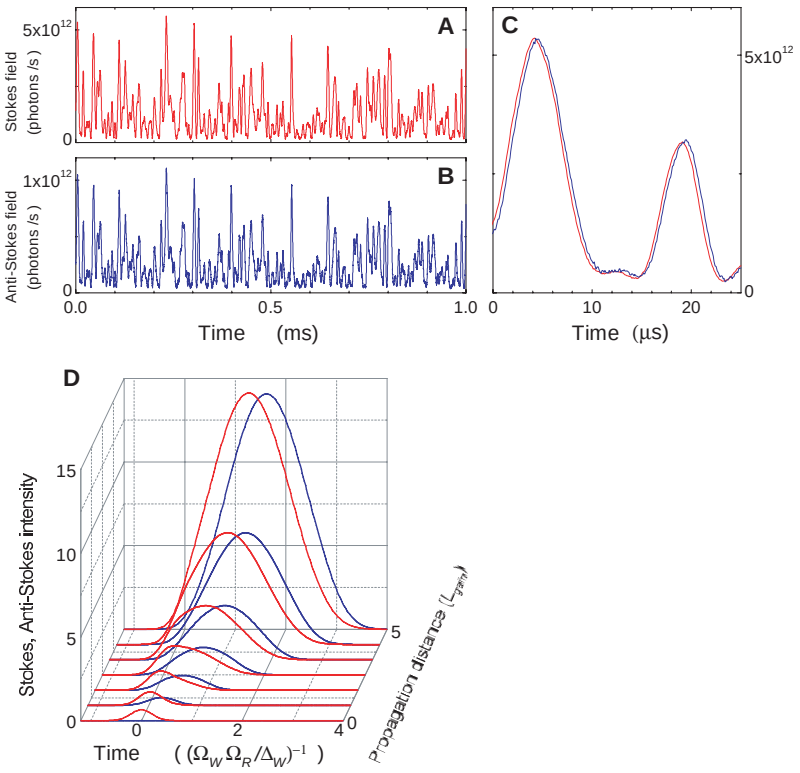

Figure 4.12: Synchronously detected Stokes (**A**) and anti-Stokes (**B**) signals showing strong intensity correlations. (**C**) The first 25 μs of the traces in (A) and (B). The anti-Stokes signal (blue) is corrected for finite retrieval efficiency, and shows a delay of 292 ns compared to the Stokes (red). (**D**) Theoretically simulated propagation dynamics of Stokes (red) and corresponding anti-Stokes (blue) intensities in the continuous-wave excitation regime.

components are still weaker than those of the Stokes light. During this interval, the group velocity of the Stokes field is close to the speed of light in vacuum c, whereas the group velocity v_g of the near-resonant anti-Stokes field is greatly reduced ($v_g \ll c$). After this initial retrieval stage, the two pulses lock together and propagate with equal group velocities, being simultaneously amplified further in a four-wave mixing process. Theoretical estimates from Fig. 4.12D for parameters corresponding to our experiment yield delays in the 100 ns - 1μs range, comparable with the experimental

observations. Thus, the observed delay corresponds to a temporal storage of the excitation in spin states.

We now turn to investigating the degree of correlations between the Stokes and anti-Stokes beams. To this end we obtained Raman signals with cw control beams, recorded signal intensities with high resolution, and analyzed the spectral densities of the Raman signal fluctuations using the discrete Fourier transform. The fluctuation spectra of the Stokes and anti-Stokes fields are peaked at low frequencies, with the large noise reflecting the super-Poissonian nature of single-mode spontaneous Raman excitations (Figure 4.13A).

At high frequencies the measured spectra generally approach a flat noise floor. Correlations between the two beams result in a large noise reduction in the spectrum of the signal that is formed by subtracting the Stokes and anti-Stokes signals in the time domain. In this difference intensity analysis it was essential to compensate for the unbalanced intensities and the delay between the Stokes and anti-Stokes beams. We routinely observed 30 dB of intensity correlations over a broad range of low frequencies. Although this level of subtraction was not sufficient to eliminate spontaneous noise entirely at low frequencies, this was readily achieved in the higher frequency range where fluctuations in the Raman fields were smaller. Whereas at large frequencies the difference intensity noise approaches a flat noise floor, at intermediate values, near the high end of the Raman bandwidth, the difference intensity noise consistently drops a few percent below that level.

To quantify the degree of correlations in this intermediate regime, we performed several experimental tests. The benchmark level representing non-classical effects is

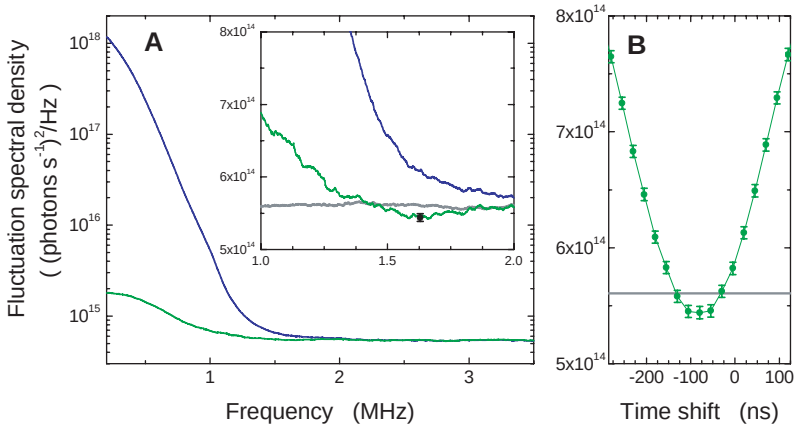

Figure 4.13: (**A**) The fluctuation spectral density of the anti-Stokes field (blue) and of the signal formed by subtraction of the Stokes and anti-Stokes signal in the time domain (green). The super-Poissonian character of the Raman signals leads to strong fluctuations at low frequencies (within the Raman bandwidth). At high frequencies, the fluctuation spectrum is flat and set by the shot-noise level for photon-detection. At frequencies near the high end of the Raman bandwidth (around 1.6 MHz, see the inset), the fluctuations in the subtracted signal fall bellow the measured PSN (gray curve in the inset). (**B**) The fluctuation spectral density levels at 1.6 MHz (green) for the green line in (A), for different values of the delay between Stokes and anti-Stokes signal before subtraction.

set by the photonic shot noise (PSN) associated with the Poissonian photon-number statistics of coherent classical light [14], and it corresponds to a flat fluctuation spectrum. We performed several checks to define the PSN level. The difference signal for two output beams from a single laser beam on a beam splitter possessed a flat fluctuation spectrum at a level that was linearly (rather than quadratically) dependent on beam intensity, characteristic for PSN. The measured level of the fluctuation spectrum is in excellent agreement with PSN values calculated using the shot-noise formula and independently determined detector and amplifier parameters. This confirms that the Stokes/anti-Stokes difference spectrum in Fig. 4.13A (green) drops at intermediate-frequencies about 4% below the PSN level. Finally, Fig. 4.13B shows that the degree

of correlations depends sensitively upon the delay compensation between the Stokes and anti-Stokes signals: the onset of non-classical correlations appears only when one properly compensates for the time that the atoms spend in a spin-flipped state. This sensitivity to delay compensation represents evidence for temporal storage of non-classical states in atomic ensembles.

4.8.2 Quantum control and generation of few-photon pulses

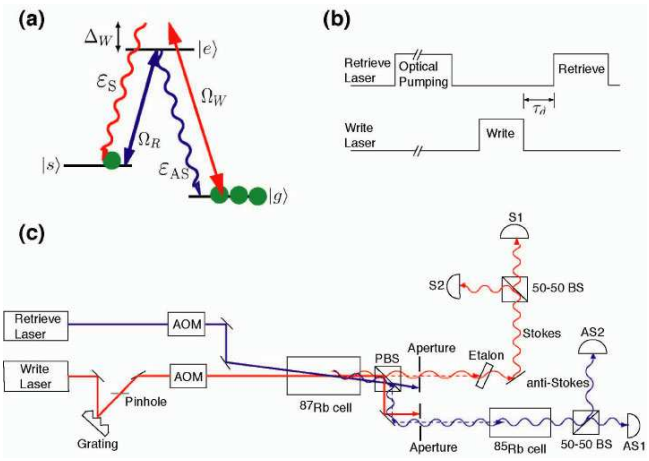

Figure 4.14: Experimental procedure and apparatus for quantum state generation via Raman scattering. (**a**) ^{87}Rb levels used in the experiments (D_1 line): $|g\rangle = |5^2S_{1/2}, F = 1\rangle$, $|s\rangle = |5^2S_{1/2}, F = 2\rangle$, and $|e\rangle$ corresponds to $|5^2P_{1/2}, F' = 1\rangle$ and $|5^2P_{1/2}, F' = 2\rangle$. (**b**) After the optical pumping pulse (provided by the retrieve laser), the 1.6 μs-long write pulse is followed by the retrieve pulse after a controllable delay τ_d. (**c**) Schematic of the experimental setup. For details see [52].

The results presented in the previous section were for CW light corresponding to 10^6 photons/μsec. We now turn to pulsed experiments, in the regime of $1 - 5$ photons/μsec.

We now describe in more detail our experiments on quantum correlated Stokes/anti-

Stokes pulse production and single-photon generation. Fig. 4.14c [159, 52] illustrates a typical experimental setup recently used by our group. Fig. 4.15a shows the average number of detected Stokes photons per unit time (photon flux) in the write channel as a function of time during the 1.6 μs-long write pulse. The photon flux is controlled by varying the excitation intensity. The shape of the Stokes pulse changes qualitatively as the total number of photons in the pulse exceeds unity: for pulses containing on average one photon or less, the flux is constant in time (more generally it follows the shape of the write laser), whereas for pulses containing more than one photon, the flux increases with time. This evolution of the Stokes pulses can be understood qualitatively by considering the mutual growth of the photon field and spin excitation: the first flipped spin *stimulates* subsequent spin excitations which are accompanied by increased probability of Stokes photon emission. The observed dynamics provide evidence for the collective nature of the atomic spin excitations.

After a time delay τ_d, we apply the retrieve beam to convert the stored spin wave into anti-Stokes photons. Fig. 4.15b demonstrates that the duration and peak flux of the anti-Stokes pulse can be controlled via the intensity of the retrieve laser. The resonant retrieve laser converts the spin coherence into a dark-state polariton [56], and eventually into an anti-Stokes photon. Since the retrieve laser establishes an EIT configuration for the generated anti-Stokes field, for larger (smaller) retrieve laser intensity, the excitation is released faster (slower), while the amplitude changes in such a way that the total number of anti-Stokes photons is always equal to the number of spin-wave excitations. In practice, decay of the spin coherence reduces the total number of anti-Stokes photons that can be retrieved, as indicated by theoretical

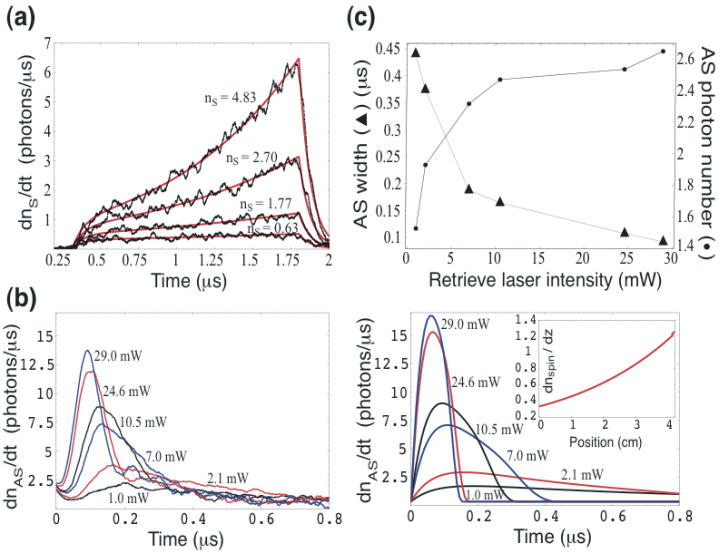

Figure 4.15: Stokes and anti-Stokes pulse shapes [52] (**a**) Experimental and theoretical values of the Stokes photon flux dn_S/dt. (**b**) Experimental (left) and theoretical (right) values of the anti-Stokes photon flux dn_{AS}/dt. The experimental pulse shapes correspond to a Stokes pulse with $n_S \approx 3$ photons, and the theoretical curves assume an initial spin wave with $n_{spin} = 3$ excitations and an optical depth of $\simeq 20$. Each curve is labeled with the power of the retrieve laser. (**b, inset**) Theoretical calculation of the number of flipped spins per unit length dn_{spin}/dz (cm^{-1}) for $n_{spin} = 3$. (**c**) Measured anti-Stokes pulse width (full-width at half-max) and total photon number as a function of the retrieve laser intensity.

calculations (Fig. 4.15b) based on Ref. [56].

At fixed laser intensities and durations, the number of Stokes and anti-Stokes photons fluctuates from event to event in a highly correlated manner [159]. To quantify these correlations, we compare the number of Stokes and anti-Stokes photons for a large number of pulsed events (each with identical parameters). The variance of the resulting distributions is then compared to the theoretical photon shot noise level $\text{PSN}_{th} = \bar{n}_S + \bar{n}_{AS}$, which represents the maximum degree of correlations possible for classical states [112]. We experimentally determine photon shot noise $\text{PSN}_{meas} = \text{var}(AS1 - AS2) + \text{var}(S1 - S2)$ by using a 50-50 beamsplitter and two

APDs per detection channel (see Fig. 4.14c).

To quantify the correlations, we consider the normalized variance

$$\mathrm{V} \;=\; \mathrm{var}(\{n_{AS} - n_S\})/\mathrm{PSN}_{meas}, \tag{4.122}$$

which is one for classically correlated pulses and zero for pulses exhibiting perfect number correlations. Fig. 4.16a shows the normalized variance V as a function of storage time τ_d. Non-classical correlations ($V < 1$) between Stokes and anti-Stokes pulses are clearly observed for storage times up to a few microseconds. This time scale arises because nonclassical correlations persist only as long as the coherence of the stored excitation is preserved. We note that at $\tau_d = 0$ the observed value $V = 0.942 \pm 0.006$ is far from the ideal value of $V = 0$. Sources of error contributing to this non-ideal value include finite retrieval efficiency, losses in the detection system, background photons, APD afterpulsing effects, and imperfect mode matching.

Since the storage and retrieval processes ideally result in identical photon numbers in the Stokes and anti-Stokes pulses [108], this technique should allow preparation of an n-photon Fock state in the anti-Stokes pulse conditioned on detection of n Stokes photons. In practice, these correlations allow for the conditional preparation of an anti-Stokes pulse with intensity fluctuations that are suppressed compared with classical light. To quantify this preparation, we measured the second-order intensity correlation function $g^{(2)}_{n_S}(AS)$ and mean number of photons $\bar{n}^{AS}_{n_S}$ for the anti-Stokes pulse conditioned on the detection of n_S photons in the Stokes channel (see Fig. 4.16b). (For classical states of light, $g^{(2)} \geq 1$; an ideal Fock state with n photons has $g^{(2)} = 1 - 1/n$.) Note that the mean number of anti-Stokes photons grows linearly with n_S, while $g^{(2)}_{n_S}(AS)$ drops below unity, indicating the non-classical character of

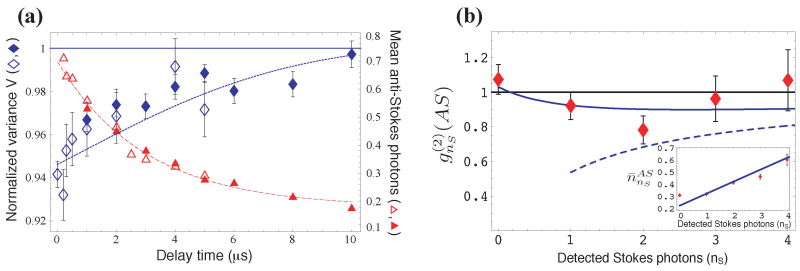

Figure 4.16: (**a**) Observation of nonclassical correlations. Normalized variance V (diamonds) and mean number of anti-Stokes photons (triangles) versus delay time τ_d. The open and closed symbols represent two experimental runs with similar experimental parameters. The dotted line is an exponential fit (characteristic time $\sim 3\mu$s) to the mean number of anti-Stokes photons. The solid line is the result of a theoretical model including the effects of loss, background, and several spatial modes on the Stokes and anti-Stokes channels. (**b**) Conditional nonclassical state generation. Diamonds show experimentally measured values $g^{(2)}(AS) = \langle AS_1 \cdot AS_2\rangle / \langle AS_1\rangle\langle AS_2\rangle$ (see Fig. 5c) as a function of the number of detected Stokes photons. The solid line shows the result of a theoretical model including background and loss on both the Stokes and anti-Stokes channels. (**Inset**) Measured mean anti-Stokes number $\bar{n}^{AS}_{n_S}$ conditioned on the Stokes photon number n_S.

the anti-Stokes photon states. In the presence of background counts, $g^{(2)}_{n_S}(AS)$ does not increase monotonically with n_S, but exhibits a minimum at $n_S = 2$. The Mandel Q parameter [112] can be calculated using $Q^{AS}_{n_S} = \bar{n}^{AS}_{n_S}(g^{(2)}_{n_S}(AS) - 1)$; from the measurements we determine $Q^{AS}_{n_S=2} = -0.09 \pm 0.03$ for conditionally generated states with $n_S = 2$ ($Q \geq 0$ for classical states and $Q = -1$ for Fock states).

It is evident that the Fock state preparation in these early measurements was far from perfect. We have recently implemented novel technical approaches that allow us to improve mode matching and to combine large signal to noise ratio with substantial retrieval efficiencies. Fulfilling these conditions simultaneously is essential for the realization of an efficient, controllable single photon source as well as for applications in quantum communication. Figure 4.17a shows a novel experimental

geometry in which ideal mode matching between the Stokes and anti-Stokes fields can be achieved automatically using single-mode optical fibers. Here, in the ideal limit of plane-wave write and retrieve lasers, the Stokes and anti-Stokes photons are emitted in counter-propagating single modes owing to the phase conjugation property of the underlying four-wave mixing interaction. In such a geometry it is possible to reduce the intensity of the write laser Ω_W such that the probability p of emitting a single Stokes photon from the atomic ensemble is much less than unity. The overall Stokes channel detection efficiency is η, thus making $p\eta$ the detection probability. The condition $p \ll 1$ then guarantees that detection of a single Stokes photon corresponds to no more than a single atomic excitation regardless of losses. Finally by optimizing the atomic density the various sources of background light can be suppressed. For example, by working in the configuration shown in Figure 4.17a we were able to increase the signal-to-noise ratio in the retrieval channel by a factor of 50 by operating at room temperature (20 C) instead of 75 C.

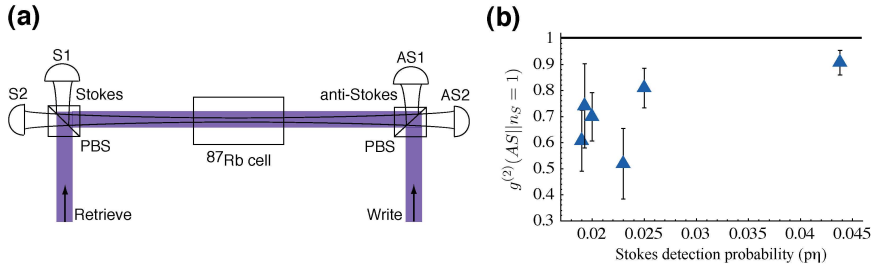

Figure 4.17: (**a**) Counter-propagating geometry for mode-matched Stoke/anti-Stokes pair creation. Note write and retrieve lasers have large beam waist size compared to Stokes/anti-Stokes modes, for ideal phase-conjugate retrieval. (**b**) Conditional single-photon generation. The second-order correlation function of the anti-Stokes field conditioned on detecting a single Stokes photon, $g^{(2)}(AS||n_S = 1)$, as a function of detection probability $p\eta$ of the Stokes channel. Data taken at an atomic ensemble temperature of 20 C, black line marks the classical limit of $g^{(2)} = 1$.

The conditional measurements of the second order correlation function for generated single photon pulses is shown in Fig. 4.17b. We clearly observe a large degree of suppression of intensity fluctuations $g^{(2)}(AS||n_S = 1) < 1$, indicating the nonclassical nature of the anti-Stokes field, with the lowest observed value $g^{(2)}(AS) = 0.52 \pm 0.14$ occurring with a conditional probability of detecting a single anti-Stokes photon in the relevant mode (retrieval efficiency) on the order of 30%. Since a larger value of p results in a decreased fidelity of preparation, $g^{(2)}(AS||n_s = 1)$ approaches the classical limit of 1 as p increases (see Fig. 4.17b). Further improvements involving operation at lower excitation power, for example, are likely. These results indicate that the present experimental approach represents a promising avenue for controlled single photon generation as well as for long-distance quantum communication.

Chapter 5

Dynamical control of the propagation properties of light pulses

5.1 Introduction

Techniques for coherent control of light-matter interaction are now actively explored for storing and manupilating quantum states of photons. In particular, using electromagnetically induced transparency (EIT) [147, 69] and adiabatic following of "dark-state polaritons" [56, 109], the group velocity of light pulses can be dramatically decelerated and their quantum state can be mapped onto metastable collective states of atomic ensembles [103, 128].

In contrast to such a coherent absorption process, this chapter describes how a propagating light pulse can be converted into a stationary excitation with non-

vanishing photonic component.

First, we describe a method for accomplishing this via controlled modification of the photonic density of states in EIT media by modulating the refractive index with an off-resonant standing light wave. By varying the properties of the resulting photonic band structure in time, the original light pulse can be converted into an excitation inside the bandgap where its propagation is forbidden. Long storage of excitations with non-vanishing photonic component may open interesting prospects for enhancement of nonlinear optical interactions [146, 73, 71].

We then describe a method based on a resonant modulation of the absorptive and refractive properties of an EIT atomic medium, achieved by using a standing wave configuration for the EIT control field [15]. We show that dynamic control of such a modulation can be used to convert propagating pulses of light into stationary excitations with non-vanishing electromagnetic component.

In particular, an intriguing and practically important [28, 122] application of this effect for interactions between few-photon fields [2] is briefly discussed.

5.2 Stationary Pulses of Light: Dispersive Case

5.2.1 Dispersive modulation via EIT

There exists a substantial litterature on photonic bandgap [83] materials and their use for strong coupling of single atoms with photons was investigated recently [161]. Especially relevant to the present work are studies of photonic bandgap due to interaction of light with atoms in an optical lattice [43] and other related work on

EIT-based control of the propagation properties of light in atomic media [93, 101].

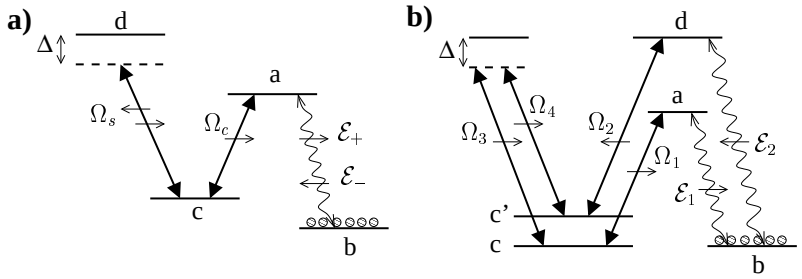

Figure 5.1: Atomic level configuration for EIT-induced photonic bandgap. a) Stationary atoms scheme, b) moving atoms scheme. The standing wave of Rabi frequency Ω_s is detuned by Δ from resonance with the $|c\rangle \rightarrow |d\rangle$ transition, giving rise to the spatially modulated light shift $\Delta_s(z,t) = |\Omega_s(z,t)|^2/\Delta$.

The key idea of the present approach can be qualitatively understood by considering a medium consisting of stationary atoms with a level structure shown in Fig. 5.1a. The atoms are interacting with a weak signal field and two strong fields. The running wave control field Ω_c is tuned close to the resonant frequency of the $a-c$ transition. In the absence of the field Ω_s, this situation corresponds to the usual EIT: in the vicinity of a frequency corresponding to two-photon resonance the medium becomes transparent for a signal field. This transparency is accompanied by a steep variation of the refractive index.

The dispersion relation can be further manipulated by applying an off-resonant standing wave field of frequency ω_s with Rabi frequency $\Omega_s(z) = 2\Omega_s \cos(k_s z)$ and detuning Δ from the $c-d$ transition. This field induces an effective shift of the resonant frequency (light shift) that varies periodically in space, resulting in a spatial modulation of the index of refraction according to $\delta n(z) = (c/v_g)4\frac{\Delta_s}{\omega_{ab}}\cos^2(k_s z)$, where $\Delta_s = \frac{\Omega_s^2}{\Delta}$ is the amplitude of the light shift modulation, ω_{ab} is the $a-b$ tran-

sition frequency and c/v_g is the ratio of speed of light in vacuum to group velocity in the medium. When the modulation depth is sufficiently large, signal light propagating near atomic resonance in the forward z direction with wavevector k near $k_s = \omega_s/c$ may undergo Bragg scattering into the backward propagating mode with wavenumber $-k$. In direct analogy to e.g., optical interferometers, the scattering of the counterpropagating fields into each other can modify the photonic density of states. In particular, a range of frequencies ("photonic bandgap") can appear for which light propagation is forbidden. To obtain the resulting band structure, we use coupled mode techniques (see [167] and description below) together with Bloch's theorem [10] $E(z+a) = e^{iKa}E(z)$ (where K is the Bloch wave vector and $a = \pi/k_s$ is the periodicity of the modulation) and obtain near two-photon resonance

$$\cos(Ka) = -\cosh\left(\frac{a}{v_g}\sqrt{\Delta_s^2 - (\omega - \omega_{ab} - \frac{v_g}{c}\Delta\omega)^2}\right), \tag{5.1}$$

where $\Delta\omega = \omega_s - \omega_{ab}$. For frequencies such that $|\omega - \omega_{ab} - \frac{v_g}{c}\Delta\omega| \leq |\Delta_s|$ a *bandgap* is created: the Bloch wavevector acquires an imaginary part and the propagation of waves in the medium is forbidden. For an outside observer such a medium can be viewed as a mirror: an incident wave with frequency inside the bandgap would undergo almost perfect reflection. Calculations in Fig. 5.2 (taking the full frequency dependence of the susceptibility into account) indicate that this qualitative result remains valid even for realistic EIT conditions, including a finite transparency bandwidth and finite ground-state decoherence rate γ_{bc}.

A specific, distinguishing feature of the present scheme is the possibility of *dynamically* changing the properties of the medium by switching in time the fields $\Omega_s(t)$ and $\Omega_c(t)$ on and off. In particular, by combining the techniques of [103, 128] with the

present idea, the following scenario can be implemented: first, with the standing wave turned off $\Omega_s = 0$, a forward propagating pulse is stored in the medium as a Raman coherence between levels $|b\rangle$ and $|c\rangle$. Then, by switching on both the "control" field Ω_c and the standing wave field Ω_s, the pulse can be released into the bandgap. In the presence of a bandgap, the forward ($\hat{\mathcal{E}}_+$) and backward ($\hat{\mathcal{E}}_-$) components are coupled due to Bragg scattering off the index grating, so that amplitude in the forward $+k$ mode is converted into the $-k$ mode and vice versa. In this case, the pulse can be effectively trapped in the photonic bandgap.

5.2.2 Dynamically controlled photonic band gap

We now turn to a detailed description of the dynamic trapping procedure. We are interested here in the propagation of fields with possibly non-trivial statistics, such as single photon fields, so that a quantum description is used. In the presence of the standing wave it is convenient to decompose the propagating signal fields into two slowly varying components $\hat{\mathcal{E}}_+$ (propagating forward) and $\hat{\mathcal{E}}_-$ (propagating backward) so that the electric field is $\hat{E}(z,t) = \sqrt{\frac{\hbar\omega_{ab}}{2\epsilon_0 V}}\left[\sum_{\sigma=\pm}\hat{\mathcal{E}}_\sigma(z,t)e^{i(\omega_{ab}/c)(\sigma z - ct)} + \text{h.c.}\right]$, the carrier frequency of the optical field being ω_{ab}. Two time dependent classical driving fields with Rabi frequencies $\Omega_s(t)$ and $\Omega_c(t)$ are used to control the propagation as shown if Fig. 5.1a.

To describe the quantum properties of the medium, we use collective slowly varying atomic operators [58] $\hat{\sigma}_{\mu\nu}(z,t) = \frac{1}{N_z}\sum_{j=1}^{N_z}|\mu_j\rangle\langle\nu_j|e^{-i\omega_{\mu\nu}t}$ where the sum is performed over a small but macroscopic volume containing $N_z \gg 1$ atoms around posi-

tion z. The interaction hamiltonian is then, in a rotating frame

$$\begin{aligned}\hat{H} &= \frac{N}{L}\int dz \left\{\Delta\hat{\sigma}_{dd} - \Big[g(\hat{\mathcal{E}}_+ e^{ik_0 z} + \hat{\mathcal{E}}_- e^{-ik_0 z})\hat{\sigma}_{ab} \right. \\ &+ \left. \Omega_c e^{ik_c z}\hat{\sigma}_{ac} + 2\Omega_s \cos(k_s z)\hat{\sigma}_{dc} + \text{h.c.}\Big]\right\}, \end{aligned} \tag{5.2}$$

where $g = \wp\sqrt{\frac{\omega_{ab}}{2\hbar\epsilon_0 V}}$ is the atom-field coupling constant, N is the number of atoms, L is the length of the medium, $\wp$ is the dipole moment of the $a-b$ transition, V the quantization volume and $k_0 = \omega_{ab}/c$.

Interaction of the two propagating fields $\hat{\mathcal{E}}_+$ and $\hat{\mathcal{E}}_-$ with the atoms gives rise to an optical coherence $\hat{\sigma}_{ba}$ as well as a Raman coherence $\hat{\sigma}_{bc}$ with specific spatial variations, i.e., varying as $e^{ik_0 z}$ for the component of $\hat{\sigma}_{ba}$ induced by $\hat{\mathcal{E}}_+$ while that due to $\hat{\mathcal{E}}_-$ will vary as $e^{-ik_0 z}$. We therefore decompose these coherences into two distinct spatial dependences $\hat{\sigma}_{ba}(z,t) = \hat{\sigma}^+_{ba}(z,t)e^{ik_0 z} + \hat{\sigma}^-_{ba}(z,t)e^{-ik_0 z}$ and $\hat{\sigma}_{bc}(z,t) = \hat{\sigma}^+_{bc}(z,t)e^{i(k_0-k_c)z} + \hat{\sigma}^-_{bc}(z,t)e^{-i(k_0+k_c)z}$. Using slowly varying envelopes, we have the equations of motion for the forward and backward modes

$$\left(\frac{\partial}{\partial t} \pm c\frac{\partial}{\partial z}\right)\hat{\mathcal{E}}_\pm(z,t) = igN\hat{\sigma}^\pm_{ba}(z,t). \tag{5.3}$$

Assuming weak quantum fields and solving perturbatively, we find to lowest order in the weak fields and in an adiabatic approximation (assuming $\Omega_s(t)$ and $\Omega_c(t)$ change in time slowly enough [56])

$$\hat{\sigma}^\pm_{ba}(z,t) = -\frac{i}{\Omega_c}\left[\frac{\partial}{\partial t}\hat{\sigma}^\pm_{bc}(z,t) - i\Delta_s e^{\pm 2i(\Delta\omega/c)z}\hat{\sigma}^\mp_{bc}(z,t)\right] \tag{5.4}$$

$$\hat{\sigma}^\pm_{bc}(z,t) = -\frac{g\hat{\mathcal{E}}_\pm(z,t)}{\Omega_c} - i\frac{\hat{F}^\pm_{ba}(t)}{\Omega_c}, \tag{5.5}$$

where $\hat{F}^\pm_{ba}(t)$ are δ-correlated noise forces. Note that in the adiabatic limit the noise

forces are negligible [56]. The propagation equations are thus

$$\left(\frac{\partial}{\partial t} \pm c\frac{\partial}{\partial z}\right)\hat{\mathcal{E}}_{\pm}(z,t) = - \frac{g^2 N}{\Omega_c}\frac{\partial}{\partial t}\frac{\hat{\mathcal{E}}_{\pm}(z,t)}{\Omega_c} + i\frac{g^2 N}{\Omega_c}\Delta_s \frac{\hat{\mathcal{E}}_{\mp}(z,t)}{\Omega_c} e^{\pm 2i(\Delta\omega/c)z}, \tag{5.6}$$

which indicates that the forward and backward slowly propagating modes become coupled. Specifically, the first term on the right-hand side gives rise to propagation at the group velocity $v_g = c/(1 + \frac{g^2 N}{\Omega_c^2})$ [74, 35, 87] while the second term gives rise to coupling between the forward and backward propagating modes. Considering first a situation involving cw fields, the equations (5.6) can be easily integrated. Solving the boundary value problem $\mathcal{E}_+(0,t) = \mathcal{E}_+^{in},\ \mathcal{E}_-(L,t) = 0$ yields directly the reflection coefficient as in Fig. 5.2b. Furthermore, integrating (5.6) over one modulation period $a = \pi/k_s$ and applying Bloch's theorem (as in [167]) yields the dispersion relation (5.1). Finally, we point out that the spatially varying part of the last term ($e^{\pm 2i(\Delta\omega/c)z}$) can be eliminated by choosing the center frequency of the signal field $\omega = \omega_{ab} + \frac{v_g}{c}\Delta\omega$ thereby fulfilling the effective phase matching condition [82]. In the limit $v_g \to 0$ this term can therefore be always neglected even for resonant fields.

To obtain a solution in the case of time-dependent fields $\Omega_c(t)$ and $\Omega_s(t)$, we introduce new quantum fields $\hat{\Psi}_+(z,t)$ and $\hat{\Psi}_-(z,t)$ (forward and backward propagating dark-state polaritons [56]) $\hat{\Psi}_{\pm}(z,t) = \cos\theta(t)\hat{\mathcal{E}}_{\pm}(z,t) - \sin\theta(t)\sqrt{N}\hat{\sigma}_{bc}^{\pm}(z,t)$, where $\tan^2\theta(t) = \frac{g^2 N}{\Omega_c(t)^2}$ is the mixing angle between the photon and matter components of the polariton. The polaritons then obey the coupled equations

$$\left(\frac{\partial}{\partial \tau} \pm c\frac{\partial}{\partial z}\right)\hat{\Psi}_{\pm} = i\Delta_s \tan^2\theta(t)\hat{\Psi}_{\mp}, \tag{5.7}$$

where $\tau(t) = \int^t dt'\ \cos^2\theta(t')$. Eq. (5.7) describes propagation with velocity $v_g(t) =$

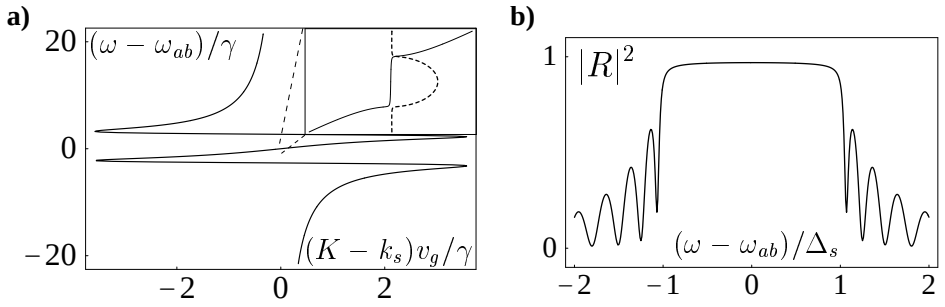

Figure 5.2: a) Dispersion relation $\omega(K)$ for waves propagating in EIT-induced bandgap medium. Plotted is the detuning from two-photon resonance $\omega - \omega_{ab}$ in units of linewidth γ vs. the Bloch wavevector K in units of γ/v_g. For $|\omega - \omega_{ab}| \gg \gamma$, we have $\omega = cK$ while near resonance $\omega = v_g K$. For $|\omega - \omega_{ab}| \leq \Delta_s$ a bandgap appears, as shown in the inset (full line: real part of $K - k_s$, dashed line: imaginary part). b) Reflection coefficient vs. frequency near EIT resonance for ^{87}Rb atoms with density $n \sim 10^{12}\text{cm}^{-3}$, length of medium $L \sim 4$cm, $\gamma_{bc} \sim 1$kHz, $\gamma \sim 5$MHz, $c/v_g \sim 10^5$, $\Omega_s \sim 2\gamma$ and $\Delta \sim 1$GHz ($\Delta_s = \frac{\Omega_s^2}{\Delta} \sim 100$kHz), giving a peak reflectivity of $\sim 97\%$.

$c\cos^2\theta(t)$ of the two polaritons (traveling in opposite directions) and coupling with rate $\Delta_s(t)\sin^2\theta(t)$. Note that in the limit $c \gg v_g$, the photonic component $\hat{\mathcal{E}}_\pm \simeq (\Omega_c/g\sqrt{N})\hat{\Psi}_\pm$ is finite for non-zero control field Ω_c.

5.2.3 Trapping of light pulses

We consider now the scenario in which the standing wave beams are initially off and the control field is on, with Rabi frequency Ω_c^{in} (corresponding to a group velocity v_g^{in}). A forward propagating photon wavepacket can then be stored in the medium in the form of a Raman coherence $\hat{\sigma}_{bc}^+(z,t)$ by turning off the control field [103, 128]. Next, to create a stationary photonic component, the standing wave field Ω_s is switched on, thereby establishing the bandgap. Simultaneously the control field is switched on to a Rabi frequency Ω_c^0 (group velocity v_g^0), thereby releasing the

pulse in the bandgap medium. In such a case, we solve (5.7) by Fourier transforming $\hat{\Psi}_{\pm}(z) = \frac{1}{2\pi}\int dk\; e^{ikz}\hat{\Psi}_{\pm}(k)$ to obtain

$$\begin{aligned}\hat{\Psi}_{+}(k,\tau) &= \left[\cos(\zeta\tau) - i\frac{kc}{\zeta}\sin(\zeta\tau)\right]\hat{\Psi}_{+}(k,0)\\ \hat{\Psi}_{-}(k,\tau) &= i\frac{\chi}{\zeta}\sin(\zeta\tau)\hat{\Psi}_{+}(k,0),\end{aligned} \tag{5.8}$$

where $\chi \equiv \Delta_s(\tau)\tan^2\theta(\tau) = \frac{g^2N}{\Delta}\frac{\Omega_c^2}{\Omega_s^2}$ (for simplicity assumed to be constant) and $\zeta = \sqrt{(kc)^2+\chi^2}$. According to (5.8), the Fourier components of the pulse cycle back and forth between the forward and backward modes at a rate which depends weakly on k. In particular when the spatial extent of the pulse inside the medium is large enough, pulse distortion is negligible and the spatial envelopes have the time dependence $\hat{\Psi}_{+}(z,\tau) = \cos(\chi\tau)\hat{\Psi}_{+}(z,0)$ and $\hat{\Psi}_{-}(z,\tau) = i\sin(\chi\tau)\hat{\Psi}_{+}(z,0)$. The wavepacket periodically cycles between a forward and backward propagating component, the result of which is *trapping* of the pulse in the medium as shown in Fig. 5.3. The wavepacket is trapped as a combination of light pulse and Raman coherence.

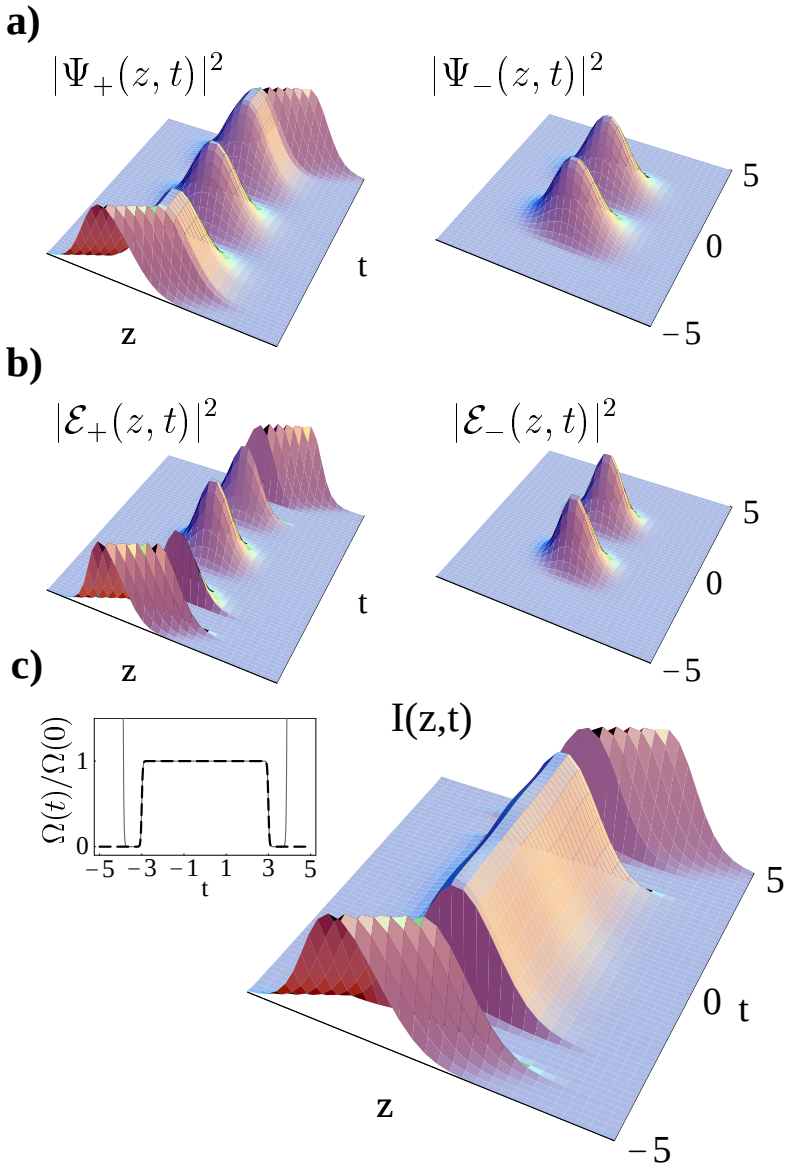

Figure 5.3: a) Evolution of forward and backward propagating polaritons $\Psi_+(z,t)$ and $\Psi_-(z,t)$ as calculated from (5.7). b) Corresponding electric fields and c) total intensity (forward and backward components) averaged over the optical wavelength. Also shown is the time-dependence of the "control" field $\Omega_c(t)$ (full grey line) and of standing wave field $\Omega_s(t)$ (dashed black line). Note that $v_g^{in}/v_g^0 \sim 15$ here so that initial motion of the pulse is noticeable on these plots. Axes are in arbitrary units.

The above analysis involves an adiabatic approximation and ignores the decay of Raman coherence at rate γ_{bc}. In order to ignore the motion compared to the coupling we require that $\chi \gg kc$ and since the maximum k can be estimated from the initial length of the pulse in the medium we find that this is equivalent to requiring that $\Delta_s T \gg \frac{v_g^0}{v_g^{in}}$, where T is the duration of the initial pulse. As seen from (5.8) the effect of non-zero values of k is that the trapped pulse become spatially distorted. Expanding $\sqrt{\chi^2 + (kc)^2}\tau \simeq [\chi + (kc)^2/(2\chi)]\tau$ we need $\tau \ll \chi/(kc)^2$, which gives after expressing τ in terms of real time t that $\frac{t_{int}}{T} \ll \Delta_s T(v_g^{in}/v_g^0)^2$, where t_{int} is the maximum time during which the pulse may be trapped without suffering distortion. Furthermore, taking into account the limits imposed by adiabaticity (i.e., modulation of index occurs within the transparency window $\Delta_s \ll (\Omega_c^0)^2/\gamma$) and the fact that the trapped pulse must fit inside the medium when travelling at the reduced group velocity, we find that the trapping or interaction time is limited by

$$t_{int} \lesssim \frac{g^2 N}{\gamma(c/L)} \frac{v_g^{in}}{v_g^0} T, \frac{1}{\gamma_{bc}}, \tag{5.9}$$

where γ is the spontaneous emission rate. The limiting quantity in this expression corresponds to the density length-product and can be rather large for optically dense medium. Note that the trapping time (5.9) can be much longer than the corresponding group delay [56] for optically dense medium.

We have shown that by spatially modulating the dispersive feature of the EIT resonance it is possible to induce a photonic bandgap. By dynamically controlling the resulting band structure, a propagating light pulse can be converted into a stationary excitation which is effectively trapped in the medium. Note that the present work is not restricted to the use of stationary or cold atoms, for example a Doppler-free

configuration involving pairs of copropagating fields is shown in Fig. 5.1b. In this case, the two polaritons are asociated with distinct atomic states $|c\rangle$ and $|c'\rangle$. Each polariton corresponds to a Doppler-free Raman configuration and they are coupled by a Doppler-free two-photon transition. Alternatively, rare-earth doped materials could be used in a regime similar to that of [157]. This work may open interesting prospects for nonlinear optics, as discussed in Chapter 6. Owing to the long trapping time (5.9), a trapped photonic excitation can be used to induce a light shift via interaction with another atom-like polariton, thereby allowing strong interaction of light pulses at low light level via the mechanism described in [146, 106]. Large nonlinear phase shifts can be expected and open up the way for possible applications in quantum non-linear optics and quantum information without the limitations associated with traveling wave configurations [71, 106] and without invoking cavity QED techniques [77, 79].

5.3 Stationary Pulses of Light: Absorptive Case

5.3.1 Basic Idea

In contrast to the purely dispersive modulation described previously, we now consider the situation where resonant counter-propagating fields are used to spatially modulate the EIT. This technique allows light propagating in a medium of warm Rb atoms to be converted into an excitation with localized, stationary electromagnetic energy, and then released after a controllable interval [15]. The key difference from the stored light technique described in [128] is the application of both forward and backward control beams, after the input signal pulse has been mapped by dy-

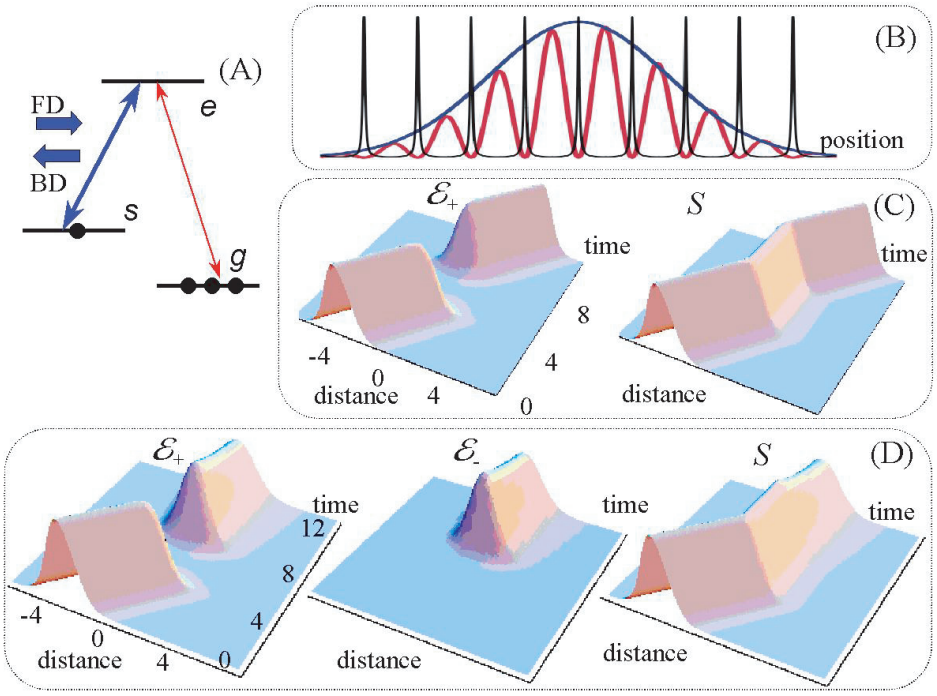

Figure 5.4: (A) Atomic level configuration. (B) Spatial variation of signal field absorption (black line), stationary pulse signal field (red line), and atomic spin coherence (blue line). (C) Storage of weak signal pulse in atomic coherence $|g\rangle\langle s|$. (D) Evolution of forward and backward signal components and atomic coherence when both control fields (FD and BD) are turned on with equal Rabi-frequencies.

namic EIT into an atomic spin-wave (see Figure 5.4). Upon their application, the counter-propagating control fields create a standing wave pattern, and EIT suppresses absorption of the signal pulse everywhere but in the nodes of the standing wave, resulting in a sharply peaked, periodic modulation of the atomic absorption for the signal light (Fig. 5.4B). Illumination by these beams also results in partial conversion of the stored atomic spin excitation into sinusoidally modulated signal light, but the latter cannot propagate in the medium due to Bragg reflections off the sharp absorption peaks, resulting in vanishing group velocity of the signal pulse, as in Fig. 5.4D. Only after one of the control beams is turned off does the signal pulse acquire a finite

velocity and leave the medium in the direction of the remaining control beam.

5.3.2 Spatially Modulated Transparency

Equations of motion

We consider two counter-propagating control fields with Rabi frequencies $\Omega_\pm$ tuned to resonance with the $|s\rangle \rightarrow |e\rangle$ transition, as shown in Fig. 5.5. The forward

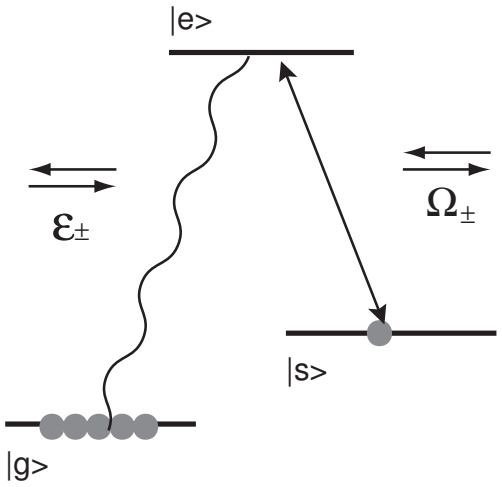

Figure 5.5: Atomic level configuration for creating stationary pulses of light. Counter-propagating control fields of Rabi frequencies $\Omega_\pm$ modulate the EIT for the forward and backward propagating components of the signal field $\hat{\mathcal{E}}_\pm$, and results in strong coupling to the spin coherence $\hat{\mathcal{S}} = \sqrt{N}\hat{\sigma}_{gs}$.

and backward propagating components of the signal field have slowly varying envelopes $\hat{E}_\pm(z,t)$, so that the slowly varying signal field is $\hat{E}_S^{(+)}(z,t) = \left[\hat{E}_+(z,t)e^{ik_s z} + \hat{E}_-(z,t)e^{-ik_s z}\right]$, where $k_s = n_s\omega_{eg}/c$, V is the quantization volume, and n_s is the background refractive index at the frequency ω_{eg}, due to off-resonant atomic levels. The interaction

Hamiltonian can be written as

$$\begin{aligned}\hat{H} &= -\frac{N}{L}\int dz\left[\left(\Omega_+ e^{iKz}+\Omega_- e^{-iKz}\right)\hat{\sigma}_{es}(z,t)\right.\\ &+ \left. g\left(\hat{E}_+(z,t)e^{ik_s z}+\hat{E}_-(z,t)e^{-ik_s z}\right)\hat{\sigma}_{eg}(z,t)+\text{H.c.}\right] \qquad (5.10)\end{aligned}$$

where $\hat{\sigma}_{eg}$ and $\hat{\sigma}_{es}$ are collective atomic operators, as described previously, and where $K=\omega_{es}/c$.

Associated with the forward/backward propagating fields are slowly varying polarization envelopes $\hat{P}_\pm(z,t)$, so that the total polarization can be written as $\sqrt{N}\hat{\sigma}_{ge}(z,t)=\hat{P}_+(z,t)e^{ik_s z}+\hat{P}_-(z,t)e^{-ik_s z}$. Similarly the ground-state spin coherence is defined as $\mathcal{S}(z,t)=\sqrt{N}\sigma_{gs}(z,t)$. Letting the wave-vector mismatch be $\Delta K = K-k_s$, and defining $\hat{\mathcal{E}}_\pm=\hat{E}_\pm e^{\mp i\Delta K z}$ and $\hat{\mathcal{P}}_\pm=\hat{P}_\pm e^{\mp i\Delta K z}$, the equations of motion for the fields can then be written as

$$(\partial_t + c\partial_z)\hat{\mathcal{E}}_+(z,t) = i\Delta K c\,\hat{\mathcal{E}}_+ + ig\sqrt{N}\hat{\mathcal{P}}_+ \qquad (5.11a)$$

$$(\partial_t - c\partial_z)\hat{\mathcal{E}}_-(z,t) = i\Delta K c\,\hat{\mathcal{E}}_- + ig\sqrt{N}\hat{\mathcal{P}}_- \qquad (5.11b)$$

while the atomic equations of motion are (to leading order in the weak fields $\hat{\mathcal{E}}_\pm$)

$$\partial_t\hat{\mathcal{P}}_+ = -\gamma\hat{\mathcal{P}}_+ + i\Omega_+\hat{\mathcal{S}} + ig\sqrt{N}\hat{\mathcal{E}}_+ + \hat{\mathcal{F}}_{P+}(z,t) \qquad (5.12a)$$

$$\partial_t\hat{\mathcal{P}}_- = -\gamma\hat{\mathcal{P}}_- + i\Omega_-\hat{\mathcal{S}} + ig\sqrt{N}\hat{\mathcal{E}}_- + \hat{\mathcal{F}}_{P-}(z,t) \qquad (5.12b)$$

$$\partial_t\hat{\mathcal{S}} = -\gamma_0\hat{\mathcal{S}} + i\Omega_+^*\hat{\mathcal{P}}_+ + i\Omega_-^*\hat{\mathcal{P}}_- + \hat{\mathcal{F}}_S(z,t), \qquad (5.12c)$$

where $\hat{\mathcal{F}}_{S,P\pm}(z,t)$ are Langevin noise forces associated with the decay terms in the equations of motion.

These equations show that the counter-propagating control fields $\Omega_\pm$ induce a coupling between $\hat{\mathcal{E}}_+$ and $\hat{\mathcal{E}}_-$, mediated through the spin coherence $\hat{\mathcal{S}}$. This leads to

the formation of new eigenmodes of propagation, where as we show below, there is one mode that is very rapidly decaying while the other decays very weakly in the large optical depth limit. This phenomenon is analogous to the "pulse matching" phenomenon, as first described by Harris [68].

Adiabatic solution

We are interested in a solution to the equations of motion in the adiabatic limit, corresponding in the time domain to slow variations of the field amplitudes, and in the frequency domain to a narrow frequency window around two-photon resonance. Thus, we look for adiabatic solutions which include terms up to first order in $\partial/\partial t$. Introducing the polariton amplitudes $\hat{\mathcal{E}}_\pm = \Omega_\pm \hat{\psi}_\pm / g\sqrt{N}$, we adiabatically eliminate the polarizations $\hat{\mathcal{P}}_\pm$, and obtain

$$\hat{\mathcal{P}}_\pm \simeq i\frac{\Omega_\pm}{\gamma}\left[\hat{\mathcal{S}} + \hat{\psi}_\pm\right] + \frac{\hat{\mathcal{F}}_{P\pm}}{\gamma} \tag{5.13}$$

$$\partial_t \hat{\mathcal{S}} = -\left[\gamma_0 + \frac{|\Omega_+|^2 + |\Omega_-|^2}{\gamma}\right]\hat{\mathcal{S}} - \frac{|\Omega_+|^2}{\gamma}\hat{\psi}_+ - \frac{|\Omega_-|^2}{\gamma}\hat{\psi}_- + \tilde{\mathcal{F}}_S, \tag{5.14}$$

where $\tilde{\mathcal{F}}_S(z,t) = \hat{\mathcal{F}}_S + i\frac{\Omega_+^*}{\gamma}\hat{\mathcal{F}}_{P+} + i\frac{\Omega_-^*}{\gamma}\hat{\mathcal{F}}_{P-}$.

The polaritons obey the equations of motion

$$(\partial_t \pm c\partial_z)\hat{\psi}_\pm = ig^2 N\frac{\hat{\mathcal{P}}_\pm}{\Omega_\pm}. \tag{5.15}$$

Solving to first order in ∂_t for $\mathcal{S}$, we find

$$\hat{\mathcal{S}} = -(\alpha_+\hat{\psi}_+ + \alpha_-\hat{\psi}_-) + \frac{\eta}{\xi}(\partial_t + \gamma_0)(\alpha_+\hat{\psi}_+ + \alpha_-\hat{\psi}_-) + \frac{\eta}{\xi}\tilde{\mathcal{F}}_S, \tag{5.16}$$

where $\eta = \frac{g^2 N}{|\Omega_+|^2 + |\Omega_-|^2}$, and plugging in the equation of motion for the polaritons, we

finally have

$$\begin{aligned}(\partial_t + c\partial_z)\hat{\psi}_+ &= i\Delta K c\hat{\psi}_+ - \eta(\partial_t + \gamma_0)(\alpha_+\hat{\psi}_+ + \alpha_-\hat{\psi}_-) \\ &- \alpha_-\xi(\hat{\psi}_+ - \hat{\psi}_-) + \hat{\mathcal{F}}_{\psi+} \qquad (5.17)\\ (\partial_t - c\partial_z)\hat{\psi}_- &= i\Delta K c\hat{\psi}_- - \eta(\partial_t + \gamma_0)(\alpha_+\hat{\psi}_+ + \alpha_-\hat{\psi}_-) \\ &+ \alpha_+\xi(\hat{\psi}_+ - \hat{\psi}_-) + \hat{\mathcal{F}}_{\psi-} \qquad (5.18)\end{aligned}$$

where $\xi = g^2N/\gamma = c/L_{abs}$. and $\alpha_\pm = \frac{|\Omega_\pm|^2}{|\Omega_+|^2+|\Omega_-|^2}$.

The counter-propagating polaritons $\psi_\pm$ are now coupled and give rise to new eigenmodes of the equations of motion. In fact, we can see by inspection of the above equations that the modes appear only in the combinations $\alpha_+\hat{\psi}_+ + \alpha_-\hat{\psi}_-$ and $\hat{\psi}_+ - \hat{\psi}_-$, corresponding to the zeroth order adiabatic solution for the spin wave $\hat{\mathcal{S}} \simeq -(\alpha_+\hat{\psi}_+ + \alpha_-\hat{\psi}_-)$, as seen from 5.16.

We thus introduce the two new modes $\hat{\Psi} \equiv \hat{\psi}_+ - \hat{\psi}_-$ and $\hat{\mathcal{S}} = -(\alpha_+\hat{\psi}_+ + \alpha_-\hat{\psi}_-)$ (we keep the symbol $\hat{\mathcal{S}}$ to denote this new mode, as a reminder that it corresponds to the spin wave excitation in the adiabatic limit). We have $\hat{\psi}_+ = \alpha_-\hat{\Psi} - \hat{\mathcal{S}}$ and $\hat{\psi}_- = -(\alpha_+\hat{\Psi} + \hat{\mathcal{S}})$, so that the equations of motion become

$$[(\eta+1)\partial_t + \eta\gamma_0]\hat{\mathcal{S}} = [i\Delta Kc - (\alpha_+ - \alpha_-)c\partial_z]\hat{\mathcal{S}} + 2\alpha_+\alpha_- c\partial_z\hat{\Psi} + \eta\hat{\mathcal{F}}_S \qquad (5.19a)$$

$$(\partial_t + \xi)\hat{\Psi} = [i\Delta Kc + (\alpha_+ - \alpha_-)c\partial_z]\hat{\Psi} + 2c\partial_z\hat{\mathcal{S}} + \hat{\mathcal{F}}_\Psi \qquad (5.19b)$$

For large optical depths, ξ is large and we may adiabatically solve for $\hat{\Psi}$ (this is a fastly decaying mode), and plugging back in the $\hat{\mathcal{S}}$ equation, we find (assuming

$\eta = c/v_g \gg 1$)

$$\hat{\Psi} \simeq \frac{2c\partial_z}{\xi}\hat{\mathcal{S}} \tag{5.20a}$$

$$\eta[\partial_t + \gamma_0]\hat{\mathcal{S}} = [i\Delta Kc - (\alpha_+ - \alpha_-)c\partial_z]\hat{\mathcal{S}} + 4\alpha_+\alpha_-\frac{(c\partial_z)^2}{\xi}\hat{\mathcal{S}} + \hat{\mathcal{F}}_S. \tag{5.20b}$$

The group velocity of the combined excitation $\hat{\mathcal{S}} = -(\alpha_+\hat{\psi}_+ + \alpha_-\hat{\psi}_-)$ is thus $v_g^{\mathcal{S}} = (\alpha_+ - \alpha_-)c/\eta$, and the effect of the weak coupling of $\hat{\mathcal{S}}$ to $\hat{\Psi}$ becomes, after adiabatic elimination of $\hat{\Psi}$, a slow spreading of the pulse in space (diffusion-like). By adjusting the relative intensity of the counter-propagating control fields $|\Omega_\pm|^2$, the group velocity of the excitation can be dynamically controlled. Note also that the wavevector mismatch ΔK is easily compensated for by a small two photon detuning $\delta = -\Delta Kc/\eta$.

Note that bound to the stationary excitation $\hat{\mathcal{S}}$ there are electromagnetic components $\hat{\mathcal{E}}_\pm$ in the forward and backward propagating modes. These components are given by

$$\hat{\mathcal{E}}_+ \simeq -\frac{\Omega_+}{g\sqrt{N}}\left(1 - \frac{2\alpha_- c\partial_z}{\xi}\right)\hat{\mathcal{S}} \tag{5.21a}$$

$$\hat{\mathcal{E}}_- \simeq -\frac{\Omega_-}{g\sqrt{N}}\left(1 + \frac{2\alpha_+ c\partial_z}{\xi}\right)\hat{\mathcal{S}}. \tag{5.21b}$$

The spatial modulation of EIT thus leads to the possibility of trapping pulses of light in an atomic medium, by converting them from propagating solutions to stationary ones, bound to the atomic spin coherence. The atomic medium behaves as an effective "cavity", trapping the light pulse by inducing a coupling between counter-propagating components of the field, analogous to the coupling induced by cavity mirrors. Denoting by $v_g = c/(2\eta) = c\frac{1}{2}\left(\frac{|\Omega_+|^2}{g^2N} + \frac{|\Omega_-|^2}{g^2N}\right)$, an effective group

velocity in the medium, we can interpret the pulse spreading in terms of an effective finesse for the "cavity" created by the atomic medium. For a gaussian pulse envelope of length l (length of the pulse inside the medium), the pulse spreads according to equation 5.20b as $\frac{l(t)^2-l^2}{l^2} = \frac{\xi t}{\eta l^2}$ (where we set $\alpha_+ = \alpha_- = \frac{1}{2}$ for simplicity). Defining the cavity decay time τ_{cav} as the time required for the pulse width to double in magnitude, we have $\tau_{cav} = 2\frac{\eta l^2}{\xi} = \frac{l}{v_g} \times \frac{l}{L_{abs}}$, where $L_{abs} = c/\xi$ is the on-resonance absorption length. The effective round-trip time of the cavity is $\tau_{rt} = \frac{l}{v_g}$, so that we may rewrite the above as $\tau_{cav} = \mathcal{F}\tau_{rt}$ where the effective finesse is $\mathcal{F} = l/L_{abs}$, i.e. it is equal to the on-resonance optical depth (over a length corresponding to the length of the pulse inside the medium). We thus conclude that large effective finesse are easily achievable in optically thick atomic media.

The lifetime of the stationary excitation in the modulated atomic medium thus scales linearly with the optical depth. This represents a large improvement over the simple pulse delay achieved by group velocity reduction in EIT, which scales as $\sqrt{d_0}$ [57]. As discussed in Chapter 6, the long storage time combined with the presence of electromagnetic components to the trapped excitation, opens up the way to strong and efficient nonlinear optical interactions, possibly at the single photon level.

5.4 Stationary Pulses of Light: Experiments

We briefly describe here a first set of experiments [15], in which we investigated the longitudinal confinement of light signals caused by spatial modulation of EIT, and the creation of stationary pulses of light by dynamical control of this modulation. In the experiments, the "absorptive" case was investigated, rather than the "dispersive"

case described previously. For warm atomic vapors, the dispersive case is difficult to achieve because it requires to establish an EIT for both the forward and backward propagation directions independently of one another. In practice, it is easier to investigate the "absorptive" case for which the modulation of EIT both establishes a transparency and introduces a controllable coupling between forward and backward propagation directions.

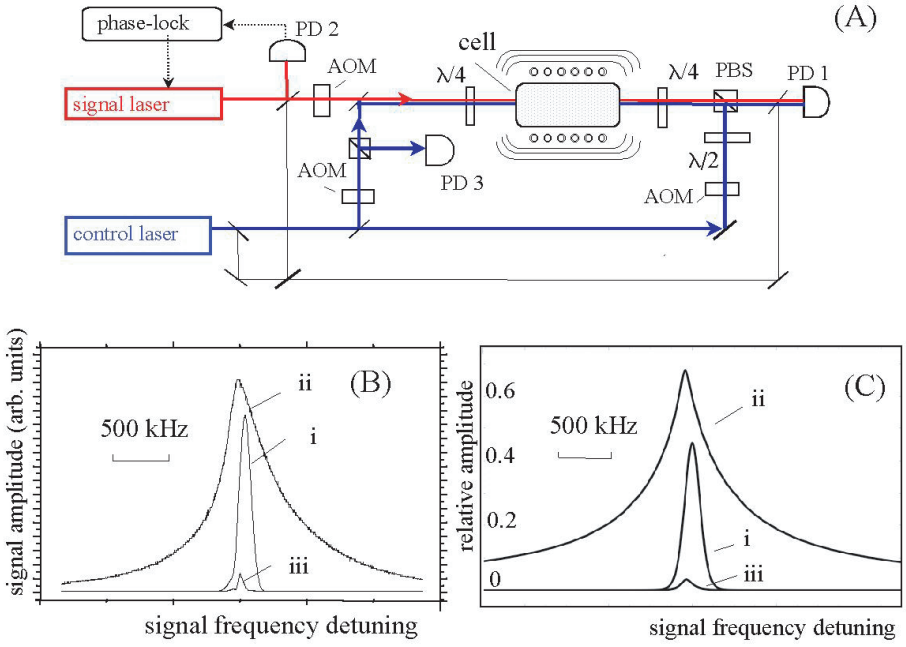

Figure 5.6: Experimental setup (A) and results of CW experiments (B). (i) EIT signal transmission with FD on, (ii-iii) reflected and transmitted signal with both FD and BD on, (C) theoretical simulations of reflected and transmitted signals.

The experimental apparatus is shown in Fig. 5.6A. We used a magnetically shielded 4 cm long ^{87}Rb vapor cell with density of $10^{12} - 10^{13}$ cm^{-3}; long-lived hyperfine sublevels of the electronic ground state $S_{1/2}$ with $F = 1, 2$ served as the storage states $|g\rangle, |s\rangle$, respectively, coupled via the excited state $P_{1/2}$. The signal field is generated

by an extended cavity diode laser and phase-locked to the control laser with a frequency offset corresponding to the hyperfine splitting of ^{87}Rb (6.84 GHz). PD1 and PD3 in Fig. 5.6A are fast photodiodes used for heterodyne detection of the the signal, followed by a spectrum analyzer.

We first consider continuous wave (CW) excitation of the atomic Rb. Without the control beams the atomic medium is completely opaque to the forward signal beam. When the FD control field is present, a sharp, few 100 kHz-wide resonance appears in the transmission spectrum of the signal beam, corresponding to EIT (curve (i) in Fig. 5.6B). Turning on the BD beam in the CW regime greatly reduces the EIT transmission (curve (iii)), while at the same time generating a reflected signal (up to $\sim 80\%$) beam that is detected in the backward direction (curve (ii)). These results demonstrate the possibility of coherent control (reflection and transmission) of light via simultaneous driving of the medium with FD and BD beams.

Turning to experiments with pulsed light, we first map the input signal pulse onto an atomic coherence of the Rb atoms, similarly to earlier stored light experiments [103, 128]. This procedure corresponds to Fig. 5.4C and its experimental observation is shown by curve (i) in Figure 5.7A. A Gaussian-shaped signal pulse of about 5 μs duration enters the medium where it is slowed to $v_g^0 \sim 6$ km/s. The FD control beam is then turned off; note that a fraction of the signal pulse leaves the cell before that, leading to the first peak of the curve (i). When the FD control field is turned back on, the stored atomic excitation is converted back into light and detected in the forward direction (second peak of the curve (i)). We next consider the retrieval of the atomic excitations by simultaneous application of the FD and BD control beams.

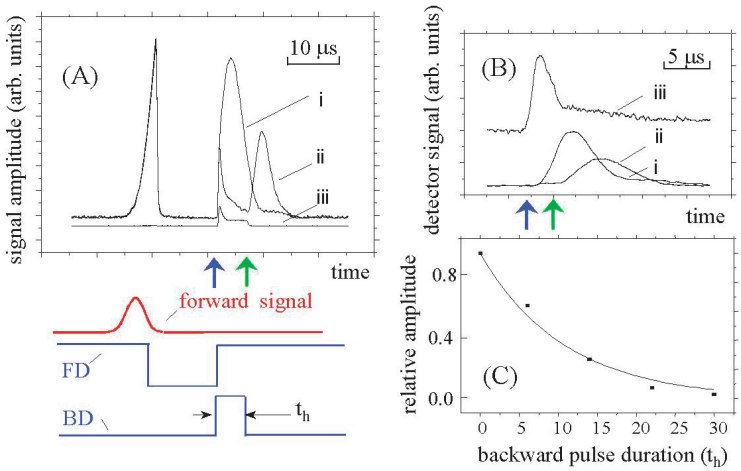

Figure 5.7: (A) Pulsed experiments, (i) storage and retrieval of signal in forward direction when FD is turned off then back on, (ii) same when FD and BD both turned on, (iii) signal in backward direction under the same conditions. (B) Rb fluorescence measured at the side of the cell, (iii) fluorescence associated with signal light during release with both FD and BD on. Curves (i) and (ii) (shown for reference) are the same as curves (i) and (ii) in Fig. 3A. (C) Dependence of released signal magnitude on BD pulse duration t_h.

When the intensities of the beams are carefully adjusted, the output signal pulses in both forward and backward directions are greatly suppressed (curves (ii) and (iii) in Fig. 5.7A). Both channels exhibit small leakage. We attribute the first peak to photons retrieved near the cell boundaries, which do not experience sufficient Bragg reflections to be trapped efficiently. The long tail is likely due to a slow spreading of the stored pulse. When the BD beam is turned off the released pulse is detected in the forward channel (curve (ii)). The presence of signal light inside the cell during the simultaneous application of the two control beams was verified directly by monitoring fluorescence from the side of the cell (Figure 5.7B). Background fluorescence associ-

ated with control beams is subtracted. For times when the signal output in forward and backward directions is greatly suppressed, we observed significant enhancement of the signal light fluorescence (curve (iii) in Figure 5.7B), due to residual atomic absorption.

These observations provide evidence for controlled conversion of the stored atomic coherence into a stationary photonic excitation in the cell. Note, in particular, that the magnitude of the fluorescence drops sharply after the BD pulse is turned off. This drop is followed by a gradual decay associated with the exit of the slow pulse from the medium. This behavior is in a qualitative agreement with our simple model, which predicts the light intensity in the stationary pulses to be double of that in the slowly propagating pulse.

Chapter 6

Nonlinear Optics with Stationary Pulses of Light

6.1 Introduction

Techniques that could facilitate controlled nonlinear interactions between few-photon light pulses are now actively explored [107]. Although research into fundamental limits of nonlinear optics has been carried out over the last three decades, there is renewed interest in these problems in part due to, e.g., potential applications in quantum information science [28]. In general, such interactions between few-photon pulses are difficult to achieve, as they require a combination of large nonlinearity, low photon loss and tight confinement of the light beams [30] . In addition, long atom-photon interaction times are required. Simultaneous implementation of all of these requirements is by now only feasible in the context of cavity QED [110, 133].

In this Letter, we describe a novel method for achieving a nonlinear interaction

between weak light pulses. Our method is based on a recently demonstrated technique [6, 15] in which light propagating in a medium of Rb atoms was converted into an excitation with localized, stationary electromagnetic energy, which could be held and released after a controllable interval. This is achieved by using Electromagnetically Induced Transparency (EIT) [69] to coherently control the pulse propagation. We show here that this method can be extended to confine stationary pulses in all three spatial dimensions, and that an efficient Kerr-like interaction between two pulses can be implemented as a sequence of linear optical processes and atomic state manipulations. Coherent, controlled nonlinear processes at optical energies corresponding to single light quanta appear feasible with our scheme.

Before proceeding, we note that the present work is closely related to recent studies on the resonant enhancement of nonlinear optical phenomena via EIT [146, 73, 71, 127, 116]. The essence of these studies is to utilize the steep atomic dispersion associated with narrow EIT resonances. In such a system, a small AC Stark shift associated with a weak off-resonant pulse of signal light, produces a large change in refractive index for a resonant probe pulse. In order to fully take advantage of this process, long interaction times between signal and probe pulses must be ensured. Although the latter can be achieved by reducing the group velocities of two interacting pulses by equal amounts [106], in practice this results only in a modest increase of the nonlinear optical efficiency since reduction of the group velocity is accompanied by a corresponding decrease of the light energy in the propagating pulse. Moreover, such nonlinear interaction is accompanied by pulse distortion, which poses a fundamental limit to nonlinear interactions. In contrast, the technique presented here allows for

long interaction times (associated with stationary light pulses) without proportional reduction of the photon energy. Furthermore, our technique enables light localization in all three spatial dimensions in the presence of atoms, and allows to entirely avoid competing effects such as pulse distortion.

6.2 Waveguiding and Three-dimensional Localization of Light Pulses

The ideas discussed in Ref. [15] allow one to localize and hold a pulse of light within a stationary envelope along the propagation direction. In practice, it is necessary to confine the signal beam in the transverse directions, in order to prevent diffraction. This can be achieved, e.g. by using a hollow core photonic crystal fiber filled with an active medium of resonant atoms [19, 94]. Such an approach is particularly attractive in that it ensures a single-mode beam quality for interacting beams. The unwanted interactions of atoms with fiber walls can be avoided by using atom guiding techniques [138, 121]. In section 6.5, we describe our photonic fiber based experiment. Alternatively, the signal pulse guiding can be accomplished by using focused control beams. Shaped control beams can be used to create a transverse variation of the index of refraction, enabling waveguiding and confinement of light pulses to small transverse dimensions.

To be specific, we consider a medium of length L consisting of an ensemble of N three-level atoms in the Λ configuration, with two metastable lower states, as shown in Fig. 6.1a. The ground states $|g\rangle, |s\rangle$ are coupled to the excited state

$|e\rangle$ via a control field applied on resonance with the $|s\rangle \rightarrow |e\rangle$ transition and a weak quantized signal field close to resonance with the $|g\rangle \rightarrow |e\rangle$ transition. The control field consists of two counter-propagating fields with spatially and temporally varying Rabi frequencies $\Omega_{\pm}(\vec{r},t)$, so that the control field Rabi frequency is $\Omega(\vec{r},t) = \Omega_{+}(\vec{r},t)e^{ik_c z} + \Omega_{-}(\vec{r},t)e^{-ik_c z}$, where $k_c = n_c\omega_{es}/c$, n_c is the background index of refraction at the frequency ω_{es}. The corresponding signal fields have slowly varying envelopes $\hat{E}_{\pm}(\vec{r},t)$, so that the slowly varying signal field is $\hat{E}_S^{(+)}(\vec{r},t) = \left[\hat{E}_{+}(\vec{r},t)e^{ik_s z} + \hat{E}_{-}(\vec{r},t)e^{-ik_s z}\right]$, where $k_s = n_s\omega_{eg}/c$, V is the quantization volume, and n_s is the background refractive index at the frequency ω_{eg} due to off-resonant atomic levels. Note that in practice n_s can be tuned, e.g., by changing the light polarization.

We describe the atomic properties with slowly varying collective operators [56] $\hat{\sigma}_{\mu\nu}(\vec{r},t) = \frac{1}{N_{\vec{r}}}\sum_{j=1}^{N_{\vec{r}}} |\mu\rangle_j \langle\nu| e^{-i\omega_{\mu\nu}t}$ where $\omega_{\mu\nu} = (E_\mu - E_\nu)/\hbar$, and where $N_{\vec{r}}$ is the number of atoms in a small but macroscopic volume around position $\vec{r}$. We define the polarization operator to be $\hat{P}(\vec{r},t) = \sqrt{N}\hat{\sigma}_{ge}(\vec{r},t)$, and the spin flip operator $\hat{S}(\vec{r},t) = \sqrt{N}\hat{\sigma}_{gs}(\vec{r},t)$. In the present situation of weak signal fields and strong control fields, most atoms are in state $|g\rangle$, with a few spin-flipped atoms in $|s\rangle$, so that the polarization and spin flip operators obey bosonic commutation relations [56]. Associated with the forward/backward propagating fields are slowly varying polarization envelopes $\hat{P}_{\pm}(\vec{r},t)$, so that the total polarization is $\hat{P}(\vec{r},t) = \hat{P}_{+}(\vec{r},t)e^{ik_s z} + \hat{P}_{-}(\vec{r},t)e^{-ik_s z}$.

Letting the wavevector mismatch between co-propagating signal and control fields be $\Delta K = k_s - k_c = (n_s\omega_{eg} - n_c\omega_{es})/c$, and defining $\hat{\mathcal{E}}_{\pm} = \hat{E}_{\pm}e^{\pm i\Delta K z}$ and $\hat{\mathcal{P}}_{\pm} = \hat{P}_{\pm}e^{\pm i\Delta K z}$, the Heisenberg equations of motion for the slowly varying operators $\hat{\mathcal{E}}_{\pm}(\vec{r},t)$

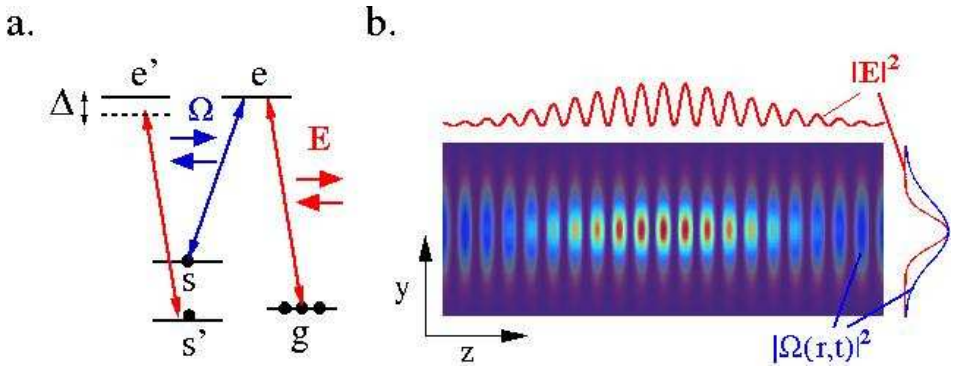

Figure 6.1: a. Three-level atoms in Λ-configuration, with auxiliary levels $|s'\rangle, |e'\rangle$ (such as hyperfine states of alkali atoms). Forward and backward propagating control fields with Rabi frequencies $\Omega_\pm$, and weak signal field $\mathcal{E}_\pm$. b. Three-dimensional confinement and waveguiding of signal light due to transverse intensity profile and longitudinal modulation of control field.

[56] can be written as (in the paraxial approximation)

$$\left(\frac{\partial}{\partial t} \pm c\frac{\partial}{\partial z} - i\frac{c\nabla_T^2}{2k_s}\right)\hat{\mathcal{E}}_\pm \;=\; i\Delta K c\hat{\mathcal{E}}_\pm + ig\sqrt{N}\hat{\mathcal{P}}_\pm, \tag{6.1}$$

where $\nabla_T^2 = \nabla^2 - \frac{d^2}{dz^2}$ is the transverse Laplacian, and where $g = \wp\left(\frac{\omega_0}{2\hbar\epsilon_0 V}\right)^{1/2}$ is the atom-field coupling constant, $\wp$ being the dipole matrix element for the $|g\rangle - |e\rangle$ transition, and V the quantization volume.

Following [56, 6] we introduce two components $\hat{\Psi}_\pm$ of a coupled excitation of light and an atomic spin wave ("dark-state polariton") corresponding to forward and backward signal fields respectively. In the experimentally relevant case of small group velocities [74, 103] the polariton components are represented by $\hat{\Psi}_\pm = g\sqrt{N}\hat{\mathcal{E}}_\pm/\Omega_\pm$. In the adiabatic limit of slowly varying pulses, disregarding the slow decay of ground

state coherence, and Fourier transforming ($\partial_t \to -i\omega$), we find

$$\left(c\frac{\partial}{\partial z} - i\frac{c\nabla_T^2}{2k_0}\right)\hat{\Psi}_+ = i\Delta K c\hat{\Psi}_+$$
$$+i\eta\omega\left(\alpha_+\hat{\Psi}_+ + \alpha_-\hat{\Psi}_-\right) - \alpha_-\xi\left(\hat{\Psi}_+ - \hat{\Psi}_-\right) + \hat{F}_+(\vec{r},\omega) \tag{6.2a}$$
$$\left(-c\frac{\partial}{\partial z} - i\frac{c\nabla_T^2}{2k_0}\right)\hat{\Psi}_- = i\Delta K c\hat{\Psi}_-$$
$$+i\eta\omega\left(\alpha_+\hat{\Psi}_+ + \alpha_-\hat{\Psi}_-\right) + \alpha_+\xi\left(\hat{\Psi}_+ - \hat{\Psi}_-\right) + \hat{F}_-(\vec{r},\omega) \tag{6.2b}$$

where $k_0 = \omega_{eg}/c$, $\eta = \frac{g^2N}{|\Omega_+|^2+|\Omega_-|^2}$, $\alpha_\pm = \frac{|\Omega_\pm|^2}{|\Omega_+|^2+|\Omega_-|^2}$, and $\xi = \frac{g^2N}{\gamma}$. We have also assumed that $k_0 a \gg 1$, where a is the typical transverse size of the control beams. These equations describe two slow waves that are coupled due to periodic modulation of atomic absorption and group velocity. The terms containing ξ on the right hand side of Eqns. (6.2) are proportional to the absorption coefficient ξ near resonant line center. $\hat{F}_\pm(\vec{r},\omega)$ are noise forces associated with dissipation. When ξ is large these terms give rise to the pulse matching phenomenon [69]: whenever one of the fields is created the other will adjust itself within a short propagation distance to match its amplitude such that $\hat{\Psi}_+ - \hat{\Psi}_- \to 0$ [15].

In order to achieve transverse confinement of light pulses, we take into account the transverse dependence of the control field intensity and the resulting variation of the index of refraction. For a focused control beam, the intensity decreases with distance from the optical axis, so that for negative two-photon detuning (as is necessary for phasematching), the index of refraction decreases with distance from the optical axis. This leads to waveguiding of the signal light. The combination of waveguiding with strong coupling of forward and backward propagating modes, permits the complete three-dimensional confinement of light pulses in the medium.

We assume a transverse spatial variation of the control field intensity, e.g. for a weakly focused gaussian beam, $|\Omega_\pm(r)|^2 = |\Omega_\pm(0)|^2 e^{-(r/a)^2}$. Expanding for $r \ll a$, we have $\eta(r) = \eta_0[1 + (r/a)^2 + \cdots]$. We consider trial solutions of (6.2) of the from $\Psi_+ = A_+ e^{i\beta z - (r/R)^2}$ and $\Psi_- = A_- e^{-i\beta z - (r/R)^2}$ where β, R and A_+/A_- are determined by requiring that the coefficients of different powers of r vanish independently. With these requirements we find the two solutions $R = \infty$ and

$$R = \left(-\frac{2a^2 c}{k_0 \eta \omega}\right)^{1/4}. \tag{6.3}$$

The eigenvector of the finite solution has $A_+/A_- = 1$, which corresponds to the stationary pulses [15] for which $\Psi_+ - \Psi_- \to 0$. We also find the dispersion relation

$$\eta\omega = \left(\frac{2c}{k_0 R(\omega)^2} - \Delta K c\right) - i\frac{(c\beta)^2}{\xi} + (\alpha_+ - \alpha_-)c\beta. \tag{6.4}$$

In the time-domain this corresponds to propagation at a group velocity $v_g = c\frac{\alpha_+ - \alpha_-}{\eta}$, which can be controlled by adjusting the intensities $I_\pm(t) \propto |\Omega_\pm(t)|^2$ of the counter-propagating control fields. Due to the imaginary term, there is also a slow spreading of the stationary pulse at a rate $\delta l/l \sim \sqrt{c^2 t/(\eta \xi l^2)}$, which determines the maximal trapping time of the stationary excitation.

We are interested in a simultaneous solution of Eqs.(6.2) when $\alpha_+ \approx \alpha_-$ and the optical depth ξ is large. This yields the radius of the stationary pulse $R = a 2^{1/4} \left[\sqrt{1 + \Delta K k_0 a^2} - 1\right]^{-1/2}$, which under conditions of strong confinements $\Delta K k_0 a^2 \gg 1$ results in

$$R = a[2/(\Delta K k_0 a^2)]^{1/4}. \tag{6.5}$$

Hence, in an optically dense medium ($\xi L/c \gg 1$) a stationary excitation confined in all three dimensions can be controllably created. To be specific, for atomic Rb

($\lambda = 0.8\,\mu$m) at density $n = 10^{14}\,\mathrm{cm}^{-3}$, we take the background refractive index due to off-resonant levels to be $n - 1 = 1.2\,10^{-2}$ [171]. For a Gaussian control beam with waist $a \sim 100\,\mu$m at the center of the atomic cell (the corresponding Rayleigh range is $z_0 = 3.9\,$cm), we find that the guided mode radius is $R = 13\,\mu$m (for which the Rayleigh range is $z_0 = 0.06\,$cm), so that the diffraction-free range is extended by a factor of 60. When the control beam is chosen in the form of a non-diffracting Bessel beam [51], waveguiding over much longer propagation distances is possible. For example, with a beam in which the radius of the first lobe of the Bessel function is $a = 20\,\mu$m, the guided mode radius is $R \sim 5.7\,\mu$m. In practice, this allows confinement over tens of cm, whereas in free space the corresponding Rayleigh range would only be 0.01 cm. Reducing the control beam radius until $R \sim a$, gives an estimate of the smallest guided mode achievable, which for an index of $n-1 = 1.2\,10^{-2}$ is $R_{min} = 1.6\,\mu$m.

6.3 Controlled Effective Kerr Nonlinearity and Single Photon Phase Shift

We next turn to the nonlinear optical interaction between two weak pulses of light. A notable feature of the step by step process described below, is that it consists of a sequence of purely linear optical interactions and atomic state manipulations, leading to an effective optical nonlinear interaction. As shown in the timing diagram Fig. 6.2a, a light pulse (signal pulse) travelling through the atomic medium is initially stored in the $|g\rangle\langle s|$ coherence. Next, a Raman or microwave π pulse (RA)

transfers the population from $|s\rangle$ to $|s'\rangle$ (see Fig. 6.2a), thereby transferring the stored excitation to the spin excitation $\hat{\mathcal{S}}' = \sqrt{N}\hat{\sigma}_{gs'}$. The signal pulse is stored as a spin wave $\sigma_{gs'}(\vec{r},t) = U_s(\vec{\rho})\hat{\mathcal{S}}'(z,t)/\sqrt{N}$, where $U_s(\vec{\rho})$ describes the transverse spin wave mode.

A second light pulse (probe pulse) is then sent through the medium and stored in the coherence $\hat{\mathcal{S}}$. The spin excitation associated with the probe pulse is then converted into a stationary optical excitation. The latter is then moved through the stored spin excitation $\hat{\mathcal{S}}'$ associated with the signal pulse by an appropriate adjustment of the intensities of the forward and backward control beams. Probe light in the modes $\hat{\mathcal{E}}_\pm$ interacts dispersively with atoms in level $|s'\rangle$ (see Fig. 6.1a), thereby acquiring a phase shift proportional to the number of excitations $\hat{\mathcal{S}}'^\dagger\hat{\mathcal{S}}'$, leading to an effective Kerr-type nonlinearity.

We focus on the situation where the transverse spatial size of the signal spin wave $\hat{\mathcal{S}}'$ is much smaller than the probe transverse size. Under these assumptions and writing the guided mode transverse dependence as $\hat{\Psi}_\pm(r,z,t) = e^{-(r/R)^2}\hat{\psi}_\pm(z,t)$, we find, in terms of the polariton components $\hat{\psi}_\pm$,

$$\begin{aligned}(\partial_t + c\partial_z)\hat{\psi}_+ &= -\eta\partial_t(\alpha_+\hat{\psi}_+ + \alpha_-\hat{\psi}_-) - \alpha_-\xi(\hat{\psi}_+ - \hat{\psi}_-) \\ &\quad + i\beta\hat{\mathcal{S}}'^\dagger\hat{\mathcal{S}}'\hat{\psi}_+ + \hat{F}_+(z,t) \qquad (6.6a)\\ (\partial_t - c\partial_z)\hat{\psi}_- &= -\eta\partial_t(\alpha_+\hat{\psi}_+ + \alpha_-\hat{\psi}_-) + \alpha_+\xi(\hat{\psi}_+ - \hat{\psi}_-) \\ &\quad + i\beta\hat{\mathcal{S}}'^\dagger\hat{\mathcal{S}}'\hat{\psi}_- + \hat{F}_-(z,t) \qquad (6.6b)\end{aligned}$$

where $\beta = \frac{\tilde{g}^2}{\Delta}(1 + i\gamma/\Delta)$, with $\tilde{g} = g\frac{A}{\pi R^2}$, A is the quantization area, and Δ is the detuning of the fields $\hat{\mathcal{E}}_\pm$ from the optical transition $|s'\rangle \to |e'\rangle$ (see Fig. 6.2a). The interaction of the localized excitation $\hat{\mathcal{S}}'$ with the guided modes $\hat{\psi}_\pm$ does not depend

on the transverse coordinate, and the effective transverse area corresponds to the mode area πR^2, in complete analogy to the interaction of localized atoms with the field mode in cavity QED [110, 133].

In the stationary pulse configuration [15], the stationary excitation is bound to the spin wave and $\hat{\mathcal{S}} \simeq -\left(\alpha_+\hat{\psi}_+ + \alpha_-\hat{\psi}_-\right)$. Solving adiabaticaly, in the limit of large optical depth ξ and writing $v_g = (\alpha_+ - \alpha_-)c/\eta$, we find

$$[\partial_t + v_g\partial_z]\hat{\mathcal{S}} = i\frac{\beta}{\eta}[\hat{\mathcal{S}'}^\dagger\hat{\mathcal{S}'}]\hat{\mathcal{S}} + \left[4\alpha_+\alpha_-\frac{(c\partial_z)^2}{\eta\xi}\right]\hat{\mathcal{S}} \tag{6.7a}$$

$$\partial_t\hat{\mathcal{S}'} = i\frac{\beta}{\eta}[\hat{\mathcal{S}}^\dagger\hat{\mathcal{S}}]\hat{\mathcal{S}'} \tag{6.7b}$$

where we have ignored for now absorption and the associated noise.

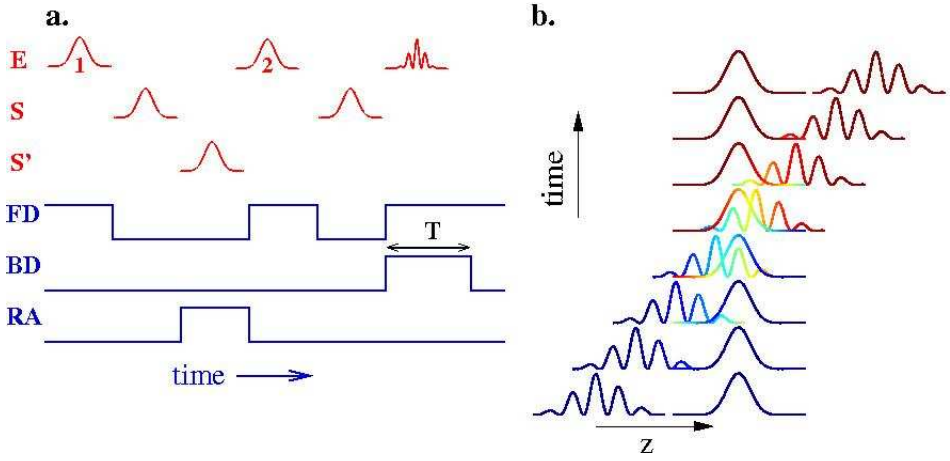

Figure 6.2: Nonlinear optical interaction with weak pulses as sequence of linear operations. a. Timing diagram: forward (FD), backward (BD), and Raman or microwave (RA) intensities vs. time. The signal pulse (E,1) is first stored in the spin wave $\mathcal{S}$ and then transfered to $\mathcal{S}'$. Next, the probe pulse (E,2) is stored in $\mathcal{S}$, and then converted to a stationary pulse excitation (E, modulated wavepacket). The stationary and the stored excitation then interact with one another for a time T. b. Illustration of Kerr interaction between slowly propagating stationary pulse $\mathcal{S}$ and stored excitation $\mathcal{S}'$ leading to phase shift (represented as changing color) of pulses.

To solve for $\hat{\mathcal{S}}(z,t)$ and $\hat{\mathcal{S}}'(z,t)$, we first ignore pulse spreading. Let $\hat{n}_1(z) = \hat{\mathcal{S}'}^\dagger\hat{\mathcal{S}'}$

(independent of t), and $\hat{n}_2(z,t) = \hat{\mathcal{S}}^\dagger\hat{\mathcal{S}}$ (which depends only on the variable $t' = t - z/v_g$). We find

$$\hat{\mathcal{S}}(z,t) = \exp\left[i\frac{\beta}{\eta v_g}\int\limits_{z-v_g t}^{z} dz'\,\hat{n}_1(z')\right]\hat{\mathcal{S}}(z-v_g t,0) \tag{6.8a}$$

$$\hat{\mathcal{S}}'(z,t) = \exp\left[i\frac{\beta}{\eta v_g}\int\limits_{0}^{v_g t-z} dz'\,\hat{n}_2(-z',0)\right]\hat{\mathcal{S}}'(z,0) \tag{6.8b}$$

When the slowly moving pulse $\hat{\mathcal{S}}$ has completely traversed the stored spin coherence $\hat{\mathcal{S}}'$, the phase shift is $\phi_S = \frac{\mathrm{Re}[\beta]}{\eta v_g} L\hat{N}_{\mathcal{S}'}$ (where $\hat{N}_{\mathcal{S}'}$ is the number of excitations initially stored in $\hat{\mathcal{S}}'$). The phase shift is proportional to the interaction time, i.e. inversely proportional to the group velocity of the slowly moving pulse $\hat{\mathcal{S}}$. To estimate the maximal phase shift, we note that the group velocity must be large enough that $v_g t \gtrsim l_{s'}$, where $l_{s'}$ is the length of spin coherence envelope. Also, non-adiabatic corrections due to the pulse spreading term in (6.7a) should be small, so that $\frac{(c/l_S)^2}{\eta\xi}t \lesssim 1$. Putting these two conditions together yields

$$\phi_S \;\lesssim\; d_0\frac{\gamma}{\Delta}\frac{\sigma}{\pi R^2}\left(\frac{l_s^2}{L l_{s'}}\right) \tag{6.9}$$

where the resonant scattering cross-section is $\sigma = \frac{3}{4\pi}\lambda^2$. Note that the nonlinear phase shift scales linearly with the optical depth d_0, in contrast to scaling with $\sqrt{d_0}$ for the case of two slowly propagating pulses [106], in which case pulse distortion effects are also significant.

Specifically, a $300\,\mu$m long, cigar shaped cloud of cold ^{87}Rb atoms confined in an optical dipole trap at a density of $n \sim 10^{14}\,\mathrm{cm}^{-3}$ has an optical depth in excess of $d_0 \sim 10^3$. Similar optical depth can be potentially achieved by guiding cold atom clouds of smaller density in a photonic crystal fiber [138, 121, 19, 94]. Taking the

guided mode radius $R \simeq 2\,\mu$m and accounting for absorption losses, we choose the detuning to be $\Delta \simeq 16\gamma$ and find that a phase shift of $\phi_S \sim \pi$ is achievable due to a single stored quantum. Under these conditions the two-photon loss probability is a few percent.

6.4 Conclusions

To summarize, we have shown that three-dimensional confinement of light pulses is possible by combining the technique of stationary light pulses with the transverse light guiding. This technique can be used to engineer efficient nonlinear optical interactions leading to significant phase shifts for weak optical pulses. Such interactions have interesting applications ranging from QND measurements [62] of few-photon pulses to quantum information processing [28].

6.5 Photonic Crystal Fiber Experiment

We now describe an experiment in which we aim to study nonlinear optical interactions in an atomic medium confined inside a hollow core photonic crystal fiber (PCF).

Nonlinear optics at the few-photon level could be a very valuable tool, with many potential applications in quantum information science [28]. For example, a quantum "phase gate" for photonic qubits could be realized with a Kerr nonlinearity [30] for which the effective Hamiltonian is $\hat{H} = \hbar\chi\hat{a}^\dagger\hat{a}\hat{b}^\dagger\hat{b}$, such that the phase of a photon wave packet in mode $\hat{a}$ can be shifted by π depending on the presence or the absence

of a photon in the second mode $\hat{b}$. This occurs when the interaction time T is such that $\chi T = \pi$.

In order to achieve nonlinear optical effects in the few-photon regime, it is necessary to have long interaction times, and thus long interaction lengths for propagating photonic wavepackets. However, strong focusing is in general also desired in order to obtain sufficient intensity to drive the nonlinear effects of interest. Because of the high diffraction losses of strongly focused beams, these two requirements are in conflict with one another. A figure of merit of nonlinear optical interactions is the product of light intensity with interaction time, which we can write as $(P/A) \times (L/c)$, where P is the optical power, A is the transverse area of the beam, and L is the length of the interaction region. For focused beams the effective interaction length is limited to the diffraction-free range (Rayleigh range for gaussian beams) $l \simeq A/\lambda$, so that the figure of merit becomes $P/(\lambda c)$, i.e. independent of interaction length or transverse beam area. Diffraction thus poses an unavoidable limit to nonlinear optical interactions.

As suggested in section 6.2, a solution to this problem is to use waveguiding to guide light over long lengths (longer than the Rayleigh range) in a single transverse mode. When the interaction length is not limited by the diffraction-free range, large optical nonlinear effects can be obtained with weak optical intensities. Furthermore, with single transverse modes, quantum optical effects that establish correlations between optical modes can be optimized to yield maximal entanglement between single transverse modes, as discussed in 4.6.3. These light modes could then easily be coupled to standard single mode fibers and distributed to distant parties for e.g. quantum

communication protocols.

In the present experiment, we use hollow core photonic crystal fibers [142] which guide light in a single transverse mode inside the hollow core of an optical crystal fiber. The nonlinear medium that we consider consists of a gas of Rubidium atoms together with a Ne buffer gas. The goal of our experiment is to study Electromagnetically Induced Transparency in the Rb gas confined inside the hollow core of the fiber, and to observe enhanced nonlinear optical effects in this medium.

6.5.1 Hollow-core Photonic Crystal Fibers

Hollow-core photonic crystal fibers [142, 92] work by using a periodic wavelength-scale lattice of microscopic holes in the cladding surrounding a central hole, as shown in Fig. 6.3. The periodic array of holes creates a periodic variation of the index of refraction and results in the creation of photonic bandgaps [83], similar to the band structures of electrons in crystal lattices.

The bandgaps arise because of Bragg reflections, making it impossible for propagating light modes to exist in certain ranges of frequencies, when their wavevector closely matches the periodicity of the lattice. The holey structure surrounding the hollow core in Fig. 6.3 can thus prevent light from escaping the core.

Hollow-core fibers have the potential for very low propagation loss, since most of the light is guided in air (e.g. for the HC-800 fiber we use, more than 95% of optical power is located in the hollow core), with the current record at 13 dB/km at $1,500$ nm [150], and losses < 10 dB/km at optical wavelengths in the near future.

Early on, it was realized that hollow core fibers could bring a solution to the

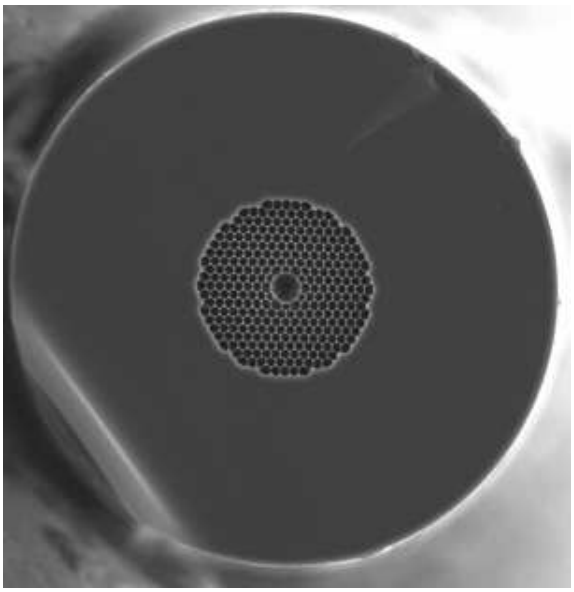

Figure 6.3: Photonic bandgap fiber (HC800 from Blaze Photonics), designed to guide light with wavelength around 840 nm. The outer diameter of the fiber is 130 μm, the spacing between holes is 2.2μm and the core diameter is 6.8μm.

long standing challenge of maximizing nonlinear interactions between lasers and low-density media such as gases (atomic or molecular). With hollow-core PCF, high intensity at low power is achievable, while offering long interaction lengths and good quality transverse beam profile. This could very soon lead to the development of enhanced ultralow-threshold gas-based nonlinear devices.

For example, efficient stimulated Raman scattering in a 1-meter-long Hydrogen-filled hollow-core PCF was recently studied by Benabid et al. [21], where it was found that the threshold for Stokes generation was nearly two orders of magnitude smaller than previously reported, with pump to Stokes conversion efficiencies of 30%. Further developments have reached 92% conversion efficiency, while the threshold power (3 nJ in a 35 m-long fiber) was more than 10^6 times lower than previously reported.

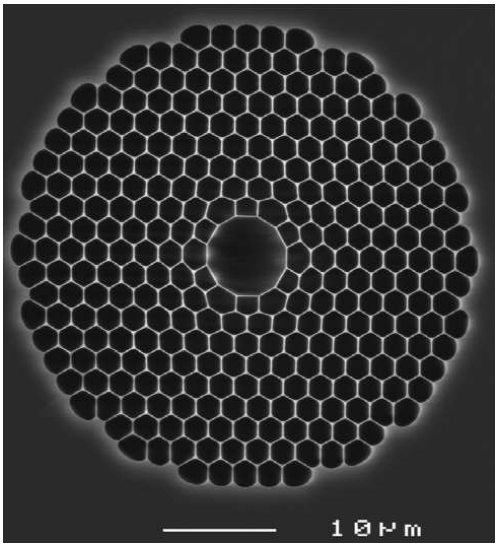

Figure 6.4: Central holey region of a photonic bandgap fiber (HC800 from Blaze Photonics). The spacing between holes is 2.2μm and the core diameter is 6.8μm.

In a recent development, the group of Phillip Russel (Bath University, UK) have reported [20] the fabrication of all-fiber gas filled cells using hollow-core PCF. These cells consists of hollow-core photonic crystal fibers filed with gas and spliced hermetically at both ends to standard single-mode optical fiber. Both hydrogen-filled cells (with gas fill pressures ranging from 6 mbar to 500 mbar) and acetylene-filled cells (C_2H_2, with gas fill pressures ranging from 5 to 10 bar) were thus made, with fiber-cell lengths of 1-5 meter. These cells were used for ultralow threshold stimulated Raman scattering and for an all-fiber-based frequency stabilization system (in the case of acetylene-filled cells).

Lastly, we note a recent experiment of interest by the Gaeta group (Cornell University) [61], in which an acetylene-filled hollow-core PCF was used to observe EIT and pulse delays due to slow-light effects. Despite the low oscillator strength of the transition (several orders of magnitude less than that for the D lines of Rubidium),

an optical thickness of approximately ~ 1 was reached in a 1.33-m-long fiber, and Electromagnetically Induced Transparency was observed, leading to an increase in transmission from $\sim 40\%$ in the absence of EIT to $\sim 65\%$ with EIT.

EIT-enhanced nonlinear optics at low light level

Electromagnetically Induced Transparency can be use to further enhance nonlinear optical phenomena [146, 73, 71, 127, 116] in the vicinity of an atomic resonance.

Due to the steep atomic dispersion associated with the narrow EIT resonance, a small shift in the atomic energy levels leads to a large change in the refractive index for the resonant EIT probe pulse. Thus, when a weak light pulse interacts with the atoms off-resonantly and gives rise to a small AC Stark shift, it can have a large effect on the phase of the probe pulse. When the index of refraction for light in mode $\hat{a}$ depends on the intensity of mode $\hat{b}$, we obtain precisely the Kerr-nonlinearity mentioned above, with effective Hamiltonian $\hat{H} = \hbar\chi\hat{a}^\dagger\hat{a}\hat{b}^\dagger\hat{b}$. Combining this enhancement of nonlinear effects due to EIT with the tight transverse confinement of light in hollow-core PCF, we anticipate that nonlinear optical effects at the few-photon level will become achievable. The prospect of reaching the new regime of *quantum nonlinear optics* is a very attractive one, with many potential applications in quantum information science, and all-optical quantum computation schemes.

Atomic media inside hollow fiber

A challenge to loading alkali gases in the narrow core of a hollow-core PCF is the wall-vapor interactions. Atoms can be lost to the walls through the process of physisorption, in which the atoms sticks to the wall for some characteristic time,

after which the are released and return to the vapor [40]. This may limit the relative fraction of Rubidium atoms in the vapor compared to those stuck to the fiber walls, and may limit the vapor density achievable inside the fiber. In a simple model of the sticking process in which a surface density of sticking sites are available to the atoms [153], the use of a buffer gas at high enough pressure may reduce the effect by occupying the sticking sites and preventing the Rb atoms from sticking to the walls. Note also that both the buffer gas and the walls give rise to a broadening and shift of the spectral lines of atoms. This large shift due to the atom-wall interaction (corresponding to the large physisorption potential) may be used as a spectroscopic signature of atoms inside the fiber.

A different strategy is to create a potential for the atoms that prevents them from approaching the walls. For example, a red-detuned laser can induce a dipole force that attracts the atoms to regions of high intensity, i.e. to the center of the hollow core region. Such an approach was pursued for guiding atoms in hollow-core fibers (capillaries, not PCF) [138, 137, 139, 140, 121], as well as micron-size particles in hollow-core fibers [22].

6.5.2 Experimental Setup

A schematic of the experimental setup is shown in Fig. 6.5. In our experiments, we use a 10 cm-long hollow core fiber (Thorlabs, HC-800), which has a bandgap centered around 840 nm. As shown in Fig. 6.5, two cells are vacuum-pumped and are connected to the ends of the hollow core fiber. In addition a set of 3 Helmholtz coils placed around the setup are used to cancel the ambient magnetic field at the fiber

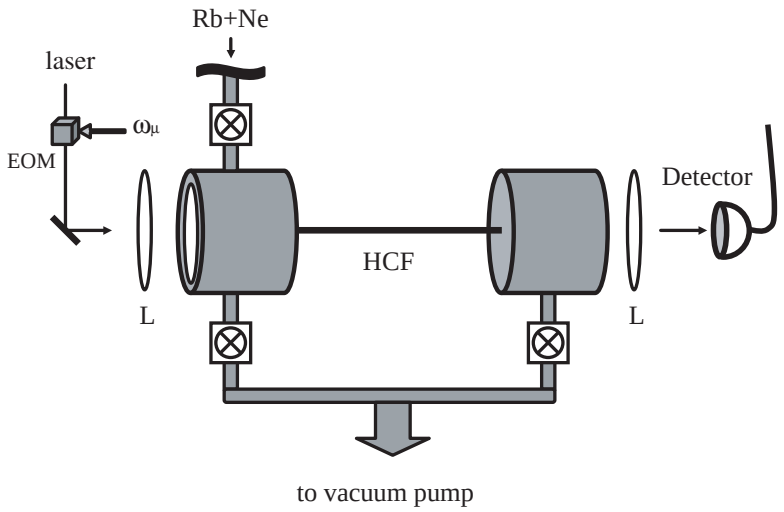

Figure 6.5: Schematic of experimental setup. The two cells are vacuum-pumped and the left cell is connected to the Rubidium source (+ buffer gas). The hollow core fiber (HCF) connects the left cell to the right cell. EOM: Electro-optic modulator for creating sidebands to the laser at frequencies $\omega_L \pm \omega_\mu$.

location. After assembly, the cells are evacuated to less than 10^{-6} Torr. A Rubidium cell is attached to one cell and can be heated to obtain a desired density of Rb vapor in the cell. In addition, Ne buffer gas can be added independently to the cell to a desired pressure, up to a few atm.

We use an external-cavity diode laser (ECDL) tuned close to the ^{87}Rb D1 line to generate a field at frequency ω_L. An electro-optic modulator fed with a microwave signal ω_μ is used to generate sidebands at frequencies $\omega_L \pm \omega_\mu$. When ω_μ is set near 3.417GHz, sidebands split by the ground-state hyperfine splitting 6.835GHz of ^{87}Rb appear and can be used to study EIT. The laser light is focused on the entrance of the fiber by an objective lens, with typical coupling efficiency of a few percent, mostly due to aberrations from the cell window. Note that we have not optimized

this coupling or made any effort to correct these aberrations so far. Note that with a near-field beam waist of $w_0 \simeq 5\mu$m [27] at the fiber, the Rayleigh range [149] is only $z_R = \frac{\pi w_0^2}{\lambda} \simeq 98\mu$m. The output light from the fiber is then detected on a fast photodiode.

The ^{87}Rb levels used in the experiments (D_1 line) are $|g\rangle = |5^2S_{1/2}, F = 1\rangle$, $|s\rangle = |5^2S_{1/2}, F = 2\rangle$, and $|e\rangle$ corresponds to $|5^2P_{1/2}, F' = 1\rangle$ and $|5^2P_{1/2}, F' = 2\rangle$, as shown in Fig. 6.6.

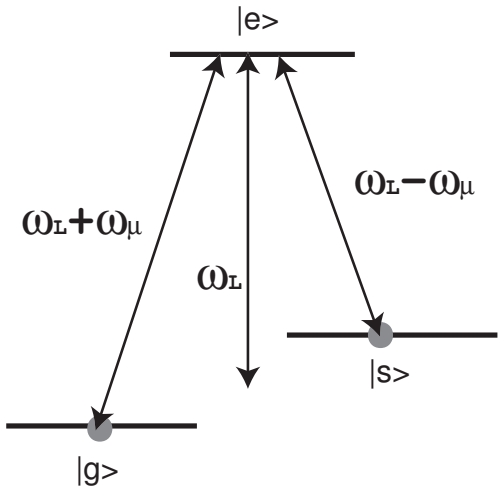

Figure 6.6: ^{87}Rb levels used in the experiments (D_1 line): $|g\rangle = |5^2S_{1/2}, F = 1\rangle$, $|s\rangle = |5^2S_{1/2}, F = 2\rangle$, and $|e\rangle$ corresponds to $|5^2P_{1/2}, F' = 1\rangle$ and $|5^2P_{1/2}, F' = 2\rangle$. The laser is tuned at frequency ω_L and the two sidebands are generated at $\omega_L \pm \omega_\mu$.

When the laser frequency ω_L is tuned close to $(\omega_{eg} + \omega_{es})/2$ and the EOM modulation frequency is equal to $\omega_{sg}/2 = 3.417$ GHz, the two sidebands difference frequency matches the hyperfine splitting and EIT can be observed. At resonance, the atoms are driven into a dark-state and do not absorb light so that the two sidebands are transmitted through the atomic sample. Modulating the EOM microwave modulation frequency ω_μ at the much smaller radio frequency ω_{RF}, results in a modulation of the

sidebands transmission at ω_{RF}, as the sidebands frequency mismatch is brought in and out of resonance with the hyperfine splitting of the atoms.

6.5.3 Current status of experiment and outlook

We now report on the preliminary results of the experiment and future directions. First, we make sure the fiber is correctly connecting the two cells by evacuating both cells to a pressure less than 10^{-6} Torr. One of the cells is then filled with Ne buffer gas, to a pressure ranging from a few Torr to a few atm. We then detect the presence of buffer gas in the second cell by monitoring the gas pressure inside it. Depending on the initial pressure it can take from a few minutes to a few hours for the pressures in the second cell to build-up. With a few atm of buffer gas in the first cell, it takes ~ 10 minutes to reach a few Torr in the second cell. These results are very promising, since they indicate that once Rb vapor is added to the buffer gas and the mixture is left to flow through the fiber, we should be able to quickly bring Rb atoms through the fiber.

Next, we check that we can bring Rb vapor to the first cell and reach sufficient densities. With the laser frequency sweeping through the D_1 line, we detect the intensity transmitted through the whole setup. This includes ~ 2 cm from the entrance window of the first cell to the fiber, through the length of the fiber and another ~ 2 cm from the end of the fiber to the exit window of the second cell. We routinely observe $\gtrsim 99\%$ absorption from Rb, which indicates that we can create a large density vapor of Rb in the cell.

Note that because of the small transverse area of the hollow core, only a few atoms

inside the fiber are sufficient to significantly scatter light. For example to reach an on-resonance optical thickness of ~ 1, only a few hundred atoms inside the fiber are necessary. We are pursuing several approaches for observing atoms loaded inside the fiber. First, due to the difference of timescales in the time required to empty the cells compared to the time required to empty the fiber (much longer because of geometrical factors), we may be able to evacuate the cells before the fiber is evacuated. This would allow us to observe the absorption signal of only those atoms that were loaded in the fiber. A second method is to look for the spectroscopic signature of atoms interacting with the walls of the fiber, which could be achieved while atoms are still present in both cells, eliminating the need to quickly evacuate them. Lastly, since the intensity of light can be large inside the fiber while small inside both cells (due to the rapid divergence of the beam upon it exit from the fiber), it may be possible to investigate nonlinear optical effects due to interaction of light with atoms inside the fiber. This would provide a signal solely due to atoms located in the high intensity regions of the field, i.e. inside the fiber.

6.5.4 Summary

To summarize, we have described the experimental setup we intend to use to investigate nonlinear optical effects of light with atoms located inside a hollow-core photonic crystal fiber. This approach to nonlinear optics at low-light level is intriguing as it may unable the combination of EIT-enhancement of nonlinear optics with the unique waveguiding properties of hollow-core fibers. The main challenge in such an experiment is the atom-wall interaction inside the fiber, and whether it can be

effectively eliminated or made irrelevant remains to be investigated.

Appendix A

Appendices to Chapter 2

A.1 Ramsey Spectroscopy

In Ramsey spectroscopy [165], a collection of N two-level atoms are made to interact with two separated fields (in time or in space). The lower and upper states (refered to as ground and excited state) have an energy difference $\hbar\omega_0$ and atoms will thus acquire a different dynamical phase $e^{-iEt/\hbar}$ depending on which state they are in. The effect of properly chosen electromagnetic fields is to perform a transformation that prepares the atoms in a superposition of the two states $|g\rangle$ and $|e\rangle$. The different parts of the wavefunction of atoms (corresponding to the ground and excited state) acquire a relative phase due to dynamical evolution and when the inverse transformation is applied, an interference effect is obtained. An exact parallel with the Mach-Zender interferometer can be drawn [45]: the transformation preparing atoms in a superposition of ground and excited states is equivalent to the transformation that lets a photon incident on a beam splitter explore the two arms of an interfer-

ometer. The relative phase acquired in the two atomic states during free evolution of duration T is the equivalent of the relative phase acquired by photons travelling in the arms of the interferometer. Finally, the second pulse that performs the inverse transformation on atoms is the equivalent of the recombination of signals from the two interferometer arms on a beam splitter. At the end of this sequence, the number of atoms in either states, equivalent to the number of photons from either output of the final beam splitter, is measured. In this way, the signal measured depends on the acquired relative phase which can thus be estimated with some accuracy.

We will now quantify this more precisely: let the frequency of the applied electromagnetic pulses be ω, and the time delay between the two zones of interaction be T. The duration and strength of the applied fields are chosen so as to lead to $\pi/2$ pulses, i.e. transformation of the atomic state according to

$$\begin{aligned} |e\rangle &\rightarrow \frac{|e\rangle - i|g\rangle}{\sqrt{2}} \\ |g\rangle &\rightarrow \frac{|e\rangle + i|g\rangle}{\sqrt{2}}. \end{aligned} \tag{A.1}$$

During their free evolution between the two zones, atoms in the ground and excited states acquire a relative phase ϕ which, in a frame rotating with the frequency of the applied field, is $\phi = (\omega - \omega_0)T$.

Before entering the first interaction zone, the atoms are prepared in their lower state $|g\rangle$ and at the exit of the second zone, the number of atoms in states $|e\rangle$ and $|g\rangle$ is measured.

For simplicity, we consider the case when the first zone leads to a $\pi/2$ pulse and the second one a $-\pi/2$ pulse. The picture of angular momentum is particularly

well suited to discuss the Ramsey interferometric scheme and leads to an intuitive pictorial representation of the scheme. The Schwinger angular momentum operators are defined as

$$\begin{aligned} \hat{J}_x &= (\hat{\Sigma}_{eg} + \hat{\Sigma}_{ge})/2 \\ \hat{J}_y &= (\hat{\Sigma}_{eg} - \hat{\Sigma}_{ge})/2i \\ \hat{J}_z &= (\hat{\Sigma}_{ee} - \hat{\Sigma}_{gg})/2 \end{aligned} \tag{A.2}$$

where $\hat{\Sigma}_{\mu\nu} = \sum_{j=1}^{N} |\mu\rangle_{jj}\langle\nu|$ are collective operators. In terms of these, a single $\pi/2$ pulse (A.1) is represented by a rotation of the pseudo angular momentum vector around the x-axis by an angle $\pi/2$. For a single atom we have the correspondence $|\uparrow\rangle = |e\rangle$ and $|\downarrow\rangle = |g\rangle$. Under a $\pi/2$ rotation about the x-axis, the state $\uparrow\rangle$ transforms to $|J_y = -1/2\rangle = (|\uparrow\rangle - i|\downarrow\rangle)/\sqrt{2}$ as indicated in (A.1). For N atoms, we can think of the N individual spin $\frac{1}{2}$ particles combining to form a pseudo angular momentum vector of length $J = N/2$. The state of the collection of N atoms can then be represented by appropriate superpositions of the states $|J, M\rangle$ where $-J \leq M \leq J$. Of course, only states within the completely symmetric subspace of the full 2^N-dimensional Hilbert space can be represented in this way, which is justified since the coherent interaction of the electromagnetic fields with the atoms couple only to this symmetric subspace (i.e. all atoms couple equally to the fields).

Free evolution in the rotating frame corresponds to rotation of the angular momentum around the z-axis at an angular velocity $\omega - \omega_0$. The whole Ramsey scheme can then be represented by the sequence: $\pi/2$ rotation about x-axis, ϕ rotation about the z-axis and $-\pi/2$ rotation about the x-axis. This is the transformation perfomed

by the unitary operator

$$\hat{U}(\phi) = e^{i\pi/2\hat{J}_x} e^{-i\phi\hat{J}_z} e^{-i\pi/2\hat{J}_x} \tag{A.3}$$

where $\phi = (\omega - \omega_0)T$ as before. At the end of the scheme, the number of atoms in states $|e\rangle$ and $|g\rangle$ is measured, or equivalently their difference $\hat{J}_z(\phi)$ where

$$\begin{aligned} \hat{J}_z(\phi) &= \hat{U}(\phi)^\dagger \hat{J}_z \hat{U}(\phi) \\ &= \hat{J}_z \cos\phi - \hat{J}_x \sin\phi. \end{aligned} \tag{A.4}$$

The Ramsey signal is thus

$$\langle \hat{J}_z(\phi) \rangle = \langle \hat{J}_z \rangle \cos\phi - \langle \hat{J}_x \rangle \sin\phi \tag{A.5}$$

and its variance $\Delta J_z(\phi)$ is

$$\begin{aligned} \Delta J_z(\phi) &= \Big[(\Delta J_z)^2 \cos^2\phi + (\Delta J_x)^2 \sin^2\phi \\ &- \cos\phi \sin\phi (\langle \hat{J}_x \hat{J}_z + \hat{J}_z \hat{J}_x \rangle - 2\langle \hat{J}_z \rangle \langle \hat{J}_x \rangle) \Big]^{1/2} \end{aligned} \tag{A.6}$$

where the variance is defined as $(\Delta A)^2 = \langle \hat{A}^2 \rangle - \langle \hat{A} \rangle^2$. From the signal one wants to estimate the phase ϕ and thus the frequency difference $\omega - \omega_0$. The phase accuracy achievable from such a measurement is related to the signal variance (the "noise") by

$$\delta\phi(\phi) = \frac{\Delta J_z(\phi)}{\left| \frac{\partial \langle \hat{J}_z(\phi) \rangle}{\partial \phi} \right|}. \tag{A.7}$$

For states such that $\langle \hat{J}_x \rangle = 0$ (all the states we will consider in this paper are of this type), the sensitivity $|\partial \langle \hat{J}_z(\phi) \rangle / \partial \phi|$ is maximal for $\phi = \pm \pi/2$ and the phase accuracy can be expressed as

$$\delta\phi(\pm\pi/2) = \frac{\Delta J_x}{|\langle \hat{J}_z \rangle|}. \tag{A.8}$$

Since ΔJ_x and $\langle \hat{J}_z \rangle$ depend on the initial state, we see that different initial states lead to different phase accuracies. Of particular importance is the accuracy achievable when all atoms are prepared in the same initial state. In this case the state of the atomic ensemble is a pure state, but it is however an uncorrelated state of the atomic ensemble (i.e. it can be factorized $|\Psi\rangle = \prod_{j=1}^{N} |\psi\rangle_j$).

Consider the case of uncorrelated atoms for which all atoms have been prepared in the lower state $|g\rangle$, sometimes called a Bloch state. The state of the atomic ensemble can thus be expressed in terms of eigenstates of the collective angular momentum operators as

$$\prod_{j=1}^{N} |g\rangle_j = |J = N/2, J_z = -N/2\rangle \tag{A.9}$$

where $J = N/2$ since there are N 2-level atoms, equivalent to N spin $\frac{1}{2}$ particles. For such a state, the expectation value of the angular momentum operators and their variances are calculated to be $\langle \hat{J}_x \rangle = \langle \hat{J}_y \rangle = 0$, $\langle \hat{J}_z \rangle = -J$, $\Delta J_x = \Delta J_y = \sqrt{J/2}$ and $\Delta J_z = 0$. The signal and its variance are thus

$$\begin{aligned} \langle \hat{J}_z(\phi) \rangle &= -J \cos\phi \\ \Delta J_z(\phi) &= \sqrt{J/2} \sin\phi. \end{aligned} \tag{A.10}$$

The maximum sensitivity is achieved at $\phi = \pm\pi/2$

$$\delta\phi(\pm\pi/2) = \frac{1}{\sqrt{2J}} = \frac{1}{\sqrt{N}} \tag{A.11}$$

which is the standard quantum limit (SQL). Performing the experiment on N independent atoms all prepared in the same initial state is thus equivalent to repeating the experiment on one atom N times and leads to an expected $1/\sqrt{N}$ factor of improvement in accuracy over the one atom result $\Delta S_x/\langle \hat{S}_z \rangle = 1$. This is the best accuracy achievable with atoms all prepared in the same initial pure quantum state. The number of atoms detected in the upper state, given by $\langle \hat{N}_+(\phi) \rangle = N/2 + \langle \hat{J}_z(\phi) \rangle$, and its variance are shown in Fig. 2.1a.

There is a lower bound on the phase accuracy, set by Heisenberg's uncertainty principle, $\Delta J_i \Delta J_j \geq \frac{1}{2}|\langle [\hat{J}_i, \hat{J}_j] \rangle|$ where $i, j = x, y, z$. It is straightforward to show that

$$\delta\phi \geq \frac{1}{N} \tag{A.12}$$

which is known as the Heisenberg limit.

We now see from (A.8) that in order to surpass the SQL, the atomic ensemble must be prepared in a state such that $\Delta J_x/|\langle J_z \rangle| \leq 1/\sqrt{N}$, which is a necessary and sufficient condition for entanglement of an atomic ensemble [49, 141]. It is thus important to have a state for which the variance ΔJ_x is reduced compared to its value for the uncorrelated state (A.9) while maintaining a large value for $\langle J_z \rangle$ so that the amplitude of the signal $\langle \hat{J}_z(\phi) \rangle = \langle \hat{J}_z \rangle \cos\phi$ is not compromised [88]. Such states which have reduced uncertainty in one observable ΔJ_x (at the expense of the conjugate

observable ΔJ_y having increased fluctuations) have been called spin-squeezed states [**?**].

A.2 Spin Squeezed States - Wigner Function Representation

We now consider the Wigner function representation of the states $|\psi(a)\rangle$. The Wigner distribution of general angular-momentum states [46] is obtained from an expansion of the density operator in terms of the multipole operators

$$\hat{\rho} = \sum_{k=0}^{2J} \sum_{q=-k}^{+k} \rho_{kq} \hat{T}_{kq} \tag{A.13}$$

where the multipole operators are

$$\begin{aligned} \hat{T}_{kq} &= \sum_{m=-J}^{+J} \sum_{m'=-J}^{+J} (-1)^{J-m} \sqrt{2k+1} \begin{pmatrix} J & k & J \\ -m & q & m' \end{pmatrix} \\ &\times |J,m\rangle\langle J,m'| \end{aligned} \tag{A.14}$$

and $\begin{pmatrix} J & k & J \\ -m & q & m' \end{pmatrix}$ is the usual Wigner $3j$ symbol.
The wigner distribution is then given by

$$W(\theta,\phi) = \sum_{k=0}^{2J} \sum_{q=-k}^{+k} Y_k^q(\theta,\phi)\rho_{kq} \tag{A.15}$$

where $\rho_{kq} = \langle \hat{T}_{kq} \rangle = \mathrm{Tr}[\hat{\rho}\hat{T}_{kq}]$ and $Y_k^q(\theta,\phi)$ are the spherical harmonics. In Fig. A.1, the Wigner function for the state $|\psi(-1)\rangle$ clearly shows the way in which

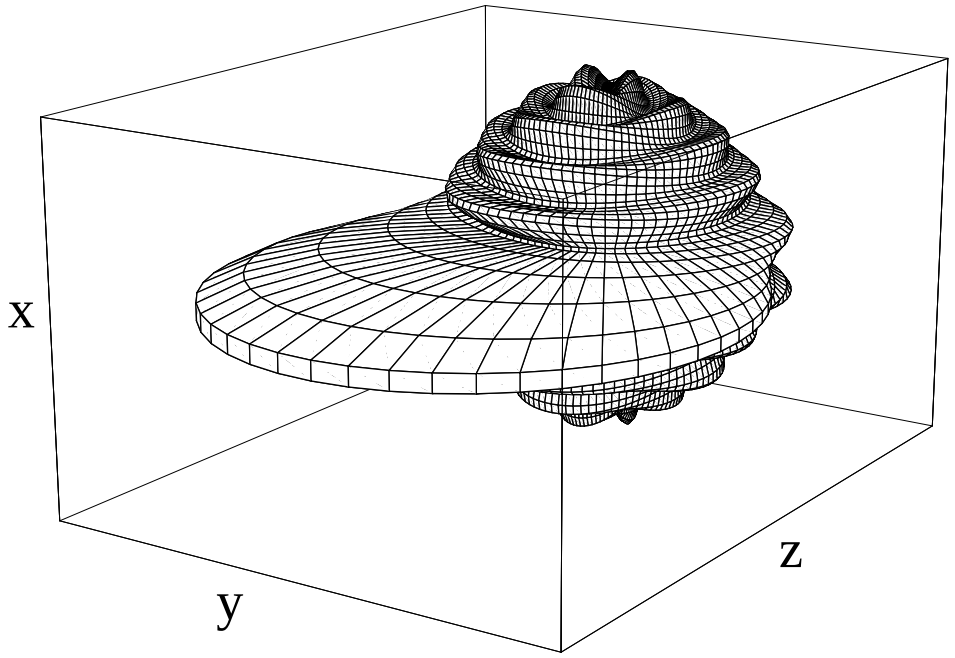

Figure A.1: Wigner function representation of the state $|\psi(a)\rangle$ with $a = -1$). Plotted is the surface $r(\theta, \phi) = W(\theta, \phi)$, showing the large and negative value of $\langle \hat{J}_z \rangle$, reduced variance ΔJ_x and correspondingly increased variance ΔJ_y.

this state has a large negative expectation value for $\hat{J}_z$, reduced variance in $\hat{J}_x$ and increased variance in $\hat{J}_y$.

A.3 Adiabatic Elimination of Excited State in Raman Scattering

From the Hamitonian (2.26), we obtain the equations of motion for the cavity mode and the ground state coherence Σ_{gb_1}

$$\dot{a} = -\kappa a - ig_1^*\Sigma_{b_1a_1} - ig_2^*\Sigma_{ga_2} + F_a(t) \quad (A.16)$$

$$\dot{\Sigma}_{gb_1} = -(\gamma_0 - i\delta_1)\Sigma_{gb_1} + i\Omega_1\Sigma_{a_1b_1} - ig_1^*a^\dagger\Sigma_{ga_1} + F_{gb_1}(t) \quad (A.17)$$

and the optical polarizations associated with Stokes emission evolve according to

$$\dot{\Sigma}_{b_1a_1} = -[\gamma - i(\Delta - \delta_1)]\Sigma_{b_1a_1} - i\Omega_1\Sigma_{b_1g} - ig_1a(\Sigma_{b_1b_1} - \Sigma_{a_1a_1}) + F_{b_1a_1}(t) \quad (A.18)$$

$$\dot{\Sigma}_{a_1g} = -(\gamma + i\Delta)\Sigma_{a_1g} - i\Omega_1^*(\Sigma_{a_1a_1} - \Sigma_{gg}) + ig_1^*a^\dagger\Sigma_{b_1g} + F_{a_1g}(t) \quad (A.19)$$

where we assume that population in the excited state $|a_1\rangle$ decays towards $|b_1\rangle$ at a rate γ_1, towards $|g\rangle$ at a rate γ_2 and we assume a dephasing rate γ_0 for ground state coherences ($\gamma = (\gamma_1 + \gamma_2)/2$ and $\gamma \gg \gamma_0$).

We proceed by adiabatic elimination of optical polarizations associated with Stokes emission. To this end we assume large single-photon detuning $\Delta \gg \gamma$ and to first order in $\hat{a}$ we obtain ($\Sigma_{gg} \sim N$)

$$\Sigma_{b_1a_1} = \frac{\Omega_1}{\Delta}(1 - i\frac{\gamma}{\Delta})\Sigma_{b_1g} + i\frac{F_{b_1a_1}(t)}{\Delta} \quad (A.20)$$

$$\Sigma_{a_1g} = \frac{\Omega_1^*}{\Delta}N(1 + i\frac{\gamma}{\Delta}) - i\frac{F_{a_1g}(t)}{\Delta} \quad (A.21)$$

which we substitute in (A.17) and obtain for the ground state spin flip operator $S_1 = \Sigma_{gb_1}/\sqrt{N}$

$$\begin{aligned}\dot{S}_1 &= -\left[(\gamma_0+\gamma_L)-i(\delta_1+\delta_L)\right]S_1 - i\frac{g_1^*\sqrt{N}\Omega_1}{\Delta}a^\dagger \\ &+ \bar{F}_{S_1}(t) \end{aligned} \tag{A.22}$$

where $\gamma_L = \gamma|\Omega_1|^2/\Delta^2$ is an optical pumping rate, $\delta_L = |\Omega_1|^2/\Delta$ is the light shift and $\bar{F}_{S_1}(t)$ is a modified noise force. Light shifts can be incorporated in a redefinition of the energies and we ignore them in the remainder of this paper. The new δ-correlated noise forces have correlations

$$\langle \bar{F}_{S_1}(t)\bar{F}^\dagger_{S_1}(t')\rangle = \left[2\gamma_0 + \frac{\gamma_2}{\gamma}\gamma_L\right]\delta(t-t') \tag{A.23}$$

$$\langle \bar{F}^\dagger_{S_1}(t)\bar{F}_{S_1}(t')\rangle = \frac{\gamma_1}{\gamma}\gamma_L\delta(t-t') \tag{A.24}$$

A.4 Adiabatic Elimination of Bright Polariton

After adiabatic elimination of the excited state $|a_1\rangle$, the relevant equations of motion are

$$\begin{aligned}\dot{S}_1^\dagger &= -(\gamma_L+\gamma_0+i\delta_1)S_1^\dagger + i\chi a + \bar{F}^\dagger_{S_1}(t) \\ \dot{a} &= -\kappa a - i\chi^* S_1^\dagger - ig_2^*\Sigma_{ga_2} + F_a(t) \\ \dot{S}_2 &= -(\gamma_L+\gamma_0+i\delta_2)S_2 - i\frac{\Omega_2^*}{\sqrt{N}}\Sigma_{ga_2} + \bar{F}_{S_2}(t) \\ \dot{\Sigma}_{ga_2} &= -(\gamma+i\delta_2)\Sigma_{ga_2} - i\Omega_2\sqrt{N}S_2 - ig_2 Na \\ &+ F_{ga_2}(t) \end{aligned} \tag{A.25}$$

where $S_2 = \Sigma_{gb_2}/\sqrt{N}$.

From (A.25) and (2.30) and in the limit of large ratio of speed of light in vacuum to group velocity of Stokes photons $\eta = |g_2|^2 N/|\Omega_2|^2 \gg 1$, we obtain the equations of motion in terms of bright and dark polaritons

$$\begin{aligned}
\dot{S}_1^\dagger &= -(\gamma_L + \gamma_0 + i\delta_1)S_1^\dagger + i\chi(P_B + \frac{P_D}{\sqrt{\eta}}) + F_{S_1}^\dagger(t) && \text{(A.26)}\\
\dot{P}_D &= -(\kappa/\eta + \Gamma_2)P_D - i\frac{\chi^*}{\sqrt{\eta}}S_1^\dagger - \frac{\kappa - \Gamma_2}{\sqrt{\eta}}P_B \\
&+ F_D(t) && \text{(A.27)}\\
\dot{P}_B &= -(\kappa + \Gamma_2/\eta)P_B - i\chi^* S_1^\dagger - \frac{\kappa - \Gamma_2}{\sqrt{\eta}}P_D \\
&- ig_2\sqrt{N}\tilde{\Sigma}_{ga_2} + F_B(t) && \text{(A.28)}\\
\dot{\tilde{\Sigma}}_{ga_2} &= -\Gamma\tilde{\Sigma}_{ga_2} - ig_2\sqrt{N}P_B + \tilde{F}_{ga_2}(t) && \text{(A.29)}
\end{aligned}$$

where $\Gamma_2 = \gamma_L + \gamma_0 + i\delta_2$, $\Gamma = \gamma + i\delta_2$ and $\tilde{\Sigma}_{ga_2} = \Sigma_{ga_2}/\sqrt{N}$ and noise forces were modified appropriately. Note that in the picture of dark and bright polaritons, only the bright polariton is coupled to the excited state through the optical coherence Σ_{ga_2}.

Under adiabatic conditions, the bright polariton evolves slowly (on a typical timescale T) and we can solve perturbatively in $1/T$. The equations (A.28) and (A.29) are of the form $\dot{\mathbf{x}} = -\mathbf{M}.\mathbf{x} + \mathbf{y}$, where $\mathbf{x}$ is the vector $(P_B, \tilde{\Sigma}_{ga_2})$, $\mathbf{M}$ is a 2×2 matrix and $\mathbf{y}$ is a source term

$$\frac{d}{dt}\begin{bmatrix} P_B \\ \tilde{\Sigma}_{ga_2} \end{bmatrix} = -\begin{pmatrix} \kappa & ig_2\sqrt{N} \\ ig_2\sqrt{N} & \Gamma \end{pmatrix}\begin{bmatrix} P_B \\ \tilde{\Sigma}_{ga_2} \end{bmatrix} + \begin{bmatrix} -i\chi^* S_1^\dagger - \frac{\kappa}{\sqrt{\eta}}P_D + F_B(t) \\ \tilde{F}_{ga_2}(t) \end{bmatrix} \tag{A.30}$$

where we have used $\kappa \gg (\gamma_L + \gamma_0)/\eta$ and where $F_B(t)$ and $\tilde{F}_{ga_2}(t)$ are appropriate noise forces. These equations can be solved easily to first order by $\mathbf{x}^{(0)}(t) = \mathbf{M}^{-1}.\mathbf{y}$, higher order approximations yielding $\mathbf{x}^{(n)}(t) = \mathbf{M}^{-1}.[\mathbf{y} - \dot{\mathbf{x}}^{(n-1)}(t)]$.

We can rewrite

$$\frac{|g_2|^2 N}{\kappa\gamma} \sim 3\pi \times \left(\frac{N}{V}L\lambda^2\right) \times \mathcal{F} \tag{A.31}$$

i.e. the density length product multiplied by the cavity finesse, so that with densities corresponding to room temperature atomic vapours, optical wavelengths and finesse of order 100 this quantity is already of order $\sim 10^4$. We can thus assume that $|g_2|^2 N/(\kappa\gamma) \gg 1$ and solve in powers of $\kappa\gamma/(|g_2|^2 N)$.

We see from (A.30) that $\mathbf{x}^{(n)}(t)$ is of order $[\kappa\gamma/(|g_2|^2 N)]^{(n+1)}$ and thus solving to lowest order we find

$$\begin{aligned} P_B &= \frac{1}{|g_2|^2 N}[-i\Gamma\chi^* S_1^\dagger - \frac{\kappa\Gamma}{\sqrt{\eta}}P_D + \Gamma F_B(t) \\ &- ig_2\sqrt{N}F_{ga_2}(t)] \end{aligned} \tag{A.32}$$

so that when $\eta \gg 1$,

$$\begin{aligned} a &\simeq \frac{P_D}{\eta} + P_B \\ &\simeq \frac{P_D}{\eta} + \frac{1}{|g_2|^2 N}[-i\Gamma\chi^* S_1^\dagger + \Gamma F_B(t) \\ &- ig_2\sqrt{N}F_{ga_2}(t)]. \end{aligned} \tag{A.33}$$

The coupled equations of motion for the dark state polariton (A.27) and the spin flip (A.26) then become

$$\begin{aligned} \dot{S}_1^\dagger &= (\frac{|g_1|^2}{|g_2|^2}\gamma_L - \gamma_L - \gamma_0 - i\delta_1)S_1^\dagger + i\frac{\chi}{\sqrt{\eta}}P_D \\ &+ \tilde{F}_{S_1}^\dagger(t) \end{aligned} \tag{A.34}$$

$$\begin{aligned} \dot{P}_D &= -(\kappa/\eta + \gamma_L + \gamma_0 + i\delta_2)P_D - i\frac{\chi^*}{\sqrt{\eta}}S_1^\dagger \\ &+ \tilde{F}_D(t) \end{aligned} \tag{A.35}$$

where $\tilde{F}_{S_1}^\dagger(t)$ and $\tilde{F}_D(t)$ are modified noise forces with correlations

$$\langle \tilde{F}_D(t)\tilde{F}_D^\dagger(t')\rangle = \left[\frac{2\kappa}{\eta} + 2\gamma_0 + \frac{\gamma_2}{\gamma}\gamma_L\right]\delta(t-t') \tag{A.36}$$

$$\langle \tilde{F}_D^\dagger(t)\tilde{F}_D(t')\rangle = 0 \tag{A.37}$$

$$\langle \tilde{F}_{S_1}(t)\tilde{F}_{S_1}^\dagger(t')\rangle = \left[2\gamma_0 + \frac{\gamma_2}{\gamma}\gamma_L\right]\delta(t-t') \tag{A.38}$$

$$\langle \tilde{F}_{S_1}^\dagger(t)\tilde{F}_{S_1}(t')\rangle = \left[\frac{\gamma_1}{\gamma}\gamma_L + 2\frac{|g_1|^2}{|g_2|^2}\gamma_L\right]\delta(t-t') \tag{A.39}$$

and all other correlations can be neglected. The coherent part of the interaction can thus be obtained from an effective hamiltonian

$$H_{eff} = \frac{\hbar\chi}{\sqrt{\eta}}S_1 P_D + \text{h.c.} \tag{A.40}$$

where the interaction rate is $\chi/\sqrt{\eta} = (g_1/g_2)\Omega_1\Omega_2/\Delta$.

We note (A.35) that cavity losses are strongly suppressed in the limit $\eta \gg 1$. Indeed, subsequent to the large group velocity reduction [74, 35, 87], the polariton is almost purely atomic and the excitation leaks very slowly out of the medium. The equation of motion for coherence S_1^+ (A.34) contains a loss term (due to isotropic spontaneous emission) and a linear gain term (due to emission into bright polariton). The two can compensate each other. However the linear phase-insensitive amplification is also accompanied by correspondingly increased fluctuations (A.39), represented by new Langevin forces $\tilde{F}_D(t), \tilde{F}_{S_1}^+(t)$. In the case that $g_1 = g_2$ and when all Rabi frequencies are taken to be real, we have the interaction rate $\xi = \chi/\sqrt{\eta} = \Omega_1\Omega_2/\Delta$.

Appendix B

Appendices to Chapter 3

B.1 Model of Frequency Control Loop

In an atomic clock, the goal is to lock the frequency of a local oscillator to the atomic transition frequency. The spectroscopic measurement is used to estimate the amount by which the L.O. frequency has drifted out of resonance during the last interrogation cycle, and in a subsequent feedback step, the L.O. frequency is steered to bring it back to resonance. Over the course of many interrogation cycles, the feedback control of the L.O. frequency leads to a stabilization of the mean frequency around the atomic resonance frequency, and an improved oscillator.

To model the stabilization of the oscillator frequency and quantify the improvement in frequency stability, we must take into account the spectroscopic measurement and its precision, as well as the feedback mechanism that controls the L.O. frequency, and its optimality must be carefully considered. The precision of the spectroscopic measurement depends on the atomic projection noise, and as discussed previously,

the use of entangled states (such as spin-squeezed states) can lead to an improved precision as compared to that achieved with uncorrelated atomic states. We consider here the situation where the main source of noise is the L.O. frequency fluctuations, rather than environmental dephasing noise. We therefore initially ignore the effect of environmental noise, and we will incorporate it in our description later.

The free-running L.O. is assumed to have frequency fluctuations described by the noise process $\delta\omega_{LO}(t)$, whose noise spectrum is $S_{LO}(\nu)$. Letting the Fourier transform of $\delta\omega_{LO}(t)$ be $\delta\Omega_{LO}(\nu) = \int dt\ e^{i\nu t}\delta\omega_{LO}(t)$, the noise spectrum is defined by

$$\langle \delta\Omega_{LO}(\nu)\delta\Omega_{LO}(\nu')\rangle \quad = \quad 2\pi\delta(\nu+\nu')S_{LO}(\nu). \tag{B.1}$$

At the discrete detection times t_k, an error signal $\mathcal{E}(t_k)$ is generated and a correction is applied to the frequency of the oscillator. The frequency offset of the slaved oscillator evolves (freely) between t_{k-1} and t_k according to

$$\delta\omega(t) \quad = \quad \delta\omega_{LO}(t) + \Delta\omega_{k-1} \tag{B.2}$$

where $\Delta\omega_{k-1}$ is the frequency correction that was applied at t_{k-1}.

In a first order feedback loop [13], the frequency correction at time t_k is updated according to

$$\Delta\omega_k \quad = \quad \Delta\omega_{k-1} + K\mathcal{E}(t_k) \tag{B.3}$$

where K is a constant that sets the strength of the feedback loop.

In an actual clock, the frequency of the oscillator is square-wave modulated with amplitude ω_m and period $2T_R$, with the modulation amplitude chosen so that $\omega_m T_R =$

$\pi/2$. Thus, during $t_{k-1} \leq t < t_k$ the frequency offset from atomic resonance is $\delta\omega(t) - (-1)^k\omega_m$, and during the next cycle $t_k \leq t < t_{k+1}$ the frequency offset is $\delta\omega(t) + (-1)^k\omega_m$.

During their interaction with the field, the atoms accumulate a phase $\pm(-1)^k\pi/2 + \delta\phi(t_k)$ relative to the oscillator, where $\delta\phi(t_k) = \int_0^T dt\ \delta\omega(t_k - t)$ is the (stochastic) phase due to fluctuations of the L.O. frequency during the interrogation time T.

As described previously, the detection signal at t_k is given by measurement of the operator

$$\begin{aligned} \hat{J}_z(t_k) &= \cos[\pm(-1)^k\pi/2 + \delta\phi(t_k)]\hat{J}_z(0) - \sin[\pm(-1)^k\pi/2 + \delta\phi(t_k)]\hat{J}_y(0) \\ &= \mp(-1)^k\left[\sin[\delta\phi(t_k)]\hat{J}_z(0) + \cos[\delta\phi(t_k)]\hat{J}_y(0)\right] \end{aligned} \tag{B.4}$$

and the error signal $\mathcal{E}(t_k)$ used to steer the frequency of the oscillator is given by the difference in detection signals at t_k and t_{k-1}, i.e.

$$\begin{aligned} \mathcal{E}(t_k) &= [\sin[\delta\phi(t_k)]\mathcal{J}_z(t_k) + \cos[\delta\phi(t_k)]\mathcal{J}_y(t_k)] \\ &+ [\sin[\delta\phi(t_{k-1})]\mathcal{J}_z(t_{k-1}) + \cos[\delta\phi(t_{k-1})]\mathcal{J}_y(t_{k-1})] \end{aligned} \tag{B.5}$$

where $\mathcal{J}_z(t_k)$ ($\mathcal{J}_y(t_k)$) represents the value of $\hat{J}_z$ ($\hat{J}_y$) obtained for the detection time t_k. We consider atomic states for which the correlator $\langle\hat{J}_z\hat{J}_y + \hat{J}_y\hat{J}_z\rangle$ vanishes, so that we may pick $\mathcal{J}_z(t_k)$ and $\mathcal{J}_y(t_k)$ as two independent random numbers distributed according to the distributions appropriate for the initial quantum state considered (uncorrelated, spin-squeezed,...etc).

We now consider the case of small $\delta\phi(t_k)$, so that we can linearize eqn. (B.5) in the phase $\delta\phi(t_k)$, and the error signal becomes

$$\begin{aligned}\mathcal{E}(t_k) &\simeq [\delta\phi(t_k) + \delta\phi(t_{k-1})]\langle\hat{J}_z\rangle + [\mathcal{J}_y(t_k) + \mathcal{J}_y(t_{k-1})] \\ &+ [\delta\phi(t_k)\delta\mathcal{J}_z(t_k) + \delta\phi(t_{k-1})\delta\mathcal{J}_z(t_{k-1})] \end{aligned} \tag{B.6}$$

where $\delta\mathcal{J}_z(t_k)$ is the value of $\hat{J}_z - \langle\hat{J}_z\rangle$ obtained at time t_k.

Plugging in (B.2) and letting $-\beta = K\langle\hat{J}_z\rangle T$, we have

$$\Delta\omega_k = \Delta\omega_{k-1} - \beta\left[\mathcal{G}\delta\omega(t_k) + \mathcal{G}\delta\omega(t_{k-1}) + \delta\mathcal{Y}_k + \delta\mathcal{Y}_{k-1}\right] \tag{B.7}$$

where $\mathcal{G}\delta\omega(t_k) = \frac{1}{T}\int_0^T dt\ \delta\omega(t_k - t)$, and $\delta\mathcal{Y}_k = \frac{\mathcal{J}_y(t_k) + \delta\mathcal{J}_z(t_k)\delta\phi(t_k)}{\langle\hat{J}_z\rangle T}$.

The dynamical behaviour of the frequency control loop can now be obtained, combining (B.2) with (B.7) to give

$$\Delta\omega_k - (1-\beta)\Delta\omega_{k-1} + \beta\Delta\omega_{k-2} = -\beta[\mathcal{W}_k + \mathcal{W}_{k-1}] \tag{B.8}$$

where $\mathcal{W}_k = \mathcal{G}\delta\omega_{LO}(t_k) + \delta\mathcal{Y}_k$.

The stability criterion for the control loop is that the modulus of the roots of its characteristic equation is smaller than unity, that equation is

$$z^2 - (1-\beta)z + \beta = 0 \tag{B.9}$$

where $z = e^{i\nu T}$, it is stable for $1 \geq \beta \geq 0$.

In the frequency domain, equation (B.8) gives $\Delta\omega(\nu) = H(\nu)\mathcal{W}(\nu)$ where

$$\begin{aligned} H(\nu) &= \frac{-\beta(1+z^{-1})}{1-(1-\beta)z^{-1}+\beta z^{-2}} \\ \mathcal{W}(\nu) &= \delta\mathcal{Y}(\nu)+\mathcal{G}(\nu)\delta\omega_{LO}(\nu) \\ \mathcal{G}(\nu) &= \frac{1-e^{-i\nu T}}{i\nu T}. \end{aligned} \tag{B.10}$$

Plugging that in (B.2), we find

$$\delta\omega(\nu) = \left[1+z^{-1}H(\nu)\mathcal{G}(\nu)\right]\delta\omega_{LO}(\nu)+\left[z^{-1}H(\nu)\right]\delta\mathcal{Y}(\nu). \tag{B.11}$$

This expression gives the noise of the stabilized oscillator $\delta\omega(\nu)$ in terms of the free-running oscillator noise $\delta\omega_{LO}(\nu)$ and the atomic projection noise $\delta\mathcal{Y}(\nu)$.

To find the noise spectrum corresponding to the atomic part, we note that $\delta\mathcal{Y}_k$ is a white noise process sampled at times $t_k = kT$. We thus find $S_Y(\nu) = \frac{\Delta J_y^2+\Delta J_z^2\langle\delta\phi^2\rangle}{T\langle J_z\rangle^2}$.

We find the noise spectrum of the slaved oscillator

$$S(\nu) = \left|1+z^{-1}H(\nu)\mathcal{G}(\nu)\right|^2 S_{LO}(\nu)+\left|H(\nu)\right|^2 S_Y(\nu) \tag{B.12}$$

Note that $|1+e^{-i\nu T}H(\nu)\mathcal{G}(\nu)|^2 \sim \left(\frac{\nu T}{2\beta}\right)^2$ for $\nu T \ll \beta$, therefore as long as the noise spectrum of the L.O. is less divergent than $1/\nu^2$ at low frequencies, its contribution to the stabilized oscillator noise vanishes at low enough frequencies. It is possible to improve the stabilization further by using a higher order feedback loop, i.e. where the feedback term depends on the past n measurements. In general such feedback loop will stabilize noise spectra as divergent as $1/\nu^n$, so that for the practically relevant case of $1/\nu^2$ noise (present in quartz crystal oscillators and resulting in $\sigma_y(\tau)^2 \sim \tau$), higher order feedback loop may be useful.

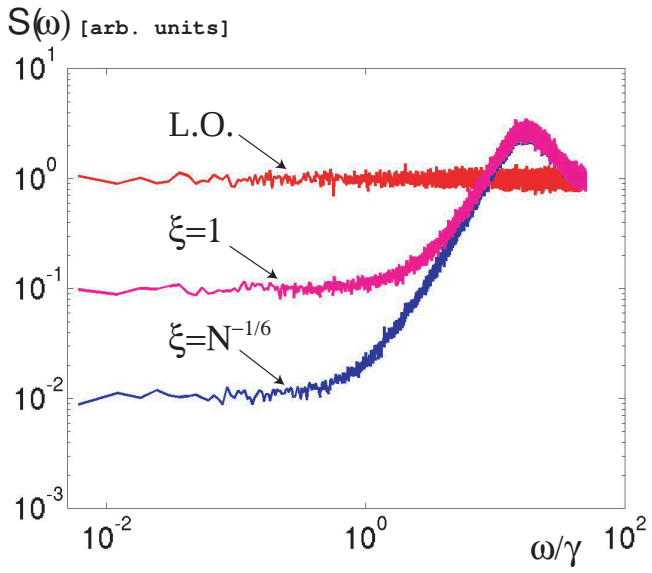

Figure B.1: Noise spectrum of local oscillator, stabilized oscillator locked to uncorrelated atoms, and stabilized oscillator locked to spin-squeezed atoms. The LO noise spectrum is initially white, $N = 1000$.

For low frequencies, $|H(\nu)|^2 \simeq 1$, so that the atomic contribution to the oscillator noise corresponds to white noise at low frequencies. In the time domain, this means that for long enough averaging times, the frequency stability is limited by the atomic projection noise. Moreover, because the atomic contribution to the stabilized oscillator noise is white at low frequencies, the frequency fluctuations average down as $\tau^{-1/2}$ with averaging time τ.

A widely used measure of frequency stability is the Allan variance [16], defined as

$$\sigma^2(\tau) \quad = \quad \frac{1}{2}\langle\left(\frac{\delta\bar{\omega}(2\tau) - \delta\bar{\omega}(\tau)}{\omega_0}\right)^2\rangle \tag{B.13}$$

where $\delta\bar{\omega}(t) = \frac{1}{\tau}\int_0^\tau dt'\ \delta\omega(t-t')$ is the frequency averaged over the averaging period $\tau \gg T$. It is easy to show [16] that for white noise $S(\nu) = \Gamma$, the Allan variance is given by $\sigma(\tau)^2 = \frac{\Gamma}{\omega_0^2\tau}$.

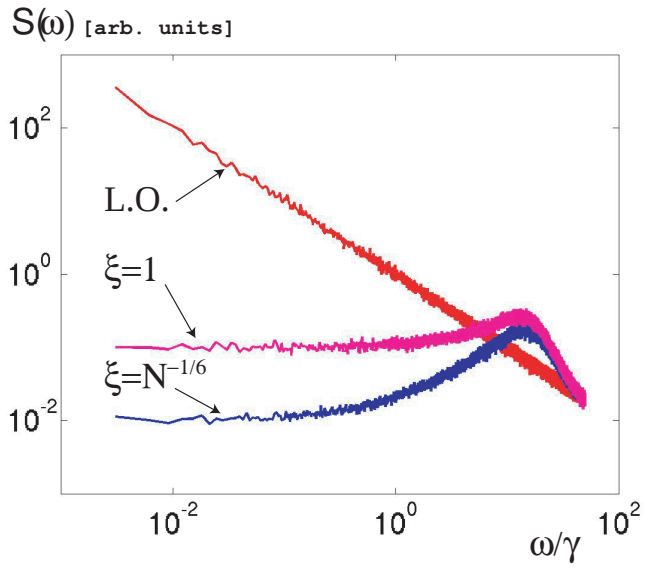

Figure B.2: Noise spectrum of local oscillator, stabilized oscillator locked to uncorrelated atoms, and stabilized oscillator locked to spin-squeezed atoms. The LO noise spectrum is $1/f$, $N = 1000$.

For low frequencies, the stabilized oscillator noise spectrum is white so that the Allan variance (for long enough averaging time τ) is given by

$$\sigma(\tau)^2 \quad = \quad \frac{\Delta J_y^2 + \Delta J_z^2 \langle \delta\phi^2 \rangle}{\omega_0^2 \tau T \langle \hat{J}_z \rangle^2} \tag{B.14}$$

where $\delta\phi = \int_0^T dt\ \delta\omega(t)$ is the phase fluctuation of the stabilized oscillator during one interrogation time T.

We recognize in (B.14), the atomic projection noise $\frac{\Delta J_y^2}{\langle \hat{J}_z \rangle^2}$ which for uncorrelated atoms is equal to $1/N$, while for highly spin-squeezed states we have $\frac{\Delta J_y^2}{\langle \hat{J}_z \rangle^2} \sim 1/N^2$. Note however that because of the second term in (B.14), proportional to $\frac{\Delta J_z^2 \langle \delta\phi^2 \rangle}{\langle \hat{J}_z \rangle^2}$, highly spin squeezed states are not desirable, since the reduction in transverse noise ΔJ_y is accompanied by an increase in longitudinal noise ΔJ_z (i.e. along the mean

spin direction).

B.2 Stochastic Differential Equation approach

Note that eq. (B.14) is derived assuming we can linearize in the phase $\delta\phi$. To investigate the nonlinear regime where terms of higher order in $\delta\phi$ lead non-negligible corrections, we resort to approximating the feedback control loop by a stochastic differential equation.

At the detection times t_k we have the error signal

$$\mathcal{E}(t_k) \;=\; \mathcal{J}_z(t_k)\sin[\delta\phi(t_k)] + \mathcal{J}_y(t_k)\cos[\delta\phi(t_k)] \tag{B.15}$$

where

$$\delta\phi(t_k) \;=\; \int_0^T \delta\omega(t_k - t)dt \tag{B.16}$$

is the phase of the slaved oscillator accumulated during the interrogation time T. The accumulated phase of the slaved oscillator $\delta\phi(t_k)$ can be decomposed as the sum of a contribution due to the free-running LO frequency fluctuations $\delta\omega_{LO}(t)$ and a contribution due to the frequency correction $\Delta\omega_{k-1}$ that was applied at time t_{k-1}, as $\delta\phi(t_k) = \delta\phi_{LO}(t_k) + \Delta\phi_{k-1}$, where $\Delta\phi_{k-1} = \Delta\omega_{k-1}T$.

Ignoring for simplicity the fact that the LO frequency is square wave modulated (this does not modify the applicability of the results below to the modulated case), the frequency correction applied at t_k is updated according to

$$\Delta\omega_k \;=\; \Delta\omega_{k-1} - \frac{\beta}{T}F[\mathcal{E}(t_k)/J] \tag{B.17}$$

where $F(x) = x$ in the case of linear feedback as considered earlier, and $F(x) = \arcsin(x)$ in the case of nonlinear feedback we consider below. Note that the linear feedback is designed to correct small phase fluctuations $\delta\phi(t_k) \ll 1$, and that it ignores higher order terms in $\delta\phi(t_k)$. Linearizing the error signal in the phase $\delta\phi(t_k)$, we have

$$\mathcal{E}(t_k) \;=\; \langle \hat{J}_z \rangle \delta\phi(t_k) + [\mathcal{J}_y(t_k) + \delta\mathcal{J}_z(t_k)\delta\phi(t_k)] + \cdots \tag{B.18}$$

The higher order terms in $\delta\phi(t_k)$ are ignored by the linear feedback, such as the next term in the expansion $\sin[\delta\phi(t_k)] = \delta\phi(t_k) - \frac{\delta\phi(t_k)^3}{3!} + \cdots$. The effect of such terms is to add noise unaccounted for in the detection signal, and just like the atomic projection noise ΔJ_y, they limit the long terms stabiliy of the clock. Before describing this stability limit in details, we can understand this easily by noting that the most important term ignored in the linearized detection signal is $-\langle \hat{J}_z \rangle \frac{\delta\phi(t_k)^3}{3!}$. As we increase the Ramsey time T, the random phase $\delta\phi(t_k) = \int_0^T \delta\omega(t_k - t)dt$ increases, so that the size of the nonlinear term we ignored increases. When the term we ignored becomes comparable to or greater than the atomic noise ΔJ_y, it becomes the dominant noise source. We can estimate that this will happen when the Ramsey time becomes large enough that $\Delta J_y^2 \simeq \langle \hat{J}_z \rangle^2 \langle \left(\frac{\delta\phi(t_k)^3}{3!} \right)^2 \rangle$. We thus see that in the linear feedback case, the maximum Ramsey time is determined by that for which the nonlinear terms become comparable to or greater than the atomic noise. In the simplest case of white frequency noise, $\langle \delta\phi(t_k)^2 \rangle = \gamma T$, and we find that for uncorrelated atoms, the condition above gives $\gamma T_{max} \sim N^{-1/3}$. Ideally, it should be possible through proper choice of feedback, to extend this to $\gamma T_{max} \sim 1$. We thus see in this example, that while ideally the frequency precision $\delta\omega(\tau) = \frac{\delta\phi_R}{\sqrt{\tau T}}$ should scale as $N^{-1/2}$ for uncorrelated atoms, in the case of linear feedback it scales as $N^{-1/3}$

instead, due to the shorter maximum interrogation time.

We now consider the case of nonlinear feedback $F(x) = \arcsin(x)$, and show that this leads to an improved frequency stability due to its ability to correct for larger phase fluctuations ($\delta\phi(t_k) \lesssim 1$), where the linear feedback strategy fails. In particular, we show below that nonlinear feedback allows to recover the ideal scaling $\delta\omega(\tau) \propto N^{-1/2}$ for uncorrelated atoms, while linear feedback only led to $\delta\omega(\tau) \propto N^{-1/3}$.

Using the frequency correction equation $\delta\phi(t_k) = \delta\phi_{LO}(t_k) + \Delta\phi_{k-1}$, we find the difference equation

$$\begin{aligned} \delta\phi(t_k) - \delta\phi(t_{k-1}) &= [\delta\phi_{LO}(t_k) - \delta\phi_{LO}(t_{k-1})] \\ &- \beta F\left[\kappa(1+\delta z_{k-1})\sin[\delta\phi(t_{k-1})] + \kappa\delta y_{k-1}\cos[\delta\phi(t_{k-1})]\right] \end{aligned} \quad \text{(B.19)}$$

where $\kappa = \langle \hat{J}_z \rangle / J$, and where δz_k and δy_k are gaussian random variables of zero mean and with variance given by $\langle \delta z_k^2 \rangle = (\Delta J_z / \langle J_z \rangle)^2$, and $\langle \delta y_k^2 \rangle = (\Delta J_y / \langle J_z \rangle)^2$. We want to estimate the long-term frequency stability, as given by the frequency averaged over a time $\tau = nT$

$$\begin{aligned} \delta\bar{\omega}(\tau) &= \frac{1}{\tau}\int_0^\tau \delta\omega(\tau - t)dt \\ &= \frac{1}{\tau}\sum_{k=1}^{n} \delta\phi(t_k). \end{aligned} \quad \text{(B.20)}$$

Since we are interested in the long term frequency stability, i.e. in time scales much longer than T, we approximate the difference equation by a differential equation. In doing so we are explicitely smoothing out time variations faster than or on the scale of T. We thus write $\delta\phi(t) \simeq T\delta\omega(t) = x(t)$, $\delta\phi_{LO}(t) \simeq T\delta\omega_{LO}(t) = \epsilon_1 z_1(t)$. In the case of white LO noise for example, we have $\langle z_1(t) z_1(t') \rangle = T\delta(t - t')$ and $\epsilon_1 = \sqrt{\gamma T}$, so that we can use ϵ_1 as a small expansion parameter. For other noise spectra, the scaling

with interrogation time will be different, and for small interrogation time we can similarly treat ϵ_1 as a small expansion parameter. We also approximate the discrete-time atomic noise processes δy_k and δz_k by continuous time delta-correlated stochastic processes $\delta y(t) = \epsilon_2 z_2(t)$, and $\delta z(t) = \epsilon_3 z_3(t)$, where $\langle z_i(t) z_j(t') \rangle = \delta_{ij} T \delta(t - t')$, $\epsilon_2 = \Delta J_y / \langle J_z \rangle$, $\epsilon_3 = \Delta J_z / \langle J_z \rangle$. Note that to keep the variance at equal times finite, we set $T\delta(0) \to 1$ and treat $\delta(t - t')$ as a usual delta function inside integrals. The difference equation thus becomes in the continuous time version the stochastic differential equation

$$\dot{x} \;=\; \epsilon_1 \dot{z}_1(t) - \frac{\beta}{T} F[\kappa(1 + \epsilon_3 z_3(t)) \sin(x) + \kappa \epsilon_2 z_2(t) \cos(x)] \tag{B.21}$$

were $F(x)$ is the feedback function. For linear feedback (LF), we choose this function to be $F(x) = x$, which we anticipate will optimally stabilize the oscillator for small values of the noise and of the phase fluctuation $\delta\phi$. We will also look at a nonlinear feedback (NLF) scheme, where we choose $F(x) = \arcsin(x)$. We show below that NLF performs better than LF, and that optimizing the interrogation time T, we find a different scaling with the number of atoms of the long-term frequency stability in these two cases. Only NLF leads to the well-known scaling $\langle (\delta\bar{\omega}(\tau)/\omega_0)^2 \rangle^{1/2} \propto 1/\sqrt{N}$, for uncorrelated atoms.

B.3 Long-term Stability

B.3.1 Linear Feedback

In appendix B.4, we show how eqn. (B.21) can be solved by a small noise perturbative expansion method. The solution for the LF case is

$$\sigma_y^2(\tau) \;=\; \frac{1}{\omega_0^2 T\tau}\left\{c\epsilon_1^6+\epsilon_2^2+\epsilon_1^2\epsilon_3^2\right\}, \tag{B.22}$$

where $c=[1-3\chi+(8/3)\chi^2]/6$, with $\chi=\beta\kappa/2$.

For white L.O. noise, we replace $\epsilon_1=\sqrt{\gamma T}$, and find

$$\sigma_y^2(\tau) \;=\; \frac{1}{\omega_0^2 T\tau}\left\{c(\gamma T)^3+\frac{\Delta J_y^2}{\langle J_z\rangle^2}+(\gamma T)\frac{\Delta J_z^2}{\langle J_z\rangle^2}\right\}. \tag{B.23}$$

To find the optimal long-term stability, we now need to optimize interrogation time T and find the optimal degree of spin-squeezing that minimizes $\sigma_y(\tau)$. Setting the derivative with respect to T equal to zero and solving for the optimal interrogation time, we find $\gamma T^*=\left(\frac{\Delta J_y^2}{2c\langle J_z\rangle^2}\right)^{1/3}$. As anticipated earlier, the optimal Ramsey time for uncorrelated atoms scales as $\gamma T^*\sim N^{-1/3}$. This corresponds to the time at which the atomic projection noise equals the noise coming from the nonlinear terms not corrected by the linear feedback loop. For longer interrogation times the nonlinear terms dominate, and the overall phase estimation accuracy decreases with increasing Ramsey time. Similarly for interrogation times shorter than the optimum, the projection noise dominates compared to the nonlinear contribution, and increasing the Ramsey time, increases the precision.

We can now plug in the optimal interrogation time in (B.23) and find the atomic state that minimizes the resulting expression. At the optimal Ramsey time, we find

the Allan variance

$$\sigma_y^2(\tau) \;=\; \frac{\gamma}{\omega_0^2\tau}\left\{\frac{3c^{1/3}}{2^{2/3}}\left(\frac{\Delta J_y}{|\langle\hat{J}_z\rangle|}\right)^{4/3}+\left(\frac{\Delta J_z}{|\langle\hat{J}_z\rangle|}\right)^2\right\} \tag{B.24}$$

For uncorrelated atoms and weak feedback ($c \to 1$), we find $\sigma_y(\tau)^2 = \frac{\gamma}{\omega_0^2\tau}\frac{3/4}{N^{2/3}}$. Note the importance of considering the feedback loop: since the Ramsey phase accuracy is $\delta\phi_R = \frac{\Delta J_y}{|\langle\hat{J}_z\rangle|} = \frac{1}{\sqrt{N}}$ for uncorrelated atoms, one would naively argue that the frequency stability after $n = \tau/T$ measurements should be $\langle\left(\frac{\delta\omega(\tau)}{\omega_0}\right)^2\rangle = \frac{1}{\omega_0^2 T\tau N}$, with $T \sim 1/\gamma$ optimally. When the Ramsey time is optimized, the scaling $\propto 1/N$ crucially depends on choosing the correct feedback loop, and as demonstrated above, a linear feedback loop is not optimal and gives a scaling $\propto 1/N^{2/3}$.

Finding the exact state that minimizes the expression (B.24) is trivial to implement algorithmically, however it may be difficult to understand physically why the optimal state is optimal. Instead, we consider a particular family of states that include the uncorrelated state and spin-squeezed states of various degree. We consider the atomic states

$$|\psi(\sigma)\rangle = \frac{1}{\mathcal{N}(\sigma)}\sum_{M=-J}^{J} e^{-(M/\sigma)^2}\,|J_y = M\rangle \tag{B.25}$$

where $J = N/2 \gg 1$, and $|J_y = M\rangle$ are eigenstates of $\hat{J}_y$ with eigenvalue M ($\mathcal{N}(\sigma)$ is a normalization factor). When $\sigma = \sqrt{2J}$, the uncorrelated atomic state with $|\langle\hat{J}_z\rangle| \simeq N/2$, $\Delta J_y \simeq \sqrt{N}/2$, and $\Delta J_z \simeq 0$ is obtained, while highly spin-squeezed states are achieved as $\sigma \to 1$.

Optimizing over this class of states, we find the optimum spin-squeezed state parameter $\sigma = 2^{-1/16}N^{1/4}$, which corresponds to $|\langle\hat{J}_z\rangle| \simeq N/2$, $\Delta J_y \sim N^{1/4}$, and $\Delta J_z \sim N^{1/2}$. We find the corresponding Allan variance $\sigma_{y,opt}(\tau)^2 = \frac{\gamma}{\omega_0^2\tau}\frac{2^{5/4}}{N}$. This

represents an improvement in long-term frequency stability (as measured by $\sigma_y(\tau)$) by a factor of $N^{1/6}$, when compared to uncorrelated atoms.

In the case of $1/f$ noise, we heuristically replace $\epsilon_1 = \sqrt{\gamma T}$, by $\epsilon_1 \propto \gamma T$, where the constant of proportionality is unknown, but can be obtained by fitting the results of the numerical simulation to the expression for $\sigma_y^2(\tau)$. We then find

$$\sigma_y^2(\tau) = \frac{1}{\omega_0^2 T\tau}\left\{c(\gamma T)^6 + \frac{\Delta J_y^2}{\langle \hat{J}_z\rangle^2} + (\gamma T)^2\frac{\Delta J_z^2}{\langle \hat{J}_z\rangle^2}\right\} \tag{B.26}$$

where c is a numerical coefficient to be determined.

For uncorrelated atoms $\sigma_y(\tau)^2 \sim \frac{1}{N^{5/6}}$, and once again we see that the linear feedback loop is not optimal, in that it does not give the scaling $\propto 1/N$ for uncorrelated atoms, but rather $\propto 1/N^{5/6}$. Optimizing once again over our family of gaussian states, we find that using optimally spin squeezed states of parameter $\sigma \sim N^{3/8}$ yields the Allan variance $\sigma_y(\tau)^2 \sim \frac{1}{N^{25/24}}$, which represents an improvement in Allan variance by a factor of $N^{5/24}$, as compared to uncorrelated atoms.

B.3.2 Nonlinear Feedback

In the NLF case, the stabilized oscillator frequency offset obeys the stochastic differential equation (B.21) with $F(x) = \arcsin(x)$. As shown in appendix B.4, the solution in this case can be found and is

$$\sigma_y^2(\tau) = \frac{1}{\omega_0^2 T\tau}\left\{c\epsilon_1^6(1-\kappa^2)^2 + \epsilon_2^2 + \epsilon_1^2\epsilon_3^2\right\}, \tag{B.27}$$

where $c = [1-3\chi+(8/3)\chi^2]/6$. Nonlinear feedback reduces the effect of the first term by a factor of $(1-\kappa^2)^2$. Note that for $N \gg 1$, using our gaussian states (see appendix

B.5), we have $1-\kappa^2 \simeq 2\Delta J_z/J$. Hence, we see that for uncorrelated atoms $\Delta J_z = 0$, nonlinear feedback completely removes the effect of that term, as we expected.

For uncorrelated atoms, $\kappa = 1$ and $\epsilon_3^2 = \Delta J_z^2/|\langle \hat{J}_z \rangle|^2 = 0$, so that the long term frequency stability is given by the usual expression

$$\sigma_y^2(\tau) \;=\; \frac{1}{\omega_0^2 T \tau N}. \tag{B.28}$$

The longest Ramsey time that can be used is then $T \sim 1/\gamma$ where $1/\gamma$ is the time over which the variance of the phase fluctuations of the local oscillator grows to $\langle \delta\phi_{LO}^2 \rangle \sim 1$.

To find the optimal long-term stability using entangled states of the atomic ensemble, we now need to find the optimal interrogation time T and the optimal degree of spin-squeezing, that minimizes $\sigma_y(\tau)$. Considering white LO noise, and putting $\epsilon_1^2 = \gamma T$ in (B.29), we find that the optimum is at $\gamma T^* \sim 1$, and that the states optimizing the Allan variance correspond to $\Delta J_y \sim \Delta J_z \sim N^{1/3}$. In this case the long-term stability is given by

$$\sigma_y^2(\tau) \;\sim\; \frac{\gamma}{\omega_0^2 \tau} \frac{1}{N^{2/3}} \tag{B.29}$$

representing an improvement by a factor of $N^{1/3}$ compared to uncorrelated atoms (a factor of $N^{1/6}$ in the frequency stability $\sigma_y(\tau)$).

Similarly, for $1/f$ noise we find the optimal Ramsey time $T^* \sim 1/\gamma$, and the same scaling of the Allan variance as in (B.29).

We thus conclude that the nonlinear feedback loop allows to use the longest possible time as the optimal Ramsey time, which is such that $\langle \delta\phi_{LO}(T)^2 \rangle \sim 1$. In this case, the effective squeezing parameter that needs to be optimized by choosing the

appropriate atomic state is given by

$$\xi = \sqrt{N}\frac{\left[\Delta J_y^2 + \alpha \Delta J_z^2\right]^{1/2}}{|\langle \hat{J}_z \rangle|} \tag{B.30}$$

where $\alpha \sim 1$ is a numerical coefficient of order unity. The squeezing parameter is $\xi = 1$ for uncorrelated atoms, and its minimum value is $\xi \sim N^{-1/6}$ for the mildly spin-squeezed states with $\Delta J_y \sim \Delta J_z \sim N^{1/3}$.

B.4 Perturbative Solution of SDE

We proceed to solve this differential equation with a small noise expansion. Assuming $\epsilon_{1,2,3} \ll 1$, we seek a solution in the form of a power series expansion in the small quantities $\epsilon_{1,2,3}$, representing the amplitude of the various noise sources entering the problem. We will find that the nonlinear term plays a role for $\epsilon_2 \sim \epsilon_1^3$, so we seek a perturbative solution that is first order in ϵ_2 and ϵ_3 and at least up to order ϵ_1^3. We use the trial solution of the form $x(t) = \sum_{n=1}^{\infty} x_{1,n}(t)\epsilon_1^n + \epsilon_2 \sum_{n=0}^{\infty} x_{2,n}(t)\epsilon_1^n + \epsilon_3 \sum_{n=0}^{\infty} x_{3,n}(t)\epsilon_1^n$.

B.4.1 Linear feedback

Plugging in the trial solution, we find that $x_{1,2n}(t) = x_{2,2n+1}(t) = x_{3,2n}(t) = 0$ and the first few relevant terms obey

$$\begin{aligned}
\dot{x}_{1,1} &= -\alpha x_{1,1} + \dot{z}_1 \\
\dot{x}_{1,3} &= -\alpha x_{1,3} + \alpha \frac{x_{1,1}^3}{3!} \\
\dot{x}_{2,0} &= -\alpha x_{2,0} + \alpha z_2 \\
\dot{x}_{3,1} &= -\alpha x_{3,1} + \alpha z_3 x_{1,1}
\end{aligned} \tag{B.31}$$

where $\alpha = \frac{\beta\kappa}{T}$.

Solving the first few terms gives

$$\begin{aligned}
x_{1,1}(t) &= \int_{-\infty}^{t} e^{-\alpha(t-t')}\dot{z}_1(t')dt' = z_1(t) - \alpha\int_{-\infty}^{t} e^{-\alpha(t-t')}z_1(t')dt' && \text{(B.32)}\\
x_{1,3}(t) &= \frac{\alpha}{3!}\int_{-\infty}^{t} e^{-\alpha(t-t')}[x_{1,1}(t')]^3dt' && \text{(B.33)}\\
x_{2,0}(t) &= \alpha\int_{-\infty}^{t} e^{-\alpha(t-t')}z_2(t')dt' && \text{(B.34)}\\
x_{3,1}(t) &= \alpha\int_{-\infty}^{t} e^{-\alpha(t-t')}z_3(t')x_{1,1}(t')dt' && \text{(B.35)}\\
&\cdots
\end{aligned}$$

The correlation function is thus

$$\begin{aligned}
\langle x(t)x(t')\rangle &= \epsilon_1^2\langle x_{1,1}(t)x_{1,1}(t')\rangle\\
&+ \epsilon_1^4\left[\langle x_{1,1}(t)x_{1,3}(t')\rangle + \langle x_{1,3}(t)x_{1,1}(t')\rangle\right] + \epsilon_1^6\langle x_{1,3}(t)x_{1,3}(t')\rangle\\
&+ \epsilon_2^2\langle x_{2,0}(t)x_{2,0}(t')\rangle\\
&+ \epsilon_3^2\epsilon_1^2\langle x_{3,1}(t)x_{3,1}(t')\rangle + \cdots && \text{(B.36)}
\end{aligned}$$

Evaluating these terms one by one gives, for $z_1(t)$ corresponding to white noise and assuming gaussian statistics,

$$\begin{aligned}
\langle x_{1,1}(t)x_{1,1}(t')\rangle &= T\delta(t-t') - \frac{\alpha T}{2}e^{-\alpha|t-t'|} && \text{(B.37)}\\
\langle x_{1,1}(t)x_{1,3}(t')\rangle + \langle x_{1,3}(t)x_{1,1}(t')\rangle &= \frac{\alpha T}{4}\left(1-\frac{\alpha T}{2}\right)[1-\alpha|t-t'|]e^{-\alpha|t-t'|} && \text{(B.38)}\\
\langle x_{2,0}(t)x_{2,0}(t')\rangle &= \frac{\alpha T}{2}e^{-\alpha|t-t'|} && \text{(B.39)}\\
\langle x_{3,1}(t)x_{3,1}(t')\rangle &= \frac{\alpha T}{2}\left(1-\frac{\alpha T}{2}\right)e^{-\alpha|t-t'|} && \text{(B.40)}
\end{aligned}$$

where we used the result $\langle x_{1,1}(t)^2\rangle = T\delta(0) - \alpha T/2 \to 1 - \alpha T/2$.

Using gaussian statistics we can write $\langle x_{1,1}(s)^3 x_{1,1}(u)^3\rangle = 6\langle x_{1,1}(s)x_{1,1}(u)\rangle^3 + 9\langle x_{1,1}(s)x_{1,1}(u)\rangle\langle x_{1,1}(s)^2\rangle\langle x_{1,1}(u)^2\rangle$, so that

$$\begin{aligned}\langle x_{1,1}(t_1)^3 x_{1,1}(t_2)^3\rangle &= 6\left\{T\delta(t_1-t_2)\left[1-3\chi+3\chi^2\right]-\chi^3 e^{-3\alpha|t_1-t_2|}\right\}\\ &+ 9[1-\chi]^2\left[T\delta(t_1-t_2)-\chi e^{-\alpha|t_1-t_2|}\right]\\ &= 3T\delta(t_1-t_2)\left[5-12\chi+9\chi^2\right]-6\chi^3 e^{-3\alpha|t_1-t_2|}\\ &- 9\chi[1-\chi]^2 e^{-\alpha|t_1-t_2|}, \end{aligned} \tag{B.41}$$

where $\chi = \alpha T/2$.

Plugging in the expression for $\langle x_{1,3}(t)x_{1,3}(t')\rangle$, we have

$$\langle x_{1,3}(t)x_{1,3}(t')\rangle = (\alpha/3!)^2\int_{-\infty}^{t} dt_1\int_{-\infty}^{t'} dt_2 e^{-\alpha[(t-t_1)+(t'-t_2)]}\langle x_{1,1}(t_1)^3 x_{1,1}(t_2)^3\rangle, \tag{B.42}$$

which gives

$$\begin{aligned}\langle x_{1,3}(t)x_{1,3}(t')\rangle &= \frac{\chi}{48}[14-36\chi+27\chi^2]e^{-\alpha|t-t'|}-\frac{\chi(1-\chi)^2}{8}\alpha|t-t'|e^{-\alpha|t-t'|}\\ &+ \frac{\chi^3}{48}e^{-3\alpha|t-t'|}. \end{aligned} \tag{B.43}$$

The correlation function $\langle x(t)x(t')\rangle$ can thus be written as

$$\begin{aligned}\langle x(t)x(t')\rangle &= \epsilon_1^2\left[T\delta(t-t')-\chi e^{-\alpha|t-t'|}\right]+\epsilon_1^4\left[\frac{\chi}{2}(1-\chi)[1-\alpha|t-t'|]e^{-\alpha|t-t'|}\right]\\ &+ \epsilon_1^6\left[\frac{\chi}{48}(14-36\chi+27\chi^2)e^{-\alpha|t-t'|}-\frac{\chi(1-\chi)^2}{8}\alpha|t-t'|e^{-\alpha|t-t'|}+\frac{\chi^3}{48}e^{-3\alpha|t-t'|}\right]\\ &+ \epsilon_2^2\left[\chi e^{-\alpha|t-t'|}\right]+\epsilon_3^2\epsilon_1^2\left[\chi(1-\chi)e^{-\alpha|t-t'|}\right] \end{aligned} \tag{B.44}$$

The long-term frequency stability is then given by

$$\begin{aligned}\sigma_y^2(\tau) &= \langle(\delta\bar{\omega}(\tau)/\omega_0)^2\rangle\\ &= \left(\frac{1}{\omega_0 T\tau}\right)^2\int_0^\tau\int_0^\tau\langle x(t)x(t')\rangle dtdt'. \end{aligned} \tag{B.45}$$

Plugging in and performing the integrals, we find (in the limit $\alpha\tau \gg 1$)

$$\int_0^\tau \int_0^\tau \langle x(t)x(t')\rangle dt dt' = \frac{\tau}{\alpha}\left\{\epsilon_1^6\left[\frac{\chi}{9}(3-9\chi+8\chi^2)\right]+2\chi\epsilon_2^2+2\chi\epsilon_3^2\epsilon_1^2\right\}, \quad \text{(B.46)}$$

so that

$$\sigma_y^2(\tau) = \frac{1}{\omega_0^2 T\tau}\left\{\frac{\epsilon_1^6}{6}[1-3\chi+(8/3)\chi^2]+\epsilon_2^2+\epsilon_1^2\epsilon_3^2\right\}. \quad \text{(B.47)}$$

B.4.2 Nonlinear feedback

In the NLF case, the stabilized oscillator frequency offset obeys the stochastic differential equation (B.21) with $F(x) = \arcsin(x)$. Plugging in our trial solution, we find the set of equations

$$\dot{x}_{1,1} = -\alpha x_{1,1} + \dot{z}_1 \quad \text{(B.48)}$$

$$\dot{x}_{1,3} = -\alpha x_{1,3} + \frac{\alpha}{3!}(1-\kappa^2)x_{1,1}(t)^3 \quad \text{(B.49)}$$

$$\dot{x}_{2,0} = -\alpha x_{2,0} - \alpha z_2 \quad \text{(B.50)}$$

$$\dot{x}_{3,1} = -\alpha x_{3,1} - \alpha z_3(t)x_{1,1}(t) \quad \text{(B.51)}$$

$$\cdots$$

Solving as in the LF case, we eventually find

$$\sigma_y^2(\tau) = \frac{1}{\omega_0^2 T\tau}\left\{c\epsilon_1^6(1-\kappa^2)^2+\epsilon_2^2+\epsilon_1^2\epsilon_3^2\right\}, \quad \text{(B.52)}$$

where $c = [1-3\chi+(8/3)\chi^2]/6$.

B.5 Gaussian States

We consider the atomic states

$$|\psi(\sigma)\rangle = \frac{1}{\mathcal{N}(\sigma)} \sum_{M=-J}^{J} e^{-(M/\sigma)^2} |J_y = M\rangle \tag{B.53}$$

where $J = N/2 \gg 1$, and $|M\rangle$ are eigenstates of $\hat{J}_y$ with eigenvalue M. We use the range from $\sigma = 1$ to $\sigma = \sqrt{2J}$, corresponding to the range from highly spin-squeezed states to uncorrelated. Morevoer, these states are near-minimum uncertainty states. We find the empirical relations when $\sigma = N^\beta$ (with $1/2 \geq \beta > 0$)

$$\begin{aligned}
\langle \hat{J}_z \rangle &= J[1 - 2^{-(1+2\beta)} J^{-2\beta} + \cdots] && \text{(B.54)} \\
\Delta J_z &\simeq 2^{-(1/2+2\beta)} J^{1-2\beta} && \text{(B.55)} \\
\Delta J_x &\simeq 2^{-\beta} J^{1-\beta} && \text{(B.56)} \\
\Delta J_y &\simeq 2^{-(1-\beta)} J^{\beta} && \text{(B.57)} \\
\Delta J_x \Delta J_y &= \frac{|\langle \hat{J}_z \rangle|}{2} [1 + O(N^{-4\beta})]. && \text{(B.58)}
\end{aligned}$$

In the limit $\sigma \to 1$, we find

$$\begin{aligned}
\langle \hat{J}_z \rangle &\to J e^{-1/2} \\
\Delta J_z &\to J \frac{1 - e^{-1}}{\sqrt{2}} \\
\Delta J_x &\to J \sqrt{\frac{1 - e^{-2}}{2}} \\
\Delta J_y &\to 1/2 && \text{(B.59)}
\end{aligned}$$

while in the limit $\sigma \to N^{1/2} = \sqrt{2J}$,

$$\begin{aligned} \langle \hat{J}_z \rangle &\rightarrow J \\ \Delta J_z &\rightarrow \frac{1}{\sqrt{6}J} \\ \Delta J_x &\rightarrow \sqrt{J/2} \\ \Delta J_y &\rightarrow \sqrt{J/2} \end{aligned} \tag{B.60}$$

which is approximately correct for a Bloch state.

Appendix C

Appendices to Chapter 4

C.1 Three-dimensional quantum description of resonant atom-field interactions

C.1.1 Equations of motion for fields

$\vec{p}\cdot\vec{A}$ Hamiltonian

A general way of obtaining the equations of motion for the field is to start from the standard hamiltonian with minimal coupling to the EM field of N atomic electrons of mass m [112]

$$\begin{aligned}\hat{H} &= \sum_{j=1}^{N}\left\{\frac{1}{2m}[\vec{P}_j - e\vec{A}(R_j)]^2 + eU(\vec{r}_j)\right\} \\ &+ \frac{1}{2}\int\left[\epsilon_0\vec{E}^2(r) + \frac{1}{\mu_0}\vec{B}(r)^2\right]d^3r \end{aligned} \tag{C.1}$$

where the dipole approximation has been made i.e. $\hat{A}(R_j)$ is evaluated at the position of the atom R_j and does not depend on the relative position of the electron to the atom (r_j).

The quantized EM field obeys the following equal-time commutation relations [112, 39]

$$\begin{aligned}
[E_i(r_1,t), B_j(r_2,t)] &= \frac{-i\hbar}{\epsilon_0}\epsilon_{ijl}\partial_{1,l}\delta(\vec{r}_1-\vec{r}_2), \\
[E_i(r_1,t), A_j(r_2,t)] &= \frac{i\hbar}{\epsilon_0}\delta^T_{ij}(r_1-r_2), \\
[B_i(r_1,t), A_j(r_2,t)] &= 0,
\end{aligned} \tag{C.2}$$

where the transverse delta function is defined as [39]

$$\delta^{\perp}_{lm}(\vec{r}-\vec{r'}) = \frac{1}{(2\pi)^3}\int d^3k\, e^{i\vec{k}(\vec{r}-\vec{r'})}\left(\delta_{lm}-\frac{k_l k_m}{k^2}\right). \tag{C.3}$$

Let the atomic dipole moment operator be defined as

$$\hat{P}_l(r,t) = \sum_{j=1}^{N}\left[\wp_i|e\rangle_j\langle g| + \wp_i^*|g\rangle_j\langle e|\right]\delta^T_{il}(r-R_j) \tag{C.4}$$

where $\vec{\wp}_{eg} = e\langle e|\vec{r}|g\rangle$.

In the Coulomb gauge, we can treat $\vec{p}$ and $\vec{A}(r,t)$ as commuting variables. From the equations of motion for atomic position, we find that $\langle e|\frac{\vec{p}}{m}|g\rangle = i\omega_{eg}\wp_{eg}$. Also, the atomic coherence $\sigma_{eg} = |e\rangle\langle g|$ obeys the equation of motion $\dot{\sigma}_{eg} = i\omega_{eg}\sigma_{eg}$, so that we can write the $\vec{p}\cdot\vec{A}$ part of the Hamiltonian as

$$-\sum_j \frac{e\vec{p}_j}{m}\cdot\vec{A}(R_j) = -\int d^3r'[\partial_t\vec{P}(r',t)]\cdot\vec{A}(r',t). \tag{C.5}$$

The equations of motion for the quantized fields then are

$$\begin{aligned} \partial_t E_j &= c^2 \left(\vec{\nabla} \times \vec{B}\right)_j - \frac{1}{\epsilon_0}\partial_t P_j \\ \partial_t B_j &= -\left(\vec{\nabla} \times \vec{E}\right)_j \end{aligned} \tag{C.6}$$

and we obtain the usual wave equation (now valid for operators)

$$[\partial_t^2 - c^2\nabla^2]\vec{E}(r,t) = -\frac{1}{\epsilon_0}\partial_t^2 \vec{P}(r,t) \tag{C.7}$$

Power-Zienau transformation

Alternatively, the Power-Zienau transformation can be applied: states $|\psi\rangle \rightarrow |\psi'\rangle = \hat{U}|\psi\rangle$ and operators $\hat{O} \rightarrow \hat{O}' = \hat{U}\hat{O}\hat{U}^\dagger$ are transformed according to the unitary operator $\hat{U} = \exp\left[-(i/\hbar)\sum_{j=1}^{N} \vec{r}_j \cdot \vec{A}(R_j)\right]$.

In the new frame, the new operators are

$$\begin{aligned} \vec{r}' &= \vec{r} \\ \vec{p}' &= \vec{p} + e\vec{A}(R,t) \\ \vec{E}(r,t)' &= \vec{E}(r,t) + \vec{P}(r,t)/\epsilon_0 \\ \vec{P}'(r,t) &= \vec{P}(r,t) \\ \vec{B}'(r,t) &= \vec{B}(r,t) \\ \vec{A}'(r,t) &= \vec{A}(r,t). \end{aligned} \tag{C.8}$$

$\vec{E}\cdot\vec{r}$ Hamiltonian

We can write the new Hamiltonian as

$$\hat{H} = \hat{H}_{at} + \frac{1}{2}\int\left[\epsilon_0 \vec{E'}^2(r) + \frac{1}{\mu_0}\vec{B'}(r)^2\right]d^3r - \int \hat{P'}(r)\cdot\vec{E'}(r)d^3r \qquad \text{(C.9)}$$

where $\hat{H}_{at}$ contains the energies of atomic energy levels...etc.

We obtain the Heisenberg equations

$$\begin{aligned}\partial_t E'_j &= c^2\left(\vec{\nabla}\times\vec{B'}\right)_j \\ \partial_t B'_j &= -\left(\vec{\nabla}\times\vec{E'}\right)_j - \frac{1}{\epsilon_0}\left(\vec{\nabla}\times\vec{P'}\right)_j \end{aligned} \qquad \text{(C.10)}$$

which can be combined to give the wave equation (since both $\vec{E}$ and $\vec{P}$ are transverse)

$$\left[\frac{\partial^2}{\partial t^2} - c^2\nabla^2\right]\vec{E'} = \frac{c^2}{\epsilon_0}\nabla^2\vec{P'}. \qquad \text{(C.11)}$$

Returning to the original frame (i.e. writing E', P' in terms of E, P) we obtain the same equations of motion as in the $\vec{p}\cdot\vec{A}$ formulation, i.e.

$$[\partial_t^2 - c^2\nabla^2]\vec{E}(r,t) = -\frac{1}{\epsilon_0}\partial_t^2\vec{P}(r,t). \qquad \text{(C.12)}$$

In conclusion either formulation is correct and generates the same equations of motion. The $\vec{E}\cdot\vec{r}$ formulation may be preferable for generating the atomic equations of motion.

C.1.2 Atom-field equations of motion

Slowly-varying envelope approximation

Consider now the interaction of a travelling-wave field with a near resonant atomic transition between levels $|g\rangle$ and $|e\rangle$. Let the resonant frequency be ω_0 and assuming the field propagates in the z-direction, let $\vec{k}_0 = (\omega_0/c)\hat{z}$, we can then write the field and polarization in terms of slowly varying amplitudes [39] (considering one polarization $\vec{\epsilon}$ and assuming the relevant frequency components are all near-resonance)

$$\vec{E}(\vec{r},t) = \left(\frac{\hbar\omega_0}{2\epsilon_0 V}\right)^{1/2}\left[\mathcal{E}(\vec{r},t)\vec{\epsilon}e^{-i\omega_0 t} + \text{h.c.}\right] \tag{C.13}$$

$$P(\vec{r},t) = \frac{N}{V}\left[(\vec{\wp}\cdot\vec{\epsilon})\sigma_{eg}(\vec{r},t)e^{-i(\vec{k}_o\cdot\vec{r}-\omega_0 t)} + \text{h.c.}\right], \tag{C.14}$$

where $\sigma_{eg}(\vec{r},t)$ is a collective slowly varying atomic operator. To describe the quantum properties of the medium, we use the atomic operators [47]

$$\hat{\sigma}_{\mu\nu}(\vec{r},t) = \frac{1}{N_{\vec{r}}}\sum_{j=1}^{N_{\vec{r}}}|\mu_j\rangle\langle\nu_j|e^{-i\omega_{\mu\nu}t}, \tag{C.15}$$

where the sum is performed over a small but macroscopic volume containing $N_{\vec{r}} \gg 1$ atoms around position $\vec{r}$.

Plugging these in the wave equation and assuming slowly varying envelopes i.e. $\omega_0\partial_t\mathcal{E} \gg \partial_t^2\mathcal{E}$ and $\omega_0\sigma_{eg} \gg \partial_t\sigma_{eg}$, we find,

$$\left[\partial_t - i\frac{\omega_0}{2}\left(1+\frac{\nabla^2}{k_0^2}\right)\right]\mathcal{E}(\vec{r},t) = igN\sigma_{ge}(\vec{r},t)e^{i\vec{k}_0\cdot\vec{r}}, \tag{C.16}$$

where $\hbar g = \left(\frac{\hbar\omega_0}{2\epsilon_0 V}\right)^{1/2}(-\vec{\wp}\cdot\vec{\epsilon})$. Note that the above equation is first-order in time and second order in space variables. A boundary condition sufficient to determine

the field at all times and at all positions inside an atomic cell with boundaries at $z = 0$ and $z = L$, is the initial condition $\mathcal{E}(\vec{r}, 0)$ and the boundary condition at the cell boundary between the "in" and "out" solutions to the equations of motion.

Paraxial approximation

If we further assume that $\mathcal{E}(r,t) = \mathcal{E}(r,t)e^{i\vec{k_0}\cdot\vec{r}}$ where $\vec{k}_0 = k_0\hat{z}$ and $k_0\partial_z\mathcal{E} \gg \partial_z^2\mathcal{E}$, we obtain the paraxial approximation to the wave equation,

$$\left[\partial_t + c\partial_z - i\frac{c\nabla_\perp^2}{2k_0}\right]\mathcal{E}(z, r_\perp, t) \;=\; igN\sigma_{ge}(z, r_\perp, t). \tag{C.17}$$

We consider a cigar-shaped cylindrical atomic sample of length L and transverse area A. The paraxial approximation is valid when the geometric angle $\theta_G \sim \sqrt{A}/L$ is small $\theta_G \ll 1$. The diffraction angle is given by $\theta_D \sim \lambda/\sqrt{A}$, and the ratio of geometric to diffraction angle is called the Fresnel number

$$\begin{aligned}\mathcal{F} &= \frac{\theta_G}{\theta_D} \\ &= \frac{A}{\lambda L}.\end{aligned} \tag{C.18}$$

Note that when $\mathcal{F} \gg 1$, several transverse modes are necessary to describe the fiels as it propagates through the atomic sample. Thus, the field description is the paraxial approximation is still a mutli-mode one (several transverse modes and a continuum of longitudinal modes to describe propagation).

Appendix D

Appendices to Chapter 5

D.1 Shaping Stationary Pulses

In this section, we present a technique to manipulate the shape of stationary pulses, with the goal of confining the pulse to a very short spatial dimension, of the order of a wavelength. Initially the pulse is stored as a spin coherence with a spatial envelope that extends over many wavelengths. By illuminating the atoms with control beams that have multiple frequency components, many corresponding frequency components are generated for the signal field. These components interfere to create a very sharp spatial envelope, confined over few wavelengths (see Fig. D.1.

Considering the case when several counter-propagating control fields, with detunings Δ_j, (complex) Rabi frequencies Ω_j, we have the total Rabi frequency (slowly varying envelope) $\Omega(z,t) = \sum_j \Omega_j e^{-i\Delta_j(t-z/c)}$, where $\Delta_j = \omega_j - \omega_0$ is the detuning from atomic resonance. Corresponding to these driving fields are signal field slowly varying amplitudes $\mathcal{E}_j(z,t)$, so that the total signal field envelope is $E(z,t) =$

$\sum_j \mathcal{E}_j(z,t)e^{-i\Delta_j(t-z/c)}$.

Assuming $\Delta_j \gg \Omega_j$ so that we can ignore coupling of the frequency components through off-resonant processes, we also expand the optical polarization as $\mathcal{P}(z,t) = \sum_j \mathcal{P}_j(z,t)e^{-i\Delta_j(t-z/c)}$. The spin coherence slowly varying envelope is $\mathcal{S}(z,t)$ and we ignore fast varying components such as $e^{2i\Delta t}$, i.e. assuming $\Delta_j \gg \Omega_j$.

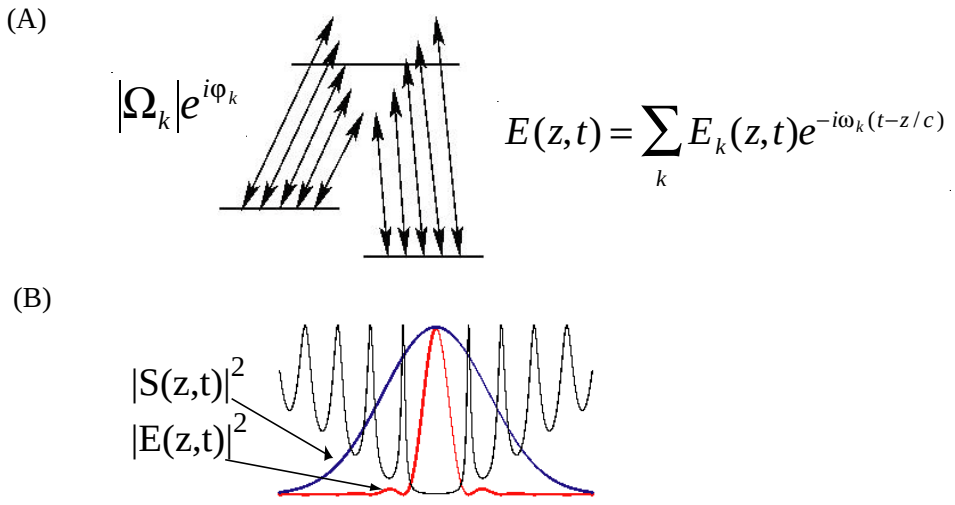

Figure D.1: (A) Atomic level structure and multiple frequency component control field $\Omega(z,t) = \sum_j \Omega_j e^{-i\Delta_j(t-z/c)}$, and generated signal field $E(z,t) = \sum_j \mathcal{E}_j(z,t)e^{-i\Delta_j(t-z/c)}$. (B) Generated signal field envelope, showing tight localization due to multiple frequency components.

The equations of motion, in a wavefunction description, are, to first order in the weak signal field E,

$$\dot{e} = \gamma e + i\Omega s + igE \tag{D.1}$$

$$\dot{s} = i\Omega^* e \tag{D.2}$$

where $e(z,t)$ denotes the probability amplitude for atoms to be in state $|e\rangle$, and $g(z,t) \simeq 1$.

Corresponding to the expansion of the polarization above, we introduce effective excited state amplitudes $e_j(z,t)$ so that $\mathcal{P}_j(z,t) = e_j(z,t)$ and

$$\dot{e}_j = -\Gamma_j e_j + i\Omega_j s + ig\mathcal{E}_j \tag{D.3}$$

$$\dot{s} = i\sum \Omega_j^* e_j \tag{D.4}$$

Solving adiabatically for e_j and plugging back in the s equation, we have

$$e_j \simeq i\frac{\Omega_j s + g\mathcal{E}_j}{\Gamma_j} \tag{D.5}$$

$$\dot{s} \simeq -\sum_j \frac{|\Omega_j|^2}{\Gamma_j} s - \sum_j \frac{\Omega_j^* g\mathcal{E}_j}{\Gamma_j} \tag{D.6}$$

which can be solved adiabatically for $s(z,t)$. To first order in the time derivative of the signal field, we find

$$s \simeq -\frac{1}{\xi}\left[\dot{s} + \sum_j \frac{\Omega_j^* g\mathcal{E}_j}{\Gamma_j}\right] \tag{D.7}$$

where $\xi = \sum_j \frac{|\Omega_j|^2}{\Gamma_j}$.

Introducing the polaritons, $\psi_j = g\mathcal{E}_j/\Omega_j$, we have

$$s \simeq -\frac{1}{\xi}\sum_j \left[\frac{|\Omega_j|^2}{\Gamma_j}\psi_j + \dot{s}\right] \tag{D.8}$$

$$\frac{e_j}{\Omega_j} \simeq i\frac{s+\psi_j}{\Gamma_j}. \tag{D.9}$$

Letting $\Delta_0 = 0$ and $\Delta_{j\neq 0} \gg \gamma, \Omega_j$, we can solve the resulting coupled equations perturbatively ($\gamma/\Delta_j \ll 1$). To leading order we have

$$\xi \simeq \frac{|\Omega_+|^2 + |\Omega_-|^2}{\gamma} \tag{D.10}$$

$$s \simeq -(\alpha_+\psi_+ + \alpha_-\psi_-) \tag{D.11}$$

and (letting $\zeta = g^2 N/\gamma$)

$$(\partial_t + c\partial_z)\psi_+ = -\eta\partial_t(\alpha_+\psi_+ + \alpha_-\psi_-) - \alpha_-\zeta(\psi_+ - \psi_-) \quad \text{(D.12)}$$

$$(\partial_t - c\partial_z)\psi_- = -\eta\partial_t(\alpha_+\psi_+ + \alpha_-\psi_-) + \alpha_+\zeta(\psi_+ - \psi_-). \quad \text{(D.13)}$$

For $\Delta_{j\neq 0}$, we have, assuming $\Delta_j \gg \gamma$,

$$\frac{e_j}{\Omega_j} \simeq -\frac{1}{\Delta_j}\left[\psi_j + s - \gamma\partial_t s\right] \quad \text{(D.14)}$$

and the equations of motion

$$(\partial_t + c\partial_z)\psi_{j+} = i\eta(\gamma/\Delta_j)\partial_t s - i\zeta(\gamma/\Delta_j)(\psi_{j+} + s) \quad \text{(D.15)}$$

$$(\partial_t - c\partial_z)\psi_{j-} = i\eta(\gamma/\Delta_j)\partial_t s - i\zeta(\gamma/\Delta_j)(\psi_{j-} + s). \quad \text{(D.16)}$$

In the limit $\gamma_0 = 0$, $\eta \gg 1$ and $\alpha_+ = \alpha_-$, we find

$$\Psi = \frac{2}{\xi}c\partial_z s \quad \text{(D.17)}$$

$$\eta\partial_t s = (1/\xi)c^2\partial_z^2 s \quad \text{(D.18)}$$

where $\Psi = \psi_+ - \psi_-$. Solving in k-space, we have $s(t,k) = \exp[-\frac{k^2c^2}{\eta\xi}t]s(0,k)$, and

$$\partial_t\psi_{j+}(t,k) = -i(kc + \xi\gamma/\Delta_j)\psi_{j+} - i\xi(\gamma/\Delta_j)(1 + (kc/\xi)^2)s(t,k) \quad \text{(D.19)}$$

$$\partial_t\psi_{j-}(t,k) = -i(-kc + \xi\gamma/\Delta_j)\psi_{j-} - i\xi(\gamma/\Delta_j)(1 + (kc/\xi)^2)s(t,k). \quad \text{(D.20)}$$

Since $\xi \gg kc$ (i.e. $l_{in} \gg L_{abs}$, where l_{in} is the spatial length of the pulse inside the medium), and assuming $\xi\gamma/\Delta_j \gg kc$, we find

$$\psi_{j+} \simeq -s \quad \text{(D.21)}$$

$$\psi_{j-} \simeq -s. \quad \text{(D.22)}$$

Similarly since $\Psi \simeq 0$, we also have $\psi_+ = \psi_- = -s$. The electric field envelope can thus be written as

$$gE(z,t) \simeq \left(\sum_j \Omega_j e^{-i\Delta_j(t-z/c)}\right) s(t,z) \quad \text{(D.23)}$$

$$= \Omega(t,z)s(t,z). \quad \text{(D.24)}$$

The electric field envelope becomes matched to the control field envelope, allowing control of the trapped pulse effective mode shape through control of the control fields amplitudes and phases.

D.2 Multi-component Spatial Coherence Grating

In this section we show that multiple atomic momentum components can be taken into account. These arise due to multiple scattering of photons in the forward and backward directions, resulting in distinctly different atomic susceptibilities when they are taken into account. For stationary atoms, such as in cold atomic samples, these multiple scattering momentum components can be populated and preserve their coherence. In contrast, for warm atomic vapors, the rapid random motion of the atoms and their collisions results in a very rapid decay of spatial coherences with period equal to or shorter than the optical wavelength.

Susceptibility

In terms of susceptibilities, the equations of motion 5.11 are

$$(-i\omega + c\partial_z)\mathcal{E}_+(z,\omega) = i\left(\Delta Kc + \frac{\omega_0}{2}\chi_{++}(\omega)\right)\mathcal{E}_+ + i\frac{\omega_0}{2}\chi_{+-}(\omega)\mathcal{E}_- \quad \text{(D.25)}$$

$$(-i\omega - c\partial_z)\mathcal{E}_-(z,t) = i\left(\Delta Kc + \frac{\omega_0}{2}\chi_{-+}(\omega)\right)\mathcal{E}_+ + i\frac{\omega_0}{2}\chi_{--}(\omega)\mathcal{E}_- \quad \text{(D.26)}$$

Taking a Fourier transform of 5.12 and solving for the polarizations, we find

$$\frac{\mathcal{P}_+(z,\omega)}{g\sqrt{N}} = i\frac{(\Gamma\Gamma_0+|\Omega_-|^2)\mathcal{E}_+(z,\omega)-\Omega_-^*\Omega_+\mathcal{E}_-(z,\omega)}{\Gamma(\Gamma\Gamma_0+|\Omega_+|^2+|\Omega_-|^2)} \tag{D.27}$$

$$\frac{\mathcal{P}_-(z,\omega)}{g\sqrt{N}} = i\frac{(\Gamma\Gamma_0+|\Omega_+|^2)\mathcal{E}_-(z,\omega)-\Omega_+^*\Omega_-\mathcal{E}_+(z,\omega)}{\Gamma(\Gamma\Gamma_0+|\Omega_+|^2+|\Omega_-|^2)} \tag{D.28}$$

$$\mathcal{S}(z,\omega) = -\frac{\Omega_+^*\mathcal{E}_+(z,\omega)+\Omega_-^*\mathcal{E}_-(z,\omega)}{\Gamma\Gamma_0+|\Omega_+|^2+|\Omega_-|^2} \tag{D.29}$$

The susceptibilities are then given by $\frac{\omega_0}{2}\chi_{\sigma\sigma'} = g\sqrt{N}\mathcal{P}_\sigma/\mathcal{E}_{\sigma'}$, where $\sigma,\sigma' = \pm$.

Polariton solution

In terms of polaritons, we have

$$\frac{\mathcal{P}_+(z,\omega)}{\Omega_+} = i\frac{(\Gamma\Gamma_0+|\Omega_-|^2)\psi_+(z,\omega)-|\Omega_-|^2\psi_-(z,\omega)}{\Gamma(\Gamma\Gamma_0+|\Omega_+|^2+|\Omega_-|^2)} \tag{D.30}$$

$$\frac{\mathcal{P}_-(z,\omega)}{\Omega_-} = i\frac{(\Gamma\Gamma_0+|\Omega_+|^2)\psi_-(z,\omega)-|\Omega_+|^2\psi_+(z,\omega)}{\Gamma(\Gamma\Gamma_0+|\Omega_+|^2+|\Omega_-|^2)} \tag{D.31}$$

$$\mathcal{S}(z,\omega) = -\frac{|\Omega_+|^2\psi_+(z,\omega)+|\Omega_-|^2\psi_-(z,\omega)}{\Gamma\Gamma_0+|\Omega_+|^2+|\Omega_-|^2} \tag{D.32}$$

where $\psi_\pm = g\sqrt{N}\mathcal{E}_\pm/\Omega_\pm$, $\Gamma = \gamma - i(\Delta+\omega)$ and $\Gamma_0 = \gamma_0 - i\omega$. Defining $\chi(\omega) = \frac{\Gamma\Gamma_0}{|\Omega_+|^2+|\Omega_-|^2}$ and $\alpha_\pm = \frac{|\Omega_\pm|^2}{|\Omega_+|^2+|\Omega_-|^2}$, we find the equations of motion

$$(c\partial_z - i\omega)\psi_+ = i\Delta Kc\psi_+ - \frac{\eta\Gamma_0}{1+\chi}(\alpha_+\psi_+ + \alpha_-\psi_-) - \alpha_-\frac{\xi}{1+\chi}(\psi_+ - \psi_-) \tag{D.33}$$

$$(-c\partial_z - i\omega)\psi_- = i\Delta Kc\psi_- - \frac{\eta\Gamma_0}{1+\chi}(\alpha_+\psi_+ + \alpha_-\psi_-) + \alpha_+\frac{\xi}{1+\chi}(\psi_+ - \psi_-) \tag{D.34}$$

where $\eta = \frac{g^2N}{|\Omega_+|^2+|\Omega_-|^2}$ and $\xi = \frac{g^2N}{\Gamma}$.

adiabatic limit

In the adiabatic limit $|\Omega_\pm|^2 \gg |\Gamma\Gamma_0|$, and we assume $|\chi| \ll 1$. Letting $-i\omega \to \partial_t$, we have to leading order (setting $\Delta K = 0$),

$$(\partial_t + c\partial_z)\psi_+ = -\eta(\partial_t + \gamma_0)(\alpha_+\psi_+ + \alpha_-\psi_-) - \alpha_-\xi(\psi_+ - \psi_-) \quad \text{(D.35)}$$

$$(\partial_t - c\partial_z)\psi_- = -\eta(\partial_t + \gamma_0)(\alpha_+\psi_+ + \alpha_-\psi_-) + \alpha_+\xi(\psi_+ - \psi_-) \quad \text{(D.36)}$$

where $\xi = g^2N/\gamma = c/L_{abs}$. The spin wave is $\mathcal{S}(z,t) \simeq -(\alpha_+\psi_+ + \alpha_-\psi_-)$. Letting $\Psi = \psi_+ - \psi_-$, we have $\psi_+ = \alpha_-\Psi - \mathcal{S}$ and $\psi_- = -(\alpha_+\Psi + \mathcal{S})$, so that the equations of motion become

$$\begin{aligned}[(\eta+1)\partial_t + \eta\gamma_0]\mathcal{S} &= -(\alpha_+ - \alpha_-)c\partial_z\mathcal{S} + 2\alpha_+\alpha_-c\partial_z\Psi \\ (\partial_t + \xi)\Psi &= (\alpha_+ - \alpha_-)c\partial_z\Psi + 2c\partial_z\mathcal{S} \end{aligned} \quad \text{(D.37)}$$

Coupled mode approach

Maxwell's equation in a spatially modulated medium in 1D is

$$c^2\frac{d^2}{dz^2}E(z,\nu) + \nu^2[1+\chi(z,\nu)]E(z,\nu) = 0. \quad \text{(D.38)}$$

Putting $E(z,\nu) = E_+(z,\omega)e^{ik_0z} + E_-(z,\omega)e^{-ik_0z}$, where $\omega = \nu - \omega_0$ and $k_0c = \omega_0$.

Letting the susceptibility be

$$\chi(z,\omega) = \frac{2g^2N}{\gamma\omega_0}\frac{i\gamma\Gamma_0}{\Gamma\Gamma_0 + |\Omega(z)|^2} \quad \text{(D.39)}$$

where $\Omega(z) = \Omega_+e^{iKz} + \Omega_-e^{-iKz}$, and $\Gamma = \gamma - i\omega$, we then use the Fourier expansion $\chi(z,\omega) = \sum_n \chi_n(\omega)e^{inKz}$ and using coupled mode analysis, we find

$$(-i\omega + c\partial_z)E_+ = i\frac{\omega_0}{2}\chi_0E_+ + i\frac{\omega_0}{2}\chi_1E_-e^{-2i\Delta Kz} \quad \text{(D.40)}$$

$$(-i\omega - c\partial_z)E_- = i\frac{\omega_0}{2}\chi_0E_- + i\frac{\omega_0}{2}\chi_{-1}E_+e^{2i\Delta Kz} \quad \text{(D.41)}$$

where $\Delta K = K - k_0$.

Defining $\mathcal{E}_\pm = E_\pm e^{\mp i\Delta K z}$ and $\mathcal{P}_\pm = P_\pm e^{\mp i\Delta K z}$, the field equation of motion can then be written as

$$(-i\omega + c\partial_z)\mathcal{E}_+(z,\omega) = i\left(\Delta Kc + \frac{\omega_0}{2}\chi_0(\omega)\right)\mathcal{E}_+ + i\frac{\omega_0}{2}\chi_1(\omega)\mathcal{E}_- \quad \text{(D.42)}$$

$$(-i\omega - c\partial_z)\mathcal{E}_-(z,t) = i\left(\Delta Kc + \frac{\omega_0}{2}\chi_0(\omega)\right)\mathcal{E}_- + i\frac{\omega_0}{2}\chi_{-1}(\omega)\mathcal{E}_+ \quad \text{(D.43)}$$

We let $|\Omega(z)|^2 = |\Omega_0|^2[1 + 2\sqrt{\alpha_+\alpha_-}\cos(2Kz)]$, where $|\Omega_0|^2 = |\Omega_+|^2 + |\Omega_-|^2$ and $\alpha_\pm = |\Omega_\pm|^2/|\Omega_0|^2$, and we use $\chi_n(\omega) = \frac{K}{\pi}\int_0^{\pi/K} e^{-2inKz}\chi(z,\omega)$.

We find (performing the integrals by contour integration and approximating near $Kz = \pi/2$ where $|\Omega(z)|^2 \ll |\Omega_0|^2$...)

$$\frac{\omega_0}{2}\chi_0(\omega) = i\frac{g^2N}{\gamma}\frac{\gamma\Gamma_0}{|\Omega_0|^2}\left\{[1 + 2\sqrt{\alpha_+\alpha_-}]^{-1} + [4\sqrt{\alpha_+\alpha_-}\Xi]^{-1}\right\} \quad \text{(D.44)}$$

$$\frac{\omega_0}{2}\chi_{\pm1}(\omega) = -i\frac{g^2N}{\gamma}\Xi\exp[-2\Xi] \quad \text{(D.45)}$$

where $\Xi^2 = \frac{1}{4\sqrt{\alpha}_+\alpha_-}\left[\frac{\Gamma\Gamma_0}{|\Omega_0|^2} + (1 - 2\sqrt{\alpha_+\alpha_-}\right]$.

These susceptibilities are very different from those obtained with the Maxwell-Bloch equations. Implicit in the derivation of the susceptibilities D.39 is the assumption of stationary atoms, so that all intermediate atomic momentum states are taken into account, in particular high spatial frequency coherences contribute to this result. All spatial components of the spin and polarization waves are taken into account, even those with momentum equal to multiples of the optical wavevector K. For warm atomic samples, these coherences rapidly decohere due to the random motion of the atoms and their collisions.

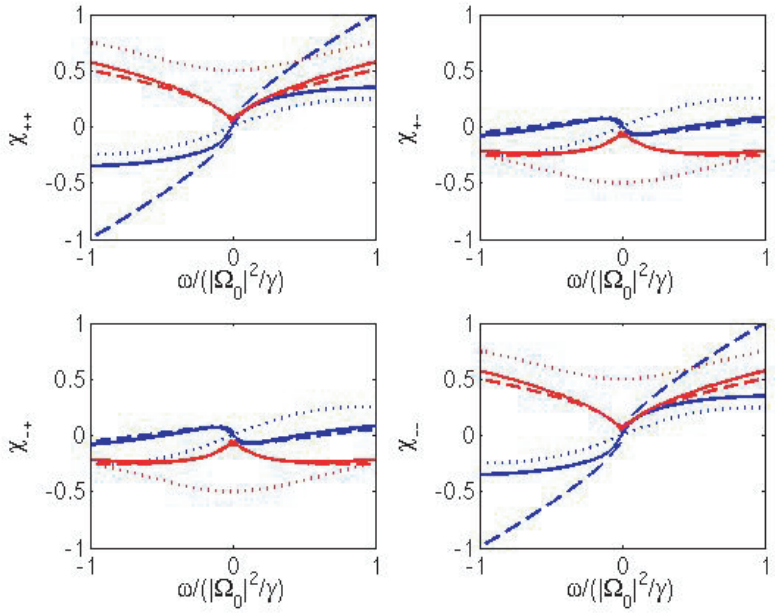

Figure D.2: Self- and cross-susceptibilites (arbitrary units) $\chi_{\pm,\pm}(\omega)$ vs. frequency ω (in units of $|\Omega_0|^2/\gamma = (|\Omega_+|^2 + |\Omega_-|^2)/\gamma$), for $\Omega_+ = \Omega_-$, $\Omega_0 = 0.1\gamma$, and $\gamma_0 = 0$. Real part (blue) and imaginary part (red), dotted line: Maxwell-Bloch equations truncated at $\mathcal{P}_{\pm 1}$, dashed line: Coupled Mode equations (analytic result), full line: Maxwell-Bloch equations truncated at $\mathcal{P}_{\pm(2n+1)}$ with $n = 5$.

Coupled polarization/spin waves approach

Explicitely, letting the polarization wave be $\mathcal{P}(z,t) = \sum_n \mathcal{P}_{2n+1}(z,t)e^{i(2n+1)Kz}$, and the spin wave be $\mathcal{S}(z,t) = \sum_n S_{2n}(z,t)e^{2inKz}$, we have the effective Hamiltonian

$$\begin{aligned} H &= \frac{-1}{L}\int dz \Big[g\sqrt{N}(\mathcal{E}_+\mathcal{P}_1^\dagger + \mathcal{E}_-\mathcal{P}_{-1}^\dagger) \\ &+ \sum_n (\Omega_+\mathcal{S}_{2n}\mathcal{P}_{2n+1}^\dagger + \Omega_-\mathcal{S}_{2n}\mathcal{P}_{2n-1}^\dagger) + h.c. \Big] \end{aligned} \tag{D.46}$$

and

$$(\partial_t + c\partial_z)\mathcal{E}_+ = i\Delta K c\mathcal{E}_+ + ig\sqrt{N}\mathcal{P}_1 \tag{D.47}$$

$$(\partial_t - c\partial_z)\mathcal{E}_- = i\Delta K c\mathcal{E}_- + ig\sqrt{N}\mathcal{P}_{-1}. \tag{D.48}$$

We also have

$$\partial_t \mathcal{P}_{2n+1} = -\gamma \mathcal{P}_{2n+1} + i\Omega_+ \mathcal{S}_{2n} + i\Omega_- \mathcal{S}_{2(n+1)} + ig\sqrt{N}\mathcal{E}_{2n+1} \quad \text{(D.49)}$$

$$\partial_t \mathcal{S}_{2n} = -\gamma_0 \mathcal{S}_{2n} + i(\Omega_+^* \mathcal{P}_{2n+1} + \Omega_-^* \mathcal{P}_{2n-1}) \quad \text{(D.50)}$$

The susceptibilites $\chi_{\sigma\sigma'}(\omega)$ can be found from these coupled equations, and truncating the polarization at $\mathcal{P}_{\pm(2n+1)}$, we can easily show that $n = 0$ reproduces our earlier result, whereas letting $n \to \infty$ reproduces the coupled mode result (see Fig. D.2).

We thus find that there is a clear difference between the multi-component case and the case when only the zero momentum component of the spin wave contributes. These two situations correspond e.g. to cold atomic samples vs. hot atomic gases, so that based on the previous considerations we expect that the stationary light pulse will be very different in cold atomic samples.

We now argue that for storage and retrieval of excitations, these large spatial wavevector coherences are mostly irrelevant. As can be seen from D.49 and D.50, the signal field (in modes $\mathcal{E}_\pm$) couples to the polarization components $\mathcal{P}_{\pm 1}$ with Rabi frequency $g\sqrt{N}$, which in the "slow" light limit is much larger than the control field Rabi frequencies $\Omega_\pm$. Therefore, starting from a stored pulse in the zero-momentum spin coherence $\mathcal{S}_0$, most of the amplitude is coupled to the signal field modes $\mathcal{E}_\pm$, while very little amplitude "leaks" to the higher momentum coherences. Thus, even for warm atomic samples, coupling to higher momentum coherences does not lead to decay of the spin coherence. We discuss this further in the next subsection.

We can also see this from the following considerations: adiabatically eliminating

the polarizations, we have

$$\mathcal{P}_{2n+1} \simeq i\frac{\Omega_+}{\gamma}\mathcal{S}_{2n} + i\frac{\Omega_-}{\gamma}\mathcal{S}_{2(n+1)} + i\frac{g\sqrt{N}}{\gamma}\mathcal{E}_{2n+1}, \tag{D.51}$$

so that, plugging the result back into the equations of motion for the spin coherences and introducing the polaritons $\psi_\pm = g\sqrt{N}\mathcal{E}_\pm/\Omega_\pm$, we find (letting $\kappa = \frac{|\Omega_+|^2+|\Omega_-|^2}{\gamma}$)

$$\partial_t\mathcal{S}_{-2} = -\kappa\mathcal{S}_{-2} - \kappa\sqrt{\alpha_+\alpha_-}(\mathcal{S}_0+\psi_-) - \kappa\sqrt{\alpha_+\alpha_-}\mathcal{S}_{-4} \tag{D.52}$$

$$\partial_t\mathcal{S}_0 = -\kappa\mathcal{S}_0 - \kappa(\alpha_+\psi_+ + \alpha_-\psi_-) - \kappa\sqrt{\alpha_+\alpha_-}(\mathcal{S}_{-2}+\mathcal{S}_{+2}) \tag{D.53}$$

$$\partial_t\mathcal{S}_{+2} = -\kappa\mathcal{S}_{+2} - \kappa\sqrt{\alpha_+\alpha_-}(\mathcal{S}_0+\psi_+) - \kappa\sqrt{\alpha_+\alpha_-}\mathcal{S}_{+4}, \tag{D.54}$$

where $\alpha_\pm = \frac{|\Omega_\pm|^2}{|\Omega_+|^2+|\Omega_-|^2}$ as before. From our discussions of stationary pulses in section 5.3, we have, in the adiabatic limit, $\mathcal{S}_0+\psi_+ \simeq -\alpha_-(\psi_+-\psi_-)$ and $\mathcal{S}_0+\psi_- \simeq -\alpha_+(\psi_+-\psi_-)$. This indicates that the spin coherences $\mathcal{S}_{\pm2}$ couple to $\psi_+ - \psi_-$, which we have previously showed is a fast decaying mode equal to $\psi_+ - \psi_- \simeq -\frac{2c\partial_z}{\xi}(\alpha_+\psi_+ + \alpha_-\psi_-)$. Thus, in the limit of large optical depth (i.e. large $g\sqrt{N}$ and large ξ) the spin coherences $\mathcal{S}_{\pm2}$ effectively decouple from the zero momentum spin coherence and thus from the stationary pulse excitation, which is a combination of $\mathcal{S}_0$ and the fields $\mathcal{E}_\pm$.

D.2.1 Release of stored pulse: multi-component approach

When the pulse is released, i.e. starting with a stored spin wave $\mathcal{S}(z,0)$ and switching on the fields $\Omega_\pm$ on at $t=0$, we want to check that atoms remain mostly in zero momentum states.

A simple wavefunction approach can illustrate this point: consider two counter-propagating single modes and assume there is at most one excitation in the system.

Initially the system atom+two modes is in the state $|s_0, 0, 0\rangle$, and we want to check that a fraction $1/\sqrt{\eta}$ of the amplitude ends up in state $(|g, 1, 0\rangle + |g, 0, 1\rangle)/\sqrt{2}$ (we assume $\alpha_+ = \alpha_-$ for simplicity), where $|g, 1, 0\rangle$ indicates that the atom is in state $|g\rangle$ (with zero momentum) while the forward propagating mode contains no photon and the backward propagating mode contains one. State $|e_{-3}, 0, 0\rangle$ indicates atom is in state $|e\rangle$ with $-3\hbar k$ momentum, no photons in either modes.

The effective Hamiltonian is thus

$$\begin{aligned} H_{eff} &= \Big[g\sqrt{N}(|e_{-1}, 0, 0\rangle\langle g, 1, 0| + |e_{+1}, 0, 0\rangle\langle g, 0, 1|) \\ &+ \sum_n (\Omega_+ |s_{-2n}, 0, 0\rangle\langle e_{-2n+1}, 0, 0| + \Omega_- |s_{-2n}, 0, 0\rangle\langle e_{-2n-1}, 0, 0|) \\ &+ \text{h.c.}] \end{aligned} \tag{D.55}$$

In Fig.D.3, the initial state is $|s_0, 0, 0\rangle$, and the system is time evolved. The probability to go into higher momentum spin states $|s_{\pm 2}, 0, 0\rangle$ is suppressed by an extra factor of $\eta = c/v_g \gg 1$, compared to the probability to go into $(|g, 1, 0\rangle + |g, 0, 1\rangle)/\sqrt{2}$, so that in the relevant limit of $\eta \gg 1$, our model (taking into account only the slowly varying envelope $\mathcal{S}_0(z, t)$, $\mathcal{P}_\pm(z, t)$ and not higher momentum states) is appropriate.

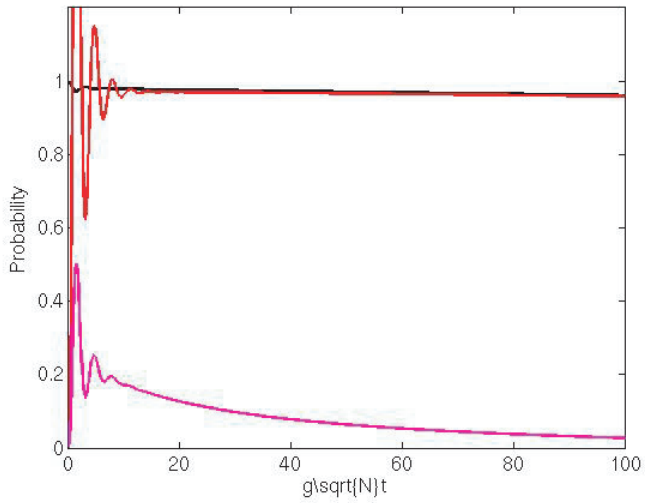

Figure D.3: Release of spin flip into trapped excitation. Probability in state $|s_0, 0, 0\rangle$ (black), probability in state $(|g, 1, 0\rangle + |g, 0, 1\rangle)/\sqrt{2}$ (red, multiplied by η), probability in state $|s_2, 0, 0\rangle$ (purple, multiplied by η^2). Parameters are $\alpha_+ = \alpha_- = 1/2$, $\Omega_+ = 0.2\gamma$, $\gamma_0 = 0.001\gamma$, $\eta = \frac{g^2 N}{|\Omega_+|^2 + |\Omega_-|^2} = 100$. Time is in units of $g\sqrt{N}$.

Bibliography

[1] D. Akamatsu, K. Akiba, and M. Kozuma. *Physical Review Letters*, 92:203602, 2004.

[2] A. André, M. Bajcsy, A. S. Zibrov, and M. D. Lukin. *Physical Review Letters*, 94:063902, 2005.

[3] A. André, L.-M. Duan, and M. D. Lukin. *Physical Review Letters*, 88:243602, 2002.

[4] A. André, M. D. Eisaman, R. L. Walsworth, A. S. Zibrov, and M. D. Lukin. *Journal of Physics B*, 38:S589, 2005.

[5] A. André and M. D. Lukin. *Physical Review A*, 65:053819, 2002.

[6] A. André and M. D. Lukin. *Physical Review Letters*, 89:143602, 2002.

[7] A. André, A. S. Sørensen, and M. D. Lukin. *Physical Review Letters*, 92:230801, 2004.

[8] J. R. Anglin and A. Vardi. *Physical Review A*, 64:013605, 2001.

[9] F. T. Arecchi, Eric Courtens, Robert Gilmore, and Harry Thomas. *Physical Review A*, 6:2211, 1972.

[10] N. W. Ashcroft and N. D. Mermin. *Solid State Physics*. Saunders College Publishing, Toronto, 1st edition, 1976.

[11] A. Aspect. *Nature*, 398:189, 1999.

[12] A. Aspect, J. Dalibard, and G. Roger. *Physical Review Letters*, 49:1804, 1982.

[13] Claude Audoin, Giorgio Santarelli, Ala'a Makdissi, and André Clairon. *IEEE Transactions on Ultrasonics, Ferroelectrics, and Frequency Control*, 45:877, 1998.

[14] O. Aytür and P. Kumar. *Physical Review Letters*, 65:1551, 1990.

[15] M. Bajcsy, A. S. Zibrov, and M. D. Lukin. *Nature*, 426:638, 2003.

[16] J. A. Barnes, A. R. Chi, L. S. Cutler, D. J. Healey, D. B. Leeson, T. E. McGunigal, J. A. Mullen JR., W. L. Smith, R. L. Sydnor, R. F. C. Vessot, and G. M. R. Winkler. *IEEE Transactions on Instrumentation and Measurement*, 20:105, 1971.

[17] P. R. Battle, J. G. Wessel, and J. L. Carlsten. *Physical Review A*, 48:707, 1993.

[18] J. S. Bell. *Physics*, 1:195, 1964.

[19] F. Benabid, G. Bouwmans, J. C. knight, P. St J. Russell, and F. Couny. *Physical Review Letters*, 93:123903, 2004.

[20] F. Benabid, F. Couny, J. C. knight, T. A. Birks, and P. St J. Russell. *Nature*, 434:488, 2005.

[21] F. Benabid, J. C. Knight, G. Antonopoulos, and P. St J. Russell. *Science*, 298:399, 2002.

[22] F. Benabid, J. C. Knight, and P. St J. Russell. *Optics Express*, 10:1195, 2002.

[23] D. J. Berkeland, J. D. Miller, J. C. Bergquist, W. M. Itano, and D. J. Wineland. *Physical Review Letters*, 80:2089, 1998.

[24] N. Bloembergen. *Nonlinear Optics*. World Scientific, 4th edition, 1996.

[25] J. J. Bollinger, W. M. Itano, D. J. Wineland, and D. J. Heinzen. *Physical Review A*, 54:R4649–R4652, 1996.

[26] Isabelle Bouchoule and Klaus Molmer. *Physical Review A*, 65:041803, 2002.

[27] G. Bouwmans, F. Luan, J. C. Knight, P. St. J. Russell, L. Farr, B. J. Mangan, and H.Sabert. *Optics Express*, 11, 2003.

[28] Dirk Bouwmeester, Arthur K. Ekert, and Anton Zeilinger, editors. *The physics of quantum information*. Springer, 1st edition, 2000.

[29] P. Bouyer and M. A. Kasevich. *Physical Review A*, 56:R1083, 1997.

[30] R. W. Boyd. *Nonlinear Optics*. Academic Press, 2nd edition, 2003.

[31] R. W. Boyd and D. J. Gauthier. *Progress in Optics*, 43:497–530, 2002.

[32] Danielle A. Braje, Vlatko Balić, Sunil Goda, G. Y. Yin, and S. E. Harris. *Physical Review Letters*, 93:183601, 2004.

[33] Danielle A. Braje, Vlatko Balić, G. Y. Yin, and S. E. Harris. *Physical Review A*, 68:041801(R), 2003.

[34] H.-J. Briegel, W. Dur, J. I. Cirac, and P. Zoller. *Physical Review Letters*, 78:3221, 1998.

[35] D. Budker, D. F. Kimball, S. M. Rochester, and V. V. Yashchuk. *Physical Review Letters*, 83:1767, 1999.

[36] L. Childress, J. M. Taylor, A. S. Sørensen, and M. D. Lukin. *quant-ph/0410123*, 2004.

[37] C. W. Chou, S. V. Polyakov, A. Kuzmich, and H. J. Kimble. *Physical Review Letters*, 92:213601, 2004.

[38] J. I. Cirac, P. Zoller, H. J. Kimble, and H. Mabuchi. *Physical Review Letters*, 78:3221, 1997.

[39] Claude Cohen-Tannoudji, Jacques Dupont-Roc, and Gilbert Grynberg. *Atom-photon Interactions*. Wiley, New York, 1998.

[40] J. H. de Boer. *The dynamical character of Adsorption*. Clarendon Press, Oxford, 1978.

[41] F. de Martini and C. Monroe, editors. *Proceedings of the International School of Physics "Enrico Fermi", Course CXLVIII, "Experimental Quantum Computation and Information"*. IOS Press, Amsterdam, 2002.

[42] I. H. Deutsch, J. C. Garrison, and E. M. Wright. *Journal of the Optical Society of America B*, 8, 1991.

[43] I. H. Deutsch, R. J. C. Spreeuw, S. L. Rolston, and W. D. Phillips. *Physical Review A*, 52:1394, 1995.

[44] S. A. Diddams, Th. Udem, J. C. Bergquist, E. A. Curtis, R. E. Drullinger, L. Hollberg, W. M. Itano, W. D. Lee, C. W. Oates, K. R. Vogel, and D. J. Wineland. *Science*, 293:825, 2001.

[45] Jonathan P. Dowling. *Physical Review A*, 57:4736–4746, 1998.

[46] Jonathan P. Dowling, G. S. Agarwal, and Wolfgang P. Schleich. *Physical Review A*, 49:4101–4109, 1994.

[47] P. D. Drummond and M. G. Raymer. *Physical Review A*, 44:2072, 1991.

[48] L. M. Duan, M. D. Lukin, J. I. Cirac, and P. Zoller. *Nature*, 68:3663, 2001.

[49] L.-M. Duan, A. Sørensen, J. I. Cirac, and P. Zoller. *Physical Review Letters*, 85:3991, 2000.

[50] W. Dur, H.-J. Briegel, J. I. Cirac, and P. Zoller. *Physical Review A*, 59:169, 1999.

[51] J. Durnin. *Journal of the Optical Society of America A*, 4:651, 1987.

[52] M. D. Eisaman, L. Childress, A. André, F. Massou, A. S. Zibrov, and M. D. Lukin. *Physical Review Letters*, 93:233602, 2004.

[53] M. D. Eisaman, F. Massou, G.-W. Li, A. André, A. S. Zibrov, and M. D. Lukin. *to be published*, 2005.

[54] J. E. Field, K. H. Hahn, and S. E. Harris. *Physical Review Letters*, 67:3062, 1991.

[55] J. Fiurášek, N. J. Cerf, and E. S. Polzik. *Physical Review Letters*, 93:180501, 2004.

[56] M. Fleischhauer and M. D. Lukin. *Physical Review Letters*, 84:5094, 2000.

[57] M. Fleischhauer and M. D. Lukin. *Physical Review A*, 65:022314, 2002.

[58] M. Fleischhauer and Th. Richter. *Physical Review A*, 51:2430, 1995.

[59] C. W. Gardiner and P. Zoller. *Quantum Noise*. Springer, 2nd edition, 2000.

[60] JM Geremia, John K. Stockton, Andrew C. Doherty, and Hideo Mabuchi. *Physical Review Letters*, 91:250801, 2003.

[61] Saikat Ghosh, Jay E. Sharping, Dimitre G. Ouzounov, and Alexander L. Gaeta. *Physical Review Letters*, 94:093902, 2005.

[62] Ph. Grangier, J.-A. Levenson, and J.-Ph. Poizat. *Nature*, 396:537, 1998.

[63] C. A. Greenhall. *IEEE Transactions on Ultrasonics, Ferroelectrics, and Frequency Control*, 45:895, 1998.

[64] Markus Greiner, Olaf Mandel andTilman Esslinger, Theodor W. Hansch, and Immanuel Bloch. *Nature*, 415:39–44, 2002.

[65] M. Gross and S. Haroche. *Physics Reports*, 93:301, 1982.

[66] J. Hald, J. L. Sørensen, C. Schori, and E. S. Polzik. *Physical Review Letters*, 83:1319, 1999.

[67] K. Hammerer, K. Mølmer, E. S. Polzik, and J. I. Cirac. *Physical Review A*, 70:044304, 2004.

[68] S. E. Harris. *Physical Review Letters*, 70:552, 1993.

[69] S. E. Harris. *Physics Today*, 50(7):36, 1997.

[70] S. E. Harris, J. E. Field, and A. Imamoğlu. *Physical Review Letters*, 64:1107, 1990.

[71] S. E. Harris and L. V. Hau. *Physical Review Letters*, 82:4611, 1999.

[72] S. E. Harris, M. K. Hoshman, and R. L. Byer. *Physical Review Letters*, 18:732, 1967.

[73] S. E. Harris and Y. Yamamoto. *Physical Review Letters*, 81:3611, 1998.

[74] Lene Vestergaard Hau, Stephen E. Harris, Zachary Dutton, and Cyrus H. Behroozi. *Nature*, 397:594, 1999.

[75] D. J. Heinzen and Roahn Wynar. *Physical Review Letters*, 84:5029–5033, 2000.

[76] P. R. Hemmer, D. P. Katz, J. Donoghue, M. Cronin-Golomb, M. S. Shahriar, and P. Kumar. *Optics Letters*, 20:982, 1995.

[77] M. Hennrich, T. Legero, A. Kuhn, and G. Rempe. *Physical Review Letters*, 85:4872, 2000.

[78] C. K. Hong, Z. Y. Ou, and L. Mandel. *Physical Review Letters*, 59:2044, 1987.

[79] Christina J. Hood, H. J. Kimble, and Jun Ye. *Physical Review A*, 64:033804, 2001.

[80] S. F. Huelga, C. Macchiavello, T. Pellizzari, A. K. Ekert, M. B. Plenio, and J. I. Cirac. *Physical Review Letters*, 79:3865–3868, 1997.

[81] W. M. Itano, J. C. Bergquist, J. J. Bollinger, J. M. Gilligan, D. J. Heinzen, F. L. Moore, M. G. Raizen, and D. J. Wineland. *Physical Review A*, 47:3554, 1993.

[82] M. Jain, G. Y. Yin, J. E. Field, and S. E. Harris. *Optics Letters*, 22:998, 1993.

[83] J. D. Joannopoulos, R. D. Meade, and J. N. Winn, editors. *Photonic Crystals: Molding the Flow of Light*. Princeton University Press, 1st edition, 1995.

[84] B. Julsgaard, J. Sherson, J. I. Cirac, J. Fiurášek, and E. S. Polzik. *Nature*, 432:482, 2004.

[85] Brian Julsgaard, Alexander Kozhekin, and Eugene S. Polzik. *Nature*, 413:400–403, 2001.

[86] Y. Kaluzny, P. Goy, M. Gross, J. M. Raimond, and S. Haroche. *Physical Review Letters*, 51:1175, 1983.

[87] Michael M. Kash, Vladimir A. Sautenkov, Alexander S. Zibrov, Leo Hollberg, George R. Welch, Mikhail D. Lukin, Yuri Rostovtsev, Edward S. Fry, and Marlan O. Scully. *Physical Review Letters*, 82:5229, 1999.

[88] Taesoo Kim, Olivier Pfister, Murray J. Holland, Jaewoo Noh, and John L. Hall. *Physical Review A*, 57:4004–4013, 1998.

[89] H. J. Kimble. *Fundamental Systems in Quantum Optics*. North-Holland, 1992.

[90] H. J. Kimble. *Physica Scripta*, 76:127, 1998.

[91] Masahiro Kitagawa and Masahito Ueda. *Physical Review A*, 47:5138, 1993.

[92] Jonathan C. Knight. *Nature*, 424:847, 2003.

[93] Olga Kocharovskaya, Yuri Rostovtsev, and Marlan O. Scully. *Physical Review Letters*, 86:628, 2001.

[94] S. O. Konorov, A. B. Fedotov, and A. M. Zheltikov. *Optics Letters*, 28:1448, 2003.

[95] A. E. Kozhekin, K. Mølmer, and E. S. Polzik. *Physical Review A*, 62:033809, 2000.

[96] A. Kuhn, M. Hennrich, and G. Rempe. *Physical Review Letters*, 89:067901, 2002.

[97] A. Kuzmich, W. P. Bowen, A. D. Boozer, A. Boca, C. W. Chou, L.-M. Duan, and H. J. Kimble. *Nature*, 423:731, 2003.

[98] A. Kuzmich, Klaus Mølmer, and E. S. Polzik. *Physical Review Letters*, 79:4782, 1997.

[99] A. Kuzmich, L. Mandel, and N. P. Bigelow. *Physical Review Letters*, 85:1594, 2000.

[100] A. Kuzmich and E. S. Polzik. 2003.

[101] Ulf Leonhardt. *Nature*, 415:406, 2002.

[102] R. S. Lipster and A. N. Shiryaev. *Statistics of Random Processes*. Springer, 2nd edition, 2001.

[103] Chien Liu, Zachary Dutton, Cyrus H. Behroozi, and Lene Vestergaard Hau. *Nature*, 409:490, 2001.

[104] M. D. Lukin. *Review of Modern Physics*, 75:457, 2003.

[105] M. D. Lukin, P. R. Hemmer, and M. O. Scully. *Advances in Atomic, Molecular and Optical Physics*, 42:347, 2000.

[106] M. D. Lukin and A. Imamoğlu. *Physical Review Letters*, 84:1419, 2000.

[107] M. D. Lukin and A. Imamoğlu. *Nature*, 413:273, 2001.

[108] M. D. Lukin, A. B. Matsko, M. Fleischhauer, and M. O. Scully. *Physical Review Letters*, 82:1847, 1999.

[109] M. D. Lukin, S. F. Yelin, and M. Fleischhauer. *Physical Review Letters*, 84:4232, 2000.

[110] H. Mabuchi and A. C. Doherty. *Science*, 298:1372, 2002.

[111] A. Mair, J. Hager, D. F. Phillips, R. L. Walsworth, , and M. D. Lukin. *Physical Review A*, 65:031802(R), 2002.

[112] L. Mandel and E. Wolf. *Optical Coherence in Quantum Optics*. Cambridge University Press, 1995.

[113] J. P. Marangos, M. Fleischhauer, and A. Imamoğlu. *Review of Modern Physics, in press*, 2005.

[114] D. N. Matsukevich and A. Kuzmich. *Science*, 306:663, 2004.

[115] Klaus Mattle, Harald Weinfurter, Paul G. Kwiat, and Anton Zeilinger. *Physical Review Letters*, 76:4656, 1996.

[116] M. Mašalas and M. fleischhauer. *Physical Review A*, 69:061801(R), 2004.

[117] J. McKeever, A. Boca, A. D. Boozer, J. R. Buck, and H. J. Kimble. *Nature*, 425:268, 2003.

[118] J. McKeever, A. Boca, A. D. Boozer, R. Miller, J. R. Buck, A. Kuzmich, and H. J. Kimble. *Science*, 303:1992, 2004.

[119] V. Meyer, M. A. Rowe, D. Kielpinski, C. A. Sackett, W. M. Itano, C. Monroe, and D. J. Wineland. *Physical Review Letters*, 86:5870–5873, 2001.

[120] P. Meystre. *Atom Optics*. Springer, 1st edition, 2001.

[121] Dirk Müller, Eric A. Cornell, Dana Z. Anderson, and Eric R. I. Abraham. *Physical Review A*, 61:033411, 2000.

[122] M. A. Nielsen and I. L. Chuang. *Quantum computation and quantum information*. Cambridge University Press, Cambridge, 1st edition, 2000.

[123] I. Novikova, A. S. Zibrov, D. F. Phillips, A. André, and R. L. Walsworth. *Physical Review A*, 69:061802, 2004.

[124] C. Orzel, A. K. Tuchman, M. L. Fenselau, M. Yasuda, and M. A. Kasevich. *Science*, 291:2386–2389, 2001.

[125] Z. Y. Ou, S. F. Pereira, H. J. Kimble, and K. C. Peng. *Physical Review Letters*, 68:3663, 1992.

[126] B. N. Perry, P. Rabinowitz, and M. Newstein. *Physical Review A*, 27:1989, 1983.

[127] D. Petrosyan and G. Kurizki. *Physical Review A*, 65:033833, 2002.

[128] D. F. Phillips, A. Fleischhauer, A. Mair, R. L. Walsworth, and M. D. Lukin. *Physical Review Letters*, 86:783, 2001.

[129] P. W. H. Pinkse, T. Fischer, P. Maunz, T. Puppe, and G. Rempe. *Journal of Modern Optics*, 47:2769–2787, 2000.

[130] P. W. H. Pinkse, T. Fischer, P. Maunz, and G. Rempe. *Nature*, 404:365–368, 2000.

[131] S. V. Polyakov, C. W. Chou, D. Felinto, and H. J. Kimble. *Physical Review Letters*, 93:263601, 2004.

[132] R. J. Rafac, B. C. Young, J. A. Beall, W. M. Itano, D. J. Wineland, and J. C. Bergquist. *Physical Review Letters*, 85:2462, 2000.

[133] J.-M. Raimond, M. Brune, and S. Haroche. *Review of Modern Physics*, 73:565, 2001.

[134] Norman F. Ramsey. *Molecular Beams*. Oxford University Press, 1985.

[135] M. G. Raymer and I. A. Walmsley. *Progress in Optics*, volume 28. North-Holland, 1996.

[136] M. G. Raymer, I. A. Walmsley, J. Mostowski, and B. Sobolewska. *Physical Review A*, 32:332, 1985.

[137] M. J. Renn, E. A. Donley, E. A. Cornell, C. E. Wieman, and D. Z. Anderson. *Physical Review A*, 53:R648, 1996.

[138] M. J. Renn, D. Montgomery, O. Vdovin, D. Z. Anderson, C. E. Wieman, and E. A. Cornell. *Physical Review Letters*, 75:3253, 1995.

[139] M. J. Renn, A. A. Zozulya, E. A. Donley, E. A. Cornell, and D. Z. Anderson. *Physical Review A*, 55:3684, 1997.

[140] Michael J. Renn, Robert Pastel, and Heather J. Lewandowski. *Physical Review Letters*, 82:1574, 1999.

[141] A. Sørensen, L.-M. Duan, J. I. Cirac, and P. Zoller. *Nature*, 409:63–66, 2001.

[142] Philip Russell. *Science*, 299:358, 2003.

[143] S. Sachdev. *Quantum phase transitions*. Camrbidge University Press, 1st edition, 1999.

[144] C. A. Sackett, D. Kielpinski, B. E. King, C. Langer, V. Meyer, C. J. Myatt, M. Rowe, Q. A. Turchette, W. M. Itano, D. J. Wineland, and C. Monroe. *Nature*, 404:256–259, 2000.

[145] G. Santarelli, Ph. Laurent, P. Lemonde, A. Clairon, A. G. Mann, S. Chang, A. N. Luiten, and C. Salomon. *Physical Review Letters*, 82:4619, 1999.

[146] H. Schmidt and A. Imamoğlu. *Optics Letters*, 21:1936, 1996.

[147] M. Scully and M. S. Zubairy. *Quantum Optics*. Cambridge University Press, 1st edition, 1997.

[148] M. Y. Shverdin, D. R. Walker, D. D. Yavuz, G. Y. Yin, and S. E. Harris. *Physical Review Letters*, 94:033904, 2005.

[149] Anthony E. Siegman. *Lasers*. University Science Books, Mll Valley, CA, 1986.

[150] C. M. Smith, N. Venkataraman, M. T. Gallagher, D. Müller, J. A. West, N. F. Borrelli, D. C. Allan, and K. W. Koch. *Nature*, 424:657, 2003.

[151] D. T. Smithey, M. Beck, M. Belsley, and M. G. Raymer. *Physical Review Letters*, 69:2650, 1992.

[152] J. Stenger, S. Inouye, D. M. Stamper-Kurn, H.-J. Miesner, A. P. Chikkatur, and W. Ketterle. *Nature*, 396:345–348, 1998.

[153] M. Stephens, R. Rhodes, and C. Wieman. *Journal of Applied Physics*, 76:3479, 1994.

[154] Masao Takamoto and Hidetoshi Katori. *Physical Review Letters*, 91:223001, 2003.

[155] L. K. Thomsen, S. Mancini, and H. M. Wiseman. *Physical Review A*, 65:061801, 2002.

[156] Hugo Touchette and Seth Lloyd. *Physical Review Letters*, 84:1156–1159, 2000.

[157] A. V. Turukhin, V. S. Sudarshanam, M. S. Shahriar, J. A. Musser, B. S. Ham, and P. R. Hemmer. *Physical Review Letters*, 88:023602, 2002.

[158] D. Ulam-Orgikh and M. Kitagawa. *Physical Review A*, 64:052106, 2001.

[159] C. H. van der Wal, M. D. Eisaman, A. André, R. L. Walsworth, D. F. Phillips, A. S. Zibrov, and M. D. Lukin. *Science*, 301:196, 2003.

[160] S. J. van Enk, J. I. Cirac, and P. Zoller. *Science*, 279:205, 1998.

[161] Jelena Vučković, Marko Loncar, Hideo Mabuchi, and Axel Scherer. *Physical Review E*, 65:016608, 2002.

[162] D. F. Walls and G. J. Milburn. *Quantum Optics*. Springer, 1st edition, 1994.

[163] J. G. Wessel, P. R. Battle, and J. L. Carlsten. *Physical Review A*, 50:2587, 1994.

[164] D. J. Wineland, J. J. Bollinger, W. M. Itano, and D. J. Heinzen. *Physical Review A*, 50:67, 1994.

[165] D. J. Wineland, J. J. Bollinger, W. M. Itano, F. L. Moore, and D. J. Heinzen. *Physical Review A*, 46:R6797, 1992.

[166] D. J. Wineland, C Monroe, W. M. Itano, D. Leibfried, B. E. King, and D. M. Meekhof. *Journal of Research of the National Institute of Standards and Technology*, 103:259, 1998.

[167] A. Yariv and P. Yeh. *Optical Waves in Crystals*. Wiley, New York, 1st edition, 1984.

[168] J. Ye, D. W. Vernooy, and H. J. Kimble. *Physical Review Letters*, 83:4987–4990, 1999.

[169] A. Zeilinger. *Review of Modern Physics*, 71:288, 1998.

[170] A. S. Zibrov, M. D. Lukin, and M. O. Scully. *Physical Review Letters*, 83:4049, 1999.

[171] A. S. Zibrov, A. B. Matsko, L. Hollbreg, and V. L. Velichansky. *Journal of Modern Optics*, 49:359, 2002.